# UNIVERSIDAD DE ALCALÁ

**ESCUELA POLITÉCNICA SUPERIOR**

**DEPARTAMENTO DE ELECTRÓNICA**


# EFFICIENT COMPLEMENTARY SEQUENCES-BASED ARCHITECTURES AND THEIR APPLICATION TO RANGING MEASUREMENTS


**Author**

Enrique García Núñez

**Advisors**

Dr. Juan Jesús García Domínguez

Dr. Jesús Ureña Ureña


**DOCTORAL THESIS**

**2013**

# Resumen

En las últimas décadas, los sistemas de medición de distancias se han beneficiado de los avances en el área de las comunicaciones inalámbricas. En los sistemas basados en CDMA (Code-Division Multiple-Access), las propiedades de correlación de las secuencias empleadas juegan un papel fundamental en el desarrollo de dispositivos de medición de altas prestaciones. Debido a las sumas ideales de correlaciones aperiódicas, los conjuntos de secuencias complementarias, CSS (Complementary Sets of Sequences), son ampliamente utilizados en sistemas CDMA. En ellos, es deseable el uso de arquitecturas eficientes que permitan generar y correlar CSS del mayor número de secuencias y longitudes posibles. Por el término eficiente se hace referencia a aquellas arquitecturas que requieren menos operaciones por muestra de entrada que con una arquitectura directa.

Esta tesis contribuye al desarrollo de arquitecturas eficientes de generación/correlación de CSS y derivadas, como son las secuencias LS (Loosely Synchronized) y GPC (Generalized Pairwise Complementary), que permitan aumentar el número de longitudes y/o de secuencias disponibles. Las contribuciones de la tesis pueden dividirse en dos bloques:

En primer lugar, las arquitecturas eficientes de generación/correlación para CSS binarios, derivadas en trabajos previos, son generalizadas al alfabeto multinivel (secuencias con valores reales) mediante el uso de matrices de Hadamard multinivel. Este planteamiento tiene dos ventajas: por un lado el aumento del número de longitudes que pueden generarse/correlarse y la eliminación de las limitaciones de las arquitecturas previas en el número de secuencias en el conjunto. Por otro lado, bajo ciertas condiciones, los parámetros de las arquitecturas generalizadas pueden ajustarse para generar/correlar eficientemente CSS binarios de mayor número de longitudes que con las arquitecturas eficientes previas.

En segundo lugar, las arquitecturas propuestas son usadas para el desarrollo de nuevos algoritmos de generación/correlación de secuencias derivadas de CSS que reducen el número de operaciones por muestra de entrada. Finalmente, se presenta la aplicación

de las secuencias estudiadas en un nuevo sistema de posicionamiento local basado en Ultra-Wideband y en un sistema de posicionamiento local basado en ultrasonidos.

# Abstract

In the last decades, ranging systems have benefited from advances in the wireless communication field, as multiple access techniques or near-far mitigation algorithms. In CDMA-based (Code-Division Multiple-Access) ranging systems, the properties of the spreading sequence used play a key role on the development of high-precision ranging measurements. This thesis proposes novel efficient generation/correlation architectures of Complementary Sets of Sequences (CSS) and sequences derived from them, as Loosely Synchronized (LS) and Generalized Pairwise Complementary (GPC) sequences. We consider the term efficient applicable whether the proposed architectures requires less operations per input sample in comparison with a straighforward implementation (a Tapped-Delay Line implementation). The contributions of the thesis can be divided into two stages:

Firstly, we generalize the efficient generation/correlation architectures for binary CSS, derived in previous works, to the multilevel (real-valued) alphabet by using multilevel Hadamard matrices. This approach has two advantages: on the one hand the increase of the feasible lengths that the architecture is capable to generate/correlate, and the elimination of the previous limitations in the number of sequences of the set; on the other hand, under certain conditions, the generalized architectures allow to particularize their inner structure to efficiently generate/correlate binary CSS with more different lengths than the ones feasible with previous efficient algorithms.

Secondly, based on the proposed architectures, we provide novel algorithms for LS and GPC sequences that reduce the number of operations per input sample. Finally, we do a comparative analysis of the performance of LS and Kasami sequences in a novel UWB indoor positioning system.

«... If practical problems exist in which the correlation function is the thing desired, a device performing the correlation calculations efficiently and with reasonably short samples would fall in the class of [an outstanding useful application]»

M. J. E. Golay

# Agradecimientos

Mis primeros agradecimientos van a mis directores de tesis, Juan Jesús García y Jesús Ureña, por su compromiso, las largas horas de revisiones y por darme la libertad para seguir mi camino, pero advertirme cuando me desviaba del objetivo.

A José Luis Martín y a Pablo Poudereux. Sin su trabajo, el desarrollo del sistema UWB hubiese sido muy diferente.

A los miembros del grupo de investigación GEINTRA de la UAH. En especial a Daniel Ruiz, por ofrecerme su ayuda cada vez que me oía resoplar.

Hago extensivo mi agradecimiento a los compañeros de laboratorio y del Departamento de Electrónica, por los buenos momentos pasados dentro y fuera del horario de trabajo.

Por último, en el terreno personal, a mis amigos, que siguen llamándome a pesar de mis negativas a descansar. Alguno dice que la tesis me ha cambiado, ¿verdad Fer?.

Sin duda, a Ana por tener tanta paciencia conmigo desde el primer momento y, por último, mis mayores agradecimientos van dirigidos a mi familia, en especial a mis padres. Este trabajo es tan suyo como mío. Sin ellos esto hubiese sido imposible.

# Contents

# List of Figures

# List of Tables

# List of Acronyms

| | |
|---|---|
| ADC | Analog to Digital Converter |
| AOA | Angle of Arrival |
| AWGN | Additive White Gaussian Noise |
| BER | Bit Error Rate |
| BPSK | Binary Phase Shift Keying |
| CAZAC | Constant Amplitude Zero Auto-Correlation |
| CC | Complete Complementary |
| CDMA | Code-Division Multiple-Access |
| CDF | Cumulative Distribution Function |
| CRLB | Cramér-Rao Lower Bound |
| CSMA | Carrier Sense Multiple-Access |
| CSS | Complementary Sets of Sequences |
| DS | Direct Sequence |
| EGC | Efficient Golay Correlator |
| EGG | Efficient Golay Generator |
| FDMA | Frequency Division Multiple-Access |
| FFT | Fast Fourier Transform |
| FIR | Finite Impulse Response |
| GCC | Generalized Cross-Correlation |
| GESO | Generalized Even-Shift Orthogonal |
| GLS | Generalized Loosely Synchronous |
| GO | Generalized Orthogonal |
| GPC | Generalized Pairwise Complementary |

| | |
|---|---|
| GPZ | Generalized Pairwise Z-complementary |
| GQO | Generalized Quasi-Orthogonal |
| IFW | Interference Free Windows |
| IGC | Inter-Group Complementary |
| IRLS | Interatively Reweighted Least Squares |
| ISI | Inter-Symbol Interference |
| ISL | Integrated Sidelobe Level |
| LCZ | Low Correlation Zone |
| LO | Local Oscillator |
| LOS | Line-of-Sight |
| LPS | Local Positioning System |
| LS | Loosely Synchronized |
| MAI | Multiple Access Interference |
| MC-CDMA | Multi-Carrier CDMA |
| NLOS | Non-Line-of-Sight |
| OVSF | Orthogonal Variable Spreading Factor |
| PAPR | Peak-to-Average Power Ratio |
| PC | Perfect Complementary |
| PMCS | Pair of Multilevel Complementary Sequences |
| PN | Pseudo-Noise |
| PR | Perfect Reconstruction |
| PSD | Power Spectral Density |
| PSL | Peak Sidelobe Level |
| QMF | Quadrature Mirror Filter |
| QS-CDMA | Quasi-synchronous CDMA |
| RMSE | Root Mean Square Error |
| RSS | Received Signal Strength |
| SACF | Sum of Auto-Correlation Functions |
| SCCF | Sum of Cross-Correlation Functions |
| SIC | Successive Interference Cancellation |

| | |
|---|---|
| SNR | Signal-to-Noise Ratio |
| SPL | Sound Pressure Level |
| SPT | Signed Power-of-Two |
| TDMA | Time Division Multiple-Access |
| TDOA | Time Difference Of Arrival |
| TOA | Time Of Arrival |
| T-ZCZ | Three-Zero Correlation Zone |
| US | Ultrasound |
| UWB | Ultra-Wideband |
| WHE | Walsh-Hadamard Expansion |
| ZCZ | Zero Correlation Zone |

# Nomenclature

| | |
|---|---|
| $\boldsymbol{\mathcal{C}}_{K_{\|MultCSS}}$ | Circulant multilevel Hadamard matrix used to generate $K_{\|MultCSS}$ multilevel CSS. |
| $\boldsymbol{\mathcal{P}}(z^{-1})$ | Paraunitary matrix used in the planar factorization. |
| $\boldsymbol{\mathcal{R}}^{(l)}(\theta^{(l)})$ | Rotation matrix used in the planar factorization. |
| $\boldsymbol{\mathcal{H}}_K$ | Hadamard matrix of order $K$ generated with Sylvester's method. |
| $\gamma_{i,j}$ | The $i$-th row and $j$-th column with modulus $\gamma$ of a Hadamard matrix. It determines the initial conditions of the multilevel CSS for $K_{\|MultCSS} \geq 3 - \{4\}$. |
| $\breve{\mathbf{S}}_j^{(q+1)}[l]$ | $j$-th multilevel CSS generated after iteration $q$ with the circulant multilevel Hadamard matrix $\boldsymbol{\mathcal{C}}_{K_{\|MultCSS}}$ in time domain. |
| $\mathbf{B}_{A^{(1,q)},W^{(1,q)}}\left(z^{-D^{(q)}}\right)$ | Basic building block defined by the parameters $A^{(1,q)}$, $W^{(1,q)}$ and $D^{(q)}$. |
| $\mathbf{D}^{(k,q)}[l]$ | Delay matrix in time domain at stage $q$ for the generation of $2^k$ CSS. |
| $\mathbf{G}^{(k+1)}_{K_{\|CSS}\cdot 2^N\cdot 10^M\cdot 26^P}(z^{-1})$ | Generation matrix of $2\cdot K_{\|CSS}$ uncorrelated CSS of length $L_{\|CSS} = K_{\|CSS}\cdot(2^N\cdot 10^M\cdot 26^P), K_{\|CSS} = 2^k$. |
| $\mathbf{H}_2^{(k+1)}(z^{-1})$ | Paraunitary matrix of order 2 employed to generalized the CSS generation algorithm to $2\cdot K_{\|CSS}$ sequences, $K_{\|CSS} = 2^k$. |
| $\mathbf{Sc}_j(z^{-1})$ | $j$-th CC set in $Z$-domain. |
| $\mathbf{S}_j^{(k,Q)}(z^{-1})$ | $j$-th CSS generated in $Q$ stages in $Z$-domain. The set size is $2^k$. |

| | |
|---|---|
| $\mathbf{S}_j^{(k,q+1)}[l]$ | $j$-th CSS generated after iteration $q$ in time domain. The set size is $2^k$. |
| $\mathbf{U}^{(j)}[l]$ | $j$-th GPC group in time domain. |
| $\mathbf{Y}^{(j)}[l]$ | $j$-th IGC group in time domain. |
| $\mathcal{E}_j\left(z^{-1}\right)$ | GESO sequence in $Z$-domain generated from the $j$-th CC set. |
| ${}^dS_{j,i}^{(Q)}(z^{-1})$ | $i$-th complementary sequence of the $j$-th set with one zero every two bits and generated in $Q$ stages. |
| $A^{(k,q)}$ | Multiplier used in the $q$-th stage of the efficient architectures for $K_{\|CSS} = 2^k$, $k > 0$ CSS in Chapter 4, $0 \leq q \leq Q-1$. In Chapters 3 and 5 it is used the notation $A^{(q)}$. |
| $B$ | Signal bandwidth. |
| $c$ | In Chapter 3, it represents the exponent of the homomorphic transformation to the CSS. In Chapter 6 we refer to the propagation speed of electromagnetic waves and in Chapter 7 to the propagation speed of acoustic signals. |
| $C_{a,b}[\tau]$ | Aperiodic correlation between sequences $a$ and $b$. |
| $D^{(q)}$ | Delay value used in the $q$-th stage of the efficient architectures for CSS. |
| $D^k s\,[l]$ | Cyclic shift of $k$ bits to the sequence $s[l]$. |
| $E_j(z^{-1})$ | $E$-sequence in $Z$-domain generated from the $j$-th Golay pair. |
| $G$ | Number of GPC sequences in the $j$-th subgroup. $G = 2^a$; $a \in \mathbb{N} - \{0\}$ |
| $K_{\|seq}$ | Number of sequences in a set of *seq* sequences. For any type of sequences we use $K$. |
| $l$ | $l$-th bit of a sequence of length $L, 0 \leq l \leq L-1$. |
| $L_{\|seq}$ | Length of the sequence *seq*. For any class of sequences we use $L$. |

| | |
|---|---|
| $M$ | Non-negative integer which determines the length of the Golay binary sequences, $L_{\|Gol} = 10^M$. |
| $N$ | Non-negative integer which determines the length of the Golay binary sequences, $L_{\|Gol} = 2^N$. |
| $N_0$ | Power spectral density of additive white gaussian noise in W/Hz. |
| $N_\ell$ | Number of amplitude levels of the multilevel CSS. |
| $P$ | Non-negative integer which determines the length of the Golay binary sequences, $L_{\|Gol} = 26^P$. |
| $Q$ | Number of iterations of the recursive algorithm for the generation of CSS. |
| $R(z^{-1})$ | Correlator input in $Z$-domain. |
| $R_{a,b}[\tau]$ | Periodic correlation between sequences $a$ and $b$. |
| $s[l]$ | Real-valued sequence of length $L$ in time domain. To indicate the elements of $s[l]$, we use the notation $\{s[0], s[1], \ldots, s[L-1]\}$. Its $Z$-transform is expressed in uppercase as $S(z^{-1})$. A set of $K$ sequences $\{s_0[l], s_1[l], \ldots s_{K-1}[l]\}$ in time domain is notated as $\mathbf{S}[l]$ and in $Z$-domain as $\mathbf{S}(z^{-1})$. |
| $S_{j,i}^{(q+1)}(z^{-1})$ | $i$-th complementary sequence of the $j$-th set generated after iteration $q$ in $Z$-domain. |
| $s_{j,i}^{(q+1)}[l]$ | $i$-th complementary sequence of the $j$-th set generated after iteration $q$ in time domain. |
| $U_{k,i}^{(j)}(z^{-1})$ | $i$-th GPC sequence in $Z$-domain of the $k$-th pair, which belongs to the $j$-th subgroup. |
| $V_\ell$ | Amplitude values of the multilevel CSS. |
| $V_k\,(z^{-1})$ | $k$-th LS sequence in $Z$-domain, $0 \leq k \leq K_{\|LS} - 1$. |
| $W^{(k,q)}$ | Complex number of unit magnitude. For real-valued CSS $W^{(k,q)} \in \{-1, +1\}$. |

$W_{|seq}$ Zero correlation zone length of the sequence *seq*. For any class of sequences we use $W_{ZCZ}$ for the zero correlation zone length and $W_{LCZ}$.

$y_{g,k}^{(j)}[l]$ $k$-th IGC sequence in time domain, of the $g$-th set belonging to the $j$-th group.

$\boldsymbol{\pi}$ Vector that represents the binary expansion of an arbitrary integer $p$, $0 \leq p \leq 2^{K_{|LS}/2-1}$.

$\delta[l]$ Kronecker delta.

$\boldsymbol{\Delta}_{left}^{(k,q)}$ Left submatrix of the Tseng and Liu expansion matrix at the $q$-th iteration and at expansion stage $k$. In Chapter 4 we use the notation $\boldsymbol{\Delta}_{left}^{(k+1)}$ to refer the left submatrix for the generation of $2 \cdot K_{|CSS}$ uncorrelated CSS.

$\boldsymbol{\Delta}_{right}^{(k,q)}$ Right submatrix of the Tseng and Liu expansion matrix at the $q$-th iteration and at expansion stage $k$. In Chapter 4 we use the notation $\boldsymbol{\Delta}_{right}^{(k+1)}$ to refer the right submatrix for the generation of $2 \cdot K_{|CSS}$ uncorrelated CSS.

$\boldsymbol{\Lambda}_{j}^{(k,q)}$ Tseng and Liu expansion matrix in time domain for the generation of the $j$-th uncorrelated CSS of $K_{|CSS} = 2^k$ sequences at iteration $q$.

$\boldsymbol{\Upsilon}^{(q)}(z^{-1})$ Interleaving matrix used in stage $q$ for the decomposition of the paraunitary matrix $\mathbf{H}_2^{(k+1)}(z^{-1})$.

$\phi_{r,s_{j,i}^{(q)}}[l]$ Partial result in time domain after the stage $q-1$ in the efficient correlator. After the final stage it results in the aperiodic correlation among $r[l]$ and $s_{j,i}^{(Q)}$.

$\tau$ Time shift of the correlation.

$\theta$ Joint correlation bound.

$\theta_{AC}$ Auto-correlation bound.

$\theta_{CC}$ Cross-correlation bound.

| | |
|---|---|
| ■ | End of proof. |
| ▲ | End of example. |
| $\lceil x \rceil$ | Smallest integer larger than or equal to $x$. |
| $\lfloor x \rfloor$ | Largest integer smaller than or equal to $x$. |
| $\odot$ | Interleaving operator. |
| $\oplus$ | Modulo-2 adder. |
| $\otimes$ | Kronecker product. |
| $\star$ | Convolution operator. |
| $\times$ | Matricial product. |
| $mod\, n$ | Modulo $n$ operation. |

# Chapter 1
# Preface

## 1.1 Thesis Background

This thesis has been developed under the research project LEMUR (ref. TIN2009-14114-C04-01), supported by the Spanish Ministry of Science and Innovation.

The thesis has also been economically supported by the University of Alcalá grant program FPI/UAH (ref. FPI/UAH2009), by the Spanish Ministry of Education grant program FPU/MEC (EDU/3083/2009) and by the University of Alcalá mobility program. The former one made possible a research stay at the Digital Signal Processing and Image Analysis (DBS) research group of the University of Oslo.

The main goal of the LEMUR project is to achieve significant improvements in Local Positioning Systems (LPS) to operate in extensive areas (including indoor and restricted outdoor environments) in a transparent form for users or services. Continuous and robust positioning is achieved by means of a combination of ultrasound and radio frequency technologies. Particularly, this thesis copes with the following objectives of the LEMUR project:

- The study of modulation, encoding and digital signal detection by using CDMA and UWB techniques to enhance optimal processing of US and RF signals.
- Implementation of a demonstrator: an integrated system for continuous localization and guidance of people in large buildings.

## 1.2 Introduction

Binary Complementary Sets of Sequences (CSS) are used intensively in a broad number of fields, as sonar [Alvar 06], MIMO radar [Li 10], Non-Destructive Test (NDT) applications

[White 92], low Peak-to-Average Power Ratio (PAPR) OFDM communication systems [Davis 99], or the second digital terrestrial television broadcasting standard (DVB-T2) [He 11], due to their ideal sum of aperiodic correlation functions. Furthermore, they are considered as a basic building block for the generation of novel Generalized Orthogonal (GO) spreading sequences for Quasi-Synchronous Code Division Multiple Access (QS-CDMA) systems [Stanc 01, Chen 06, Li 08]. Those applications would benefit from generation and correlation architectures capable of dealing with CSS of a large number of feasible lengths and set sizes, and correlate them with a reduced number of operations per input sample. In this sense, there has been a sustained research effort in the last decades for the design of flexible CSS and CSS-derived GO sequences [Darne 88, Kemp 89, Gavis 94, Fan 96, Trinh 06, Chen 06, Fan 07, Li 11a, Budis 11, Bi 12] and of correlation architectures for CSS and CSS-derived GO sequences with a reduced number of hardware resources [Budis 91, Alvar 04, De Ma 07, Perez 08, Donat 09b, Perez 09b, Perez 10, Coker 10, De Ma 11, Budis 11].

This thesis contributes to the increase on the versatility of the efficient architectures for the generation and correlation of CSS and CCS-derived GO sequences, as Generalized Pairwise Complementary (GPC) and Loosely Synchronous (LS) sequences. It also focuses on the application of the spreading sequences in ranging systems by proposing a CDMA-based Ultra-Wideband (UWB) indoor positioning system, which is used as a test-bed for the performance comparison of LS and Kasami spreading sequences. Furthermore, an ultrasonic local positioning system has been used for the analysis of CSS-derived GO spreading sequences.

## 1.3 Summary

The proposals of the thesis have been divided into the following chapters:

- Chapter 2: *"State of the Art and Problem Statement"*. In this chapter we introduce the signal processing techniques employed in ranging measurements and review the generation algorithms of the classical and the newest spreading sequences available in literature. Later, we revise the performance of two types of ranging systems: Ultra-Wideband-based and ultrasound-based local positioning systems. From the previous review we derive the problems in ranging systems and introduce the objectives and proposals of this thesis.

- Chapter 3: *"Generalization of Efficient Architectures for the Generation and Correlation of Multilevel CSS"*. In this chapter we cope with the first objective of the thesis and propose efficient architectures for the generation and correlation of multilevel CSS. With these architectures it is possible the generation/correlation of multilevel CSS with more flexible lengths and without limitations in the number of sequences of the set. The proposals of this chapter have been submitted for publication in the international journal IEEE Transactions on Signal Processing.

- Chapter 4: *"Efficient Architectures for the Generation and Correlation of Binary CSS"*. This chapter deals with the generalization of the efficient generation/correlation architectures of $K_{|CSS}$ binary CSS of lengths $L_{|CSS} = K_{|CSS}^{Q}$ to $K_{|CSS}$ binary CSS of length $L_{|CSS} = \left(K_{|CSS}/2\right) \cdot 2^N \cdot 10^M \cdot 26^P$, with $N$, $M$ and $P$ non-negative integers and $Q$ and integer so that $Q \geq 1$. The proposal of the architecture for $K_{|CSS} = 2$ binary CSS (the so-called Golay sequence pairs) has been published in the International Journal of Circuit Theory and Applications and its extension to $K_{|CSS} = 2^k$, $k \in \mathbb{N} - \{0\}$, binary CSS has been submitted for publication in the journal IEEE Transactions on Signal Processing.

- Chapter 5: "*Novel Algorithms for the Generation and Correlation of Generalized Orthogonal Sequences*". In this chapter we propose a generalization of binary LS sequences to multilevel LS sequences, by applying the algorithms of Chapter 3 and a novel generation/correlation architecture for GPC sequences, by using the algorithm introduced in Chapter 4. Finally we show the theoretical link between LS and GPC sequences and this leads to the proposal of a novel and efficient generation and correlation algorithm for LS sequences. The proposals of this chapter have been published in the international journals Electronics Letters and IEEE Communications Letters.

- Chapter 6: *"Application to Ultra-Wideband Ranging Systems"*. In this chapter we present an indoor positioning system based on Ultra-Wideband which is used as a test-bed for the performance comparison of two spreading sequences, LS and Kasami sequences [Kasam 66]. The work derived from this chapter is being prepared for submission to the international journal Sensors & Actuators A: Physical.

- Chapter 7: *"Application to Ultrasonic Ranging Systems"*. In this chapter we use the GO sequences studied in the thesis in an ultrasonic indoor positioning system to

analyze the advantages and disadvantages of each spreading sequence and modulation scheme.

- Chapter 8: "*Conclusions and Future Works*". In this chapter we include the most significant conclusions derived from the contributions of this thesis; later we show the references to the publications in indexed international journals and international conferences derived from this thesis. Finally, we propose some research lines that could be tackled with these contributions.

# Chapter 2

# State of the Art and Problem Statement

## 2.1 Introduction

There are certain desirable properties in ranging and wireless communication systems as a large spectral and energy efficiency, immunity to interferences and low hardware complexity.

In the last years, ranging systems have benefited from the advances in the wireless communication field. In this way, among all the existent methods to carry out mechanisms for sharing the channel between users[1], the most used is Code-Division Multiple-Access (CDMA), also known as Spread Spectrum Multiple-Access (SSMA), where the channel division is carried out by means of spreading sequences with good correlation properties. Its main advantages in comparison with other multiple access schemes are its spectral efficiency, the capability of simultaneous access to the channel by the users and the processing gain that it provides [Fan 96]. This processing gain conferes a large robustness to Additive White Gaussian Noise (AWGN) and to narrowband interferences [Chen 07]. Nevertheless, the properties of the particular spreading sequence used for multiple access significantly affect to the system performance.

First, this chapter introduces the typical signal processing techniques used for ranging measurements. Later, we review the classical and the newest spreading sequences available in the literature; finally, we show the architectures traditionally used for the implementation of a matched filter.

[1] In this thesis the term "user" is adopted in a broad sense, referring to a sensor transmitting an assigned spreading sequence.

## 2.2 Signal Detection and Ranging Measurements

The problem of signal detection and ranging measurements dates from the mid-twentieth century and since then, there has been an intensive work to reduce the false alarm probability in the detection and ranging errors. In this section, we review a compendium of the most common signal processing techniques used for signal detection and ranging measurements.

### 2.2.1 Envelope Detection

This type of detection is used in applications where it is not needed high accuracies in ranging estimation. This kind of detection has been intensively used in ultrasound systems [Boren 88], where the envelope is obtained by rectifying the received signal and integrating it over the time. If the envelope exceeds a given threshold it is considered that the signal is present. In spite of being easy to implement, these systems have several drawbacks, and the main ones are the followings [Alvar 05]:

- Low immunity to noise: If there are interferences in the working frequency band it is possible to exceed the threshold regardless of not receiving the signal of interest.
- Low ranging accuracy: By using this method it is not possible to know the exact time instant in which the signal is received.
- Difficulty in working properly in multiuser environments: If the available bandwidth is reduced, a multiple access scheme, as Time Division Multiple-Access (TDMA) or Carrier Sense Multiple-Access (CSMA), in which only one device is transmitting at a given time is needed. This is because if the same frequency band is used for all the devices at the same time, there is no chance to distinguish the contribution to the envelope amplitude of each user.
- Low update rate: Due to the previous limitations, if TDMA or CSMA is used, the update rate falls as the number of users increase.

Nevertheless, this kind of receivers are still used in ranging applications due to its simplicity, as in low-cost UWB ranging systems [Lie 05].

### 2.2.2 Correlation and Matched Filter

Given a sequence of length $L$, $s[l] = \{s_0,\ s_1, \ldots,\ s_{L-1}\}$, a matched filter is a Finite Impulse Response (FIR) filter with an impulse response, $h[l]$, equal to the time reversed version of the sequence $s[l]$, i.e. $h[l] = s[-l]\,;\ s[-l] = \{s_{L-1},\ s_{L-2}, \ldots,\ s_0\}$. This filter maximises the SNR at its output in the presence of AWGN. Considering that $s[l]$ is a binary sequence, $s[l] \in \{+1,\ -1\}$, and that the received signal, $r[l]$ is equal to $r[l] = s[l] + n[l]$; where $n[l]$ is AWGN with a two-sided Power Spectral Density (PSD) equal to $\frac{N_0}{2}$ W/Hz, then the output of the matched filter is equal to:

$$\begin{aligned} o[l] &= r[l] \star h[l] \\ &= s[l] \star s[-l] + n[l] \star s[-l] \end{aligned} \tag{2.1}$$

where the symbol $\star$ refers to the convolution operation. The first term $s[l] \star s[-l]$ of the equation 2.1 is equal to the auto-correlation function of the sequence $s[l]$ and only depends on its properties. The second term $n[l] \star s[-l]$ of the equation 2.1, is equivalent to the cross-correlation of $n[l]$ and $s[l]$.

The maximum SNR is obtained at the output of the matched filter, at the zero time shift, when matching happens, and for binary sequences is equal to [Proak 00]:

$$SNR_{out_{max}} = \frac{2 \cdot L}{N_0} \tag{2.2}$$

Notice that the SNR at the output of the matched filter depends on the energy of the input sequence (in the binary case equal to $L$) and on the PSD of the AWGN noise ($N_0$), but not on the particular characteristics of the sequence [Proak 00].

Given two real and unitary[2] sequences of length $L$, $\{s_n[l],\ s_m[l]\}\,;\ 0 \leq l \leq L-1$, it is defined the periodic correlation function as

$$R_{s_n,s_m}[\tau] = \sum_{l=0}^{L-1} s_n[l] \cdot s_m[l+\tau] \tag{2.3}$$

when $n = m$, equation 2.3 turns out to be the periodic auto-correlation function, whereas if $n \neq m$, the equation 2.3 is the periodic cross-correlation function.

[2]This term is used to refer those sequences whose correlation properties depend solely on their inner characteristics.

The aperiodic correlation function is defined as

$$C_{s_n,s_m}[\tau] = \begin{cases} \sum_{l=0}^{L-1-\tau} s_n[l] \cdot s_m[l+\tau], & 0 \leq \tau \leq L-1 \\ \sum_{l=0}^{L-1+\tau} s_n[l-\tau] \cdot s_m[l], & 1-L \leq \tau < 0 \\ 0, & |\tau| \geq L \end{cases} \tag{2.4}$$

Equation 2.4 represents the aperiodic auto-correlation function when $n = m$, and the aperiodic cross-correlation function when $n \neq m$. Notice that independently of the correlation function applied, aperiodic or periodic auto-correlation, the maximum SNR at the correlator output is given by the equation 2.2. Figure 2.1 depicts the periodic and aperiodic correlation function of the sequence $s[l] = \{+1, +1, +1, -1\}$. Notice the differences between aperiodic and periodic correlation functions: in the periodic correlation function no gaps between the periods of the sequence $s[l]$ is considered; in the aperiodic correlation function, different periods of the sequence $s[l]$ do not overlap in the correlation process. This is what happens in bursting transmissions, typically used in wireless sensor networks, ultrasound and UWB ranging systems. The sequence $s[l]$ is called in the literature as a *perfect binary sequence*, as its periodic auto-correlation function is ideal. Nevertheless, its aperiodic auto-correlation function is far from being ideal. For this reason, the term *perfect sequence* is normally referred to those with an ideal periodic correlation function.

In this thesis, we will use by default aperiodic correlation functions.

### 2.2.3 Generalized Matched Filters

As was shown previously, matched filters are optimum in the sense that maximize the SNR at their output when the noise is AWGN. In the presence of coloured noise, this is not true, and the matched filter can be preceded by a weight function (also known as pre-whitening filter). This filter in cascade with the matched filter is commonly named as generalized matched filter or Generalized Cross-Correlation (GCC) function [Knapp 76] and it has found applications to ranging estimation [Villa 11]. Nevertheless, in practice the GCC tends to an error-prone range estimation, especially at low SNR.

### 2.2.4 Mismatched Filters

In the last decades, mismatched filters have been broadly used in the radar field to sidelobe suppression [Ackro 73, Levan 04]. There are mainly two approaches in the sidelobe

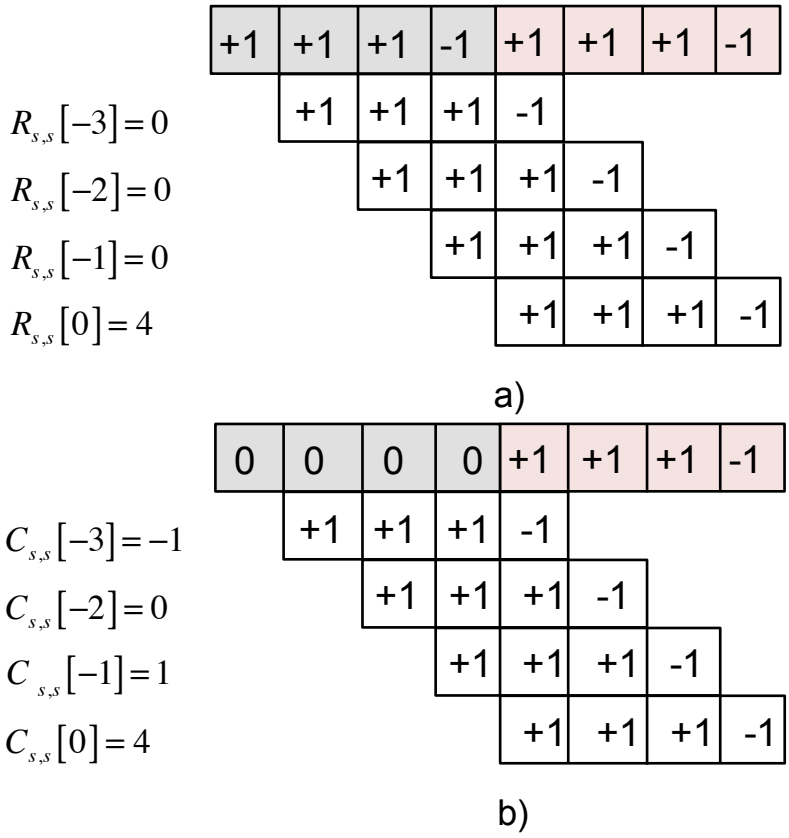


Figure 2.1: a) Periodic correlation of the perfect sequence $\{+1, +1, +1, -1\}$, b) Aperiodic correlation

suppression with mismatched filters: the first one consists on the use of a mismatched filter alone [Griep 95, Levan 05] and the second one uses a mismatched filter in cascade with a matched filter [Rihac 71, Schol 00]. Both introduce a SNR loss and are commonly designed as a FIR filter. The coefficients of this filter are computed by means of an optimization algorithm, as Least Squares or Iteratively Reweighted Least Squares (IRLS) [Green 84].

This algorithm has been also extended to cope with multiuser environments [Griep 95] or Doppler shifts [Zejak 91] and normally tries to minimize the Integrated Sidelobe Levels (ISL) or the Peak Sidelobe Levels (PSL), (which is computationally much more demanding) of the correlation function.

We will review the algorithm introduced in [Griep 95, Levan 05] to compute the filter coefficients that minimizes the ISL metric, considering only here the case of only one user. Define the real-valued sequence $s[l]$ of length $L_1$, which expressed in a vectorial form, is $\mathbf{s} = [\ s[0] \quad s[1] \quad \dots \quad s[L_1 - 1]\ ]^T$ and the mismatched filter coefficients $h[\ell]$ of length $L_2$

in a vectorial form $\mathbf{h} = [\ h[0] \quad h[1] \quad \dots \quad h[L_2-1]\ ]^T$. The correlation operation can be expressed in a matricial form as $\mathbf{y} = \mathbf{h} \times \mathbf{S}$, where $\mathbf{y}$ represents the output of the correlation operation with length $\mathcal{L} = (L_1 + L_2 - 1)$, the symbol $\times$ is the matricial product and $\mathbf{S}$ is the Toeplitz matrix of the sequence $\mathbf{s}$ of dimensions $L_2 \times \mathcal{L}$ and it is defined as

$$\mathbf{S} = \begin{bmatrix} s[L_1-1] & \dots & s[1] & s[0] & 0 & \cdots & 0 \\ 0 & s[L_1-1] & \dots & s[1] & \ddots & & \vdots \\ \vdots & \ddots & \ddots & & \ddots & s[0] & 0 \\ 0 & \cdots & 0 & s[L_1-1] & \dots & s[1] & s[0] \end{bmatrix} \tag{2.5}$$

Define now a square weighting diagonal matrix $\mathbf{F}$ of order $\mathcal{L}$, with a diagonal equal to

$$diag(\mathbf{F}) = \begin{bmatrix} f^2[-\mathcal{L}+1] & \dots & f^2[0] & \dots & f^2[\mathcal{L}-1] \end{bmatrix} \tag{2.6}$$

where $\mathbf{f}$ is a vector whose entries have an arbitrary weight. If $f[0] = 0$, the total energy of the sidelobes of $\mathbf{y}$ can be defined as

$$\begin{aligned} E &= \mathbf{y} \times \mathbf{F} \times \mathbf{y}^T \\ &= \mathbf{h} \times (\mathbf{S} \times \mathbf{F} \times \mathbf{S}^T) \times \mathbf{h}^T \\ &= \mathbf{h} \times \mathbf{A} \times \mathbf{h}^T \end{aligned} \tag{2.7}$$

The vector $\mathbf{h}$ that minimizes the sidelobes energy is equal to

$$\mathbf{h} = \frac{\mathbf{s} \times \mathbf{A}^{-1} \times \left(\mathbf{s} \times \mathbf{s}^T\right)}{\mathbf{s} \times \mathbf{A}^{-1} \times \mathbf{s}^T} \tag{2.8}$$

with the constraints that the matrix $\mathbf{A}$ is not singular and that $\mathbf{s} \times \mathbf{h}^T = \mathbf{s} \times \mathbf{s}^T$, i.e. the filter $\mathbf{h}$ is normalized to have the same response at zero time shift as the matched filter.

Nonetheless, without the normalization of the filter $\mathbf{h}$, the SNR loss introduced by the mismatched filter is computed as

$$SNR_{loss} = \frac{\varepsilon^2}{C_p^2} \tag{2.9}$$

where $\varepsilon$ is the maximum output of the mismatched filter at zero time shift and $C_p$ is the correlation peak of the received signal. Figure 2.2 depicts the output of a matched filter when a zero-padded Barker sequence of length 13 is received and Figure 2.3 shows the

output of a mismatched filter, whose real-valued coefficients are obtained by means of the Least Squares algorithm for minimizing the ISL. Finally, Figure 2.4 shows the coefficients of the mismatched filter, which are real-valued coefficients.

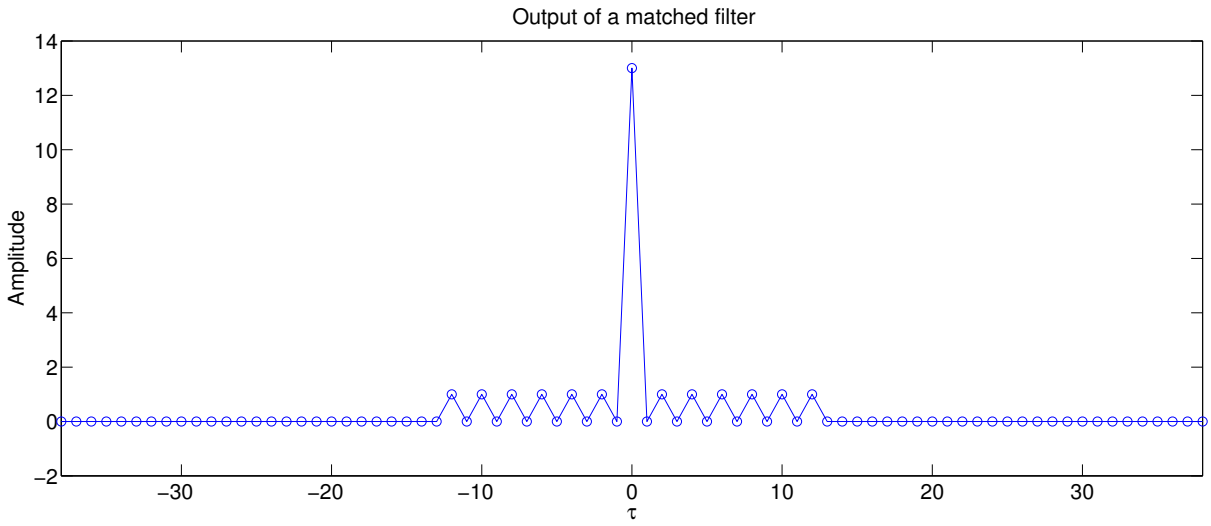


Figure 2.2: Output of a matched filter when a zero-padded Barker sequence of length 13 is received and the template signal is itself.

### 2.2.5 Coherent/Non-Coherent Detection

Coherent receivers use complex systems for phase and frequency estimation of the emitter Local Oscillator (LO) and thus adjust the receiver LO for their synchronization. Later, the demodulation process is done by multiplying the received signal by the LO. This process (ideally) does not generate Inter-symbol Interference (ISI) and the signal detection is known as coherent detection. On the contrary, non-coherent receivers, easier to implement than the coherent ones, recover neither the phase nor the frequency of the transmitter oscillator. In the case of using matched filters for signal detection, the demodulation process is done by correlating the received signal with the carrier symbol [Proak 00]; this results in ISI, even in the case of an ideal channel, as the auto-correlation of the band-limited symbol is not a Kronecker delta. The demodulated signal should pass through a matched filter in order to carry out the signal detection. In non-coherent demodulation schemes ISI appears as correlation sidelobes, which degrade the SNR of the system. Figure 2.5 shows the aperiodic auto-correlation of a CDMA signal when the signal pass through a root-raised cosine filter and is coherently demodulated; Figure 2.6 depicts the auto-correlation

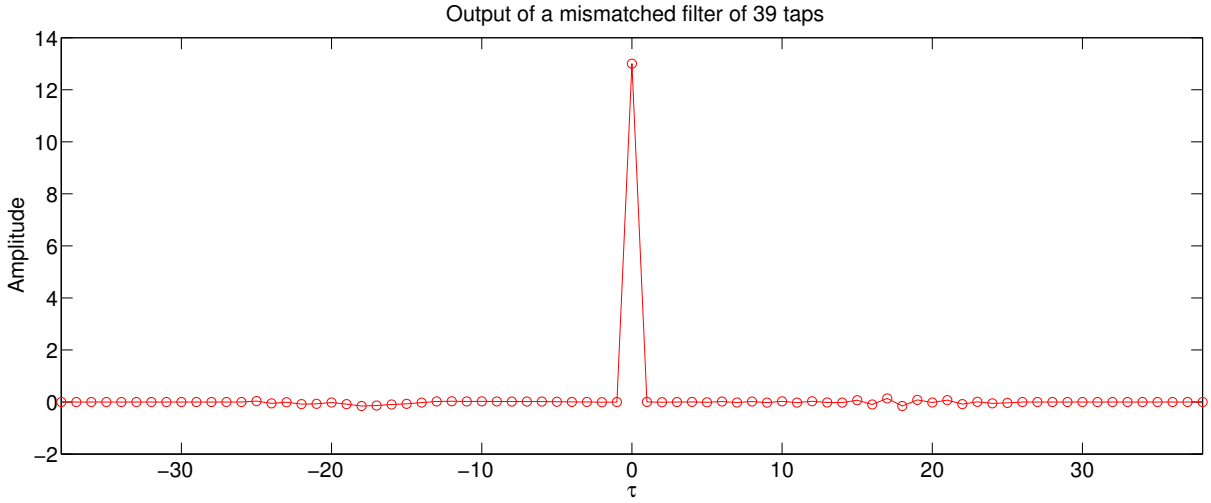


Figure 2.3: Output of a mismatched filter of 39 taps when the received signal is a zero-padded Barker sequence of length 13.

of the same CDMA signal with non-coherent demodulation. As depicted, the degradation in the auto-correlation of Figure 2.6 is due to ISI generated in the demodulation process.

Possible solutions for reducing correlation sidelobes due to non-coherent demodulation is the use of carrier symbols with reduced correlation sidelobes and a controlled spectrum, as repeating Barker codes [Pinke 92], the use of equalizers at the output of the matched filter [Johns 98], or the use of differential modulation/demodulation schemes [Proak 00].

## 2.3 Benefits of Coding and Spreading Sequences

Additionally to the maximization of the SNR at the output of a matched filter in AWGN channels, the use of coding conferes a SNR gain at its output. This is also known as processing gain and it is derived briefly in this section. The SNR gain, $SNRG$, due to coding is defined as the relation between the SNR at the output of the matched filter, $SNR_{out}$, and the SNR at the input, $SNR_{in}$. Mathematically it is expressed as

$$SNRG = \frac{SNR_{out}}{SNR_{in}} \tag{2.10}$$

For narrowband signals, the SNR at the output of the matched filter, $SNR_{out}$, is equal to $SNR_{out} = \frac{SNR_{out_{max}}}{2}$. This is due to the fact that the average power at any time instance is approximately half the instantaneous peak power at the same time instance [Misar 05]. The $SNR_{in}$ is expressed as $SNR_{in} = \frac{P_{in}}{N_0 \cdot B}$, where $B$ is the signal bandwidth, $P_{in} = \frac{L}{T_d}$ is

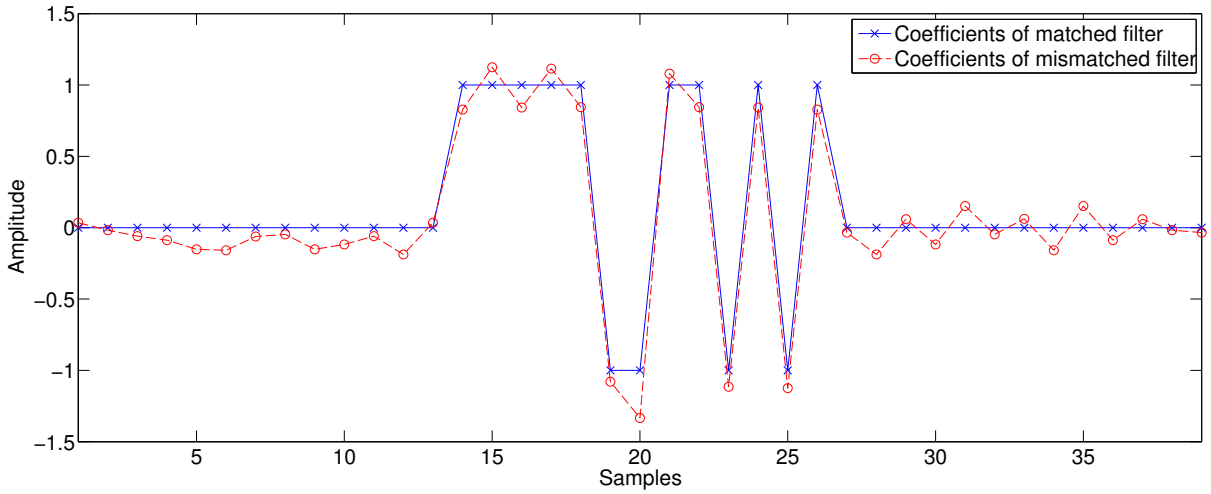


Figure 2.4: Comparison of the coefficients of the matched and mismatched filter. The coefficients of the matched filter are a zero-padded Barker sequence of length 13.

the average power of the input signal, $L$ is the sequence length, $T_d = L \cdot T_s$ is the signal duration and $T_s$ is the symbol duration. So the $SNRG$ can be expressed as

$$SNRG = \frac{\frac{\frac{2 \cdot L}{N_0}}{2}}{\frac{P_{in}}{N_0 \cdot B}} = \frac{\frac{P_{in} \cdot T_d}{N_0}}{\frac{P_{in}}{N_0 \cdot B}} = B \cdot T_d \tag{2.11}$$

Therefore, the SNR gain can be expressed as $SNRG = B \cdot L \cdot T_s$, which is approximately equal to $SNRG = L$ as $\frac{1}{T_s} \cong B$. The $SNRG$ is also known as processing gain and normally it is expressed in decibels.

Note that for systems in which the users transmit pair of sequences (each one of length $L$), in the receiver it is performed the sum of correlation (so the sequences are not unitary) and consequently, the auto-correlation at zero time shift ($\tau = 0$) is equal to $2 \cdot L$. Therefore, the SNR gain for those systems will be $SNRG = 2 \cdot L$. This gain gives large robustness to noise and to narrowband interferences [Chen 07].

In [Garci 11] a comparison of the link budget between a coded and a non-coded ultrasonic ranging system is presented. It is demonstrated that the use of spreading codes in an ultrasonic LPS gives the same maximum range distance as a low bandwidth non-coded ultrasonic LPS system, but with the feasibility of accurate ranging. Unfortunately, there is no free lunch and the use of spreading sequences implies several challenges and trade-offs in ranging systems:

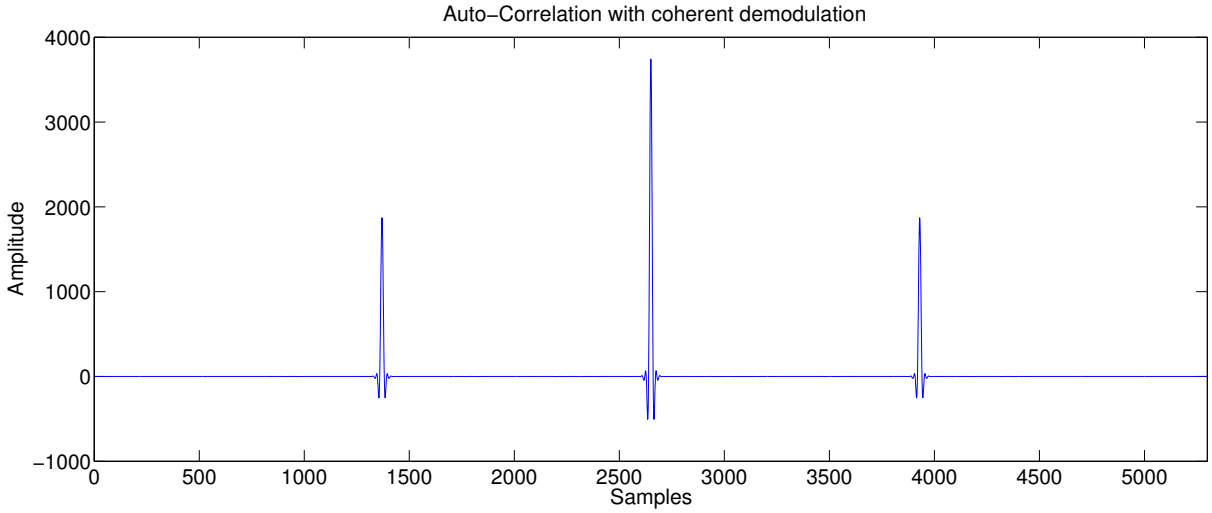


Figure 2.5: Auto-correlation of a CDMA signal with coherent demodulation and a root-raised cosine filter.

- The processing gain, which is proportional to the sequence length, $L$, is restricted by the maximum allowable emission time and hardware capabilities. Larger sequences imply larger hardware requirements on the receiver side and larger emission times, which depending on the relative velocity emitter-receiver, can be prohibitively large due to Doppler shifts [Pared 11].

- In asynchronous CDMA multiuser ranging systems, where $K$ users transmit simultaneously, near-far effect is a major issue. This effect occurs when the signal of an user impinges the receiver close to it with a larger energy than the one of other users. As a consequence, weaker signals from users further away cannot be detected because their auto-correlation functions will be masked by the sidelobe peaks caused by the signal with more energy. In CDMA satellite communication systems they commonly use power-controlled emissions in order to receive a similar energy from all the users. On the receiver side, there are several techniques to cope with the near-far effect, such as the use of Successive Interference Cancellation (SIC) [Viter 02]. The SIC method consists on subtracting from the received signals the emitted ones as they are being detected, improving the detection of the other emitters. Power control approach is complex, expensive and leads to bulky solutions. SIC approach introduces a large complexity in the receiver side and has a limited performance at low SNR. Another solution is the use of time multiplexing, i.e. TDMA. Unfortunately this solution implies emission times more than $K$ times longer than those required with

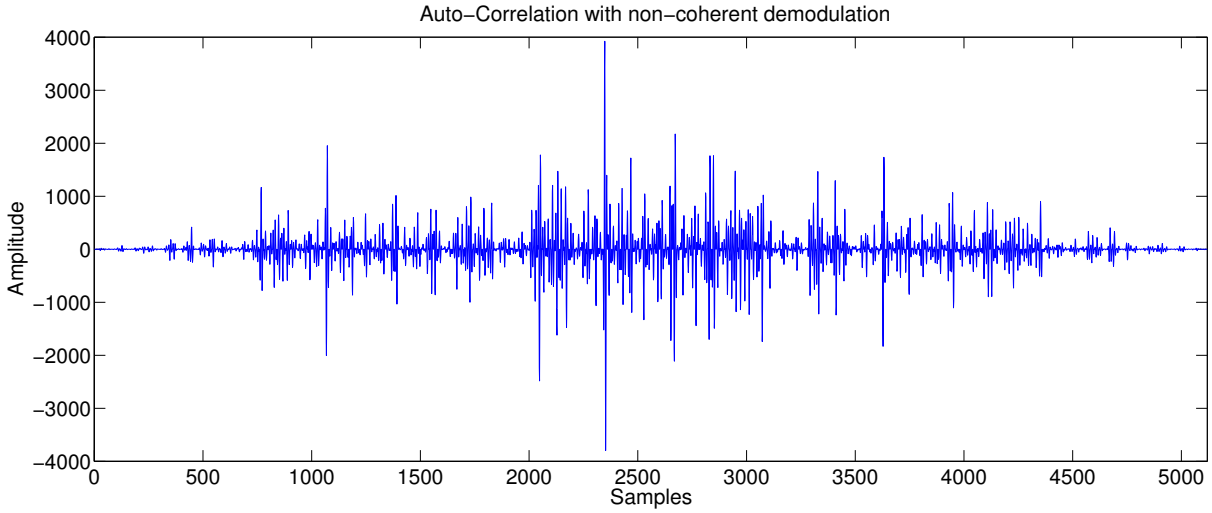


Figure 2.6: Auto-correlation of a CDMA signal with non-coherent demodulation.

CDMA. Again, this can be unfeasible due to Doppler shifts, especially in ultrasound ranging systems. Finally, the use of Frequency Division Multiple-Access (FDMA), resolves the near-far effect at the expense of requiring a larger bandwidth.

In general terms, spread spectrum sequences can be classified as shown in Figure 2.7, where polyphase, real and binary sequences are distinguished. The most used polyphase sequences are the so-called Constant Amplitude Zero Auto-Correlation (CAZAC) sequences and in second place Huffman sequences. CAZAC sequences are polyphase sequences with an ideal periodic auto-correlation and unitary magnitude, i.e. constant envelope, and for this reason, they are commonly used as a preamble for synchronization of mobile devices. Nevertheless, CAZAC sequences have favourable aperiodic correlation functions for their use in asynchronous radar systems [Frank 63, Krets 88]. Among the CAZAC sequences with good aperiodic correlation functions, can be mentioned Frank sequences [Frank 62] and its variations P1, P2 [Lewis 81] and P3, P4 [Lewis 82] as well as Zadoff-Chu sequences [Chu 72], which have been recently proposed for their use in Long Term Evolution (LTE) communication systems.

In what follows, we review the spreading sequences represented in Figure 2.7, with the exception of polyphase sequences, whose analysis and optimization are beyond the scope of this thesis. Additionally, in order to make this chapter more readable, Chaotic sequences and Pseudo-Noise (PN) sequences are reviewed in Appendix A.

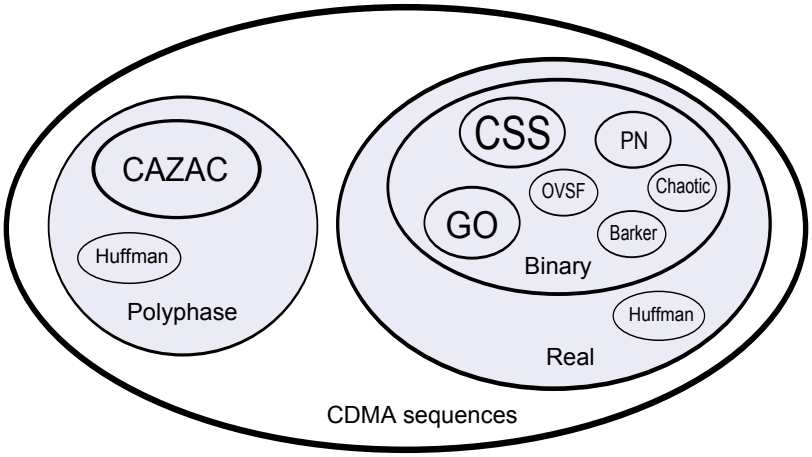


Figure 2.7: General classification of CDMA sequences.

### 2.3.1 Walsh-Hadamard Sequences

Walsh-Hadamard sequences, also known as Orthogonal Variable Spreading Factor (OVSF) sequences are orthogonal sequences with applications in synchronous CDMA systems and used intensively as a basic building block for the generation of Generalized Orthogonal (GO) sequences. These sequences are the rows or columns of a Hadamard matrix[3] [Seber 92], which can be generated from any construction method, as the one proposed by J. J. Sylvester [Sylve 67]. By using the previous method, a Hadamard matrix $\boldsymbol{\mathcal{H}}_{2^a}$ of order $2^a$, $a \in \mathbb{N}$, can be generated recursively as follows:

$$\boldsymbol{\mathcal{H}}_1 = [1]\,;\, \boldsymbol{\mathcal{H}}_{2^{\Psi+1}} = \begin{bmatrix} \boldsymbol{\mathcal{H}}_{2^\Psi} & \boldsymbol{\mathcal{H}}_{2^\Psi} \\ \boldsymbol{\mathcal{H}}_{2^\Psi} & -\boldsymbol{\mathcal{H}}_{2^\Psi} \end{bmatrix}; \Psi \in \{0, 1, \ldots, a-1\} \tag{2.12}$$

For instance, if $a = 2$, the resultant Hadamard matrix, $\boldsymbol{\mathcal{H}}_4$ is equal to

$$\boldsymbol{\mathcal{H}}_4 = \begin{bmatrix} +1 & +1 & +1 & +1 \\ +1 & -1 & +1 & -1 \\ +1 & +1 & -1 & -1 \\ +1 & -1 & -1 & +1 \end{bmatrix}$$

[3] A $K \times K$ matrix $\boldsymbol{\mathcal{H}}_K$ with entries $\pm 1$ is a Hadamard matrix if $\boldsymbol{\mathcal{H}}_K^T \times \boldsymbol{\mathcal{H}}_K = K \cdot \mathbf{I}_K$.

where the rows or columns of the matrix $\boldsymbol{\mathcal{H}}_4$ are mutually orthogonal and they represents Walsh-Hadamard sequences.

### 2.3.2 Barker Sequences

A binary sequence, $s\,[l]$ of length $L_{|Barker}$ is a Barker sequence if the absolute value of the sidelobes of its aperiodic auto-correlation are lower than one. Expressed mathematically leads to the expression

$$\left| \sum_{l=0}^{L_{|Barker}-\tau-1} s\,[l] \cdot s\,[l+\tau] \right| \leq 1;\ \tau \neq 0 \tag{2.13}$$

Barker sequences have very good aperiodic auto-correlation functions. In fact, the Barker sequence of length 13 has the largest merit factor known [Jedwa 04]. Unfortunately, the known number of Barker sequences is very limited, reducing their use to sonar, medical ultrasound imaging applications with low processing gain requirements [Pinke 92, Zhao 07] and to channel estimation in the IEEE 802.11.b standard [IEEE 99]. There are strong evidences that other binary Barker sequences than those represented in Table 2.1 do not exist [Turyn 61, Turyn 67].

| Length $L_{\|Barker}$ | Barker Sequence |
|---|---|
| 2 | $\{+1\ +1\}$ |
| 3 | $\{+1\ +1\ -1\}$ |
| 4 | $\{+1\ +1\ +1\ -1\}; \{+1\ +1\ -1\ +1\}$ |
| 5 | $\{+1\ +1\ +1\ -1\ +1\}$ |
| 7 | $\{+1\ +1\ +1\ -1\ -1\ +1\ -1\}$ |
| 11 | $\{+1\ +1\ +1\ -1\ -1\ -1\ +1\ -1\ -1\ +1\ -1\}$ |
| 13 | $\{+1\ +1\ +1\ +1\ +1\ -1\ -1\ +1\ +1\ -1, +1\ -1\ +1\}$ |

Table 2.1: Barker sequences known up-to-date.

### 2.3.3 Huffman Sequences

Huffman sequences were proposed in 1962 [Huffm 62] as real/complex sequences with near perfect aperiodic auto-correlation functions. For this reason they are also known as impulse-equivalent pulse trains, as they almost have a Kronecker delta auto-correlation function. Obviously, the energy of Huffman sequences are not distributed in only one

pulse as a Kronecker delta, but they do not have an uniform envelope [White 77]. Given a polynomial with $R$ roots expressed in the $Z$-domain as shown in equation 2.14, it represents a Huffman sequence if its roots are chosen so that they are uniformly distributed in the complex plane (i.e. at equal angular intervals), with each of the zeros located either in a circle of radius $A$ or one of radius $A^{-1}$ [Huffm 62]. In order to obtain real Huffman sequences, the zeros of the polynomial must appear in conjugate pairs, in other cases they will be polyphase [Ackro 72].

$$S\left(z^{-1}\right) = s_0 + s_1 \cdot z^{-1} + \cdots + s_R \cdot z^{-R} \tag{2.14}$$

Following the previous rule, there are $2^R$ zero patterns and consequently, $K_{|Huffman} = 2^R$ Huffman sequences, $s_k[l]$, $0 \leq k \leq 2^R - 1$ of length $L_{|Huffman} = R + 1$, $0 \leq l \leq R$, that have a near perfect aperiodic auto-correlation, defined as depicted in equation 2.15.

$$C_{s_k,\, s_k}[\tau] = \sum_{l=0}^{L_{|Huffman}-1-\tau} s_k[l] \cdot s_k[l+\tau] = \begin{cases} P_0, & \text{for } \tau = 0 \\ 0 & \text{for } 1 \leq |\tau| \leq R-1 \\ \frac{P_0 \cdot A^{-R}}{1-A^{-2 \cdot R}} & \text{for } |\tau| = R \end{cases} \tag{2.15}$$

where $P_0$ is the energy of the Huffman sequence.

Nevertheless, each of the zero pattern of the polynomial $S(z^{-1})$, results in Huffman sequences with a different ambiguity function[4] distribution in the time-frequency plane and with a different energy efficiency [Ackro 70, Ackro 72]. Figure 2.8 shows the auto-correlation of a real Huffman sequence, which is depicted in Figure 2.9.

### 2.3.4 Golay Binary Pairs and Complementary Sets of Sequences

In 1961, M. Golay analyzed pairs of binary sequences whose Sum of Aperiodic Auto-correlation Functions (SACF) is a Kronecker delta and their Sum of Aperiodic Cross-correlation Functions (SCCF) is zero for all time shifts $\tau$ [Golay 61]. These sequences are currently known as Golay binary sequences pairs.

He gave non-recursive algorithms for the generation of Golay pairs of length $2 \cdot L_1$, by interleaving, and lengths $2 \cdot L_1 \cdot L_2$ by concatenating Golay pairs of lengths $L_1$ and $L_2$;

[4]Represents the time-frequency plane formed by the output of a matched filter for different Doppler displacements [Woodw 53].

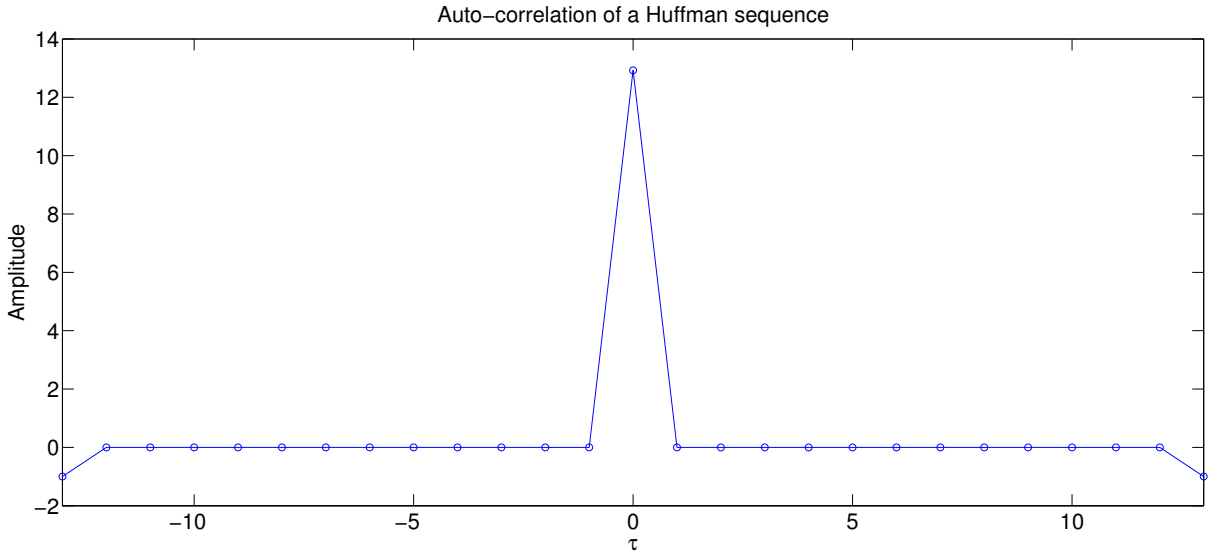


Figure 2.8: Auto-correlation function of a Huffman sequence.

and found operations of equivalence between sequence pairs. M. Golay also found pairs that cannot be generated from the proposed algorithms (the so-called Golay kernels) of lengths 10 [Golay 61] and 26 [Golay 62] (also called as Golay kernels 10 and 26). Later in [Jaure 62], Jauregui found by means of an exhaustive computer search that there are no more non-equivalent kernels of length 26 that the one found by Golay using a "by hand technique". More recently, Borwein and Ferguson reported the existence of the Golay kernel of length 20 [Borwe 03].

In 1974, Turyn proposed a non-recursive algorithm to generate Golay pairs of lengths $L_{|Gol} = 2^N \cdot 10^M \cdot 26^P$ where $N$ , $M$ and $P$ are non-negative integers, by combining the Golay kernels [Turyn 74]. There is still unknown Golay binary pairs of different lengths from $L_{|Gol} = 2^N \cdot 10^M \cdot 26^P$.

In 1972, Tseng and Liu expanded Golay pairs to binary Complementary Sets of Sequences (CSS) [Tseng 72]. They proposed to increase the number of sequences in the set from two (in the case of Golay binary pairs) to $K_{|CSS} = 2^k$, where $k \in \mathbb{N} - \{0\}$.

A set of $K_{|CSS}$ sequences $s_{j,i}[l]\,;\, 0 \leq j, i \leq K_{|CSS} - 1$ of length $L_{|CSS}$ whose SACF is a Kronecker delta is called a CSS. Mathematically is expressed as

$$\sum_{i=0}^{K_{|CSS}-1} C_{s_{j,i}}[\tau] = \eta \cdot \delta[\tau]\,;\; 0 \leq j \leq K_{|CSS} - 1;\; \eta \in \mathbb{R} - \{0\} \tag{2.16}$$

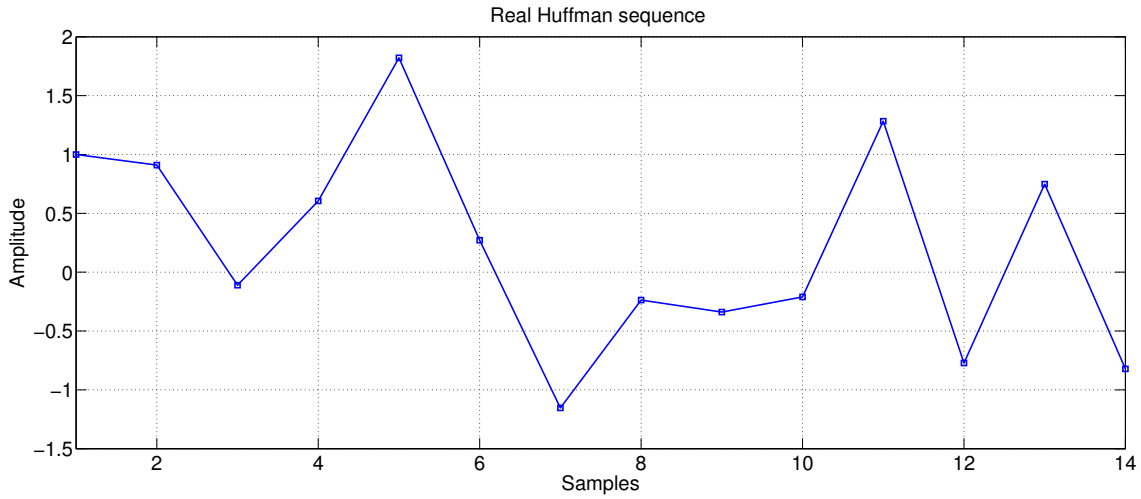


Figure 2.9: Real Huffman sequence of 14 bits.

Notice that if $K_{|CSS} = 2$, the CSS is equal to a Golay binary pair. Furthermore, $T_{|CSS} = K_{|CSS}$ CSS are called uncorrelated CSS if their SCCF is zero for all shifts $\tau$. This can be expressed as

$$\sum_{i=0}^{K_{|CSS}-1} C_{s_{j,i},s_{j',i}}[\tau] = 0;\ \forall\tau;\ 0 \leq j \neq j' \leq T_{|CSS} - 1 \tag{2.17}$$

Nowadays, due to the ideal SACF and SCCF of Golay binary sequence pairs and of their generalization, CSS, they are used as a basic building block for the generation of many other sequences for Quasi-Synchronous CDMA (QS-CDMA) systems, as depicted in Figure 2.10.

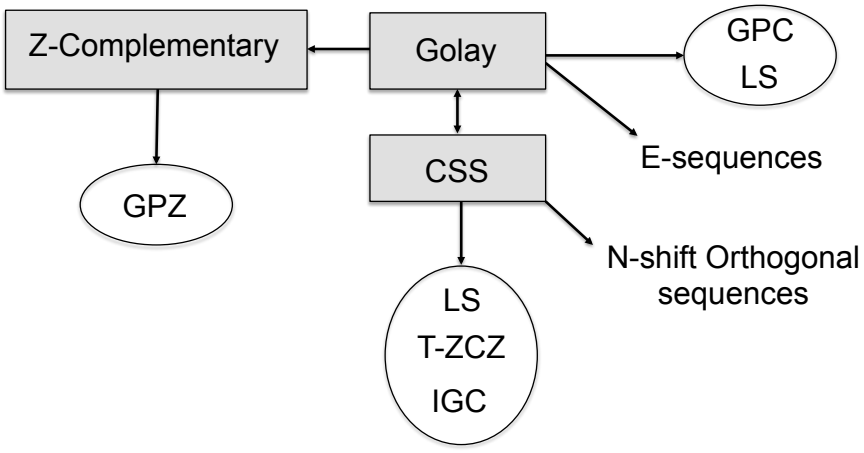


Figure 2.10: Block diagram of CSS derived sequences.

Since 1961, the number of applications found for Golay binary pairs and CSS go from MIMO radar [Li 10], Non-Destructive Test (NDT) applications [White 92], low Peak-to-Average Power Ratio (PAPR) OFDM communication systems [Davis 99], or the second digital terrestrial television broadcasting standard (DVB-T2) [He 11]. The intensive research work done since 1961 produces that a large amount of terminologies exist in the literature. To avoid confusions, Figure 2.11 includes the basic terminology used for different subclasses of complementary sequences. In [Suehi 88] the term of Complete Complementary (CC) sequences was introduced to define a set of $K_{|CC} = 2^k$; $k \in \mathbb{N} - \{0\}$ sequences of length $L_{|CC} = K_{|CC}^2$ whose SACF is a Kronecker delta and their SCCF is zero for all shifts $\tau$. Notice that these sequences have the same correlation properties as the uncorrelated CSS. Additionally, some authors [Chen 01, Perez 08] use the term orthogonal CSS to designate those sequences whose SCCF holds the equation 2.17. This thesis uses the notation of [Fan 96] and [Perez 09a] instead, and reserves the term orthogonal CSS for those complementary sets of sequences whose SCCF is only zero at $\tau = 0$ (i.e. the sum of dot products is zero). This is an important clarification as it is known that the maximum number of uncorrelated CSS[5] is equal to $T_{|CSS} = K_{|CSS}$ while for orthogonal CSS, the number of sets is limited by the expression $T_{|CSS} \leq K_{|CSS} \cdot L_{|CSS}$ [chapter 13, Fan 96].

Later, H.-H. Chen introduced the term Perfect Complementary (PC) sequences [Chen 04]. These sequences are uncorrelated CSS, generated from an algebraic approach that can take into account the real scenario in the sequence design, as multipath effect or MAI.

Budišin coined the term of supercomplementary sequences to define a special class of complex complementary sequences with a good ambiguity function [Budis 87]. Later, Sivaswamy introduced a set of composite signals generated from complementary sequences and called subcomplementary sets of sequences. The sum of the aperiodic correlation functions of these sequences has a zone with low correlation sidelobes and a good ambiguity function [Sivas 78a, Sivas 82]. Later, Popović and Budišin generalized this generation algorithm, calling the new sequences generalized subcomplementary sequences [Popov 87]. In the last years these types of sequences are known as Low Zero Correlation Zone (LCZ) sequences instead of being considered as a subclass of complementary sequences [Tang 01b]. Both kind of sequences, subcomplementary and generalized sub-

[5]In what follows, for CSS we will use equivalently $T_{|CSS}$ and $K_{|CSS}$ by using the expression $K_{|CSS}-$CSS to refer $K_{|CSS}$ uncorrelated CSS of $K_{|CSS}$ sequences.

complementary, are not strictly complementary sequences and they should be considered as a type of GO sequences.

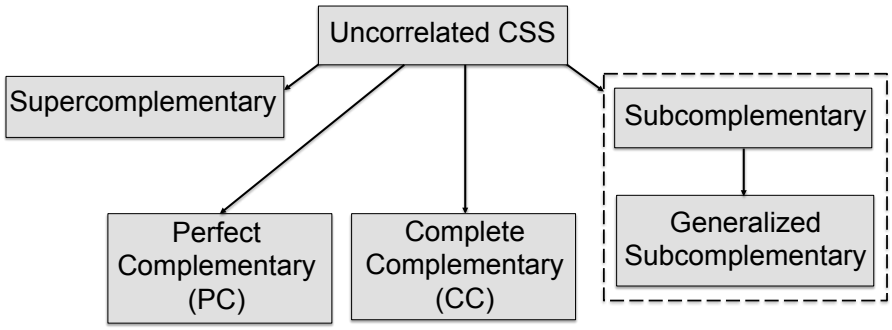


Figure 2.11: Different subclasses of complementary sequences.

M. Darnell expanded the concept of CSS to the multilevel alphabet, proposing a non-recursive algorithm to generate multilevel CSS without limitations in the length of sequences or in the number of sequences in the set [Darne 88, Kemp 89]. Later, Budišin proposed a recursive algorithm for the generation of a pair of multilevel complementary of sequences [Budis 90b]. Sivaswamy [Sivas 78b] and Frank [Frank 80] carried out a similar generalization to the polyphase alphabet.

### 2.3.5 Generalized Orthogonal Sequences

In synchronous CDMA systems, sequences with an orthogonal behaviour (i.e. cross-correlation is zero for the time shift $\tau = 0$) between sequences of the family set, as Walsh-Hadamard sequences (or OVSF sequences) are used. Nevertheless, in practice for loosely synchronous systems, where receivers and emitters are not strictly synchronized, the cross-correlation is not zero for $\tau = 0$. Independently of the synchronization accuracy, multipath provokes the received signal to contain multiple, delayed and attenuated copies of the transmitted signal; so the orthogonality between received and transmitted signal is affected.

Therefore, the ideal solution would be to find sequences with ideal auto-correlation and cross-correlation functions. They would allow to work in a completely asynchronous manner, independently of the relative delays among users and mitigating ISI and Multiple-Access Interferences (MAI). Nevertheless, these ideal sequences do not exist [Welch 74, Leven 99, Sarwa 79], so when ISI is mitigated by reducing the auto-correlation sidelobes, MAI increases, worsening the cross-correlation function and viceversa. Traditionally, in CDMA systems, sequences with good (but not ideal) aperiodic correlation properties

as Kasami sequences have been used. In contrast to mobile communication systems, a large majority of Local Positioning Systems (LPS) do not use power-controlled emissions to receive an equal amount of signal energy from each emitter. This implies that with conventional sequences, the system is severely affected by near-far effect. Therefore, positioning with a low level of errors is only feasible in those positions where the energy of received signals from each beacon is equal.

Although CSS have ideal sums of aperiodic correlation functions, they increase the complexity of the transmission scheme, as each user has to transmit a set of sequences. Furthermore, the emission time depends on the number of users as the number of sequences in a CSS set increase with the number of users. The typical transmission scheme in communication systems is Multi-Carrier CDMA (MC-CDMA), using a carrier frequency for each sequence of the set [Tseng 00]. In narrowband ranging systems, for the case of $K_{|CSS} = 2$ CCS, the use of quadrature modulation schemes as QPSK is common [Herna 04], whereas for larger complementary sets, transmissions schemes based on the concatenation or interleaving of the set of sequences is used [Alvar 06], worsening in this way the correlation properties of the CSS [De Ma 06].

For this reason, in the last years the interest for QS-CDMA systems have boosted [Suehi 94, Fan 03, Li 03]. These systems use Generalized Orthogonal (GO) or Generalized Quasi-Orthogonal (GQO) sequences. GO sequences have a Zero Correlation Zone (ZCZ) $W_{ZCZ}$ in the vicinity of the correlation time shift $\tau = 0$, or equivalently an Interference Free Window (IFW), where IFW $= 2 \cdot W_{ZCZ} + 1$, i.e. the double-sided ZCZ, due to the symmetric properties of the correlation functions. GQO sequences, instead of having a ZCZ, have a Low Correlation Zone (LCZ) next to the time shift $\tau = 0$ where the amplitude of the correlation sidelobes are limited to a certain value.

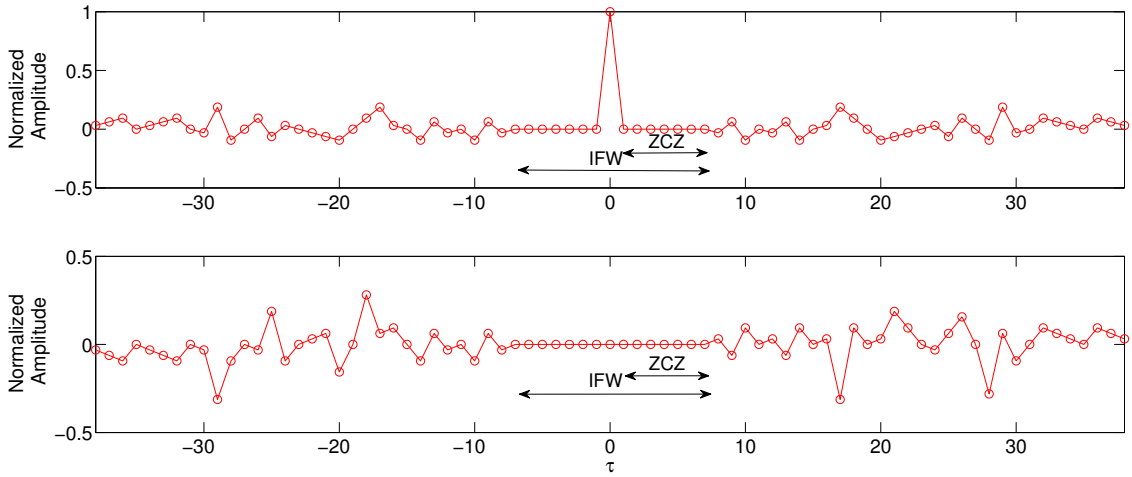


Figure 2.12: Normalized aperiodic correlation functions of a class of GO sequence.

Figure 2.12 depicts the aperiodic correlation functions of a GO sequence with the IFW and ZCZ marked to differentiate both zones. Notice that the correlation sidelobes outside of the IFW are larger than some non-GO sequences as PN sequences. For this reason, it is important to ensure that the maximum delay between users is lower than $W_{ZCZ}$ and to limit the zone of interest to the IFW.

GO sequences are sub-optimum solutions because of the unfeasibility to generate unitary sequences with ideal aperiodic correlation functions. Figure 2.13 shows a classification of GO sequences which will be introduced in the following sections.

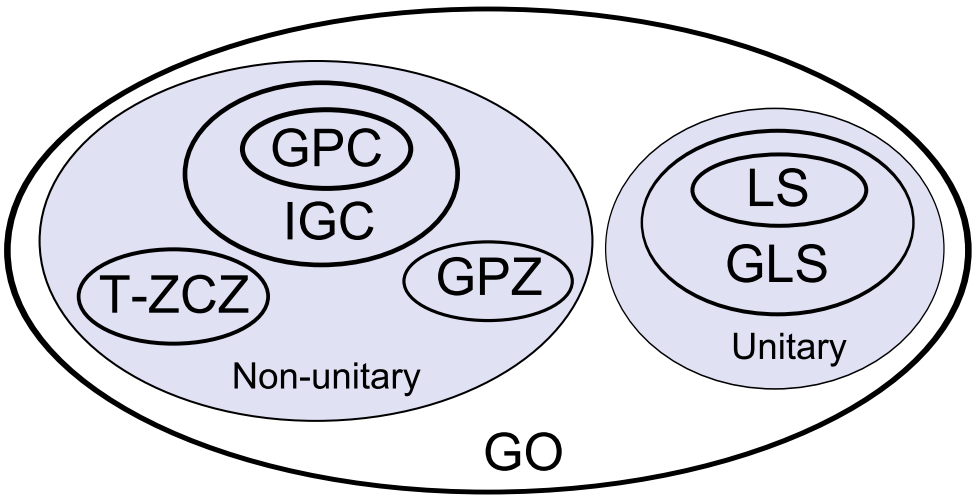


Figure 2.13: General classification of GO sequences.

### Z-Complementary Sequences

Fan *et al.* propose Z-Complementary sequences [Fan 07], as a generalization of the Golay binary sequence pairs to cope with their limitation in length. As shown previously, the lengths of the Golay binary sequences pairs, $L_{|Gol}$, are limited to $L_{|Gol} = 2^N \cdot 10^M \cdot 26^P$, being $N$, $M$ and $P$ non-negative integers [Golay 61, Borwe 03]. The limitation in length of Golay binary sequences pairs as well as the reduced number of uncorrelated pairs (also known as mates) make difficult their use in practice. Nevertheless, they are commonly considered as a building block for the generation of GO sequences [Stanc 01, Chen 06, Zhang 04]. Consequently, the former limitations of Golay binary sequence pairs are also applicable to GO sequences derived from them.

For this reason, Fan *et al.* propose a generation algorithm of complementary sequences with sub-optimum aperiodic correlation properties (i.e. with ZCZ) [Fan 07], so the limitation in length is relaxed and the number of sequences available is enlarged.

The same generation algorithms and equivalence rules as those used in Golay binary sequence pairs can be used for Z-complementary sequences. Similarly to Golay binary pairs, there are Z-complementary pairs which cannot be generated from the Golay rules [Golay 61], the so-called kernels. In [Fan 07] Fan *et al.* present a list of the kernels up to length $L_{|ZC} = 26$ with maximum ZCZ, $W_{|ZC}$. Those kernels include Golay kernels of lengths $L_{|Gol} = 2$, $L_{|Gol} = 10$ and $L_{|Gol} = 26$ with $W_{|ZC} = L_{|ZC}$.

Following the generation rules used for complementary sets [Tseng 72], Fan *et al.* conjecture that for certain values of $W_{|ZC}$, Z-complementary sequences exist for all lengths. Later, Li *et al.* demonstrate in [Li 11a] the existence of Z-complementary pairs of lengths $L_{|ZC} \geq 4$ for $W_{|ZC} = 3$ , $L_{|ZC} \geq 6$ for $W_{|ZC} = 4$, $L_{|ZC} \geq 8$ for $W_{|ZC} = 5$ and $L_{|ZC} \geq 10$ for $W_{|ZC} = 6$. Additionally, they derive the ZCZ size upper bound for binary Z-complementary pairs of length $L_{|ZC}$ odd and is equal to

$$W_{|ZC} \leq \frac{L_{|ZC} + 1}{2} \tag{2.18}$$

For the case of Z-complementary sets, the number of sets $T_{ZC}$ is bounded by the expression

$$T_{|ZC} \leq K_{|ZC} \cdot \left\lfloor \frac{L_{|ZC}}{W_{|ZC}} \right\rfloor \tag{2.19}$$

where $K_{|ZC}$ represents the number of sequences in the set and $\lfloor x \rfloor$ represents the largest integer less than or equal to $x$. Notice that if $W_{|ZC} = L_{|ZC}$, Z-complementary sequences

result in uncorrelated CSS and the set size upper bound becomes equal to $T_{|ZC} \leq K_{|ZC}$. Additionally, if $W_{|ZC} = 1$, the Z-complementary sequences become orthogonal complementary sequences.

### Loosely Synchronized Sequences

In 2000, LinkAir company proposed Loosely Synchronized (LS) sequences as a candidate for the 3G wireless communications standard to cope with ISI and MAI in QS-CDMA systems [Li 00]. These unitary and ternary sequences over the alphabet $\{-1, 0, +1\}$ have ideal aperiodic correlation functions in a window IFW, placed in the vicinity of the correlation shift $\tau = 0$. There are two generation algorithms for LS sequences, namely:

1. *Generation of LS sequences from Golay binary pairs*:

   In [Stanc 01], a comprehensive study of the LS generation method of [Li 00] was presented. This algorithm generates a set of $K_{|LS} = 2^a$; $a \in \mathbb{N} - \{0\}$ LS sequences of length $L_{|LS} = K_{|LS} \cdot L_{|Gol} + W_{|LS}$ and is based on the concatenation of Golay binary sequence pairs following a code tree and the insertion of a chain of zeros of length $W_{|LS}$ in the middle of the concatenated sequence. The length of this chain is equal to the ZCZ length if and only if $W_{|LS} \leq L_{|Gol} - 1$. The generation algorithm of these sequences is introduced in Chapter 5.

2. *Generation of LS sequences from CSS*:

   In [Zhang 05] Zhang *et al.* propose a generation algorithm of LS sequences from $K_{|CC}$ CC sequences of length $L_{|CC}$ is proposed. This algorithm generates $K_{|LS} = K_{|CC}^{(1+\alpha)}$ LS sequences of length $L_{|LS} = K_{|CC}^{(1+\alpha)} \cdot L_{|CC} + (K_{|CC} - 1) \cdot W_{|LS}$ and it requires $\alpha$ iterations to increase the number and length of the LS sequences, ($\alpha \in \mathbb{N} - \{0\}$). Both, the number and length of LS sequences can be equivalently adjusted by using $K_{|CSS}$ CSS of length $L_{|CSS}$, $\mathbf{S}_j(z^{-1}) = \{S_{j,0}(z^{-1}), S_{j,1}(z^{-1}), \ldots, S_{j,K_{|CSS}-1}(z^{-1})\}$; $0 \leq j \leq K_{|CSS} - 1$ and $P$=1 iterations instead of using $\alpha > 1$ iterations and CC sequences [Perez 08]. So $K_{|LS} = K_{|CSS}^2$ LS sequences of length $L_{|LS} = K_{|CSS}^2 \cdot L_{|CSS} + \left(K_{|CSS} - 1\right) \cdot W_{|LS}$ can be generated by following the recursive equation

$$V_{g,k}\left(z^{-1}\right) = \sum_{i=0}^{K_{|CSS}-1} h_{k,i} \cdot z^{-i \cdot L_{|CSS}} \cdot \left[ \sum_{j=0}^{K_{|CSS}-1} z^{-j \cdot \left(K_{|CSS} \cdot L_{|CSS} + W_{|LS}\right)} \cdot S_{\pi_{g,i},j}\left(z^{-1}\right) \right] \tag{2.20}$$

where $0 \leq g, k \leq K_{|CSS} - 1$, $h_{k,i}$ are the elements of a Hadamard matrix of order $K_{|CSS}$ and $\pi_{g,i} = (g + i) \bmod K_{|CSS}$. As stated in equation 2.20 LS sequences are generated by concatenating the $j$-th complementary sequence of the set $\pi_{g,i}$, $S_{\pi_{g,i},j}(z^{-1})$, with the polarity given by the Hadamard entry $h_{k,i}$ and by inserting a chain of zeros $W_{|LS} = L_{|CSS} - 1$ every $K_{|CSS}$ concatenated sequences. This algorithm is more general than the previous one from Golay binary sequence pairs. In fact, if $K_{|CSS} = 2$ and $K_{|LS} = 4$ both algorithms are equivalent.

### Generalized LS Sequences

Tang and Mow propose in [Tang 06] the generation of groups of Generalized Loosely Synchronized (GLS) sequences with favourable intergroup cross-correlation functions, while maintaining the sequence and ZCZ length of the original LS sequences. The generation algorithm of GLS sequences is a generalization of the one for LS from Golay binary pairs. The generation of GLS sequences clearly shows the problem of generating large families of GO sequences for a given length and with the largest theoretical ZCZ length. Tang and Mow found a generation algorithm of GLS sequences that almost reach the theoretical maximum number of sequences that can be generated for a given sequence length and ZCZ length. $T_{|GLS}$ groups of $K_{|GLS} = K_{|LS} = 2^a$; $a \in \mathbb{N} - \{0\}$ GLS sequences of length $L_{|GLS} = L_{|LS}$ are generated from $T_{|GLS}$ sets of Hadamard matrices of order $2^{a-1}$ [Yang 00], which are constructed from sequences with good cross-correlation properties, as Kerdock codes [Kerdo 72] (used when $a$ is even, $T_{|GLS} = 2^{a-2}$) or Gold sequences (used when $a$ is odd, $T_{|GLS} = 2^{a-1}$).

The aperiodic auto-correlation and cross-correlation properties of GLS sequences of the same group is the same as those of LS sequences. Nonetheless, for the cross-correlations of GLS sequences from different groups (i.e. generated from a different Hadamard matrix) appears an interference at the time shift $\tau = 0$ with a maximum value lower than $2^{\left(\frac{a+1}{2}\right)} \cdot L_{|GLS}$ when $a$ is even and lower than $2^{\left(\frac{a+2}{2}\right)} \cdot L_{|GLS}$ when $a$ is odd. This is an important issue, as the cross-correlation interference at $\tau = 0$ could be erroneously detected as an auto-correlation peak. There exists a trade-off between ZCZ length, sequence length and family size; this problem would be more tractable if a set of non-equivalent Hadamard matrices exists whose rows and/or columns are orthogonal with the rows and/or columns of any other non-equivalent Hadamard matrix of the set.

### Generalized Pairwise Complementary Sequences

One of the main disadvantages of LS sequences is their limited energy efficiency, as the IFW is obtained by inserting a chain of zeros in the middle of the sequence. Moreover, when the number of users is considerable, the IFW is reduced to avoid very large sequences. In 2006, the research group of Hsiao-Hwa Chen proposed a novel kind of binary pairs of spreading sequences, known as Generalized Pairwise Complementary (GPC) sequences [Chen 06]; these sequences are energy efficient, can be easily implemented and have a controllable IFW.

$T_{|GPC} = 2 \cdot G$; $G = 2^a$; $a \in \mathbb{N} - \{0\}$ pairs of GPC sequences ($K_{|GPC} = 2$) of length $L_{|GPC} = 4 \cdot G \cdot L_{|CC}$ are generated from CC sequences of length $L_{|CC}$ and Generalized Even Shift Orthogonal Sequences (GESO), which confers to the sequences sums of aperiodic correlation functions with sparse interferences, at know locations. GPC sequences are divided into two groups; the SACF has an IFW of length IFW $= 8 \cdot L_{|CC} - 1$, while the SCCF of GPC sequences has bi-valued properties: the intra-group SCCF has an IFW of length IFW $= 8 \cdot L_{|CC} - 1$, while the inter-group SCCF is zero for all shifts $\tau$. These sequences will be analyzed thoroughly in Chapter 5.

### Generalized Pairwise Z-Complementary Sequences

Generalized Pairwise Z-complementary (GPZ) sequences, pairs derived from Z-complementary sequences, are a variation of GPC sequences and they are proposed with the objective of increasing the number of sequences available. As the number of CC mates are lower than the number of Z-complementary sets for a given sequence length $L$ (refer to equation 2.19), GPZ sequences, generated from Z-complementary sequences, have a larger number of pairs, $T_{|GPZ}$, than the one of GPC sequences for a given length.

Furthermore, the lengths of CC sequences are theoretically limited to $L_{|CC} = 2^N \cdot 10^M \cdot 26^P$, whereas the lengths of Z-complementary sequences have less restrictions [Li 11a]; this implies that GPZ sequences are more flexible than GPC sequences. Apart from the use of Z-complementary sequences instead of CC sequences for the generation of GPZ sequences, the later steps are equal to the GPC algorithm. In fact, the sum of aperiodic correlation functions maintains the bi-valued correlation property, with a reduction on the IFW length. The GPZ set is defined as GPZ($T_{|GPZ}$, $L_{|GPZ}$, IFW), where $T_{|GPZ} = T_{|ZC} \cdot G$ is the number of GPZ pairs of sequences ($K_{|GPZ} = 2$) and $G$ is the Walsh-Hadamard expansion factor; $L_{|GPZ} = 4 \cdot L_{|ZC} \cdot G$ is the length of GPZ sequences and the IFW is equal to IFW $= 8 \cdot W_{|ZC} + 1$.

### Inter-Group Complementary Sequences

The SACF of both, GPC and GPZ sequences have bi-valued properties. The generalization of GPC sequences, named Inter-Group Complementary (IGC) sequences is proposed in [Li 08] to increase the number of groups from two of GPC sequences to $K_{|PC}$.

Given $T_{|PC} = K_{|PC}$ binary PC sets of $K_{|PC}$ sequences of length $L_{|PC} = W_{|IGC} + 1$, $\mathbf{S}_j[\ell] = \left\{ s_{j,0}\left[\ell\right], s_{j,1}\left[\ell\right], \ldots, s_{j,K_{|PC}-1}\left[\ell\right] \right\}; \, 0 \leq j \leq K_{|PC} - 1; \, 0 \leq \ell \leq L_{|PC} - 1$ and a Hadamard matrix of order $G$, $\boldsymbol{\mathcal{H}}_G$, IGC sequences are generated by applying the Kronecker product $\boldsymbol{\mathcal{H}}_G \otimes \mathbf{S}_j[l]; \, 0 \leq j \leq K_{|PC} - 1$. The $j$-th IGC group is defined as $\mathbf{Y}^{(j)}[l] = \{y^{(j)}_{g,0}[l], y^{(j)}_{g,1}[l], \ldots, y^{(j)}_{g,K_{|PC}-1}[l]\}$ where $y^{(j)}_{g.k}\left[l\right]$ is the $k$-th sequence of the $g$-th set belonging to the $j$-th group, $0 \leq l \leq L_{|IGC} - 1; \, 0 \leq g \leq G - 1; \, 0 \leq k, j \leq K_{|PC} - 1$, with $L_{|IGC} = G \cdot L_{|PC}$ and it is generated as:

$$y^{(j)}_{g,k}\left[l\right] = h_{g,0} \cdot s_{j,k}\left[l\right] + h_{g,1} \cdot s_{j,k}\left[l - L_{|PC}\right] + \cdots + h_{g,G-1} \cdot s_{j,k}\left[l - (G-1) \cdot L_{|PC}\right] \quad (2.21)$$

where $h_{u,v} \in \{+1, -1\}; \, 0 \leq u, v \leq G - 1$ are the entries of the Hadamard matrix $\boldsymbol{\mathcal{H}}_G$. The previous algorithm generates $T_{|IGC} = G \cdot K_{|PC}$ sets of $K_{|IGC} = K_{|PC}$ IGC sequences in each set; and the entire set size is divided into $K_{|PC}$ complementary groups. Finally, the sums of aperiodic correlation functions of IGC sequences have the following properties:

$$\begin{aligned} SACF[\tau] &= \sum_{k=0}^{K_{|IGC}} \sum_{l=0}^{L_{|IGC}-1-\tau} y^{(j)}_{g,k}[l] \cdot y^{(j)}_{g,k}[l+\tau] \\ &= \begin{cases} C_p & \text{if } \tau = 0 \\ 0 & \text{if } 1 \leq |\tau| \leq W_{|IGC} \end{cases} \quad 0 \leq g \leq G-1; \, 0 \leq j \leq K_{|IGC}-1; \, C_p \in \mathbb{R} - \{0\} \end{aligned} \quad (2.22)$$

$$\begin{aligned} SCCF[\tau] &= \sum_{k=0}^{K_{|IGC}} \sum_{l=0}^{L_{|IGC}-1-\tau} y^{(j)}_{g,k}[l] \cdot y^{(j')}_{g',k}[l+\tau] \\ &= \begin{cases} 0 & \text{if } 0 \leq |\tau| \leq W_{|IGC}; j = j' \\ 0 & \text{if } \forall \tau; j \neq j' \end{cases} \quad 0 \leq g, g' \leq G-1; \, g \neq g'; \, 0 \leq j, j' \leq K_{|IGC}-1 \end{aligned} \quad (2.23)$$

So IGC sequences have also bi-valued aperiodic correlation properties.

**T-ZCZ Sequences**

Zhang *et al.* propose in [Zhang 04] Three-Zero Correlation Zone (T-ZCZ) sequences and, similarly to GPC sequences, they are a class of GO binary sequence pairs. These sequences have a ZCZ in the vicinity of $\tau = 0$ and two more in the final part of the aperiodic correlation functions. They are constructed by rearranging the Tseng and Liu generation matrix [Tseng 72]; the form in which it is rearranged leads to a family of T-ZCZ sequences with different ZCZ lengths. In any case, the ZCZ length of these sequences is lower than the one obtained with GPC sequences. For a detailed description of the generation algorithm of T-ZCZ sequences refer to [Zhang 04, Zhang 05, Perez 09a].

## 2.4 Theoretical Bounds and Merit Factors

There are several metrics to determine the goodness of a spreading sequence $s[l]$ of length $L$. Golay proposed the so-called Merit Factor, which is defined as follows [Golay 72]:

$$\text{Merit Factor} = \frac{C_{s,s}[0]^2}{2 \cdot \sum_{\tau=1}^{L-1} |C_{s,s}[\tau]|^2} \tag{2.24}$$

Notice that the Merit Factor evaluates the relationship between the squared energy of $s[l]$, measured with the auto-correlation peak at zero time shift ($\tau$=0) and the total energy of the auto-correlation sidelobes. More general metrics to evaluate the correlation functions of spreading sequences are the ISL and the PSL. Given a family of $K$ sequences $\mathbf{S}[l] = \{s_0[l], s_1[l], \ldots, s_{K-1}[l]\}$ of length $L$, the ISL determines the total energy of the auto-correlation and cross-correlation sidelobes. Mathematically it is defined as

$$\text{ISL} = \sum_{i=0}^{K-1} \sum_{\substack{\tau=-L+1 \\ \tau \neq 0}}^{L-1} |C_{s_i,s_i}[\tau]|^2 + \sum_{i=0}^{K-1} \sum_{\substack{j=0 \\ j \neq i}}^{K-1} \sum_{\tau=-L+1}^{L-1} \left|C_{s_i,s_j}[\tau]\right|^2 \tag{2.25}$$

and the PSL computes the maximum peak sidelobe of the correlation functions, i.e. the PSL is equal to

$$\text{PSL} = \max\left\{C_{s_i,s_j}[\tau]\right\};\ 0 \leq i,j \leq K-1;\ \forall \tau \,\text{if}\, i \neq j;\ \forall \tau \neq 0 \,\text{if}\, i = j \tag{2.26}$$

An equivalent metric to the PSL are the auto-correlation and cross-correlation bounds, $\theta_{AC}$ and $\theta_{CC}$ respectively. These metrics are defined for a family of $K$ sequences $\mathbf{S}[l] = \{s_0[l], s_1[l], \ldots, s_{K-1}[l]\}$ of length $L$ as follows:

$$\begin{aligned} \theta_{AC} &= \max\left\{\frac{|C_{s_i,s_i}[\tau]|}{C_{s_i,s_i}[0]}\right\}; \forall\tau \neq 0;\ 0 \leq i \leq K-1 \\ \theta_{CC} &= \max\left\{\frac{\left|C_{s_i,s_j}[\tau]\right|}{C_{s_i,s_i}[0]}\right\}; \forall\tau;\ 0 \leq i,j \leq K-1;\ i \neq j \\ \theta &= \max\{\theta_{AC}, \theta_{CC}\} = \frac{\mathrm{PSL}}{L} \end{aligned} \tag{2.27}$$

Consequently, the joint correlation bound, $\theta$, $0 \leq \theta \leq 1$, is the normalized PSL and determines the correlation properties of a set of sequences, where the lowest bound means that the sequence set has the best correlation properties.

Theoretical lower bounds for these metrics have been derived. They determine mathematically the minimum values which can be accomplished for a given family of $K$ spreading sequences of length $L$. These theoretical bounds can be divided into four groups: theoretical bounds for unitary and non-GO/GQO sequences, theoretical bounds for non-unitary and non-GO/GQO sequences, theoretical bounds for unitary and GO/GQO sequences and theoretical bounds for non-unitary and GO/GQO sequences. There is a considerable amount of effort done to derive the tightest lower bounds, i.e. best theoretical lower bounds to evaluate the correlation properties of a set of sequences. Here only the current tightest bound is included; for a comprehensive overview of the theoretical lower bounds refer to [Fan 04].

### 2.4.1 Theoretical Bounds for Unitary and Non-GO/GQO Sequences

In this group are included sequences as Walsh-Hadamard (also known as OVSF sequences) or PN sequences (refer to the classification of Figure 2.7). The tightest lower bounds for these class of sequences are the Peng-Fan lower bounds [Peng 04], which are stronger than Welch [Welch 74], Sarwate [Sarwa 79] and Levenshtein [Leven 99] lower bounds. They are expressed as follows:

$$\frac{\sqrt{3}\cdot L - \sqrt{K}}{\left(\sqrt{3}\cdot K - 2\cdot\sqrt{K}\right)\cdot L^2}\cdot\theta_{AC}^2 + \frac{\sqrt{3}\cdot(K-1)}{\left(\sqrt{3}\cdot K - 2\cdot\sqrt{K}\right)\cdot L}\cdot\theta_{CC}^2 \geq 1 \tag{2.28}$$

$$\theta \geq L \cdot \sqrt{\frac{\sqrt{3 \cdot K} - 2}{\sqrt{3 \cdot K} \cdot L - 1}};\ \text{for}\ K \geq 3,\ L \geq 2 \tag{2.29}$$

### 2.4.2 Theoretical Bounds for Non-unitary and Non-GO/GQO Sequences

This group includes sequences as Golay binary sequence pairs and CSS (refer to the classification of Figure 2.7). If $T_{|CSS} = K_{|CSS}$ CSS are used, each of them composed of $K_{|CSS}$ sequences, then the theoretical bound is zero, but this is not true when it is transmitted more than $K_{|CSS}$ sets of sequences simultaneously. In general, Welch derived the theoretical lower bound for a system of $T$ sets of $K$ sequences, each of them of length $L$ that transmits $T > K$ sets; This lower bound is equal to:

$$\theta \geq T \cdot L \cdot \sqrt{\frac{\frac{K}{T} - 1}{K \cdot (2 \cdot L - 1) - 1}} \tag{2.30}$$

Notice that if the number of sets $T$ is equal to $T = 1$, then the Welch lower bound of equation 2.30 turns out in the conventional Welch lower bound used for binary unitary sequences.

Recently Liu proposed the following theoretical lower bound for multichannel systems [Liu 11a]:

$$\theta \geq \sqrt{\frac{T \cdot L^2 \cdot K - T^2 \cdot L^2 - \frac{T \cdot K \cdot (L^2 - 1)}{3}}{L \cdot K - 1}} \tag{2.31}$$

The proposed bound is stronger than the Welch lower bound for multichannel systems if one of the following conditions holds:

1. $K = 4 \cdot T - 1$, $T > 2$ and $L > \frac{2}{1 - \frac{1}{T}}$, or
2. $K \geq 4 \cdot T$, $T > 2$ and $L \geq 2$

### 2.4.3 Theoretical Bounds for Unitary GO/GQO Sequences

The lower bounds derived for unitary GO/GQO sequences are generalizations of some of the previous lower bounds and the tightest ones are the Peng-Fan lower bounds [Peng 04]. They are derived for $K$ unitary GO/GQO sequences of length $L$ over complex roots of unit, as LS sequences. They include the Tang-Fan [Tang 01a], Welch [Welch 74], Sarwate

[Sarwa 79] and Levenshtein [Leven 99] lower bounds when the length of the LCZ (or ZCZ) window is equal to $W_{LCZ} = L - 1$:

$$3 \cdot \gamma \cdot \theta_{AC}^2 + 3 \cdot (\gamma + 1) \cdot (K - 1) \cdot \theta_{CC}^2 \geq 3 \cdot K \cdot L - 3 \cdot L^2 + 3 \cdot K \cdot \gamma \cdot L - 2 \cdot K \cdot \gamma - K \cdot \gamma^2; \text{for any } 0 \leq \gamma \leq W_{LCZ} \tag{2.32}$$

$$\frac{\sqrt{3} \cdot L - \sqrt{K}}{\left(\sqrt{3} \cdot K - 2 \cdot \sqrt{K}\right) \cdot L^2} \cdot \theta_{AC}^2 + \frac{\sqrt{3} \cdot (K - 1)}{\left(\sqrt{3} \cdot K - 2 \cdot \sqrt{K}\right) \cdot L} \cdot \theta_{CC}^2 \geq 1; \quad \text{for } K > 3,\ L > 2,\ W_{LCZ} > \sqrt{\frac{3}{K}} \cdot L - 1 \tag{2.33}$$

$$2 \cdot (4^\gamma - 1) \cdot \theta_{AC}^2 + 3 \cdot (K - 1) \cdot 4^\gamma \cdot \theta_{CC}^2 \geq \left(3 \cdot K \cdot L - L^2 - 4 \cdot K\right) \cdot 4^\gamma + 6 \cdot (\gamma - 2) \cdot 2^\gamma \cdot K + 6 \cdot K \cdot \gamma + 16 \cdot K - 2 \cdot L^2; \text{ for any } 0 \leq \gamma \leq W_{LCZ} \tag{2.34}$$

$$\left\{1 - \frac{(32 - 3 \cdot \pi^2) \cdot (L^2 - K)^2 \cdot \left(2 \cdot L^2 - \sqrt{2 \cdot K \cdot L^2 - K^2}\right)}{128 \cdot L^2 \cdot K \cdot (2 \cdot L^2 - K) \cdot \sqrt{2 \cdot K \cdot L^2 - K^2}}\right\} \cdot \theta^2 \geq L - \left\lceil \frac{\pi \cdot L}{\sqrt{8 \cdot K}} \right\rceil; \text{ for } K \leq L^2,\ 0 < \varphi \leq \frac{\pi}{2},\ W_{LCZ} \geq \frac{\pi}{\varphi};\ \varphi = \arccos\left(1 - \frac{K}{L^2}\right) \tag{2.35}$$

$$\theta \geq \sqrt{\frac{3 \cdot K \cdot L - 3 \cdot L^2 + 3 \cdot K \cdot L \cdot \gamma - 2 \cdot K \cdot \gamma - K \cdot \gamma^2}{3 \cdot (K \cdot \gamma + K - 1)}} \quad \text{for any } 0 \leq \gamma \leq W_{LCZ} \tag{2.36}$$

$$\left\{1 - \frac{(32 - 3 \cdot \pi^2) \cdot (L^2 - K)^2 \cdot \left(2 \cdot L^2 - \sqrt{2 \cdot K \cdot L^2 - K^2}\right)}{128 \cdot L^2 \cdot K \cdot (2 \cdot L^2 - K) \cdot \sqrt{2 \cdot K \cdot L^2 - K^2}}\right\} \cdot \theta^2 \geq L - \left\lceil \frac{\pi \cdot L}{\sqrt{8 \cdot K}} \right\rceil; \text{ for } K \leq L^2,\ 0 < \varphi \leq \frac{\pi}{2},\ W_{LCZ} \geq \frac{\pi}{\varphi};\ \varphi = \arccos\left(1 - \frac{K}{L^2}\right) \tag{2.37}$$

### 2.4.4 Theoretical Bounds for Non-unitary GO/GQO Sequences

The previous theoretical lower bounds do not contemplate sets of GO/GQO sequences as GPC, T-ZCZ, IGC or Z-Complementary sequences. Recently some novel theoretical bounds for families of $T$ sets of $K$ GO/GQO sequences have been derived. In this case, the tightest lower bound is the one of Liu [Liu 11b]. Given $T$ sets of $K$ sequences of length $L$, with energy $E$ and LCZ window $W_{LCZ}$, the Liu theoretical lower bound is equal to:

$$\theta \geq E \cdot \sqrt{\frac{\left(\frac{T}{K} - 1\right) \cdot W_{LCZ} - L + 1}{(T \cdot W_{LCZ} - 1) \cdot (L + W_{LCZ} - 1)}} \tag{2.38}$$

If $K = 1$, then the lower bound of equation 2.38 will be the same as the Tang-Fan theoretical bound [Tang 01a]. Furthermore, in [Liu 11b] the upper bound of the number of sets, $T$ is derived and expressed as

$$T \leq \frac{(1 - \theta^2 \cdot E^2) \cdot K \cdot (L + W_{LCZ} - 1)}{[(1 - K \cdot (L + W_{LCZ} - 1) \cdot \theta^2 \cdot E^2)] \cdot W_{LCZ}};\ for\, \theta < \frac{1}{E \cdot \sqrt{K \cdot (L + W_{LCZ} - 1)}} \tag{2.39}$$

The upper bound of equation 2.39 is reached if a Hadamard matrix of order $T$ is used to expand the set size to $T = K \cdot \left\lfloor \frac{L}{W_{ZCZ}} \right\rfloor + K$ and the sequence sets are ternary GO sequences with the same energy $E$, i.e. there are a ZCZ ($W_{ZCZ}$) instead of a LCZ window ($W_{LCZ}$) in the aperiodic correlation functions.

## 2.5 Matched Filter Architectures for Signal Detection and Ranging Systems

For practical signal detection and ranging applications, not only it is important the use of spreading sequences with good correlation properties, but also the design of efficient architectures for their generation and, which is more critical, their correlation. The term efficient is used here in the sense of requiring less operations than the straightforward correlator. In the literature, to the author's knowledge, most of the efficient architectures are based on some orthogonal transforms: Fast Walsh Transform (FWT) [Budis 89], Fast Fourier Transform (FFT) [Van N 91] or Discrete Wavelet Transform (DWT) [Coker 10]. All of those transformations can be analyzed using a filter bank approach. In what follows, we review the most common architectures used for implementing matched filters in signal detection and ranging systems.

### 2.5.1 Tapped Delay Line Architecture

This architecture is also known as the straightforward implementation of a matched filter (or by extension of any FIR filter). Consider the real sequence $s\,[l] = \{s_0,\, s_1, \ldots,\, s_{L-1}\}$ of length $L$ and with Z-transform $S(z^{-1})$, whose elements can be represented with $b$ bits and the input signal $r\,[l]$ with Z-transform $R(z^{-1})$. Then, the Tapped Delay Line architecture for the correlation of $r\,[l]$ is the one represented in Figure 2.14. Notice that the coefficients of the matched filter are the time reversed version of the sequence elements of $s\,[l]$, and that this architecture has $L-1$ stages. Therefore, it requires $L$ multiplications, $L-1$ additions per input sample and $L-1$ delays. Clearly, if the sequence is binary, $s\,[l] \in \{+1, -1\}$, then no multiplications are required.

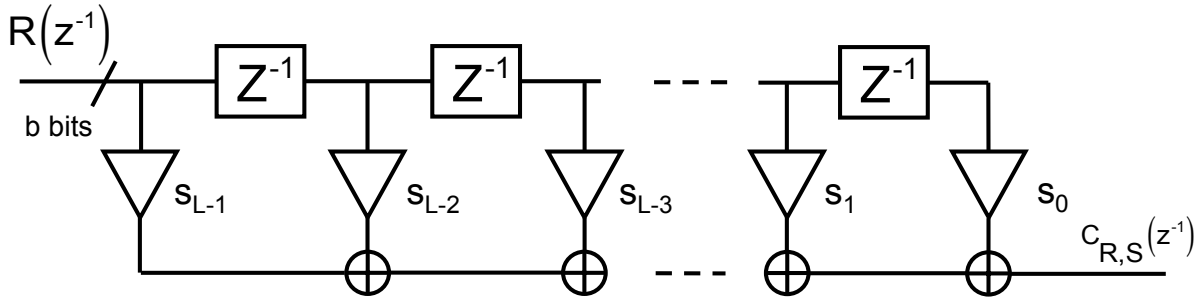


Figure 2.14: Tapped Delay Line implementation of a straightforward matched filter.

### 2.5.2 Lattice Architectures and FFT

Lattice architectures are very popular in adaptive filters and multirate filter banks due to its desirable properties, as modularity, resilience to quantization effects or losslessness in the case multirate filter banks [Vaidy 90]. The coefficients $\beta_l$ $(0 \leq l \leq L-1)$ of the standard lattice architecture can be directly derived from the coefficients of the Tapped Delay Line (straightforward) FIR architecture [Proak 96] and it requires $2 \cdot (L-1)$ multiplications and additions and $L-1$ delays for correlating a signal $R(z^{-1})$ of length $L$ with $s[l]$ (with Z-transform equal to $S(z^{-1})$ ) in $Q = L-1$ stages. It can be expressed as depicted in Figure 2.15.

In 1991, Budišin [Budis 91], and later Popović [Popov 99a], proposed an efficient correlator for Golay binary pairs of sequences of lengths $L_{|Gol} = 2^N$; $N \in \mathbb{N} - \{0\}$ with an efficient lattice architecture (depicted in Figure 2.16) that requires only $Q = N$ stages for the correlation of a sequence of the Golay pair, which we will reference from now on

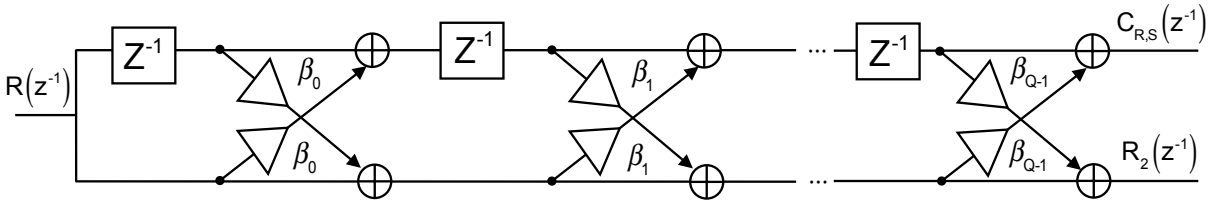


Figure 2.15: Standard lattice architecture for filtering the input $R(z^{-1})$ in $Q = L - 1$ stages. The output $R_2(z^{-1})$ is not used.

as $\{s_{j,0}^{(Q)}[l], s_{j,1}^{(Q)}[l]\}$ for $0 \leq j \leq 1$ by adding the superscript $(Q)$ to the original notation to indicate the number of stages for generating/correlating them. The coefficients $W^{(1,q)}$, $0 \leq q \leq Q-1$, are complex numbers of unit modulus and $D^{(q)}$ is a delay whose value is any permutation of the set $\{2^0, 2^1, \ldots 2^{Q-1}\}$. Therefore, the implementation of the Golay pair SACF with this architecture requires only $4 \cdot log_2\left(L_{|Gol}\right) + 1$ additions/subtractions per input sample and $2 \cdot (L_{|Gol} - 1)$ delays.

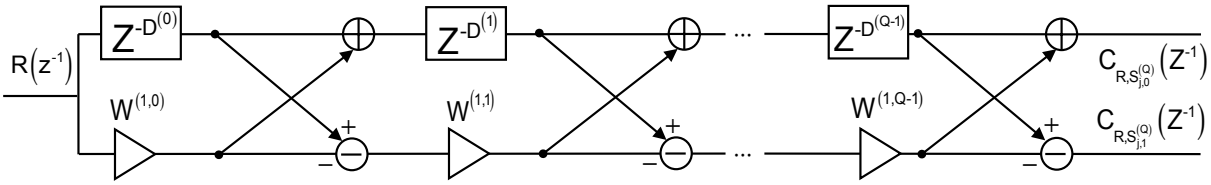


Figure 2.16: Efficient Golay correlator [Budis 91, Popov 99a].

From a filter bank point of view, the ideal Golay binary pairs SACF (and hence their sum of their power spectrum is a constant of amplitude $2 \cdot L_{|Gol}$) makes that their correlator can be implemented by using a two-channel Perfect Reconstruction Quadrature Mirror Filter (PR-QMF). In fact, the architecture proposed by Budišin and Popović is quite similar to the analysis bank of the two channel PR-QMF [p. 305, Vaidy 93, Meyer 01]. Nonetheless, the number of stages for the correlator of [Budis 91, Popov 99a] is only $log_2(L_{|Gol})$, whereas for the PR-QMF, the length of the analysis bank is equal to the length of the input signal, $L$. Figure 2.17 shows the block diagram of a two-channel PR-QMF, where $\hat{R}(z^{-1})$ represents the filtered version of the input $R(z^{-1})$.

De Marziani *et al.* have generalized the efficient correlator of [Budis 91, Popov 99a] to $K_{|CSS} = 2^k$; $k \in \mathbb{N} - \{0\}$ CSS of length $L_{|CSS} = K_{|CSS}^{Q}$, $Q \in \mathbb{N} - \{0\}$, and it has an architecture quite similar to the $K_{|CSS}$-channel Perfect Reconstruction (PR) filter [De Ma 07]. These architectures has been also applied to the efficient generation and correlation of GO sequences [Perez 08, Perez 09b].

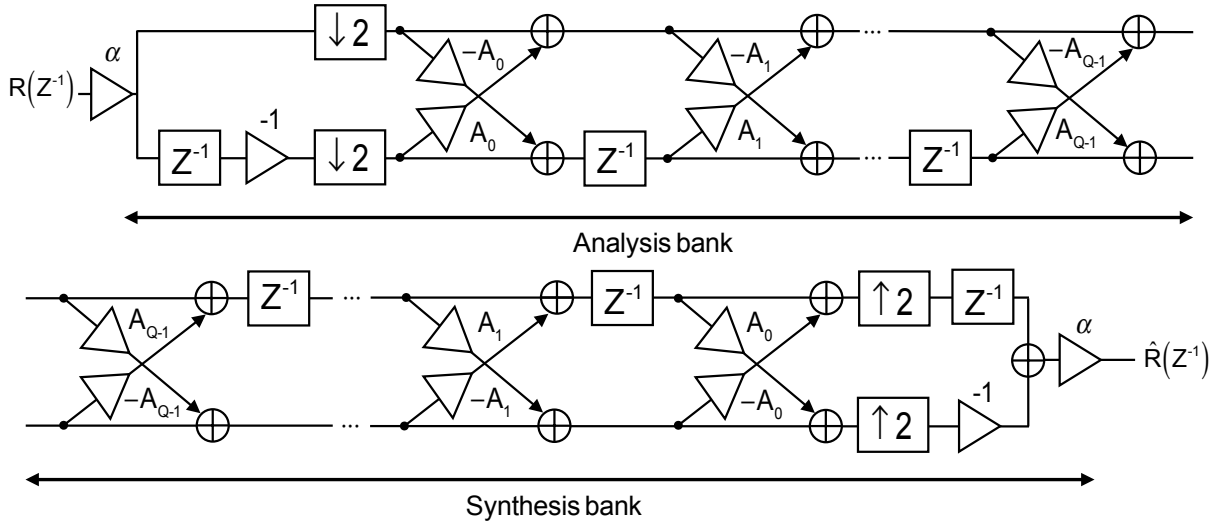


Figure 2.17: Analysis and synthesis bank of a two-channel PR-QMF [p. 305, Vaidy 93].

Recently, Donato *et al.* have modified the architecture proposed in [Budis 91, Popov 99a] to perform simultaneously the SACF [Donat 09a]. Again, this proposal has a strong similarity to the synthesis bank of the two channel PR-QMF (refer to Figure 2.18), but it requires only $log_2(L_{|Gol})$ stages in comparison with the synthesis bank of the PR-QMF (its length is equal to the length of the input signal $L$). Consequently, the proposal of [Donat 09a] requires only $log_2\left(L_{|Gol}\right) + 1$ additions and $L_{|Gol} - 1$ delays to perform the SACF of a Golay.

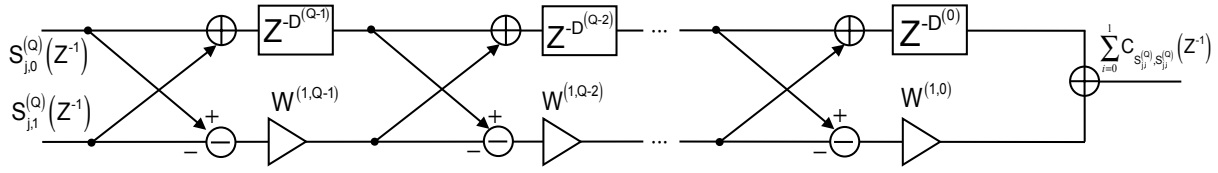


Figure 2.18: Optimized Golay Correlator of a Golay pair in $Q = N$ stages [Donat 09b].

Donato *et al.* and De Marziani *et al.* have generalized the improved architecture of [Donat 09a] to $K_{|CSS} = 2^k$; $k \in \mathbb{N} - \{0\}$ CSS of length $L_{|CSS} = K_{|CSS}^{Q}$ in $Q$ stages [Donat 09b, De Ma 11] and also it has been applied to the efficient generation and correlation of GO sequences [Perez 10, Perez 11].

Other efficient correlation architectures take advantage of the correlation properties in the frequency domain, by using the FFT [Coole 65]. Compared to the architectures proposed for Golay pairs, FFT-based architectures are not specific for a given type of spreading sequence, but this approach requires an FFT, the complex multiplication of the

result with a pre-computed complex vector stored in memory (FFT of the correlation template) and an Inverse Fast Fourier Transform (IFFT). By using a radix-2 FFT algorithm (decimation-in-time or decimation-in-frequency), each FFT/IFFT requires $\frac{L}{2} \cdot log_2 L$ complex multiplications and $L \cdot log_2 L$ complex additions, where $L$ is a power-of-two number larger than or equal to the signal length (and equal to the number of FFT points); the complex product between the pre-computed complex vector and the result of the FFT requires $L$ complex multiplications and $L-1$ additions [pp. 477-478 Proak 96].

Finally, other orthogonal transforms have been used to design efficient correlators; for example, Budišin proposed an efficient correlator for $m$-sequences of length $L_{|m-seq}$ by using the Fast Walsh Transform (FWT) [Budis 89]. This architecture requires only $2 \cdot L_{|m-seq} \cdot log_2 \left(L_{|m-seq}\right)$ additions/subtractions. In [Coker 10], Coker and Tewfik exploits the concepts of the Discrete Wavelet Transform (DWT) and the properties of the $E$-sequences to generate an efficient architecture, which curiously has the same structure as the one proposed in [Budis 91, Popov 99a].

## 2.6 Coding in Local Positioning Systems

In the last years, there has been a significant increase of interest for mobile devices that offer location based services (the so-called location aware systems) have been increased dramatically. According to the market research carried out by IDTechEx [IDTec 12], the Real Time Locating Systems (RTLS) market will rise from 293 million dollars in 2012 up to 4 billion dollars in 2022.

The requirements on the location accuracy depend on the application and impose the technology to be used; the accuracies can go from the sub-millimetre range for InfraRed (IR) systems, to hundreds of meters for E-911 emergency location systems.

In this section, we review the most representative works related to Ultra-Wideband (UWB) and ultrasound (US)-based local positioning systems.

### 2.6.1 Ultra-Wideband Local Positioning Systems

UWB is defined as any signal with a center frequency larger than 2.5 GHz and a bandwidth larger than 500 MHz or alternatively, any signal with center frequency lower than 2.5 GHz and relative bandwidth larger than 20% [Feder 02]. In 2002 the Federal Communications Commission (FCC) liberated the frequency band that goes from 3.1 GHz to 10.6 GHz with a power emission limit of $-41.3$ dBm/MHz.

Due to the generic definition of UWB and the broad range of operational frequencies, in the literature there is a considerable variety of UWB-based Local Positioning Systems (LPS), working in different conditions and with very different performances. So, it is hard to make a correct comparison of the reported systems.

Consider the Cramér-Rao theoretical limit for the Root Mean Square Error (RMSE) in the estimation of the Time Of Arrival (TOA) of a signal [Sahin 08] as

$$\mathrm{RMSE}_{\mathrm{TOA}} \geq \frac{c}{2 \cdot \sqrt{2}\pi \cdot \sqrt{\mathrm{SNR}} \cdot B} \tag{2.40}$$

where $c$ is the speed of light. Notice that the theoretical limit for TOA estimation depends inversely on the effective signal bandwidth, $B$, and on the SNR. Also, the center frequency determines the penetration capabilities of the UWB signal over the materials. Considering the TOA measurements are statistically independent and their estimator is unbiased, the Cramér-Rao theoretical limit for the RMSE in the estimation of the Time Differences Of Arrival (TDOA) of a signal is equal to:

$$\mathrm{RMSE}_{\mathrm{TDOA}} \geq \frac{c}{2 \cdot \pi \cdot \sqrt{\mathrm{SNR}} \cdot B} \tag{2.41}$$

For the sake of clarity, Table 2.2 depicts the most representative systems available in the literature.

### 2.6.2 Ultrasound-based Local Positioning Systems

One of the first US-based LPS was the *Active Bat* system, developed by AT&T [Ward 97]. This location system is based on ultrasonic emitter tags (carried by the unit to locate) and US base stations (receivers placed on the ceiling). Close to the base stations, the system uses RF for synchronization purposes, so it triggers the emission of an uncoded ultrasonic signal by the tag. The US base stations send the estimated distance measurements to a centralized computer to obtain the estimated user position. The channel division is based on TDMA, thus limiting the system update rate. In its first version, the positioning errors were lower than 9 cm for the 95% of the readings.

Later, another US-based location system known as *Cricket*, was developed [Priya 00]. Similar to *Active Bat*, the system uses RF signalling for synchronization purposes, TDMA channel division and an uncoded pulse transmission.

| System | [Stoic 06] | [Schro 05] | [Pietr 10] | MSSI [Fonta 03] | Ubisense [Ubise 12] |
|---|---|---|---|---|---|
| Ranging Accuracy | $\pm$1.5 m conf. 95% NLOS | – | $<$ 2 cm LOS | – | – |
| Positioning Accuracy | – | $<$ 73.5 cm LOS 2D | – | $<$ 30.48 cm 2D | $<$ 30 cm 3D |
| Coverage Area | – | 3 m straight line | 5 m straight line | 30.48 $\times$ 15.24 m | 50 m straight line |
| Type of Emitter | IR-UWB | IR-UWB | IR-UWB | – | IR-UWB |
| Multiple Access | – | TDMA | – | – | – |
| Bandwidth | 3.1 – 4.1 GHz | 1.6 GHz | 1.91 – 9.01 GHz | 1.25 GHz | 5.8 – 7.2 GHz |
| Type of Receiver | Energy Detector | Matched Filter | Energy Detector | Tunnel detector | – |
| Sampling Rate | – | 5 GS/s | 0.5 – 1 GS/s | – | – |

| System | DART [Zebra 12] | [Mahfo 08] | [Irahh 06] | [Segur 10] |
|---|---|---|---|---|
| Ranging Accuracy | – | 1.49 mm | 8.05 cm LOS/ 15.78 cm NLOS | – |
| Positioning Accuracy | $<$ 30 cm 3D | 5.77 mm 3D | – | $<$ 20 cm 2D |
| Coverage Area | 90 m straight line | $<$ 1.86 m straight line | 10 m straight line | 8 $\times$ 5 m |
| Type of Emitter | IR-UWB | IR-UWB | IR-UWB | IR-UWB |
| Multiple Access | – | TDMA | – | TDMA |
| Bandwidth | – | 6 GHz | 2 GHz | 1 GHz |
| Type of Receiver | – | Matched Filter | Energy Detector | Matched Filter |
| Sampling Rate | – | 100 GS/s | 100 GS/s | 3 GS/s |

Table 2.2: Characteristics of the most representative UWB LPS available in the literature.

On the contrary, *Cricket* is a privacy-oriented system, so US transmitters are placed on the ceiling and the received signal is processed in the mobile device. The positioning errors of *Cricket* are lower than 123.7 cm for the 95% of the readings with a non-valid measurements rate of the 39.18%.

*Atlintida* system, [Gonza 09], improves the positioning accuracy of the *Cricket* system to 16.6 cm for the 95% of the readings and the rate of non-valid measurements to 4.25% by using spreading sequences of length $L$.

All the previous systems use narrowband US transducers: in the case of *Atlintida* system the transducers bandwidth is approximately 2 kHz. Therefore, in order to accommodate the encoded signalling of the *Atlintida* system to the transducer bandwidth, the emission duration increases by a factor $L$ compared with *Cricket* emission time.

Hazas and Ward proposed a novel centralized and broadband location system, called *Dolphin* [Hazas 02]. The novelty of the centralized location version of the *Dolphin* system, lies in the use of ad-hoc broadband transducers and simultaneous emissions, encoded with Gold spreading sequences; i.e. the use of CDMA techniques. The positioning accuracy of the centralized *Dolphin* system is better than 2.34 cm with a 95% of confidence level.

Later, Hazas and Ward proposed an asynchronous privacy-oriented *Dolphin* system with a location accuracy better than 26.6 cm in the 95 % of the measurements [Hazas 03].

Prieto *et al.* presented a high-accuracy US LPS, named 3D-LOCUS [Priet 07]. The system uses Golay binary sequence pairs, assigning each sequence of the pair (modulated in BPSK) to a different transducer, and reaches positioning accuracies better than 1 cm in the 90% of the measurements in a reduced area of $2 \times 0.4$ metres.

Ureña *et al.* proposed an encoded US LPS, with asynchronous detection and privacy-oriented [Urena 07]. In this system, the transmitted signals are modulated in BPSK with Kasami codes of 255 bits and the accuracies obtained are in the sub-centimetre range. This work is improved later in [Perez 09c] by using LS sequences, with accuracies better than 2.5 cm even in hard multipath environments.

In [Garci 11], García *et al.* carry out a comparison between the link budget of the uncoded LPS system of [Holm 05] and the one of [Perez 09c]. Although the LPS system of [Holm 05] uses uncoded and low-bandwidth signals, it gives a similar immunity to ultrasound noise to that provided by the processing gain obtained with coding. For avoiding signal collisions, this proposal needs a channel multiplexing mechanism, as CSMA. Despite of the small signal duration, the update rate of the system of [Holm 05] can fall to less than 0.5 positions per second due to channel sensing; this problem is eliminated later in [Holm 09]. Notice that this problem does not happen with a CDMA-based system

as the one proposed in [Perez 09c]. Nevertheless CDMA-based systems can be adversely affected by near-far problem if non-GO spreading sequences are used, or if there is not implemented a power control stage in transmissions. This makes difficult the localization in positions where the power of the received signals from each beacon are very different.

Finally, it is noteworthy the recent work of [Saad 12]. It provides 3-D positioning with accuracies better than 9.5 cm in 99% of the measurements. The proposed system is privacy-oriented and the mobile device determines its position based on the Angle Of Arrival (AOA) and the Time Of Flight (TOF) of the transmitted signals from fixed positions. In the same way as the US LPS of [Perez 09c], the work of [Saad 12] does not need synchronization between emitters and receivers. The use of broadband transducers allows to modulate the transmitted signals by using Frequency Hopping Spread Spectrum (FHSS) techniques.

Table 2.3 depicts a resume of the most representative ultrasound-based local positioning systems, where the term MA refers to the Multiple-Access scheme used.

| System | Accuracy Errors | Coverage | MA | Coding |
|---|---|---|---|---|
| *Active Bat* [Ward 97] | $<$ 9 cm 95% conf. | 280 $m^3$ | TDMA | No |
| *Cricket* [Priya 00] | $<$ 123.7 cm 95% conf. | scalable | TDMA | No |
| *Dolphin* [Hazas 02] | $<$ 2.34 cm 95% conf. | $3.5 \times 2.6 \times 2.3$ m | CDMA | Yes |
| [Holm 05] | Room level | scalable | CSMA | No |
| 3D-LOCUS [Priet 07] | $<$ 1 cm 90% conf. | $2 \times 2 \times 0.4$ m | CDMA | Yes |
| [Urena 07] | $<$ 1 cm | $1 \times 1$ m | CDMA | Yes |
| [Perez 09c] | $<$ 2.5 cm 95% conf.[6] | $4.5 \times 3.5$ m | CDMA | Yes |
| *Atlintida* [Gonza 09] | $<$ 16.6 cm 95% conf. | $8.78 \times 4.40$ m | TDMA | Yes |
| [Saad 12] | $<$ 9.5 cm 99% conf. | $3.50 \times 2.85 \times 2.70$ m | FDMA | Yes |

Table 2.3: Characteristics of the most representative US LPS available in the literature.

## 2.7 Problem Statement and Thesis Objectives

The properties of the spreading sequences used play a key role on the development of high-precision ranging measurements. For practical ranging systems, there are important issues to be considered, such as: the aperiodic correlation properties, available number of sequences for a given sequence length, ZCZ length or the number of hardware resources

[6] In an environment with large multipath components.

needed for correlation implementation. Therefore, they would benefit from generation and correlation architectures that require a low number of operations per input sample and capable to deal with binary CSS, which have constraints both in the number of sequences of the set and in the sequence lengths. Unfortunately, at the present moment, binary CSS are only known to exist for limited lengths and set sizes [Seber 92, Borwe 03]. In [Phoon 05], Phoong and Chang summarize the known methods for the generation of antipodal paraunitary matrices[7] (which it is equivalent to the generation of binary CSS); for clarity, we have included them in Table 2.4. The set size $K$ generated with Wornell and Butterfly method is constrained by the known dimensions of Hadamard matrices [Seber 92].

| | Set size $K$ | Sequence length $L$ |
|---|---|---|
| Turyn and Taki method [Taki 69, Turyn 74] | 2 | $2^N \cdot 10^M \cdot 26^P$ |
| Golay-Rudin-Shapiro method [Shapi 51, Rudin 59, Golay 61] | 2 | $2^N$ |
| Tseng-Liu interleaving and concatenating method [Tseng 72] | $2^k$ | $2^k \cdot L_1$ |
| Generalized Kronecker product method [Phoon 05] | $K_1 \cdot K_2$ | $L_1 \cdot L_2$ |
| Wornell method [Worne 95] | 2 or $4 \cdot k$ | $K^N$ |
| Generalized Agayan-Sarukhanyan (AS) method [Seber 92] | $\frac{K_1 \cdot K_2}{2}$ | $L_1 \cdot L_2$ |
| Butterfly method [Phoon 05] | 2 or $4 \cdot k$ | $2^N$ |

Table 2.4: Different methods to generate binary CSS of $K$ sequences and length $L$. $K_i$ and $L_i$ are integers for which binary CSS of $K_i$ sequences and length $L_i$ exist. $N$, $M$, $P$ and $k$ are non-negative integers [Phoon 05].

Additionally, among the known methods for the generation of binary CSS, the efficient architectures for their generation and correlation only deal with $K_{|CSS} = 2^k$ binary CSS of lengths $L_{|CSS} = K^Q_{|CSS}$, $(k, Q \in \mathbb{N} - \{0\})$ [De Ma 07, Funes 10], with the exception of the architecture proposed by Budišin for Golay binary sequence pairs of lengths $L_{|Gol} = 2^N \cdot 10^M$ (where $N$, $M$ are non-negative integers) [Budis 11].

Interestingly, the current limitations on the set size ($K_{|CSS}$) and sequence length ($L_{|CSS}$) with binary CSS do not occur with multilevel (real-valued) CSS [Darne 88].

This thesis contributes to the design of efficient generation and correlation algorithms of CSS with more flexible lengths and set sizes and take advantage of them to propose novel

[7] A $K \times K$ polynomial matrix $\boldsymbol{\mathcal{P}}(z^{-1})$ is said to be antipodal if the matrix coefficients are $\pm 1$ and it is paraunitary if $\boldsymbol{\mathcal{P}}(z^{-1}) \times \boldsymbol{\mathcal{P}}^T(z) = c \cdot \mathbf{I}_K$, where $c \in \mathbb{R} - \{0\}$ and $\mathbf{I}_K$ is the identity matrix of order $K$ [Phoon 05].

architectures and generation/correlation algorithms for LS [Li 00] and GPC sequences [Chen 06], both used in QS-CDMA.

This thesis has the following objectives:

- *Design of modular and efficient architectures for the generation and correlation of flexible CSS*: Due to the fact that CSS are used as a building block for the generation of spreading sequences for aperiodic correlation, we will focus mainly on the development of architectures for generate/correlate flexible CSS. This is carried out by using two different approaches:

  - By expanding the CSS to the multilevel alphabet by using multilevel Hadamard matrices. With this approach, the multilevel CSS have sequence lengths that are a multiple number of the set size, and thus there are no constraints on it.
  - By using the generation/correlation algorithm for multilevel complementary pairs to generate binary sequences in the final stage of the algorithm. In this way, a novel form to decompose the Golay kernel 26 is proposed. This is later combined with the Golay kernel 10 decomposition proposed by Budišin [Budis 11], to generate $K_{|CSS} = 2$ binary CSS of all the currently known lengths. Finally, the algorithm is expanded to $K_{|CSS} = 2^k; k \in \mathbb{N} - \{0\}$ binary CSS of length $L_{|CSS} = (\frac{K_{|CSS}}{2}) \cdot 2^N \cdot 10^M \cdot 26^P$, where $N$, $M$ and $P$ are non-negative integers.

- *Design of efficient architectures to generate and correlate GO sequences*: The application of the previous novel architectures to GO spreading sequences is desired, as they will benefit from the flexibility achieved with the proposed architectures for CSS. This thesis proposes a novel and efficient generator/correlator for GPC sequences and shows the theoretical link between LS and GPC sequences. This allows the proposal of a new and very efficient LS generation and correlation algorithm.

- *Application of the spreading sequences to ranging measurements*: Finally the spreading sequences analyzed in this thesis will be applied to different LPS: an ultrasonic LPS and a novel CDMA-based UWB LPS. This will allows to analyze the advantages and disadvantages of each spreading sequence.

# Chapter 3

# Generalization of Efficient Architectures for the Generation and Correlation of Multilevel CSS

In this chapter we present two generalizations of efficient architectures for the generation and correlation of $K_{|MultCSS}$ multilevel CSS: the first one for $K_{|MultCSS} = 2^k$, $k \in \mathbb{N} - \{0\}$ multilevel CSS and the second one for $K_{|MultCSS} \geq 3 - \{4\}$ multilevel CSS. Therefore with both algorithms it is possible to generate/correlate efficiently $K_{|MultCSS}$ multilevel CSS, with $K_{|MultCSS} \geq 2$ and their lengths can be adjusted without constraints. These architectures not only are interesting from the theoretical point of view, but also because they can be the basis for the generation of multilevel CSS with low Peak-to-Average Power Ratio (PAPR) and flexible length. Furthermore, the first algorithm introduced for $K_{|MultCSS} = 2^k$ multilevel CSS, will be used in the following chapters for the proposal of efficient architectures for other types of spreading sequences.

Along this chapter we will use the algorithms shown in Table 2.4 (refer to Chapter 2, section 2.7) to explain the efficient architectures presented here for multilevel CSS: Golay-Rudin-Shapiro, Wornell, and Tseng-Liu interleaving algorithms.

Consequently, the main contribution of this chapter is the design of efficient architectures for multilevel CSS to generate/correlate complementary sets of sequences of more lengths and set sizes than the currently reported for binary CSS.

## 3.1 Foundations of Efficient Algorithms for Complementary Sequences

In this section we will review and unify the recursive generation algorithms for Golay binary sequences, polyphase and multilevel complementary pairs. The resultant algorithm will be the basis for further generalizations along the thesis. The non-recursive algorithms presented by Golay in [Golay 61] for the generation of Golay sequence pairs $\{s_{j,0}^{(Q)}[l], s_{j,1}^{(Q)}[l]\}$ can be expressed in a recursive form as follows:

$$\begin{aligned} s_{j,0}^{(0)}[l] &= \delta[l] \\ s_{j,1}^{(0)}[l] &= \delta[l] \\ s_{j,0}^{(q+1)}[l] &= s_{j,0}^{(q)}[l] + s_{j,1}^{(q)}[l-2^q] \\ s_{j,1}^{(q+1)}[l] &= s_{j,0}^{(q)}[l] - s_{j,1}^{(q)}[l-2^q] \end{aligned} \tag{3.1}$$

where the following parameters are defined:

- $s_{j,i}^{(q+1)}[l]$ for $0 \leq i \leq 1$ is the $i$-th Golay sequence of the $j$-th uncorrelated pair after iteration $q$.[1] This recursive algorithm can only generate a Golay pair of a given length $L_{|Gol}$ and it is not capable of generating uncorrelated Golay pairs (for clarity we can assume that $j = 0$).
- $L_{|Gol}$ is the length of the Golay pair, $L_{|Gol} = 2^N$ and $N$ a non-negative integer.
- $q$ is the iteration number, $0 \leq q \leq Q-1$ and $Q = N$, $Q \geq 1$, the total number of iterations, $Q = log_2(L_{|Gol})$.[2]
- $l$ is an integer number with values $0 \leq l \leq L_{|Gol} - 1$.

Both Saphiro [Shapi 51] and Rudin [Rudin 59] found this recursive algorithm independently when researching on flat polynomials on the unit circle of the complex plane (i.e sequences with a flat power spectra and amplitude equal to their length). Because of that, this recursive algorithm is known as Golay-Rudin-Shapiro.

[1] Observe that the superscript $(q+1)$ refers to the result after the iteration $q$ and the superscript $(q)$, the result after the iteration $(q-1)$.

[2] The term $N$ is used to define the length $2^N$ of the sequence and $Q$ to indicate the number of iterations (stages) of the algorithm.

Later, Sivaswamy [Sivas 78b] generalized the Golay-Rudin-Shapiro algorithm to the polyphase alphabet by introducing the parameter $W^{(1,q)}$, which is a complex number of unit magnitude and sometimes called the "seed" of the complementary sets. The algorithm of Sivaswamy is expressed as

$$\begin{aligned} s_{j,0}^{(0)}[l] &= \delta[l] \\ s_{j,1}^{(0)}[l] &= \delta[l] \\ s_{j,0}^{(q+1)}[l] &= s_{j,0}^{(q)}[l] + W^{(1,q)} \cdot s_{j,1}^{(q)}[l - 2^q] \\ s_{j,1}^{(q+1)}[l] &= s_{j,0}^{(q)}[l] - W^{(1,q)} \cdot s_{j,1}^{(q)}[l - 2^q] \end{aligned} \tag{3.2}$$

This algorithm is capable of generating two uncorrelated Golay binary sequence pairs (i.e. $0 \leq j \leq 1$) by setting $W^{(1,q)} \in \{-1, +1\}$ and choosing different values in the first stage $q = 0$ for each Golay pair and by maintaining the same values for both pairs in the stages $1 \leq q \leq Q - 1$ [Alvar 04].

In 1990, Budišin [Budis 90a] proposed a generalization of the Golay-Rudin-Saphiro and Sivaswamy algorithm by changing the delays to $D^{(q)}$, whose value in each iteration $q$ is chosen from any of the $Q!$ permutations without repetition of the set $\{2^0, \ldots, 2^{Q-1}\}$. The generalized algorithm of Budišin is capable of generating all the complementary pairs that can be obtained by means of the non-recursive methods of Golay (in fact $2^Q \cdot Q!$ by combining different delay permutations and $W^{(1,q)}$ values, although only two are mutually uncorrelated, $0 \leq j \leq 1$), as well as polyphase complementary pairs and even multilevel complementary pairs for certain delay distributions, different from the given definition of $D^{(q)}$. This generalization is expressed as

$$\begin{aligned} s_{j,0}^{(0)}[l] &= \delta[l] \\ s_{j,1}^{(0)}[l] &= \delta[l] \\ s_{j,0}^{(q+1)}[l] &= s_{j,0}^{(q)}[l] + W^{(1,q)} \cdot s_{j,1}^{(q)}\left[l - D^{(q)}\right] \\ s_{j,1}^{(q+1)}[l] &= s_{j,0}^{(q)}[l] - W^{(1,q)} \cdot s_{j,1}^{(q)}\left[l - D^{(q)}\right] \end{aligned} \tag{3.3}$$

The previous algorithm is the cornerstone of the Efficient Golay Correlator (EGC) proposed by Budišin [Budis 91] and later by Popović [Popov 99a] (refer to Chapter 2, section 2.5.2), who demonstrated that the number of memory bits required can be minimized if the delays permutation is $\{2^{Q-1}, \ldots 2^0\}$.

Also in 1990, Budišin proposed a generation algorithm for pairs of multilevel complementary sequences (PMCS), (number of sequences equal to $K_{|MultCSS} = 2$) [Budis 90b], and it is expressed as

$$\begin{aligned} s_{j,0}^{(0)}[l] &= \delta[l] \\ s_{j,1}^{(0)}[l] &= 0 \\ s_{j,0}^{(q+1)}[l] &= s_{j,0}^{(q)}[l] + A^{(q)} \cdot s_{j,1}^{(q)}\left[l - D^{(q)}\right] \\ s_{j,1}^{(q+1)}[l] &= A^{(q)} \cdot s_{j,0}^{(q)}[l] - s_{j,1}^{(q)}\left[l - D^{(q)}\right] \end{aligned} \tag{3.4}$$

where the new parameter $A^{(q)}$ is defined as an arbitrary real number and again the parameter $D^{(q)}$ is defined as any permutation of the set $\{2^0, \ldots, 2^{Q-1}\}$, (although this restriction is not necessary to generate multilevel complementary pairs). It is noteworthy that the delays values $D^{(q)}$, as in the algorithm 3.3, are chosen to avoid overlaps in intermediate stages, and gaps (i.e. zero elements) in the final iteration. In this way, the length, $L_{|MultCSS}$ of the generated multilevel complementary pair is equal to $L_{|MultCSS} = 2^Q$.

Notice that with the previous algorithm we cannot generate uncorrelated complementary pairs, and the generated pair will assume to be the pair $\{s_{0,0}^{(Q)}[l], s_{0.1}^{(Q)}[l]\}$, $j = 0$, $0 \leq l \leq L_{|MultCSS} - 1$.

In the following generalizations, the delay values are chosen according to the mentioned conditions and later we analyze what happens when other delay distributions are chosen (i.e. we will firstly generalize the generation algorithms, and then, the parameters of these algorithms).

All the previous generation algorithms can be easily unified by adding the parameter $W^{(1,q)}$ to the algorithm 3.4 and by changing the initial condition of the sequence $s_{j,1}^{(0)}[l]$. Hence, the generalized algorithm is as follows:

$$\begin{aligned} s_{j,0}^{(0)}[l] &= \delta[l] \\ s_{j,1}^{(0)}[l] &= \delta[l] \\ s_{j,0}^{(q+1)}[l] &= s_{j,0}^{(q)}[l] + A^{(q)} \cdot W^{(1,q)} \cdot s_{j,1}^{(q)}\left[l - D^{(q)}\right] \\ s_{j,1}^{(q+1)}[l] &= A^{(q)} \cdot s_{j,0}^{(q)}[l] - W^{(1,q)} \cdot s_{j,1}^{(q)}\left[l - D^{(q)}\right] \end{aligned} \tag{3.5}$$

where the seed values $W^{(1,q)}$ are again complex number of unit modulus; for the generation of real-valued complementary pairs, which is the objective here, $W^{(1,q)} \in \{-1, +1\}$. This parameter, as in the binary case allows the generation of $K_{|MultCSS} = 2$ multilevel and uncorrelated complementary pairs: $\{s_{0,0}^{(Q)}[l], s_{0,1}^{(Q)}[l]\}$ for $j = 0$ and $\{s_{1,0}^{(Q)}[l], s_{1,1}^{(Q)}[l]\}$ for $j = 1$, $(0 \leq j \leq 1)$. It is interesting to note that although the initial condition of the sequence $s_{j,1}^{(Q)}[l]$ in equation 3.4 has been changed regarding equation 3.5, the generated pairs remain complementary.

*Proof.* For this proof we will change the notation of the seeds to $W_j^{(1,q)}$, where $0 \leq j \leq 1$ indicates the number of the complementary set that is generated, so we can distinguish the seed values of each of them. Consider now the equation 3.5 particularized for the generation of the pair $\{s_{0,0}^{(Q)}[l], s_{0,1}^{(Q)}[l]\}$ for $j = 0$ and the pair $\{s_{1,0}^{(Q)}[l], s_{1,1}^{(Q)}[l]\}$ for $j = 1$, as shown in equations 3.6 and 3.7 respectively:

$$\begin{aligned} s_{0,0}^{(0)}[l] &= \delta[l] \\ s_{0,1}^{(0)}[l] &= \delta[l] \\ s_{0,0}^{(q+1)}[l] &= s_{0,0}^{(q)}[l] + A^{(q)} \cdot W_0^{(1,q)} \cdot s_{0,1}^{(q)}\left[l - D^{(q)}\right] \\ s_{0,1}^{(q+1)}[l] &= A^{(q)} \cdot s_{0,0}^{(q)}[l] - W_0^{(1,q)} \cdot s_{0,1}^{(q)}\left[l - D^{(q)}\right] \end{aligned} \tag{3.6}$$

$$\begin{aligned} s_{1,0}^{(0)}[l] &= \delta[l] \\ s_{1,1}^{(0)}[l] &= \delta[l] \\ s_{1,0}^{(q+1)}[l] &= s_{1,0}^{(q)}[l] + A^{(q)} \cdot W_1^{(1,q)} \cdot s_{1,1}^{(q)}\left[l - D^{(q)}\right] \\ s_{1,1}^{(q+1)}[l] &= A^{(q)} \cdot s_{1,0}^{(q)}[l] - W_1^{(1,q)} \cdot s_{1,1}^{(q)}\left[l - D^{(q)}\right] \end{aligned} \tag{3.7}$$

As was shown in the definition of uncorrelated complementary sequences (refer to equation 2.17), two complementary pairs of sequences are uncorrelated if their SCCF is a delta of Kronecker. Hence, if we express the aperiodic correlations between the sequences

of two different pairs, we have

$$C_{s_{0,0}^{(Q)},s_{1,0}^{(Q)}}[\tau] = \sum_{l=0}^{L_{|MultCSS}-1-\tau} \left(s_{0,0}^{(Q-1)}[l] + A^{(Q-1)} \cdot W_0^{(1,Q-1)} \cdot s_{0,1}^{(Q-1)}\left[l - D^{(Q-1)}\right]\right) \cdot \left(s_{1,0}^{(Q-1)}[l+\tau] + A^{(Q-1)} \cdot W_1^{(1,Q-1)} \cdot s_{1,1}^{(Q-1)}\left[l - D^{(Q-1)} + \tau\right]\right)$$

$$C_{s_{0,1}^{(Q)},s_{1,1}^{(Q)}}[\tau] = \sum_{l=0}^{L_{|MultCSS}-1-\tau} \left(A^{(Q-1)} \cdot s_{0,0}^{(Q-1)}[l] - W_0^{(1,Q-1)} \cdot s_{0,1}^{(Q-1)}\left[l - D^{(Q-1)}\right]\right) \cdot \left(A^{(Q-1)} \cdot s_{1,0}^{(Q-1)}[l+\tau] - W_1^{(1,Q-1)} \cdot s_{1,1}^{(Q-1)}\left[l - D^{(Q-1)} + \tau\right]\right) \tag{3.8}$$

If we expand the previous equations, they can be expressed as

$$C_{s_{0,0}^{(Q)},s_{1,0}^{(Q)}}[\tau] = C_{s_{0,0}^{(Q-1)},s_{1,0}^{(Q-1)}}[\tau] + \left(A^{(Q-1)}\right)^2 \cdot W_0^{(Q-1)} \cdot W_1^{(Q-1)} \cdot C_{s_{0,1}^{(Q-1)},s_{1,1}^{(Q-1)}}[\tau] + \sum_{l=0}^{L_{|MultCSS}-1-\tau} \left(A^{(Q-1)} \cdot W_1^{(1,Q-1)} \cdot s_{0,0}^{(Q-1)}[l] \cdot s_{1,1}^{(Q-1)}\left[l - D^{(Q-1)} + \tau\right] + A^{(Q-1)} \cdot W_0^{(1,Q-1)} \cdot s_{0,1}^{(Q-1)}\left[l - D^{(Q-1)}\right] \cdot s_{1,0}^{(Q-1)}[l+\tau]\right)$$

$$C_{s_{0,1}^{(Q)},s_{1,1}^{(Q)}}[\tau] = \left(A^{(Q-1)}\right)^2 \cdot C_{s_{0,0}^{(Q-1)},s_{1,0}^{(Q-1)}}[\tau] + W_0^{(1,Q-1)} \cdot W_1^{(1,Q-1)} \cdot C_{s_{0,1}^{(Q-1)},s_{1,1}^{(Q-1)}}[\tau] - \sum_{l=0}^{L_{|MultCSS}-1-\tau} \left(A^{(Q-1)} \cdot W_1^{(1,Q-1)} \cdot s_{0,0}^{(Q-1)}[l] \cdot s_{1,1}^{(Q-1)}\left[l - D^{(Q-1)} + \tau\right] + A^{(Q-1)} \cdot W_0^{(1,Q-1)} \cdot s_{1,0}^{(Q-1)}[l+\tau] \cdot s_{0,1}^{(Q-1)}\left[l - D^{(Q-1)}\right]\right) \tag{3.9}$$

By adding the previous equations we obtain that the SCCF after stage $Q-1$ is equal to:

$$C_{s_{0,0}^{(Q)},s_{1,0}^{(Q)}}[\tau] + C_{s_{0,1}^{(Q)},s_{1,1}^{(Q)}}[\tau] = \left[1 + \left(A^{(Q-1)}\right)^2\right] \cdot \left(C_{s_{0,0}^{(Q-1)},s_{1,0}^{(Q-1)}}[\tau] + W_0^{(1,Q-1)} \cdot W_1^{(1,Q-1)} \cdot C_{s_{0,1}^{(Q-1)},s_{1,1}^{(Q-1)}}[\tau]\right) \tag{3.10}$$

Finally, in order to recursively iterate and to cancel the summation terms of equation 3.9, the seed values $W_0^{(1,q)}$ and $W_1^{(1,q)}$ for $1 \leq q \leq Q-1$ must be equal and have unitary modulus. Hence, by iterating $Q-1$ times more, and taking into account that the initial conditions of the complementary pairs are a Kronecker delta (and thus the

cross-correlation is also a delta), we obtain the following expression:

$$C_{s_{0,0}^{(Q)},s_{1,0}^{(Q)}}[\tau] + C_{s_{0,1}^{(Q)},s_{1,1}^{(Q)}}[\tau] = \prod_{q=0}^{Q-1}\left[1+\left(A^{(q)}\right)^2\right]\cdot\left(\delta[\tau] + W_0^{(1,0)}\cdot W_1^{(1,0)}\cdot\delta[\tau]\right) \quad (3.11)$$

In order to make the SCCF equal to zero, the seeds values at stage $q = 0$, ($W_0^{(1,0)}$ and $W_1^{(1,0)}$) must be of unitary modulus and hold the expression $W_0^{(1,0)} = -W_1^{(1,0)}$. Furthermore, the seed values in the other stages $1 \leq q \leq Q-1$, must be also of unitary modulus and hold the expression $W_0^{(1,q)} = W_1^{(1,q)}$. ■

Going back to the initial notation, from the previous proof we state that the seeds $W^{(1,q)}$ are defined in $W^{(1,q)} \in \{-1,+1\}$ for the generation of real-valued complementary pairs. Although this is a very straightforward generalization, it will have a great importance for further generalizations proposed in this thesis.

## 3.2 Generalization of Efficient Algorithms for CSS to the Multilevel Alphabet

In 1995 Wornell [Worne 95] proposed an efficient algorithm for the generation of $K_{|CSS}$ of length $L_{|CSS} = K_{|CSS}^{Q}$ that is defined as

$$\begin{aligned}\mathbf{S}_j^{(k,0)}[l] &= \boldsymbol{\mathcal{H}}_{K_{|CSS}} \\ \mathbf{S}_j^{(k,q+1)}[l] &= \boldsymbol{\mathcal{H}}_{K_{|CSS}} \times \mathbf{D}^{(k,q)}[l] \times \mathbf{S}_j^{(k,q)}[l]\end{aligned} \quad (3.12)$$

where the following parameters are defined:

- $\boldsymbol{\mathcal{H}}_{K_{|CSS}}$ is a Hadamard matrix generated with the Sylvester's recursive method (refer to Chapter 2, section 2.3.1), $K_{|CSS} = 2^k$.
- $k$ is the number of iterations of the Sylvester's algorithm needed for generating the Hadamard matrix $\boldsymbol{\mathcal{H}}_{K_{|CSS}}$, $k = log_2 K_{|CSS}$, $k \geq 1$.
- $\mathbf{S}_j^{(k,q+1)}[l]$ is the $j$-th CSS of $K_{|CSS}$ sequences of length $L_{|CSS}$ after iteration $q$. $\mathbf{S}_j^{(k,q+1)}[l] = [\ s_{j,0}^{(q+1)}[l] \ \cdots \ s_{j,K_{|CSS}-1}^{(q+1)}[l]\ ]^T$. The Wornell algorithm can only generate one CSS. Hence for clarity we will assume that $j = 0$.
- $q$ is the number of iteration of the Wornell algorithm, $0 \leq q \leq Q-1$, $Q \in \mathbb{N} - \{0\}$.

- $\mathbf{D}^{(k,q)}$ is a delay matrix defined as

$$\mathbf{D}^{(k,q)}[l] = \begin{bmatrix} \delta[l] & 0 & \cdots & 0 \\ 0 & \delta\left[l - K_{|CSS}^{q}\right] & 0 & \vdots \\ \vdots & 0 & \ddots & 0 \\ 0 & \cdots & 0 & \delta\left[l - (K_{|CSS} - 1) \cdot K_{|CSS}^{q}\right] \end{bmatrix} \tag{3.13}$$

Notice that this algorithm is a generalization of the Golay-Rudin-Shapiro algorithm previously explained, and it can only generate one CSS of $K_{|CSS}$ sequences.

Álvarez *et al.* generalized the algorithm of Wornell for $K_{|CSS} = 4$ uncorrelated binary CSS [Alvar 04] and De Marziani *et al.* [De Ma 07], for $K_{|CSS} = 2^k$ uncorrelated binary CSS.

The generalization proposed in [De Ma 07] of the Wornell algorithm can be expressed in discrete time domain as

$$\begin{aligned} \mathbf{S}_j^{(k,0)}[l] &= \delta[l] \cdot \begin{bmatrix} 1 & \cdots & 1 \end{bmatrix}_{1,K_{|CSS}}^{T} \\ \mathbf{S}_j^{(k,q+1)}[l] &= \mathbf{\Lambda}_j^{(k,q)}[l] \times \mathbf{D}^{(k,q)}[l] \times \mathbf{S}_j^{(k,q)}[l] \end{aligned} \tag{3.14}$$

where the matrix $\mathbf{\Lambda}_j^{(k,q)}$ is a Hadamard matrix of order $K_{|CSS} = 2^k$, $k \in \mathbb{N} - \{0\}$, generated with the Tseng-Liu interleaving method [Tseng 72]; the term $\mathbf{S}_j^{(k,q+1)}[l]$ denotes the $j$-th complementary set ($0 \leq j \leq K_{|CSS} - 1$), composed by $K_{|CSS}$ binary sequences after iteration $q$ ($0 \leq q \leq Q - 1$), i.e. $\mathbf{S}_j^{(k,q+1)}[l] = \begin{bmatrix} s_{j,0}^{(q+1)}[l] & \cdots & s_{j,K_{|CSS}-1}^{(q+1)}[l] \end{bmatrix}^T$. The matrix $\mathbf{D}^{(k,q)}[l]$ is a diagonal matrix defined as

$$\mathbf{D}^{(k,q)}[l] = \begin{bmatrix} \delta[l] & 0 & \cdots & 0 \\ 0 & \delta\left[l - D^{(q)}\right] & 0 & \vdots \\ \vdots & 0 & \ddots & 0 \\ 0 & \cdots & 0 & \delta\left[l - (K_{|CSS} - 1) \cdot D^{(q)}\right] \end{bmatrix} \tag{3.15}$$

where the delay elements $D^{(q)}$ are chosen as any permutation of the values $\{K_{|CSS}^{0}, K_{|CSS}^{1}, \ldots, K_{|CSS}^{Q-1}\}$. Therefore, the generation algorithm of [De Ma 07] is a generalization of the Wornell algorithm analogous to what Budišin did with the Golay-Rudin-Shapiro algorithm.

The Hadamard matrices $\mathbf{\Lambda}_j^{(k,q)}$ of order $K_{|CSS}$ have been generated with the Tseng-Liu interleaving method for a given complementary set $\mathbf{S}_j^{(k,Q)}[l]$. The Tseng-Liu recursive expansion method allows the generation of $K_{|CSS}$ uncorrelated CSS. This method can be expressed as follows:

$$\begin{aligned}
\mathbf{\Lambda}_j^{(k,q)} &= \left[ \begin{array}{cc} \mathbf{\Delta}_{left}^{(k,q)} & \mathbf{\Delta}_{right}^{(k,q)} \end{array} \right] \\
\mathbf{\Delta}_{left}^{(k,q)} &= \left[ \begin{array}{c} \mathbf{\Lambda}_j^{(k-1,q)} \odot \mathbf{\Lambda}_j^{(k-1,q)} \\ -\mathbf{\Lambda}_j^{(k-1,q)} \odot \mathbf{\Lambda}_j^{(k-1,q)} \end{array} \right] \\
\mathbf{\Delta}_{right}^{(k,q)} &= \left[ \begin{array}{c} -\mathbf{\Lambda}_j^{(k-1,q)} \odot \mathbf{\Lambda}_j^{(k-1,q)} \\ \mathbf{\Lambda}_j^{(k-1,q)} \odot \mathbf{\Lambda}_j^{(k-1,q)} \end{array} \right]
\end{aligned} \tag{3.16}$$

where the symbol $\odot$ represents the interleaving operation.

This method that starts for $k = 2$, generates in each expansion step $k$ two new matrices: the left matrix $\mathbf{\Delta}_{left}^{(k,q)}$, which represents a CSS of $2^k$ sequences of length $2^k$ and the right matrix, $\mathbf{\Delta}_{right}^{(k,q)}$, that represents another CSS of $2^k$ sequences of length $2^k$ and uncorrelated with the CSS set $\mathbf{\Delta}_{left}^{(k,q)}$. Therefore, this algorithm generates in each step $k$, two uncorrelated CSS of $2^k$ sequences of length $2^k$. The previous algorithm is unified in [De Ma 07] as

$$\mathbf{\Lambda}_j^{(k,q)} = \left[ \begin{array}{c} \mathbf{\Lambda}_j^{(k-1,q)} \odot \left( -W^{(k,q)} \cdot \mathbf{\Lambda}_j^{(k-1,q)} \right) \\ \mathbf{\Lambda}_j^{(k-1,q)} \odot \left( W^{(k,q)} \cdot \mathbf{\Lambda}_j^{(k-1,q)} \right) \end{array} \right] \tag{3.17}$$

In order to generate $K_{|CSS}$ uncorrelated CSS of length $L_{|CSS} = K_{|CSS}^Q$, we have to use all the variations with repetition of the seeds $W^{(k,0)} \in \{-1, +1\}$ at the first iteration ($q = 0$), taken from $k$ in $k$. The $j$-th variation, $0 \leq j \leq K_{|CSS} - 1$, generates the $j$-th uncorrelated CSS of length $L_{|MultCSS} = K_{|MultCSS}^Q$. The seed values for the other iterations, $\{W^{(k,1)}, \ldots, W^{(k,Q-1)}\}$ must be equal for all the sets.

The algorithm proposed in [De Ma 07] has two advantages over the recursive algorithm of Wornell [Worne 95]. Firstly, it allows the generation of $K_{|CSS}$ uncorrelated binary CSS by simply varying the sign of the seeds $W^{(k,0)}$ for $1 \leq k \leq log_2(K_{|CSS})$. Secondly, the algorithm can minimize the number of memory bits by choosing the delay permutation $\{K_{|CSS}^{Q-1}, K_{|CSS}^{Q-2}, \ldots, K_{|CSS}^0\}$.

In order to accomplish the generalization of the efficient algorithm of De Marziani *et al.* to the multilevel alphabet, the generation algorithm 3.5 for $K_{|MultCSS} = 2$ is expressed

in a matricial form as follows:

$$\begin{bmatrix} s_{j,0}^{(q+1)}[l] \\ s_{j,1}^{(q+1)}[l] \end{bmatrix} = \begin{bmatrix} 1 & A^{(q)} \cdot W^{(1,q)} \\ A^{(q)} & -W^{(1,q)} \end{bmatrix} \times \begin{bmatrix} \delta[l] & 0 \\ 0 & \delta\left[l - D^{(q)}\right] \end{bmatrix} \times \begin{bmatrix} s_{j,0}^{(q)}[l] \\ s_{j,1}^{(q)}[l] \end{bmatrix} \tag{3.18}$$

which comes directly expressed as the De Marziani *et al.* efficient algorithm if we define the matrix $\mathbf{\Lambda}_j^{(1,q)}$ as

$$\mathbf{\Lambda}_j^{(1,q)} = \begin{bmatrix} 1 & A^{(q)} \cdot W^{(1,q)} \\ A^{(q)} & -W^{(1,q)} \end{bmatrix} \tag{3.19}$$

and redefine the term $\mathbf{S}_j^{(k,q+1)}[l]$ as the $j$-th multilevel complementary set ($0 \leq j \leq K_{|MultCSS} - 1$), composed by $K_{|MultCSS} = 2^k$ ($k \in \mathbb{N} - \{0\}$) multilevel sequences after iteration $q$ ($0 \leq q \leq Q - 1$), i.e. $\mathbf{S}_j^{(k,q+1)}[l] = [\ s_{j,0}^{(q+1)}[l] \ \cdots \ s_{j,K_{|MultCSS}-1}^{(q+1)}[l]\ ]^T$ and the the matrix $\mathbf{D}^{(k,q)}[l]$ as

$$\mathbf{D}^{(k,q)}[l] = \begin{bmatrix} \delta[l] & 0 & \cdots & 0 \\ 0 & \delta\left[l - D^{(q)}\right] & 0 & \vdots \\ \vdots & 0 & \ddots & 0 \\ 0 & \cdots & 0 & \delta\left[l - (K_{|MultCSS} - 1) \cdot D^{(q)}\right] \end{bmatrix} \tag{3.20}$$

As we will show later, with this generalization, the delay values $D^{(q)}$ do not have to be chosen as a permutation of the set $\{K_{|MultCSS}^0, K_{|MultCSS}^1, \ldots, K_{|MultCSS}^{Q-1}\}$ and this will provide interesting properties to the generalized algorithm.

**Example.** Consider the generation of $K_{|MultCSS} = 2^2 = 4$ (i.e. $k = 2$) of length $L_{|MultCSS} = 4^2 = 16$ with the generalized algorithm of [De Ma 07]. The number of stages of this algorithm is equal to $Q = 2$, the delays $D^{(q)}$ are chosen as $D^{(q)} = \{4^1, 4^0\}$ and the values of $A^{(q)}$ as $A^{(q)} = \{1, 3\}$. By using the recursive equation 3.17, the matrix

| $\mathbf{\Lambda}_0^{(2,0)};\ W^{(1,0)}=+1, W^{(2,0)}=+1$ | $\mathbf{\Lambda}_1^{(2,0)};\ W^{(1,0)}=-1, W^{(2,0)}=+1$ |
|---|---|
| $\begin{bmatrix} 1 & -1 & A^{(0)} & -A^{(0)} \\ A^{(0)} & -A^{(0)} & -1 & 1 \\ 1 & 1 & A^{(0)} & A^{(0)} \\ A^{(0)} & A^{(0)} & -1 & -1 \end{bmatrix}$ | $\begin{bmatrix} 1 & -1 & -A^{(0)} & A^{(0)} \\ A^{(0)} & -A^{(0)} & 1 & -1 \\ 1 & 1 & A^{(0)} & -A^{(0)} \\ A^{(0)} & A^{(0)} & -1 & 1 \end{bmatrix}$ |
| $\mathbf{\Lambda}_2^{(2,0)};\ W^{(1,0)}=+1, W^{(2,0)}=-1$ | $\mathbf{\Lambda}_3^{(2,0)};\ W^{(1,0)}=-1, W^{(2,0)}=-1$ |
| $\begin{bmatrix} 1 & 1 & A^{(0)} & A^{(0)} \\ A^{(0)} & A^{(0)} & -1 & -1 \\ 1 & -1 & A^{(0)} & -A^{(0)} \\ A^{(0)} & -A^{(0)} & -1 & 1 \end{bmatrix}$ | $\begin{bmatrix} 1 & 1 & -A^{(0)} & -A^{(0)} \\ A^{(0)} & A^{(0)} & 1 & 1 \\ 1 & -1 & -A^{(0)} & A^{(0)} \\ A^{(0)} & -A^{(0)} & 1 & -1 \end{bmatrix}$ |

Table 3.1: Matrices $\mathbf{\Lambda}_j^{(2,0)}$ for the generation of 4 CSS obtained as the variations with repetition of the seed values at the first stage.

$\mathbf{\Lambda}_j^{(2,q)}$ results as follows:

$$\mathbf{\Lambda}_j^{(2,q)} = \begin{bmatrix} \mathbf{\Lambda}_j^{(1,q)} \odot \left(-W^{(2,q)} \cdot \mathbf{\Lambda}_j^{(1,q)}\right) \\ \mathbf{\Lambda}_j^{(1,q)} \odot \left(W^{(2,q)} \cdot \mathbf{\Lambda}_j^{(1,q)}\right) \end{bmatrix} = \begin{bmatrix} 1 & -W^{(2,q)} & W^{(1,q)} \cdot A^{(q)} & -W^{(1,q)} \cdot W^{(2,q)} \cdot A^{(q)} \\ A^{(q)} & -W^{(2,q)} \cdot A^{(q)} & -W^{(1,q)} & W^{(1,q)} \cdot W^{(2,q)} \\ 1 & W^{(2,q)} & W^{(1,q)} \cdot A^{(q)} & W^{(1,q)} \cdot W^{(2,q)} \cdot A^{(q)} \\ A^{(q)} & W^{(2,q)} \cdot A^{(q)} & -W^{(1,q)} & -W^{(1,q)} \cdot W^{(2,q)} \end{bmatrix}$$

Table 3.1 shows the $K_{|MultCSS} = 4$ variations with repetition of the seed values $W^{(1,0)}$, $W^{(2,0)}$ and the resultant matrices $\mathbf{\Lambda}_j^{(2,0)}$.

Then by using the multilevel Hadamard matrix $\mathbf{\Lambda}_j^{(2,q)}$ belonging to the algorithm of equation 3.14, the efficient generation algorithm for $K_{|MultCSS} = 4$ uncorrelated CSS is defined as stated in equation 3.21.

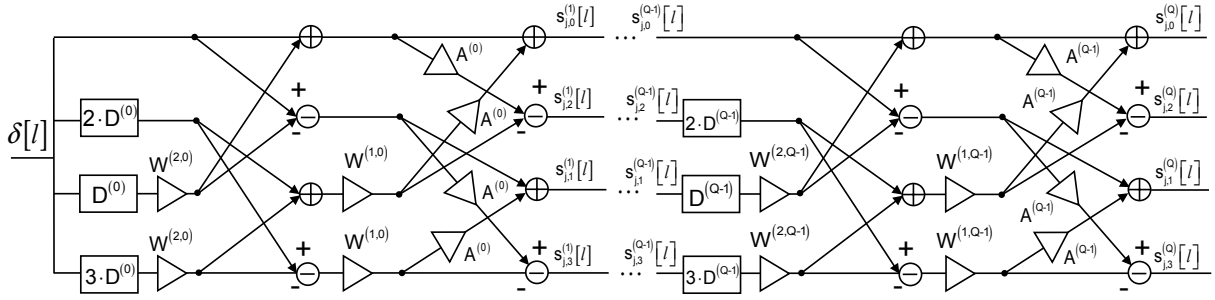


Figure 3.1: Architecture of the generation algorithm of four multilevel complementary sets of sequences, $0 \leq j \leq 3$.

$$s_{j,0}^{(0)}[l] = s_{j,1}^{(0)}[l] = s_{j,2}^{(0)}[l] = s_{j,3}^{(0)}[l] = \delta[l]$$

$$\begin{aligned}
s_{j,0}^{(q+1)}[l] &= s_{j,0}^{(q)}[l] - W^{(2,q)} \cdot s_{j,1}^{(q)}[l - D^{(q)}] + W^{(1,q)} \cdot A^{(q)} \cdot s_{j,2}^{(q)}[l - 2 \cdot D^{(q)}] \\
&\quad - A^{(q)} \cdot W^{(1.q)} \cdot W^{(2,q)} \cdot s_{j,3}^{(q)}[l - 3 \cdot D^{(q)}] \\
s_{j,1}^{(q+1)}[l] &= A^{(q)} \cdot s_{j,0}^{(q)}[l] - W^{(2,q)} \cdot A^{(q)} \cdot s_{j,1}^{(q)}[l - D^{(q)}] - W^{(1,q)} \cdot s_{j,2}^{(q)}[l - 2 \cdot D^{(q)}] \\
&\quad + W^{(1.q)} \cdot W^{(2,q)} \cdot s_{j,3}^{(q)}[l - 3 \cdot D^{(q)}] \\
s_{j,2}^{(q+1)}[l] &= s_{j,0}^{(q)}[l] + W^{(2,q)} \cdot s_{j,1}^{(q)}[l - D^{(q)}] + W^{(1,q)} \cdot A^{(q)} \cdot s_{j,2}^{(q)}[l - 2 \cdot D^{(q)}] \\
&\quad + A^{(q)} \cdot W^{(1.q)} \cdot W^{(2,q)} \cdot s_{j,3}^{(q)}[l - 3 \cdot D^{(q)}] \\
s_{j,3}^{(q+1)}[l] &= A^{(q)} \cdot s_{j,0}^{(q)}[l] + W^{(2,q)} \cdot A^{(q)} \cdot s_{j,1}^{(q)}[l - D^{(q)}] - W^{(1,q)} \cdot s_{j,2}^{(q)}[l - 2 \cdot D^{(q)}] \\
&\quad - W^{(1.q)} \cdot W^{(2,q)} \cdot s_{j,3}^{(q)}[l - 3 \cdot D^{(q)}]
\end{aligned} \tag{3.21}$$

Figure 3.1 shows the architecture of the generation algorithm for $K_{|MultCSS} = 4$ multilevel CSS of length $L_{|MultCSS} = K_{|MultCSS}^{Q}$ with the output rearrangement proposed in [Perez 07a] for the De Marziani *et al.* architecture.

We will consider only the generation of the multilevel complementary set with the variation $W^{(1,0)} = -1$ and $W^{(2,0)} = -1$ (assigned to the generation of the fourth multilevel CSS with the matrix $\mathbf{\Lambda}_3^{(2,0)}$, refer to Table 3.1). Their values in the stage $q = 1$ are equal to $W^{(1,1)} = -1$ and $W^{(2,1)} = -1$. Therefore, considering all the parameter values we have that the generation process of four multilevel CSS in two stages is equal to:

*Initial conditions*:

$$
\begin{aligned}
s^{(0)}_{3,0}[l] &= \Big\{+1,\ 0,\ 0,\ 0,\ 0,\ 0,\ 0,\ 0,\ 0,\ 0,\ 0,\ 0,\ 0,\ 0,\ 0,\ 0\Big\}\\
s^{(0)}_{3,1}[l] &= \Big\{+1,\ 0,\ 0,\ 0,\ 0,\ 0,\ 0,\ 0,\ 0,\ 0,\ 0,\ 0,\ 0,\ 0,\ 0,\ 0\Big\}\\
s^{(0)}_{3,2}[l] &= \Big\{+1,\ 0,\ 0,\ 0,\ 0,\ 0,\ 0,\ 0,\ 0,\ 0,\ 0,\ 0,\ 0,\ 0,\ 0,\ 0\Big\}\\
s^{(0)}_{3,3}[l] &= \Big\{+1,\ 0,\ 0,\ 0,\ 0,\ 0,\ 0,\ 0,\ 0,\ 0,\ 0,\ 0,\ 0,\ 0,\ 0,\ 0\Big\}
\end{aligned}
$$

*Zero stage* ($q = 0$):

$$
\begin{aligned}
s^{(1)}_{3,0}[l] &= s^{(0)}_{3,0}[l] + s^{(0)}_{3,1}[l-4] - s^{(0)}_{3,2}[l-8] - s^{(0)}_{3,3}[l-12]\\
s^{(1)}_{3,1}[l] &= s^{(0)}_{3,0}[l] + s^{(0)}_{3,1}[l-4] + s^{(0)}_{3,2}[l-8] + s^{(0)}_{3,3}[l-12]\\
s^{(1)}_{3,2}[l] &= s^{(0)}_{3,0}[l] - s^{(0)}_{3,1}[l-4] - s^{(0)}_{3,2}[l-8] + s^{(0)}_{3,3}[l-12]\\
s^{(1)}_{3,3}[l] &= s^{(0)}_{3,0}[l] - s^{(0)}_{3,1}[l-4] + s^{(0)}_{3,2}[l-8] - s^{(0)}_{3,3}[l-12]
\end{aligned}
$$

$$
\begin{aligned}
s^{(1)}_{3,0}[l] &= \Big\{+1,\ 0,\ 0,\ 0,\ +1,\ 0,\ 0,\ 0,\ -1,\ 0,\ 0,\ 0,\ -1,\ 0,\ 0,\ 0\Big\}\\
s^{(1)}_{3,1}[l] &= \Big\{+1,\ 0,\ 0,\ 0,\ +1,\ 0,\ 0,\ 0,\ +1,\ 0,\ 0,\ 0,\ +1,\ 0,\ 0,\ 0\Big\}\\
s^{(1)}_{3,2}[l] &= \Big\{+1,\ 0,\ 0,\ 0,\ -1,\ 0,\ 0,\ 0,\ -1,\ 0,\ 0,\ 0,\ +1,\ 0,\ 0,\ 0\Big\}\\
s^{(1)}_{3,3}[l] &= \Big\{+1,\ 0,\ 0,\ 0,\ -1,\ 0,\ 0,\ 0,\ +1,\ 0,\ 0,\ 0,\ -1,\ 0,\ 0,\ 0\Big\}
\end{aligned}
$$

*First stage* ($q = 1$):

$$
\begin{aligned}
s^{(2)}_{3,0}[l] &= s^{(1)}_{3,0}[l] + s^{(1)}_{3,1}[l-1] - 3\cdot s^{(1)}_{3,2}[l-2] - 3\cdot s^{(1)}_{3,3}[l-3]\\
s^{(2)}_{3,1}[l] &= 3\cdot s^{(1)}_{3,0}[l] + 3\cdot s^{(1)}_{3,1}[l-1] + s^{(1)}_{3,2}[l-2] + s^{(1)}_{3,3}[l-3]\\
s^{(2)}_{3,2}[l] &= s^{(1)}_{3,0}[l] - s^{(1)}_{3,1}[l-1] - 3\cdot s^{(1)}_{3,2}[l-2] + 3\cdot s^{(1)}_{3,3}[l-3]\\
s^{(2)}_{3,3}[l] &= 3\cdot s^{(1)}_{3,0}[l] - 3\cdot s^{(1)}_{3,1}[l-1] + s^{(1)}_{3,2}[l-2] - s^{(1)}_{3,3}[l-3]
\end{aligned}
$$

| | $Q$ | 1 | 2 | 3 | 4 | | $Q$ | 1 | 2 | 3 | 4 |
|---|---|---|---|---|---|---|---|---|---|---|---|
| $K_{\|MultCSS}=2$ | $\varphi=0$ | 3 | 6 | 12 | 24 | $K_{\|MultCSS}>2$ | $\varphi=0$ | 4 | 8 | 16 | 32 |
| | $\varphi=1$ | 2 | 4 | 8 | 16 | | $\varphi=1$ | 2 | 4 | 8 | 16 |
| | $\varphi=2$ | – | 2 | 4 | 8 | | $\varphi=2$ | – | 2 | 4 | 8 |
| | $\varphi=3$ | – | – | 2 | 4 | | $\varphi=3$ | – | – | 2 | 4 |

Table 3.2: Number of amplitude levels ($N_\ell$) for $K_{|MultCSS}$ when $1 \leq Q \leq 4$ and $1 \leq \varphi \leq 3$.

$$s^{(2)}_{3,0}[l] = \Big\{+1,\ +1,\ -3,\ -3,\ +1,\ +1,\ +3,\ +3,\ -1,\ +1,\ +3,\ -3,\ -1,\ +1,\ -3,\ +3\Big\}$$
$$s^{(2)}_{3,1}[l] = \Big\{+3,\ +3,\ +1,\ +1,\ +3,\ +3,\ -1,\ -1,\ -3,\ +3,\ -1,\ +1,\ -3,\ +3,\ +1,\ -1\Big\}$$
$$s^{(2)}_{3,2}[l] = \Big\{+1,\ -1,\ -3,\ +3,\ +1,\ -1,\ +3,\ -3,\ -1,\ -1,\ +3,\ +3,\ -1,\ -1,\ -3,\ -3\Big\}$$
$$s^{(2)}_{3,3}[l] = \Big\{+3,\ -3,\ +1,\ -1,\ +3,\ -3,\ -1,\ +1,\ -3,\ -3,\ -1,\ -1,\ -3,\ -3,\ +1,\ +1\Big\}$$

▲

### 3.2.1 Number of Amplitude Levels and Amplitude Values

Considering that the values $A^{(q)}$, $0 \leq q \leq Q-1$, are co-prime numbers, i.e. they cannot be expressed as the products of the others, the maximum number of amplitude levels of the multilevel CSS ($N_\ell$) is equal to:

$$N_\ell \leq \begin{cases} 3 \cdot 2^{Q-1} & for\ \varphi = 0\ and\ K_{|MultCSS} = 2 \\ 2^{Q-\varphi+1} & otherwise \end{cases} \tag{3.22}$$

where $\varphi$ is the number of values of $A^{(q)}$ of unit magnitude.

*Proof.* Consider first the case of being $K_{|MultCSS} = 2$ and $\varphi = 0$. In this case, the number of levels in the matrix $\mathbf{\Lambda}^{(1,0)}_j$ is equal to three as the term $A^{(0)}$ is different from zero (refer to equation 3.19). Refer to Table 3.2, which shows the number of amplitude levels ($N_\ell$) for $K_{|MultCSS}$ CSS obtained for $1 \leq Q \leq 4$ and $1 \leq \varphi \leq 3$. In each stage $q$, for a given value of $\varphi$, the number of levels increase by two as it appears a new parameter $A^{(q)}$ multiplying the sequence of the previous stage $q-1$.

Equation 3.23 represents a combinatorial approach to the maximum number of levels ($N_\ell$) for $\varphi = 0$ and $K_{|MultCSS} = 2$:

$$N_\ell \leq 3 \cdot \sum_{\nu=0}^{Q-1} \begin{pmatrix} Q-1 \\ \nu \end{pmatrix} \tag{3.23}$$

where it represents the combinations without repetition of the products of values $A^{(q)}$. By using the properties of the binomial coefficients [Rade 04], equation 3.23 can be expressed as $N_\ell \leq 3 \cdot 2^{Q-1}$.

The same demonstration can be carried out for the other cases of equation 3.22 knowing that the number of levels in the matrix $\mathbf{\Lambda}_j^{(k,0)}$ ($k = log_2 K_{|MultCSS}$) is at the most four when $\varphi = 0$ and $q = 0$, i.e. $K_{|MultCSS} > 2$ (refer to equation 3.17 and Table 3.1) and that the number of levels are divided by two with the increase of $\varphi$. Equation 3.24 represents these considerations.

$$N_\ell \leq 4 \cdot \sum_{\nu=0}^{Q-1-\varphi} \begin{pmatrix} Q-1-\varphi \\ \nu \end{pmatrix} \tag{3.24}$$

Hence the number of levels is bounded by the expression $N_\ell \leq 2^{Q-\varphi+1}$. ■

The amplitude levels of the multilevel CSS generated with this algorithm depend on the values $A^{(q)}$ of each iteration.

**Example.** Consider the generation of a complementary set of $K_{|MultCSS} = 2$ sequences of length $L_{|CSS} = 4$. If we iterate the algorithm depicted in equation 3.5 we have:

*Initial conditions*:

$$\begin{aligned} s_{j,0}^{(0)}[l] &= \Big\{1, \quad 0, \quad 0, \quad 0\Big\} \\ s_{j,1}^{(0)}[l] &= \Big\{1, \quad 0, \quad 0, \quad 0\Big\} \end{aligned}$$

*Zero stage* ($q = 0$):

$$\begin{aligned} s_{j,0}^{(1)}[l] &= \Big\{1, \quad A^{(0)} \cdot W^{(1,0)}, \quad 0, \quad 0\Big\} \\ s_{j,1}^{(1)}[l] &= \Big\{A^{(0)}, \quad -W^{(1,0)}, \quad 0, \quad 0\Big\} \end{aligned}$$

*First stage* ($q = 1$):

$$\begin{aligned} s_{j,0}^{(2)}[l] &= \Big\{1, \quad A^{(0)} \cdot W^{(1,0)}, \quad A^{(1)} \cdot A^{(0)} \cdot W^{(1,1)}, \quad -A^{(1)} \cdot W^{(1,0)} \cdot W^{(1,1)}\Big\} \\ s_{j,1}^{(2)}[l] &= \Big\{A^{(1)}, \quad A^{(1)} \cdot A^{(0)} \cdot W^{(1,0)} \quad -W^{(1,1)} \cdot A^{(0)}, \quad W^{(1,1)} \cdot W^{(1,0)}\Big\} \end{aligned}$$

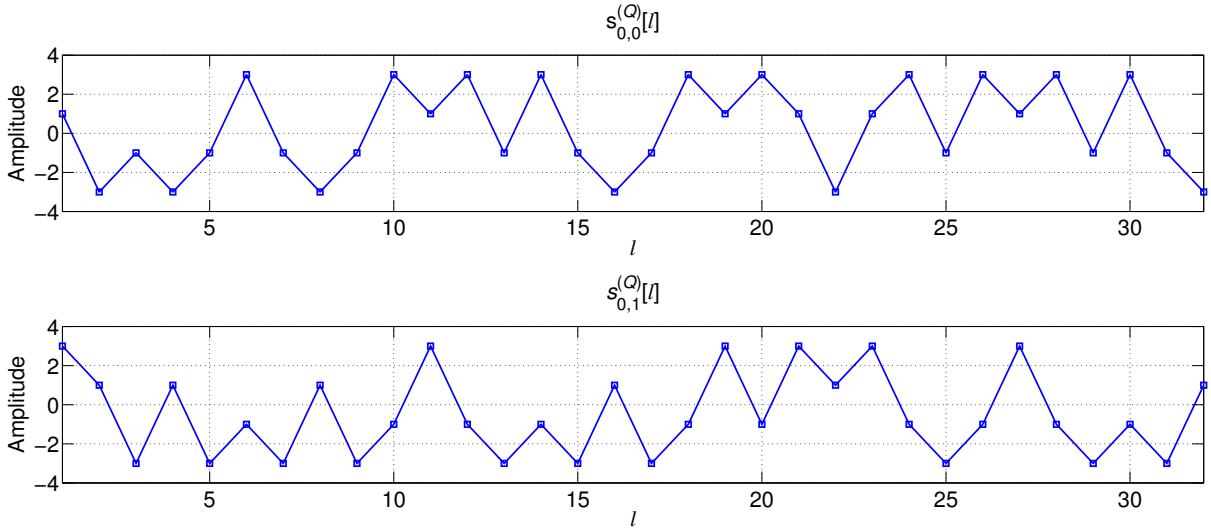


Figure 3.2: Multilevel complementary sequence pair of length 32 with amplitudes in the QAM alphabet $\{(\pm 1, \pm 3) \times (\pm 1, \pm 3)\}$.

Therefore, for the case $K_{|MultCSS} = 2$ it is possible to obtain a four-level complementary pairs of sequences that can be matched to the QAM alphabet $\{s^{(Q)}_{j,0}[l], s^{(Q)}_{j,1}[l]\} \in \{(\pm 1, \pm 3) \times (\pm 1, \pm 3)\}$ by choosing for example the values $A^{(q)} = \{+1, \cdots, +1, +3\}$ and assigning each sequence of the pair to a branch of a quadrature modulator. Figure 3.2 shows such a multilevel complementary pair of length $L_{|MultCSS} = 32$ ($Q = 5$) generated by using the values $A^{(q)} = \{+1, \cdots, +1, +3\}$, delays $D^{(q)} = \{4^4, 4^3, ..., 4^0\}$ and seeds $W^{(1,q)} = \{-1, -1, \cdots, -1\}$.

▲

There are two homomorphic transformations that can be applied to the multilevel CSS of length $K^{Q}_{|MultCSS}$. The first transformation is ${}^{t}s^{(Q)}_{j,i}[l] = c \cdot s^{(Q)}_{j,i}[l]$ for $0 \leq i, j \leq K_{|MultCSS} - 1$, $0 \leq l \leq L_{|MultCSS} - 1$ and $c \in \mathbb{R} - \{0\}$; where ${}^{t}s^{(Q)}_{j,i}[l]$ represents the $i$-th transformed complementary sequence of the $j$-th set, and the transformation represents an amplification factor. The second transformation is proposed in [Budis 90b], which is the solution to the Cauchy's power equation [Aczél 89, Dummi 04], and that is expressed as

$$ {}^{t}s^{(Q)}_{j,i}[l] = \left| s^{(Q)}_{j,i}[l] \right|^{c} \cdot sign\left( s^{(Q)}_{j,i}[l] \right) \tag{3.25} $$

Notice that in the second transformation, if $c = 0$, binary CSS are generated and the proposed generalization is reduced to the same algorithm for binary CSS of [De Ma 07]. The transformation of equation 3.25 implies that the correlation properties of multilevel

CSS of length $K^{Q}_{|MultCSS}$ generated with this generalization, are not affected by clipping. This is an important property when considering the effects of non-linear power amplifiers.

## 3.3 Novel Generation Algorithm of $K_{|MultCSS} \geq 3 - \{4\}$ Multilevel CSS

As shown in the previous section, the core of the generation algorithm of $K_{|MultCSS} = 2^k$ uncorrelated and multilevel CSS is the multilevel Hadamard matrix $\mathbf{\Lambda}_j^{(k,q)}$ of order $2^k$. In this section we introduce a novel generation algorithm, for any $K_{|MultCSS} \geq 3 - \{4\}$. Therefore, with both algorithms it is possible to generate multilevel CSS with any number of sequences in the set and with the same number of uncorrelated sets $K_{|MultCSS}$.

Observe that the number of sequences in the binary CSS (which is equal to the number of uncorrelated CSS) generated with the algorithm of De Marziani *et al.* is given by $K_{|MultCSS} = 2^k$, $k \in \mathbb{N} - \{0\}$. This limitation is because of the use of Tseng-Liu recursive method for expanding the CSS set size [Tseng 72], and because binary Hadamard matrices are only known to exist for orders two and multiple of four [Seber 92].

Nonetheless, there exist multilevel Hadamard matrices of any order. Trinh *et al.* show in [Trinh 06] the existence of circulant multilevel Hadamard matrices $\boldsymbol{\mathcal{C}}_{K_{|MultCSS}}$ of any order $K_{|MultCSS} \geq 2$ whose entries have only two real values $c_1$ and $c_2$, and they apply them to the generation of multilevel ZCZ sequences. This kind of matrices have been also used for the construction of multilevel perfect sequences over integers [Li 11b]. This circulant matrix is defined as

$$\boldsymbol{\mathcal{C}}_{K_{|MultCSS}} = \begin{bmatrix} c_1 & c_2 & c_2 & \cdots & c_2 \\ c_2 & c_1 & c_2 & \cdots & c_2 \\ \vdots & \ddots & \ddots & \ddots & \vdots \\ c_2 & \cdots & c_2 & c_1 & c_2 \\ c_2 & \cdots & c_2 & c_2 & c_1 \end{bmatrix} \tag{3.26}$$

where the entries of $\boldsymbol{\mathcal{C}}_{K_{|MultCSS}}$ have to satisfy the following relationship to be a multilevel Hadamard matrix:

$$2 \cdot c_1 \cdot c_2 + \left(K_{|MultCSS} - 2\right) \cdot c_2^2 = 0 \tag{3.27}$$

If the matrix $\mathbf{\Lambda}_j^{(k,q)}$ of the recursive generation algorithm 3.17 (generated with the Tseng-Liu expansion method) is substituted by the multilevel Hadamard matrix of equation 3.26, the resultant algorithm can generate $K_{|MultCSS}$ multilevel CSS, each of them composed of $K_{|MultCSS}$ sequences of length $L_{|MultCSS} = K_{|MultCSS}^{Q}$; with $K_{|MultCSS} \geq 3 - \{4\}$. Notice that for $K_{|MultCSS} = 4$, with the restrictions on the values of the entries $c_1$ and $c_2$ imposed by equation 3.27, the resultant Hadamard matrix is binary ($c_1 = -c_2$) or the entry $c_2$ is equal to zero. Moreover, if $K_{|MultCSS} = 2$, the entry $c_1$ or $c_2$, or both, are equal to zero. This is a non-valid matrix, as the algorithm will lead to the generation of a delta of Kronecker.

Therefore, the generation algorithm of a multilevel CSS of $K_{|MultCSS} \geq 3 - \{4\}$ sequences of length $L_{|MultCSS} = K_{|MultCSS}^{Q}$ is as follows:

$$\begin{aligned} \breve{\mathbf{S}}_j^{(0)}[l] &= \delta[l] \cdot \left[ \begin{array}{ccc} 1 & \cdots & 1 \end{array} \right]_{1,K_{|MultCSS}}^{T} \\ \breve{\mathbf{S}}_j^{(q+1)}[l] &= \boldsymbol{\mathcal{C}}_{K_{|MultCSS}} \times \breve{\mathbf{D}}^{(q)} \times \breve{\mathbf{S}}_j^{(q)} \end{aligned} \tag{3.28}$$

Notice that we have change the notation of $\mathbf{S}_j^{(k,q+1)}[l]$, $\mathbf{D}^{(k,q)}[l]$ and $\mathbf{S}_j^{(k,q)}[l]$ to $\breve{\mathbf{S}}_j^{(q+1)}[l]$, $\breve{\mathbf{D}}^{(q)}[l]$ and $\breve{\mathbf{S}}_j^{(q)}[l]$ because in this algorithm there are no expansion factor, $k$. The term $\breve{\mathbf{S}}_j^{(q+1)}[l]$ is also defined as $\breve{\mathbf{S}}_j^{(q+1)}[l] = [\ s_{j,0}^{(q+1)}[l] \quad \cdots \quad s_{j,K_{|MultCSS}-1}^{(q+1)}[l]\ ]^T$. The matrix $\breve{\mathbf{D}}^{(q)}[l]$ has the same entries of the one of equation 3.20, and $K_{|MultCSS}$ is now $K_{|MultCSS} \geq 3 - \{4\}$. As in the previous section, the delays $D^{(q)}$ are chosen as any permutation of the set $\{K_{|MultCSS}^0, K_{|MultCSS}^1, \ldots, K_{|MultCSS}^{Q-1}\}$, although their values will be generalized in the next section.

Equation 3.28 generates $K_{|MultCSS}$ ($K_{|MultCSS} \geq 3 - \{4\}$) multilevel CSS, albeit they are not necessarily uncorrelated.

*Proof.* For the sake of clarity it is demonstrated for $K_{|MultCSS} = 3$ multilevel CSS. If the matrices of equation 3.28 are multiplied, the generation algorithm is as follows:

$$\breve{\mathbf{S}}_j^{(0)}[l] = \delta[l] \cdot \left[ \begin{array}{ccc} 1 & 1 & 1 \end{array} \right]^T$$

$$\begin{aligned} s_{j,0}^{(q+1)}[l] &= c_1 \cdot s_{j,0}^{(q)}[l] + c_2 \cdot s_{j,1}^{(q)}[l - D^{(q)}] + c_2 \cdot s_{j,2}^{(q)}[l - 2 \cdot D^{(q)}] \\ s_{j,1}^{(q+1)}[l] &= c_2 \cdot s_{j,0}^{(q)}[l] + c_1 \cdot s_{j,1}^{(q)}[l - D^{(q)}] + c_2 \cdot s_{j,2}^{(q)}[l - 2 \cdot D^{(q)}] \\ s_{j,2}^{(q+1)}[l] &= c_2 \cdot s_{j,0}^{(q)}[l] + c_2 \cdot s_{j,1}^{(q)}[l - D^{(q)}] + c_1 \cdot s_{j,2}^{(q)}[l - 2 \cdot D^{(q)}] \end{aligned} \tag{3.29}$$

Recalling the definition 2.16 of a CSS (Chapter 2, section 2.3.4), the sum of the aperiodic correlations of the sequences after $Q$ iterations, must be a Kronecker delta. The aperiodic correlations of the sequences after iteration $q$ are equal to:

$$\begin{aligned}
C_{s_{j,0}^{(q+1)},s_{j,0}^{(q+1)}}[\tau] = & \sum_{l=0}^{L_{|MultCSS}-1-\tau} \left(c_1 \cdot s_{j,0}^{(q)}[l] + c_2 \cdot s_{j,1}^{(q)}\left[l - D^{(q)}\right] + c_2 \cdot s_{j,2}^{(q)}\left[l - 2 \cdot D^{(q)}\right]\right) \\
& \cdot \left(c_1 \cdot s_{j,0}^{(q)}[l+\tau] + c_2 \cdot s_{j,1}^{(q)}\left[l - D^{(q)} + \tau\right] + c_2 \cdot s_{j,2}^{(q)}\left[l - 2 \cdot D^{(q)} + \tau\right]\right) \\
C_{s_{j,1}^{(q+1)},s_{j,1}^{(q+1)}}[\tau] = & \sum_{l=0}^{L_{|MultCSS}-1-\tau} \left(c_2 \cdot s_{j,0}^{(q)}[l] + c_1 \cdot s_{j,1}^{(q)}\left[l - D^{(q)}\right] + c_2 \cdot s_{j,2}^{(q)}\left[l - 2 \cdot D^{(q)}\right]\right) \\
& \cdot \left(c_2 \cdot s_{j,0}^{(q)}[l+\tau] + c_1 \cdot s_{j,1}^{(q)}\left[l - D^{(q)} + \tau\right] + c_2 \cdot s_{j,2}^{(q)}\left[l - 2 \cdot D^{(q)} + \tau\right]\right) \\
C_{s_{j,2}^{(q+1)},s_{j,2}^{(q+1)}}[\tau] = & \sum_{l=0}^{L_{|MultCSS}-1-\tau} \left(c_2 \cdot s_{j,0}^{(q)}[l] + c_2 \cdot s_{j,1}^{(q)}\left[l - D^{(q)}\right] + c_1 \cdot s_{j,2}^{(q)}\left[l - 2 \cdot D^{(q)}\right]\right) \\
& \cdot \left(c_2 \cdot s_{j,0}^{(q)}[l+\tau] + c_2 \cdot s_{j,1}^{(q)}\left[l - D^{(q)} + \tau\right] + c_1 \cdot s_{j,2}^{(q)}\left[l - 2 \cdot D^{(q)} + \tau\right]\right)
\end{aligned} \tag{3.30}$$

Then, for the demonstration, the SACF of equation 3.30 after iteration $q$ is expressed as a function of the aperiodic correlations after the previous iteration $q-1$, as

$$\begin{aligned}
C_{s_{j,0}^{(q+1)},s_{j,0}^{(q+1)}}[\tau] + C_{s_{j,1}^{(q+1)},s_{j,1}^{(q+1)}}[\tau] + C_{s_{j,2}^{(q+1)},s_{j,2}^{(q+1)}}[\tau] = & \left(c_1^2 + 2 \cdot c_2^2\right) \\
& \cdot \left(C_{s_{j,0}^{(q)},s_{j,0}^{(q)}}[\tau] + C_{s_{j,1}^{(q)},s_{j,1}^{(q)}}[\tau] + C_{s_{j,2}^{(q)},s_{j,2}^{(q)}}[\tau]\right) \\
& + \left(c_2^2 + 2 \cdot c_1 \cdot c_2\right) \cdot \xi[\tau]
\end{aligned} \tag{3.31}$$

where $\xi[\tau]$ is equal to:

$$\begin{aligned}
\xi[\tau] = & \sum_{l=0}^{L_{|MultCSS}-1-\tau} \left[s_{j,0}^{(q)}[l] \cdot \left(s_{j,1}^{(q)}\left[l - D^{(q)} + \tau\right] + s_{j,2}^{(q)}\left[l - 2 \cdot D^{(q)} + \tau\right]\right)\right. \\
& + s_{j,1}^{(q)}\left[l - D^{(q)}\right] \cdot \left(s_{j,0}^{(q)}[l+\tau] + s_{j,2}^{(q)}\left[l - 2 \cdot D^{(q)} + \tau\right]\right) \\
& \left. + s_{j,2}^{(q)}\left[l - 2 \cdot D^{(q)}\right] \cdot \left(s_{j,0}^{(q)}[l+\tau] + s_{j,1}^{(q)}\left[l - D^{(q)} + \tau\right]\right)\right]
\end{aligned} \tag{3.32}$$

In order to cancel the cross-term $\xi[\tau]$, the term $c_2^2 + 2 \cdot c_1 \cdot c_2$ must be zero. Notice that this condition is the same as stated in equation 3.27 for $K_{|MultCSS} = 3$. Now, iterating $Q-1$ times more the expression 3.31 it is obtained the SACF as a function of the initial

conditions as

$$C_{s_{j,0}^{(Q)},s_{j,0}^{(Q)}}[\tau] + C_{s_{j,1}^{(Q)},s_{j,1}^{(Q)}}[\tau] + C_{s_{j,2}^{(Q)},s_{j,2}^{(Q)}}[\tau] = (c_1^2 + 2\cdot c_2^2)^Q \cdot \left(C_{s_{j,0}^{(0)},s_{j,0}^{(0)}}[\tau] + C_{s_{j,1}^{(0)},s_{j,1}^{(0)}}[\tau] + C_{s_{j,2}^{(0)},s_{j,2}^{(0)}}[\tau]\right) = 3\cdot\left(c_1^2 + 2\cdot c_2^2\right)^Q \cdot \delta[\tau] \quad (3.33)$$

■

In general, the SACF for a multilevel CSS of $K_{|MultCSS}$ sequences generated as previously defined is

$$\sum_{i=0}^{K_{|MultCSS}-1} C_{s_{j,i}^{(Q)},s_{j,i}^{(Q)}}[\tau] = \left[c_1^2 + \left(K_{|MultCSS}-1\right)\cdot c_2^2\right]^Q \cdot \sum_{i=0}^{K_{|MultCSS}-1} C_{s_{j,i}^{(0)},s_{j,i}^{(0)}}[\tau] = K_{|MultCSS}\cdot\left[c_1^2 + \left(K_{|MultCSS}-1\right)\cdot c_2^2\right]^Q \cdot \delta[\tau] \quad (3.34)$$

where the term $[c_1^2 + (K_{|MultCSS}-1)\cdot c_2^2]^Q$ represents the energy of the sequences of the set.

Now, for generating $K_{|MultCSS}$ uncorrelated multilevel CSS, the proper initial conditions in the equation 3.28 must be chosen; and we demonstrate that the initial conditions must be equal to:

$$\left[\begin{array}{cccc} \breve{\mathbf{S}}_0^{(0)}[l] & \breve{\mathbf{S}}_1^{(0)}[l] & \cdots & \breve{\mathbf{S}}_{K_{|MultCSS}-1}^{(0)}[l] \end{array}\right]^T = \delta[l]\cdot\mathcal{F}_{K_{|MultCSS}} \quad (3.35)$$

where $\mathcal{F}_{K_{|MultCSS}}$ is an arbitrary Hadamard matrix of order $K_{|MultCSS}$.

*Proof.* Again, for the sake of clarity the demonstration is carried out for $K_{|MultCSS} = 3$ uncorrelated multilevel CSS. As stated in equation 2.17 (Chapter 2, section 2.3.4), two CSS are uncorrelated if the sum of the aperiodic correlation functions are zero for all time shifts $\tau$. The aperiodic correlations between the sequences of the $j$-th complementary set

and the sequences of the $j'$-th set ($j \neq j'$) are as follows:

$$\begin{aligned}
C_{s_{j,0}^{(q+1)},s_{j',0}^{(q+1)}}[\tau] = & \sum_{l=0}^{L_{|MultCSS}-1-\tau} \left(c_1 \cdot s_{j,0}^{(q)}[l] + c_2 \cdot s_{j,1}^{(q)}\left[l - D^{(q)}\right] + c_2 \cdot s_{j,2}^{(q)}\left[l - 2 \cdot D^{(q)}\right]\right) \\
& \cdot \left(c_1 \cdot s_{j',0}^{(q)}[l+\tau] + c_2 \cdot s_{j',1}^{(q)}\left[l - D^{(q)} + \tau\right] + c_2 \cdot s_{j',2}^{(q)}\left[l - 2 \cdot D^{(q)} + \tau\right]\right) \\
C_{s_{j,1}^{(q+1)},s_{j',1}^{(q+1)}}[\tau] = & \sum_{l=0}^{L_{|MultCSS}-1-\tau} \left(c_2 \cdot s_{j,0}^{(q)}[l] + c_1 \cdot s_{j,1}^{(q)}\left[l - D^{(q)}\right] + c_2 \cdot s_{j,2}^{(q)}\left[l - 2 \cdot D^{(q)}\right]\right) \\
& \cdot \left(c_2 \cdot s_{j',0}^{(q)}[l+\tau] + c_1 \cdot s_{j',1}^{(q)}\left[l - D^{(q)} + \tau\right] + c_1 \cdot s_{j',2}^{(q)}\left[l - 2 \cdot D^{(q)} + \tau\right]\right) \\
C_{s_{j,2}^{(q+1)},s_{j',2}^{(q+1)}}[\tau] = & \sum_{l=0}^{L_{|MultCSS}-1-\tau} \left(c_2 \cdot s_{j,0}^{(q)}[l] + c_2 \cdot s_{j,1}^{(q)}\left[l - D^{(q)}\right] + c_1 \cdot s_{j,2}^{(q)}\left[l - 2 \cdot D^{(q)}\right]\right) \\
& \cdot \left(c_2 \cdot s_{j',0}^{(q)}[l+\tau] + c_2 \cdot s_{j',1}^{(q)}\left[l - D^{(q)} + \tau\right] + c_1 \cdot s_{j',2}^{(q)}\left[l - 2 \cdot D^{(q)} + \tau\right]\right)
\end{aligned} \tag{3.36}$$

The restriction of equation 3.27 in the entries of the Hadamard matrix $\boldsymbol{\mathcal{C}}_{K_{|MultCSS}}$ for $K_{|MultCSS} = 3$, implies that $c_2 = -2 \cdot c_1$. Considering this relation and developing equation 3.36, the sum of cross-correlation functions between the $j$-th set and the $j'$-th set after iteration $q$ can be expressed as a function of the correlations after iteration $q-1$ as

$$\sum_{i=0}^{2} C_{s_{j,i}^{(q+1)},s_{j',i}^{(q+1)}}[\tau] = \left(2 \cdot c_2^2 + c_1^2\right) \cdot \sum_{i=0}^{2} C_{s_{j,i}^{(q)},s_{j',i}^{(q)}}[\tau] \tag{3.37}$$

Now, iterating equation 3.37 $Q-1$ times, the SCCF is expressed as

$$\sum_{i=0}^{2} C_{s_{j,i}^{(q+1)},s_{j',i}^{(q+1)}}[\tau] = \left(2 \cdot c_2^2 + c_1^2\right)^Q \cdot \sum_{i=0}^{2} C_{s_{j,i}^{(0)},s_{j',i}^{(0)}}[\tau] \tag{3.38}$$

Recalling the definition of uncorrelated CSS (refer to equation 2.17), and considering the initial condition of the $i$-th sequence of the $j$-th set as $\gamma_{i,j} \cdot \delta[l]$ ($0 \leq j, i \leq K_{|MultCSS}-1$) where $\gamma_{i,j} \in \mathbb{R} - \{0\}$, the following expression must be hold to generate uncorrelated CSS:

$$\sum_{i=0}^{2} \gamma_{i,j} \cdot \gamma_{i,j'} = 0 \tag{3.39}$$

Notice that the previous expression is held by the entries of any existent Hadamard matrix of order $K_{|MultCSS} = 3$ if $\gamma_{i,j}$ is assumed to be the entry of the row $i$ and the column $j$ with modulus $\gamma$. ■

Here it is assumed that the matrix defined in equation 3.26 is used to determine the initial conditions. Therefore, in general, the modulus of the initial conditions $\gamma_{i,j}$ are defined for any $K_{|MultCSS} \geq 3 - \{4\}$ as follows:

$$\begin{bmatrix} \gamma_{0,0} & \gamma_{0,1} & \gamma_{0,2} & \cdots & \gamma_{0,K_{|MultCSS}-1} \\ \gamma_{1,0} & \gamma_{1,1} & \gamma_{1,2} & \cdots & \gamma_{1,K_{|MultCSS}-1} \\ \vdots & \vdots & \vdots & \ddots & \vdots \\ \gamma_{K_{|MultCSS}-2,0} & \gamma_{K_{|MultCSS}-2,1} & \gamma_{K_{|MultCSS}-2,2} & \cdots & \gamma_{K_{|MultCSS}-2,K_{|MultCSS}-1} \\ \gamma_{K_{|MultCSS}-1,0} & \gamma_{K_{|MultCSS}-1,1} & \gamma_{K_{|MultCSS}-1,2} & \cdots & \gamma_{K_{|MultCSS}-1,K_{|MultCSS}-1} \end{bmatrix} = \begin{bmatrix} c_1 & c_2 & c_2 & \cdots & c_2 \\ c_2 & c_1 & c_2 & \cdots & c_2 \\ \vdots & \ddots & \ddots & \ddots & \vdots \\ c_2 & \cdots & c_2 & c_1 & c_2 \\ c_2 & \cdots & c_2 & c_2 & c_1 \end{bmatrix} \tag{3.40}$$

and the initial conditions of the algorithm must be equal to:

$$\begin{bmatrix} s^{(0)}_{0,0}[l] & s^{(0)}_{1,0}[l] & \cdots & s^{(0)}_{K_{|MultCSS}-1,0}[l] \\ s^{(0)}_{0,1}[l] & s^{(0)}_{1,1}[l] & \cdots & s^{(0)}_{K_{|MultCSS}-1,1}[l] \\ \vdots & \vdots & \ddots & \vdots \\ s^{(0)}_{0,K_{|MultCSS}-1}[l] & s^{(0)}_{1,K_{|MultCSS}-1}[l] & \cdots & s^{(0)}_{K_{|MultCSS}-1,K_{|MultCSS}-1}[l] \end{bmatrix} = \delta[l] \cdot \boldsymbol{\mathcal{C}}_{K_{|MultCSS}} \tag{3.41}$$

Hence, the algorithm stated in equation 3.28 is redefined in order to generate $K_{|MultCSS} \geq 3 - \{4\}$ uncorrelated multilevel CSS of length $L_{|MultCSS} = K^{Q}_{|MultCSS}$ as

$$\begin{bmatrix} \breve{\mathbf{S}}^{(0)}_0[l] & \breve{\mathbf{S}}^{(0)}_1[l] & \cdots & \breve{\mathbf{S}}^{(0)}_{K_{|MultCSS}-1}[l] \end{bmatrix} = \delta[l] \cdot \boldsymbol{\mathcal{C}}_{K_{|MultCSS}}$$
$$\breve{\mathbf{S}}^{(q+1)}_j[l] = \boldsymbol{\mathcal{C}}_{K_{|MultCSS}} \times \breve{\mathbf{D}}^{(q)}[l] \times \breve{\mathbf{S}}^{(q)}_j[l] \tag{3.42}$$

Figure 3.3 depicts the architecture of the proposed algorithm for $K_{|MultCSS} \geq 3 - \{4\}$ uncorrelated multilevel CSS.

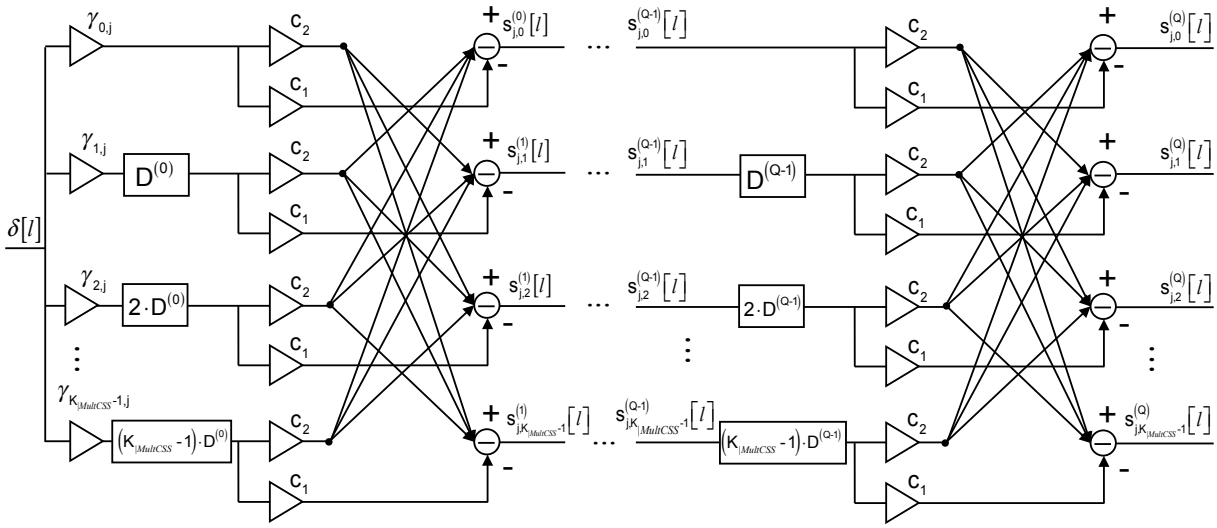


Figure 3.3: Architecture of the generation algorithm for $K_{|MultCSS} \geq 3-\{4\}$ uncorrelated multilevel CSS.

### 3.3.1 Number of Amplitude Levels and Amplitude Values

The number of amplitude levels of the multilevel CSS generated with the algorithm of equation 3.42 is equal to:

$$N_\ell = Q + 2 \tag{3.43}$$

The previous expression can be demonstrated considering that:

- The number of amplitude levels of the matrix $\boldsymbol{\mathcal{C}}_{K_{|MultCSS}}$ is equal to two (the entries $c_1$ and $c_2$).
- There is no overlaps in each stage due to the fact that the delay values $D^{(q)}$ are chosen as any permutation of the set $\{K^0_{|MultCSS}, K^1_{|MultCSS}, \ldots, K^{Q-1}_{|MultCSS}\}$
- The initial conditions are chosen from the same matrix $\boldsymbol{\mathcal{C}}_{K_{|MultCSS}}$.

Table 3.3 shows the number of amplitude levels and their values for different $K_{|MultCSS}$ and number of stages $Q$. In order to construct multilevel CSS with an integer alphabet, the entries of the Hadamard matrix $\boldsymbol{\mathcal{C}}_{K_{|MultCSS}}$ ($c_1$ and $c_2$) are chosen as $c_1 = \frac{(K_{|MultCSS}-2)}{2}$, $c_2 = -1$ for $K_{|MultCSS}$ even and $c_1 = K_{|MultCSS} - 2$, $c_2 = -2$ for $K_{|MultCSS}$ odd.

| $K_{\|MultCSS}$ | $Q$ | $N_\ell$ | $V_\ell$ | | | | |
|---|---|---|---|---|---|---|---|
| 3 | 1 | 3 | 1 | −2 | 4 | – | – |
| | 2 | 4 | 1 | −2 | 4 | −8 | – |
| | 3 | 5 | 1 | −2 | 4 | −8 | 16 |
| 5 | 1 | 3 | 4 | −6 | 9 | – | – |
| | 2 | 4 | −8 | 12 | −18 | 27 | – |
| | 3 | 5 | 16 | −24 | 36 | −54 | 81 |
| 6 | 1 | 3 | 1 | −2 | 4 | – | – |
| | 2 | 4 | −1 | 2 | −4 | 8 | – |
| | 3 | 5 | 1 | −2 | 4 | −8 | 16 |

Table 3.3: Number and amplitude levels for different $K_{|MultCSS}$-CSS obtained for $1 \leq Q \leq 3$.

Hence, it can be demonstrated that the amplitude values, $V_\ell$ , of the sequences are as follows:

$$V_\ell = \begin{cases} (-1)^{Q+1+\Phi} \cdot \left(\frac{K_{|MultCSS}-2}{2}\right)^{\Phi} & for\ K_{|MultCSS}\ even \\ (-2)^{Q+1} \cdot \left(\frac{2-K_{|MultCSS}}{2}\right)^{\Phi} & for\ K_{|MultCSS} \neq 3\ odd \\ \left[2 \cdot \left(2 - K_{|MultCSS}\right)\right]^{\Phi} & for\ K_{|MultCSS} = 3 \end{cases} \tag{3.44}$$

where $\Phi \in \{0, \ldots, Q+1\}$, $Q \geq 1$.

**Example.** If we generate $K_{|MultCSS} = 3$ multilevel CSS of length $L_{|MultCSS} = 27$ ($Q = 3$), obtained with the parameter values $c_1 = 1$, $c_2 = -2$ and initial conditions equal to the ones shown in equation 3.45, the number of amplitude values are given by the combinations without repetition of the sets $\{(1,-2) \times (1,-2) \times (1,-2) \times (1,-2)\}$. The first set is due to the initial conditions and the other three because of the number of stages, $Q$).

$$\begin{aligned} \begin{bmatrix} s_{0,0}^{(0)}[l] & s_{1,0}^{(0)}[l] & s_{2,0}^{(0)}[l] \\ s_{0,1}^{(0)}[l] & s_{1,1}^{(0)}[l] & s_{2,1}^{(0)}[l] \\ s_{0,2}^{(0)}[l] & s_{1,2}^{(0)}[l] & s_{2,2}^{(0)}[l] \end{bmatrix} &= \delta[l] \cdot \begin{bmatrix} \gamma_{0,0} & \gamma_{0,1} & \gamma_{0,2} \\ \gamma_{1,0} & \gamma_{1,1} & \gamma_{1,2} \\ \gamma_{2,0} & \gamma_{2,1} & \gamma_{2,2} \end{bmatrix} \\ &= \delta[l] \cdot \begin{bmatrix} 1 & -2 & -2 \\ -2 & 1 & -2 \\ -2 & -2 & 1 \end{bmatrix} \end{aligned} \tag{3.45}$$

Therefore, the number of levels of the sequences is $N_\ell = 5$ and their values are $V_\ell = \{1, -2, 4, -8, 16\}$ (refer also to Table 3.3). Figure 3.4 depicts the first set $\breve{\mathbf{S}}_0^{(Q)}[l]$ generated with the previous parameter values and the delay distribution $\{3^2, 3^1, 3^0\}$, while Figure

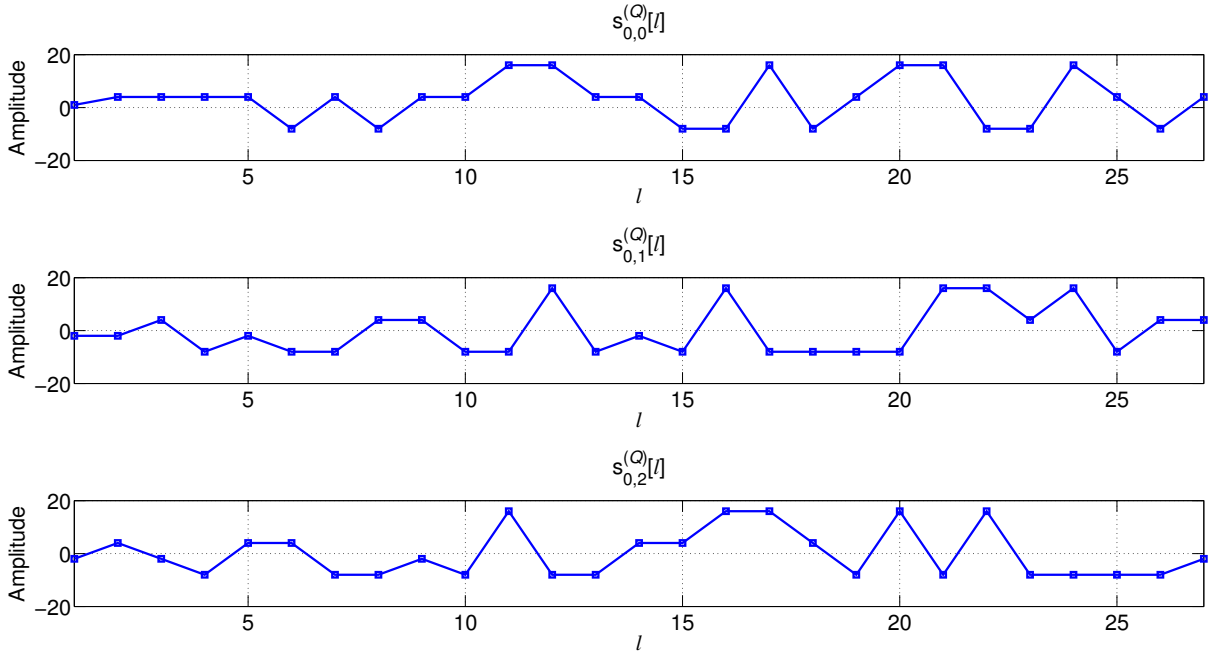


Figure 3.4: Multilevel complementary set $\breve{\mathbf{S}}_0^{(Q)}[l]$ of $K_{|MultCSS} = 3$ sequences of length $L_{|MultCSS} = 27$.

3.5 shows the aperiodic auto-correlations and the SACF of this set and the aperiodic cross-correlations and SCCF with the multilevel CSS $\breve{\mathbf{S}}_1^{(Q)}[l]$ (the same SCCF is obtained with the other multilevel CSS $\breve{\mathbf{S}}_2^{(Q)}[l]$).

▲

## 3.4 Feasible Lengths of the Multilevel CSS

In the previous sections we have shown modular architectures for the generation of $K_{|MultCSS}$ multilevel CSS of length $L_{|MultCSS} = K^Q_{|MultCSS}$, based on generalizations of previous algorithms for binary CSS. In those algorithms, the length of the generated sequences is determined by the entry values $D^{(q)}$ of the matrices $\mathbf{D}^{(k,q)}[l]$ and $\breve{\mathbf{D}}^{(q)}[l]$ (refer to equation 3.15), which is chosen as any permutation of the set $\{K^0_{|MultCSS}, K^1_{|MultCSS}, \ldots, K^{Q-1}_{|MultCSS}\}$. In the multilevel case, these entries can be chosen as:

1. Any permutation of the set $\{K^0_{|MultCSS}, K^1_{|MultCSS}, \ldots, K^{Q-1}_{|MultCSS}\}$ in order to avoid overlaps in the generation process and to generate the complementary set in a reduced number of stages, $Q = \frac{log_2(L_{|MultCSS})}{log_2(K_{|MultCSS})}$. This is convenient for reducing computational costs. In fact, this is the basis of the construction of efficient al-

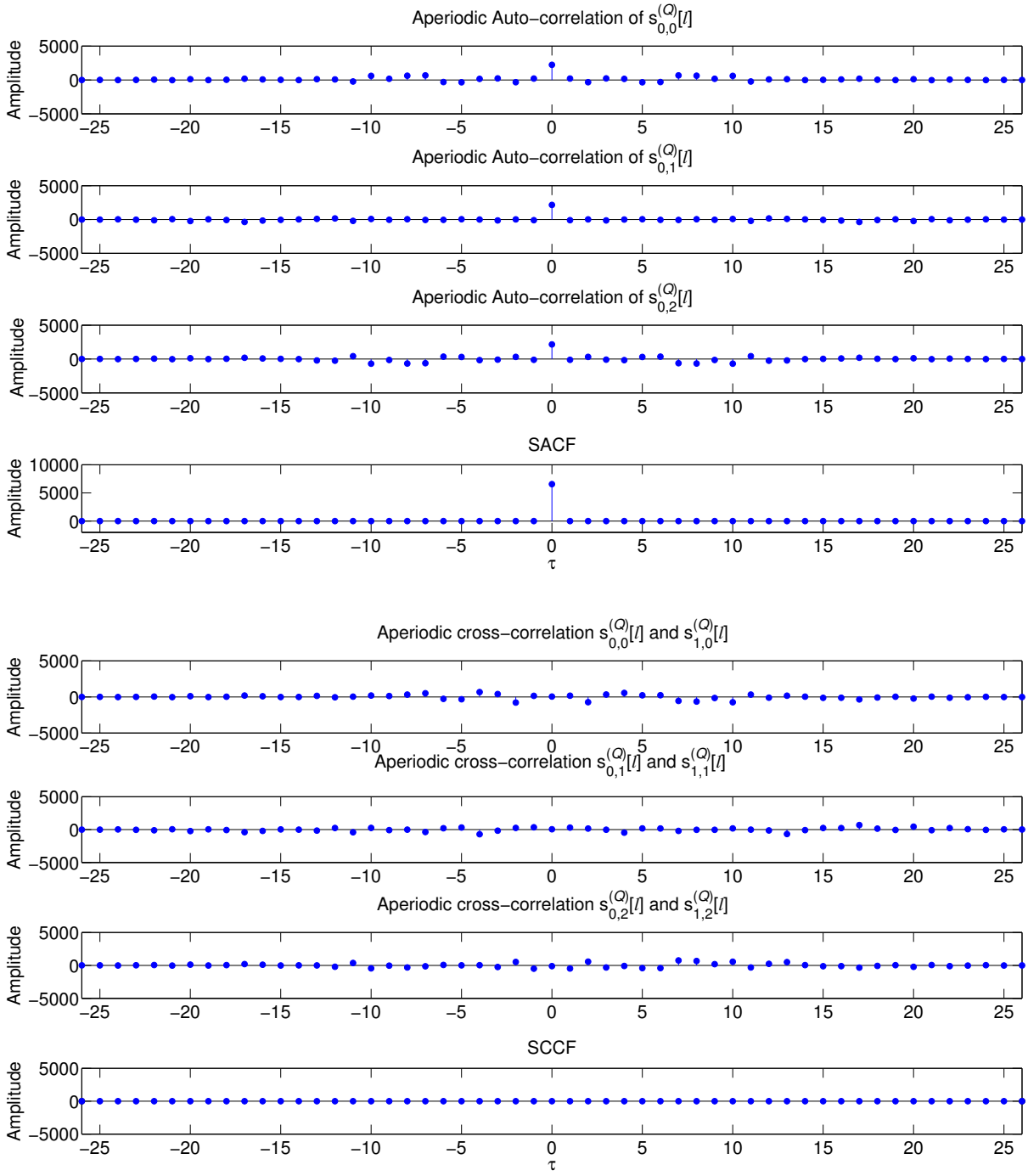


Figure 3.5: SACF of the multilevel CSS $\breve{\mathbf{S}}_0^{(Q)}[l]$ of Figure 3.4 and the SCCF with the multilevel CSS $\breve{\mathbf{S}}_1^{(Q)}[l]$.

gorithms for any CSS. In order to reduce the total number of memory bits it is suggested in [Alvar 04, Perez 07a] for the binary case the permutation $\{K_{|MultCSS}^{Q-1}, K_{|MultCSS}^{Q-2}, \ldots, K_{|MultCSS}^{0}\}$. In this case, the number of levels of the multilevel CSS generated are defined by equation 3.22 (when the terms $A^{(q)}$ are co-prime numbers) and equation 3.43.

2. Any delay values $D^{(q)}$, $D^{(q)} > 0$ so the multilevel CSS generated have a length equal to $L_{|MultCSS} = (K_{|MultCSS}-1)\cdot\sum_{q=0}^{Q-1} D^{(q)}+1$. Notice that the modular architectures presented in this chapter generate $K_{|MultCSS}$ uncorrelated CSS, independently of the entry values $D^{(q)}$ of the matrices $\mathbf{D}^{(k,q)}[l]$ or $\breve{\mathbf{D}}^{(q)}[l]$. In this case, the number and value of levels depend on: the overlaps introduced by the delay arrangement, the parameters $A^{(q)}$ for the generation algorithm of $K_{|MultCSS} = 2^k$ multilevel CSS, and $c_1$ and $c_2$ for the generation algorithm of $K_{|MultCSS} \geq 3 - \{4\}$ multilevel CSS. This approximation can serve as a basis for the search of the optimal parameters that efficiently generates multilevel CSS with low PAPR, as we will show later.

3. A trade-off solution between the number of stages ($Q$) and the flexibility of the generated CSS lengths is to maintain the delays $D^{(q)}$ of the first $Q-1$ iterations to $D^{(q)} = \{K_{|MultCSS}^{0}, K_{|MultCSS}^{1}, \ldots, K_{|MultCSS}^{Q-2}\}$ and to modify the delays of the last iteration, $D^{(Q-1)}$, in order to hold the following expression:

$$D^{(Q-1)} = \left\lceil \frac{L_{|MultCSS} - K_{|MultCSS}^{Q-1}}{K_{|MultCSS} - 1} \right\rceil \tag{3.46}$$

where $\lceil x \rceil$ represents the smallest integer larger of equal to $x$. In equation 3.46 the difference between the final length $L_{|MultCSS}$ and the CSS length at iteration $Q-1$ is divided by $K_{|MultCSS}-1$ because at a given stage $q$, the same delay $D^{(q)}$ is applied to the sequences $\{s_{j,0}^{(q)}[l], \ldots, s_{j,K_{|MultCSS-1}}^{(q)}[l]\}$, (refer to equation 3.20). Hence, in the case that the final sequence length $L_{|MultCSS}$ is not equal to $K_{|MultCSS}^{Q}$, the delay of the last stage is not a power-of-two number and the number of stages of the algorithm is equal to:

$$Q = \left\lceil \frac{log_2\left(L_{|MultCSS}\right)}{log_2\left(K_{|MultCSS}\right)} \right\rceil \tag{3.47}$$

## 3.5 Multilevel CSS with Low PAPR

In order to demonstrate the feasibility of generating multilevel CSS with low Peak-to-Average Power Ratio (PAPR) we have carried out a computer search by means of an evolutionary algorithm. Given a real sequence $x[l]$ of length $L$, $0 \leq l \leq L-1$, the PAPR is defined as [Popov 99b]:

$$PAPR = \frac{\max |x\,[l]|^2}{\frac{1}{L} \cdot \sum_{l=0}^{L-1} |x\,[l]|^2} \tag{3.48}$$

This parameter is commonly used in multi-carrier communication systems to analyze the linearity requirements of the power amplifiers at the emission stage. In order to improve the energy efficiency, it is desired sequences with a low PAPR, i.e. sequences the most uniform as possible.

We have used a genetic algorithm to find the parameters $D^{(q)}$, $A^{(q)}$, $W^{(1,q)}$ and $Q$ that generates $K_{|MultCSS} = 2$ multilevel CSS with a reduced PAPR. For that we have considered values $A^{(q)}$ bounded by $-1 \leq A^{(q)} \leq 1$, seed values $W^{(1,q)} \in \{-1, +1\}$ and delays $D^{(q)}$, $1 \leq q \leq Q-1$, which can take the values $1 \leq D^{(q)} \leq L_{|MultCSS} - Q$.

Interestingly, the algorithm is capable to find a combination of parameters $D^{(q)}$, $A^{(q)}$, $W^{(1,q)}$ and $Q$, and it turns out that the generated sequences are some of the optimal ternary complementary pairs found in [Gavis 94, Gysin 01] over the alphabet $\{+1, -1, 0\}$ up to normalization. The term optimal is used in the sense that the ternary complementary pairs have the minimum number of zero elements. Table 3.4 depicts the optimal ternary complementary pairs up to length 12, generated with the proposed generalized algorithm for $K_{|MultCSS} = 2$.

For the sake of compactness, the ternary complementary pairs have been depicted assuming that the elements with signs + and − have unit modulus. Notice that binary complementary pairs exist for the lengths 2, 4, 8, and 10 and thus they are not included in the Table 3.4; observe also that for each given length, the uncorrelated pair can be generated by changing the sign of the seed value $W^{(1,0)}$. To the best knowledge of the author, there is only known optimal ternary complementary pairs up to length 22 [Gysin 01], although it is known the minimum feasible number of zero elements in ternary complementary pairs for lengths up to 100 [Craig 06]. For lengths larger than 3, the proposed generalized algorithm for $K_{|MultCSS} = 2$ generates optimal ternary complementary pairs in less stages than the standard lattice filter, and therefore with less number of operations (refer to Chapter 2, Figure 2.15).

| Length | Pair | $Q$ | $A^{(q)}$ | $W^{(1,q)}$ | $D^{(q)}$ |
|---|---|---|---|---|---|
| 3 | $++-$<br>$+0+$ | 2 | $\{\frac{1}{2},+1\}$ | $\{+1,+1\}$ | $\{1,1\}$ |
| 5 | $+-0++$<br>$-+0++$ | 2 | $\{-1,-1\}$ | $\{+1,+1\}$ | $\{1,3\}$ |
| 6 | $++-0-+$<br>$++0+-$ | 3 | $\{+1,-\frac{1}{2},+1\}$ | $\{+1,+1,+1\}$ | $\{1,2,2\}$ |
| 7 | $+--0+0+$<br>$+0+0++-$ | 3 | $\{+1,-\frac{1}{2},+1\}$ | $\{+1,+1,+1\}$ | $\{4,1,1\}$ |
| 9 | $+++-0++-+$<br>$+++-0--+-$ | 3 | $\{+1,+1,+1\}$ | $\{+1,+1,+1\}$ | $\{1,2,5\}$ |
| 11 | $+---000-+--$<br>$--+-000+++-$ | 3 | $\{-1,+1,-1\}$ | $\{+1,+1,+1\}$ | $\{7,2,1\}$ |
| 12 | $+-+++-+00-+++$<br>$+-++00+++---$ | 4 | $\{+1,+1,-\frac{1}{2},+1\}$ | $\{-1,+1,+1,+1\}$ | $\{1,2,4,4\}$ |

Table 3.4: Optimal ternary complementary pairs up to length 12 given in [Gavis 94, Gysin 01]. They are generated with the proposed generalized algorithm for $K_{|MultCSS} = 2$.

## 3.6 Efficient Correlators for Multilevel CSS

With the two previous modular architectures, we can generate $K_{|MultCSS}$ multilevel CSS for any $K_{|MultCSS} > 2$. Both architectures are FIR filters whose impulse responses are the multilevel CSS. Consequently, it is possible to design modular architectures for the correlation of $K_{|MultCSS}$ multilevel CSS if the proposed generators are modified to generate the reversed sequences (refer to the definition of aperiodic correlation of equation 2.4 in Chapter 2, section 2.3.4). This is simply done by interchanging the order of the delays in each stage of the generators depicted in Figure 3.1 and Figure 3.3, resulting in the correlators of Figure 3.7 and Figure 3.6 respectively, where the terms $\phi_{r,s_{j,i}^{(q)}}[l]$ are intermediate results, different from the aperiodic correlation function, which only appears at the end of the final stage.

The proposed generalized architectures for multilevel CSS of lengths $K^{Q}_{|MultCSS}$ permit to reduce the computational load needed to perform the generation/correlation of the multilevel CSS in comparison with the Tapped Delay Line (i.e. straightforward) architecture. This is accomplished thanks to the delay matrix of the Wornell algorithm that reduces the number of stages needed for a given length $K^{Q}_{|MultCSS}$. Table 3.5 shows a comparison between the number of operations needed for the generation and correlation of a multilevel complementary sequence from a CSS of $K_{|MultCSS}$ sequences with a straightforward architecture and with the ones analyzed here. To perform the sum of aperiodic

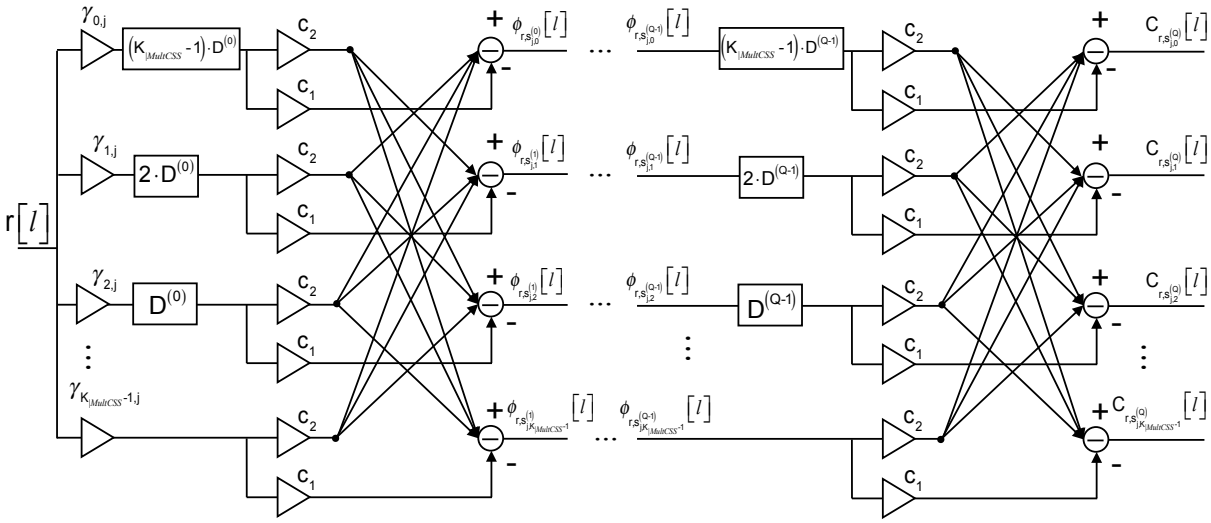

Figure 3.6: Architecture of the correlator for $K_{|MultCSS} \geq 3 - \{4\}$ multilevel complementary sets of sequences.

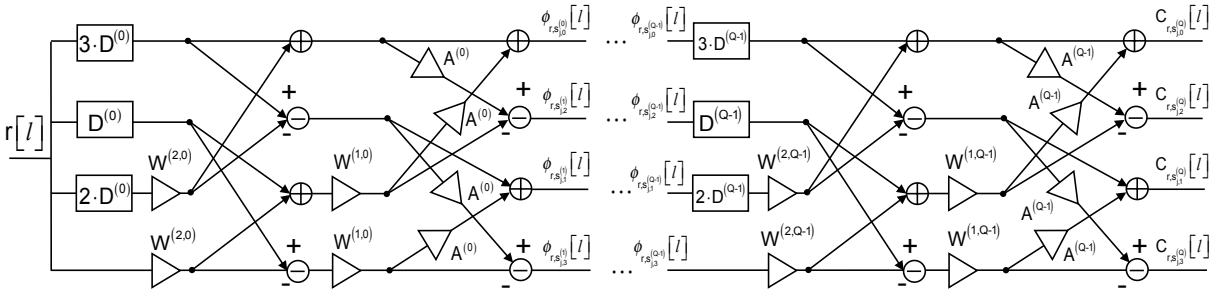

Figure 3.7: Architecture of the correlator for $K_{|MultCSS} = 2^k$ multilevel complementary sets of sequences.

| | Implementation | Multiplications | Additions |
|---|---|---|---|
| Any $K_{\|MultCSS}$ | Straightforward | $K^{Q}_{\|MultCSS}$ | $K^{Q}_{\|MultCSS} - 1$ |
| $K_{\|MultCSS} = 2^k$ | Efficient | $Q \cdot K_{\|MultCSS}$ | $Q \cdot K_{\|MultCSS} \cdot log_2(K_{\|MultCSS})$ |
| $K_{\|MultCSS} \geq 3 - \{4\}$ | Efficient | $K_{\|MultCSS} \cdot (1 + 2 \cdot Q)$ | $Q \cdot K_{\|MultCSS} \cdot (K_{\|MultCSS} - 1)$ |

Table 3.5: Operations needed for the generation/correlation of a multilevel CSS of $K_{|MultCSS}$ sequences with the straightforward architecture and with the proposed one with the delay distribution of [De Ma 07].

correlations functions, it is necessary to replicate the architectures (straightforward and the proposed) $K_{|MultCSS} - 1$ times more and to carry out an extra addition.

Additionally, Table 3.6 represents some examples of the required operations for a given CSS. For example, the number of additions and products needed for the correlation of $K_{|MultCSS} = 6$ multilevel CSS of length $L_{|MultCSS} = 216$ with the proposed architecture is more than three times lower than those needed with a straightforward correlator. It is important to notice that the proposed architectures still require less operations than FFT-based correlations (refer to Chapter 2, section 2.5.2).

The multipliers indicated in Table 3.5 and Table 3.6 can be implemented in an efficient form, by using the Signed Power-of-Two (SPT) representation [Lim 99], requiring only shifts and additions for their implementation. This is preferable to the use of dedicated multipliers, which are limited in number in reconfigurable platforms as FPGAs-based. Due to the internal operations carried out in these architectures, the data bus width must be increased in each stage to avoid overflow, and therefore, the total number of memory bits can be higher than the required in a straightforward architecture [Alvar 04, Perez 07a]. Nevertheless, it is demonstrated in [Alvar 04] that in these architectures the total number of memory bits can be minimized if the delay permutation is chosen as $\{K^{Q-1}_{|MultCSS}, K^{Q-2}_{|MultCSS}, \ldots, K^{0}_{|MultCSS}\}$ (notice that this does not happen in the Wornell algorithm). Additionally, it is demonstrated in [Vaidy 90] that the lattice architectures, as the ones proposed here, are very robust to severe quantization effects.

## 3.7 Conclusions

In this chapter we have introduced generalizations of efficient algorithms for $K_{|MultCSS} = 2$ (generalization of Budišin's algorithms) and for $K_{|MultCSS} = 2^k$ ($k \in \mathbb{N} - \{0\}$) (generalization of De Marziani's algorithm). We have also proposed a novel algorithm for $K_{|MultCSS} \geq 3 - \{4\}$ by using circulant multilevel Hadamard matrices and certain initial

| | Implementation | $(K_{\|MultCSS}, L_{\|MultCSS}, Q)$ | Multiplications | Additions |
|---|---|---|---|---|
| $K_{\|MultCSS} = 2^k$ | Straightforward | $(2, 128, 7)$ | 128 | 127 |
| | | $(4, 64, 3)$ | 64 | 63 |
| | | $(8, 64, 2)$ | 64 | 63 |
| | Efficient | $(2, 128, 7)$ | 14 | 14 |
| | | $(4, 64, 3)$ | 12 | 24 |
| | | $(8, 64, 2)$ | 16 | 48 |
| $K_{\|MultCSS} \geq 3 - \{4\}$ | Straightforward | $(3, 81, 4)$ | 81 | 80 |
| | | $(5, 125, 3)$ | 125 | 124 |
| | | $(6, 216, 3)$ | 216 | 215 |
| | Efficient | $(3, 81, 4)$ | 27 | 24 |
| | | $(5, 125, 3)$ | 35 | 60 |
| | | $(6, 216, 3)$ | 42 | 90 |

Table 3.6: Examples of the operations needed for the generation/correlation of $K_{|MultCSS}$ multilevel CSS with the straightforward architecture and with the proposed one for several lengths.

conditions. Both generalizations permit to generate and correlate efficiently any multilevel CSS with $K_{|MultCSS} > 2$.

On the other hand, by penalizing the efficiency of the generalized algorithms, it is possible to use different delay patterns to generate and correlate multilevel CSS of more number of lengths than in the binary case. By searching the parameters $A^{(q)}$, $D^{(q)}$, $W^{(1,q)}$ and $Q$ that generate multilevel complementary pairs with low PAPR, we have demonstrated for lengths lower than 13, that the generalization of Budišin's algorithm can generate and correlate optimal ternary complementary sequences. For lengths larger than 3, the algorithm generates them in less stages than the standard lattice filter. Therefore, the proposals can be the basis for the search of the parameters that generate multilevel CSS with low PAPR without changing the architecture of the generator/correlator.

# Chapter 4

# Efficient Architectures for the Generation and Correlation of Binary CSS

In Chapter 2, section 2.7, we saw that the efficient architectures for the generation and correlation of binary CSS only dealt with $K_{|CSS} = 2^k$ binary CSS of lengths $L_{|CSS} = K_{|CSS}^Q$ [De Ma 07, Funes 10], with the exception of the architecture proposed by Budišin for Golay binary sequence pairs ($K_{|CSS} = 2$) of lengths $L_{|Gol} = 2^N \cdot 10^M$ (where $N$, $M$ are non-negative integers and $k, Q \in \mathbb{N}\text{-}\{0\}$) [Budis 11]. Also from Table 2.4 of Chapter 2, we concluded that efficient architectures could be proposed for lengths $L_1 \cdot 2^N \cdot 10^M \cdot 26^P$, where $L_1$ is an integer for which binary CSS of length $L_1$ exist, and $N$, $M$ and $P$ are non-negative integers.

This chapter presents the following contributions:

- Firstly, we demonstrate that the Golay kernel 26 has an inner structure by proposing a decomposition of this kernel.

- Secondly, we propose an efficient generator/correlator for $K_{|CSS} = 2$ binary CSS (also known as Golay sequence pairs) of length $L_{|Gol} = 2^N \cdot 10^M \cdot 26^P$ made up of $Q = N+4\cdot M+12\cdot P$ stages of a lattice filter. This contribution uses the architecture introduced in Chapter 2 for the generation/correlation of $K_{|MultCSS} = 2$ multilevel CSS, the Golay kernel 10 decomposition introduced by Budišin [Budis 11] and the decomposition of the Golay kernel 26 proposed also in this chapter.

- Finally, we generalize the previous efficient architecture to $K_{|CSS} = 2^k$ binary CSS of length $L_{|CSS} = \frac{K_{|CSS}}{2} \cdot 2^N \cdot 10^M \cdot 26^P$ by using the Tseng-Liu interleaving method

(equivalent to the generalized Kronecker product with $M_1 = N_1$ the dimensions of a Hadamard matrix generated with Sylvester's method [Sylve 67]).

These contributions improve the versatility of the previous efficient architectures which only generate $K_{|CSS} = 2^k$ CSS of length $K^Q_{|CSS}$ in $Q = N$ stages.

## 4.1 Golay Kernels Decomposition

In [Budis 11] Budišin demonstrates that the Golay kernel has an inner structure by decomposing it in four stages of an efficient generator. He also suggests that the Golay kernels 20 and 26 have an inner structure, but he did not decomposed them. Moreover, in [Budis 11] the decomposition of the Golay kernel 10 was not shown by using a decomposition method.

In this section we introduce a recursive method for the decomposition of the Golay kernels and we demonstrate that, the Golay kernel 26 has really an inner structure by carrying out its decomposition. The Golay kernel 20 is not decomposed for practical considerations, as the aim of the Golay kernels decomposition is the generation of binary CSS of lengths $L_{|CSS} = L_1 \cdot 2^N \cdot 10^M \cdot 26^P$, but not the mathematical derivation of all the existent complementary sequences for a given length. The length $L_{|Gol} = 20$ can be generated by choosing the exponents $N = 1$, $M = 1$ and $P = 0$.

For the following demonstrations, it is needed to recall the generation algorithm for two Pairs of Multilevel Complementary Sequences (PMCS) introduced in the equation 3.5 (refer to Chapter 3, section 3.1). For convenience, in this chapter we will work in the $Z$-domain and change the nomenclature of the terms $A^{(q)}$ for $A^{(k,q)}$, with $k = log_2 K_{|CSS}$ any integer larger than zero. So, equation 3.5 is expressed as

$$\begin{aligned}
S^{(0)}_{j,0}(z^{-1}) &= 1 \\
S^{(0)}_{j,1}(z^{-1}) &= 1 \\
S^{(q+1)}_{j,0}(z^{-1}) &= S^{(q)}_{j,0}(z^{-1}) + A^{(1,q)} \cdot W^{(1,q)} \cdot S^{(q)}_{j,1}(z^{-1}) \cdot z^{-D^{(q)}} \\
S^{(q+1)}_{j,1}(z^{-1}) &= A^{(1,q)} \cdot S^{(q)}_{j,0}(z^{-1}) - W^{(1,q)} \cdot S^{(q)}_{j,1}(z^{-1}) \cdot z^{-D^{(q)}}
\end{aligned} \tag{4.1}$$

As shown in [Budis 11] for the Golay kernel 10, this algorithm can also generate Golay binary pairs of length $L_{|Gol} = 2^N \cdot 10^M$. Here we will extend the algorithm to generate Golay binary pairs of length $L_{|Gol} = 2^N \cdot 10^M \cdot 26^P$ by using a filter bank approach.

Any $2 \times 1$ FIR lossless system of degree $L-1$ with transfer function $\mathbf{S}(z^{-1})$ and with real coefficients, can be factorized as [Vaidy 90]:

$$\mathbf{S}\left(z^{-1}\right) = \beta \cdot \prod_{l=L-1}^{0} \left\{ \boldsymbol{\mathcal{R}}^{(l)}\left(\theta^{(l)}\right) \times \boldsymbol{\mathcal{P}}\left(z^{-1}\right) \right\} \times \begin{bmatrix} cos\varphi \\ -sin\varphi \end{bmatrix}; \beta, \varphi \in \mathbb{R} \tag{4.2}$$

where $\boldsymbol{\mathcal{R}}^{(l)}(\theta^{(l)})$ represents the following rotation matrix:

$$\boldsymbol{\mathcal{R}}^{(l)}\left(\theta^{(l)}\right) = \begin{bmatrix} cos\theta^{(l)} & sin\theta^{(l)} \\ -sin\theta^{(l)} & cos\theta^{(l)} \end{bmatrix}; \theta^{(l)} \in \mathbb{R} \tag{4.3}$$

and $\boldsymbol{\mathcal{P}}(z^{-1})$ is a paraunitary matrix of the form:

$$\boldsymbol{\mathcal{P}}\left(z^{-1}\right) = \begin{bmatrix} 1 & 0 \\ 0 & z^{-1} \end{bmatrix} \tag{4.4}$$

Notice that this factorization generates a $2 \times 1$ FIR lossless filter regardless of the values of $\beta$ and $\theta^{(l)}$ [Vaidy 90]. Therefore, the previous equation 4.2, known as planar factorization, can be expressed in an equivalent form as

$$\mathbf{S}_j^{(1,Q)}\left(z^{-1}\right) = \alpha \cdot \prod_{q=Q-1}^{0} \left\{ \boldsymbol{\mathcal{R}}^{(q)}\left(\theta^{(q)}\right) \times \boldsymbol{\mathcal{P}}\left(z^{-1}\right) \right\} \times \begin{bmatrix} 1 \\ 1 \end{bmatrix}; \alpha \in \mathbb{R} \tag{4.5}$$

where the rotation matrix, $\boldsymbol{\mathcal{R}}^{(q)}(\theta^{(q)})$ is redefined as [Coker 10]

$$\boldsymbol{\mathcal{R}}^{(q)}\left(\theta^{(q)}\right) = \begin{cases} \begin{bmatrix} 0 & sin\theta^{(q)} \\ -sin\theta^{(q)} & 0 \end{bmatrix} & \text{if } \theta^{(q)} = \pm\dfrac{\pi}{2} \\ \begin{bmatrix} 1 & tan\theta^{(q)} \\ -tan\theta^{(q)} & 1 \end{bmatrix} & \text{otherwise} \end{cases} \tag{4.6}$$

and the matrix $\boldsymbol{\mathcal{P}}^{(q)}(z^{-1})$ is expressed in the following form:

$$\boldsymbol{\mathcal{P}}^{(q)}\left(z^{-1}\right) = \begin{bmatrix} 1 & 0 \\ 0 & W^{(1,q)} \cdot z^{-D^{(q)}} \end{bmatrix} \tag{4.7}$$

This matrix is also a paraunitary matrix as $\boldsymbol{\mathcal{P}}^{(q)}(z^{-1}) \times [\boldsymbol{\mathcal{P}}^{(q)}(z)]^T = \mathbf{I}_2$; $D^{(q)}$ is a delay lower than $L$, which maintains the filter as a causal one and $W^{(1,q)}$ is a complex number of unit magnitude. The generation algorithm of equation 4.1 can be expressed in a matricial form as follows:

$$\begin{aligned}
\mathbf{S}_j^{(1,0)}(z^{-1}) &= \begin{bmatrix} 1 & 1 \end{bmatrix}^T \\
\mathbf{S}_j^{(1,q+1)}(z^{-1}) &= \begin{bmatrix} 1 & A^{(1,q)} \cdot W^{(1,q)} \cdot z^{-D^{(q)}} \\ A^{(1,q)} & -W^{(1,q)} \cdot z^{-D^{(q)}} \end{bmatrix} \times \mathbf{S}_j^{(1,q)}(z^{-1}) \\
&= \mathbf{B}^{(1)}_{A^{(1,q)},W^{(1,q)}}(z^{-D^{(q)}}) \times \mathbf{S}_j^{(1,q)}(z^{-1})
\end{aligned} \tag{4.8}$$

where the basic building block is defined as

$$\mathbf{B}^{(1)}_{A^{(1,q)},W^{(1,q)}}\left(z^{-D^{(q)}}\right) = \begin{bmatrix} 1 & A^{(1,q)} \cdot W^{(1,q)} \cdot z^{-D^{(q)}} \\ A^{(1,q)} & -W^{(1,q)} \cdot z^{-D^{(q)}} \end{bmatrix} \tag{4.9}$$

The previous building block is equivalent to the product $\boldsymbol{\mathcal{R}}^{(q)}(\theta^{(q)}) \times \boldsymbol{\mathcal{P}}(z^{-1})$ of equation 4.5 and therefore, the Golay kernels can be generated by cascading the basic building blocks $\mathbf{B}^{(1)}_{A^{(1,q)},W^{(1,q)}}(z^{-D^{(q)}})$. This factorization leads to a very efficient lattice structure [Budis 91, Popov 99a].

**Example.** In Chapter 2, section 2.7 we stated that the generation of antipodal paraunitary matrices is equivalent to the generation of complementary sets of sequences. A detailed demonstration can be found in [Phoon 05]; here for clarity we show this equivalence with an example. Consider the basic building block of equation 4.9 for the stage $q = 0$. The rows of this matrix conform a multilevel complementary pair of sequences of length $L_{|MultCSS} = D^{(0)} + 1$, for any $D^{(0)} \geq 1$ as we concluded in Chapter 3. For the sake of clarity, we will consider only the delay $D^{(0)} = 1$ for $q = 0$. Hence, the basic building block to analyze is equal to:

$$\mathbf{B}^{(1)}_{A^{(1,0)},W^{(1,0)}}\left(z^{-1}\right) = \begin{bmatrix} 1 & A^{(1,0)} \cdot W^{(1,0)} \cdot z^{-1} \\ A^{(1,0)} & -W^{(1,0)} \cdot z^{-1} \end{bmatrix}$$

and the pairs of multilevel complementary sequences are obtained by means of equation 4.8, and they are equal to:

$$\begin{bmatrix} S_{j,0}^{(1)}(z^{-1}) \\ S_{j,1}^{(1)}(z^{-1}) \end{bmatrix} = \begin{bmatrix} 1 & A^{(1,0)} \cdot W^{(1,0)} \cdot z^{-1} \\ A^{(1,0)} & -W^{(1,0)} \cdot z^{-1} \end{bmatrix} \times \begin{bmatrix} 1 \\ 1 \end{bmatrix}$$
$$= \begin{bmatrix} 1 + A^{(1,0)} \cdot W^{(1,0)} \cdot z^{-1} \\ A^{(1,0)} - W^{(1,0)} \cdot z^{-1} \end{bmatrix}$$

It is defined now the aperiodic correlation between two sequences $x[l]$ and $y[l]$, with $Z$-transforms equal to $X(z^{-1})$ and $Y(z^{-1})$, in $Z$-domain as $X(z^{-1}) \cdot Y(z)$. Therefore the SACF of the pair $\{S_{j,0}^{(1)}(z^{-1}), S_{j,1}^{(1)}(z^{-1})\}$ is developed as

$$SACF = (1+A^{(1,0)} \cdot W^{(1,0)} z^{-1}) \cdot (1+A^{(1,0)} \cdot W^{(1,0)} \cdot z) + (A^{(1,0)} - W^{(1,0)} \cdot z^{-1}) \cdot (A^{(1,0)} - W^{(1,0)} \cdot z)$$

and knowing that $W^{(1,q)}$ is a number of unit magnitude we have that $SACF = 2 \cdot [1 + (A^{(1,0)})^2]$

Now, if we apply the condition of paraunitary matrix to the basic building block $\mathbf{B}_{A^{(1,0)},W^{(1,0)}}^{(1)}(z^{-1})$, we have

$$\begin{bmatrix} 1 & A^{(1,0)} \cdot W^{(1,0)} \cdot z^{-1} \\ A^{(1,0)} & -W^{(1,0)} \cdot z^{-1} \end{bmatrix} \times \begin{bmatrix} 1 & A^{(1,0)} \\ A^{(1,0)} \cdot W^{(1,0)} \cdot z & -W^{(1,0)} \cdot z \end{bmatrix} = [1 + (A^{(1,0)})^2] \cdot \mathbf{I}_2$$

where the diagonal elements of the resultant matrix represent the aperiodic auto-correlation at time shift $\tau = 0$. Hence, $SACF = 2 \cdot [1 + (A^{(1,0)})^2]$.

▲

### 4.1.1 Golay Kernel 2

For the generation of Golay binary pairs of sequences of length $L_{|Gol} = 2^N$, the coefficients $A^{(1,q)}$ are equal to $A^{(1,q)} = +1$, i.e. $\theta^{(q)} = -\frac{\pi}{4}$, the delay values $D^{(q)}$ are any permutation of the set $\{2^0, 2^1, \ldots, 2^{N-1}\}$ and $W^{(1,q)} \in \{+1, -1\}$ [Budis 91, Popov 99a]. This is the case of the algorithms reviewed in Chapter 3, section 3.1.

### 4.1.2 Golay Kernel 10 Decomposition

It is known that exist two non-equivalent Golay kernels of length $L_{|Gol} = 10$. Here, we consider the first kernel 10 defined in [Golay 61] and decomposed in [Budis 11], whose polynomial matrix form is shown in equation 4.10 (the same development could be done if the other kernel were chosen).

$$\begin{aligned} s_{1,0}^{(Q)}[l] &= \{1, \ -1, \ -1, \ 1, \ 1, \ 1, \ 1, \ 1, \ 1, \ -1\} \\ s_{1,1}^{(Q)}[l] &= \{1, \ -1, \ -1, \ -1, \ 1, \ -1, \ 1, \ -1, \ -1, \ 1\} \\ \mathbf{S}_j^{(1,Q)} &= \begin{bmatrix} \sum_{l=0}^{9} s_{1,0}^{(Q)}[l] \cdot z^{-l} \\ \sum_{l=0}^{9} s_{1,1}^{(Q)}[l] \cdot z^{-l} \end{bmatrix} \end{aligned} \tag{4.10}$$

Notice that according to the notation $s_{j,i}^{(Q)}[l]$ we are assuming that we deal with the $j$-th complementary pair $j = 1$. This is an arbitrary assumption of no consequences. Now, we carry out the Golay kernel 10 decomposition by proposing a recursive method. The objective of the decomposition is to express the kernel in the following form:

$$\mathbf{S}_j^{(1,Q)}\left(z^{-1}\right) = \mathbf{G}_{10}^{(1)}\left(z^{-1}\right) \times \begin{bmatrix} 1 & 1 \end{bmatrix}^T \tag{4.11}$$

where the generation matrix of the Golay kernel 10, $\mathbf{G}_{10}^{(1)}(z^{-1})$, is defined as the product of four building blocks and each one has the structure shown in equation 4.9. To compute the coefficients of each building block, the recursive algorithm of equation 4.8 must be iterated backwards. Therefore, the next recursive steps have to be followed:

- *Step 1*: Find by inspection the monomials $s_{1,0}^{(Q)}[l] \cdot z^{-l}$ and $s_{1,1}^{(Q)}[l] \cdot z^{-l}$ of lowest value of $l$ that hold equation 4.12 for certain values of $A^{(1,q)}$, $D^{(q)}$ and $W^{(1,q)}$.

$$\begin{bmatrix} 1 & A^{(1,Q-1)} \cdot W^{(1,Q-1)} \cdot z^{-D^{(Q-1)}} \\ A^{(1,Q-1)} & -W^{(1,Q-1)} \cdot z^{-D^{(Q-1)}} \end{bmatrix} = \begin{bmatrix} s_{1,0}^{(Q)}[l] & s_{1,0}^{(Q)}[l] \cdot z^{-l} \\ s_{1,1}^{(Q)}[l] & s_{1,1}^{(Q)}[l] \cdot z^{-l} \end{bmatrix} \tag{4.12}$$

  In the case of the first non-equivalent Golay kernel 10 (refer to equation 4.10), the first monomials which hold equation 4.12 are $s_{1,0}^{(Q)}[3] \cdot z^{-3}$ and $s_{1,1}^{(Q)}[3] \cdot z^{-3}$ with parameter values $A^{(1,q)} = 1$, $W^{(1,q)} = 1$ and $D^{(q)} = 3$. Consequently, the building block at iteration $Q - 1$ is equal to $\mathbf{B}_{1,1}^{(1)}(z^{-3})$.

- *Step 2*: Solve the following system of equations to find the pair of sequences $\mathbf{S}_j^{(1,Q-1)}(z^{-1})$:

$$\mathbf{S}_j^{(1,Q)}\left(z^{-1}\right) = \mathbf{B}^{(1)}_{A^{(1,Q-1)},W^{(1,Q-1)}}\left(z^{-D^{(Q-1)}}\right) \times \mathbf{S}_j^{(1,Q-1)}\left(z^{-1}\right);$$

$$\mathbf{S}_j^{(1,Q)}\left(z^{-1}\right) = \begin{bmatrix} 1 & A^{(1,Q-1)} \cdot W^{(1,Q-1)} \cdot z^{-D^{(Q-1)}} \\ A^{(1,Q-1)} & -W^{(1,Q-1)} \cdot z^{-D^{(Q-1)}} \end{bmatrix} \times$$

$$\begin{bmatrix} s_{1,0}^{(Q-1)}[0] \cdot z^{-0} + s_{1,0}^{(Q-1)}[1] \cdot z^{-1} + \cdots + s_{1,0}^{(Q-1)}\left[L_{|Gol} - D^{(Q-1)} - 1\right] \cdot z^{-\left(L_{|Gol} - D^{(Q-1)} - 1\right)} \\ s_{1,1}^{(Q-1)}[0] \cdot z^{-0} + s_{1,1}^{(Q-1)}[1] \cdot z^{-1} + \cdots + s_{1,1}^{(Q-1)}\left[L_{|Gol} - D^{(Q-1)} - 1\right] \cdot z^{-\left(L_{|Gol} - D^{(Q-1)} - 1\right)} \end{bmatrix} \tag{4.13}$$

  Solving the system of equation of (4.13) for the Golay kernel 10 (shown in equation (4.10)) at the stage $Q-1$, leads to

$$\mathbf{S}_j^{(1,Q)}\left(z^{-1}\right) = \begin{bmatrix} 1 & z^{-3} \\ 1 & -z^{-3} \end{bmatrix} \times \begin{bmatrix} \sum_{l=0}^{6} s_{1,0}^{(Q-1)}[l] \cdot z^{-l} \\ \sum_{l=0}^{6} s_{1,1}^{(Q-1)}[l] \cdot z^{-l} \end{bmatrix} \Rightarrow$$

$$\mathbf{S}_j^{(1,Q-1)}\left(z^{-1}\right) = \begin{bmatrix} 1 - z^{-1} - z^{-2} + z^{-4} + z^{-6} \\ 1 + z^{-2} + z^{-4} + z^{-5} - z^{-6} \end{bmatrix} \tag{4.14}$$

- *Step 3*: Once the new polynomial matrix $\mathbf{S}_j^{(1,Q-1)}(z^{-1})$ is generated, the previous stages must be repeated until the initial conditions $\mathbf{S}_j^{(1,0)}(z^{-1}) = [\ 1 \quad 1\ ]^T$ are obtained. If in any stage $q < Q-1$, the matrix $\mathbf{S}_j^{(1,q)}(z^{-1})$ has a row with a monomial equal to zero (that is, a missing monomial, either $s_{1,0}^{(q)}[l] \cdot z^{-l}$ or $s_{1,1}^{(q)}[l] \cdot z^{-l}$), for $l$ lower than that obtained by the application of equation (4.12), then those monomials must be chosen to obtain the parameters $A^{(1,q)}$, $W^{(1,q)}$ and $D^{(q)}$. For example, in equation (4.14) these monomials are $s_{1,0}^{(Q-1)}[1] \cdot z^{-1}$ and $s_{1,1}^{(Q-1)}[1] \cdot z^{-1}$. In this way, the building block at the iteration $Q-2$ is equal to $\mathbf{B}_{1,-1}^{(1)}(z^{-1})$.

Iterating the previous procedure four times, the generation matrix of the first Golay kernel 10 is the one shown in [Budis 11]:

$$\mathbf{G}_{10}^{(1)}\left(z^{-1}\right) = \mathbf{B}_{1,1}^{(1)}(z^{-3}) \times \mathbf{B}_{1,-1}^{(1)}(z^{-1}) \times \mathbf{B}_{1/2,-1}^{(1)}(z^{-1}) \times \mathbf{B}_{1,1}^{(1)}(z^{-4}) \tag{4.15}$$

Notice that the coefficients $A^{(1,q)}$ are mostly equal to 1 except one of them, which is equal to $\frac{1}{2}$. This multiplication can be carried out by shifting.

### 4.1.3 Golay Kernel 26 Decomposition

The Golay kernel 26 is defined as

$$s_{1,0}^{(Q)}[l] = \Big\{ +1,+1,+1,+1,-1,+1,+1,-1,-1,+1,-1,+1,-1,+1,-1,-1,+1,-1,+1,+1,+1,-1,-1,+1,+1,+1 \Big\}$$
$$s_{1,1}^{(Q)}[l] = \Big\{ +1,+1,+1,+1,-1,+1,+1,-1,-1,+1,-1,+1,+1,+1,+1,+1,-1,+1,-1,-1,-1,+1,+1,-1,-1,-1 \Big\}$$

$$\mathbf{s}_j^{(1,Q)}(z^{-1}) = \begin{bmatrix} \sum_{l=0}^{25} s_{1,0}^{(Q)}[l] \cdot z^{-l} \\ \sum_{l=0}^{25} s_{1,1}^{(Q)}[l] \cdot z^{-l} \end{bmatrix} \tag{4.16}$$

Again, by using the notation $s_{j,i}^{(Q)}[l]$ we consider here that $j = 1$. The Golay kernel 26 can be decomposed by following the recursive procedure explained in the previous section and generated in 12 stages as follows:

$$\begin{aligned} \mathbf{S}_j^{(1,12)}\left(z^{-1}\right) &= \mathbf{B}_{1,-1}^{(1)}(z^{-12}) \times \mathbf{B}_{1,1}^{(1)}(z^{-1}) \times \mathbf{B}_{1/2,1}^{(1)}(z^{-1}) \times \mathbf{B}_{1/5,-1}^{(1)}(z^{-1}) \\ &\quad \times \mathbf{B}_{4/13,-1}^{(1)}(z^{-1}) \times \mathbf{B}_{3/37,1}^{(1)}(z^{-1}) \times \mathbf{B}_{81/106,-1}^{(1)}(z^{-1}) \times \mathbf{B}_{3/37,1}^{(1)}(z^{-1}) \\ &\quad \times \mathbf{B}_{4/13,1}^{(1)}(z^{-1}) \times \mathbf{B}_{1/5,-1}^{(1)}(z^{-1}) \times \mathbf{B}_{1/2,1}^{(1)}(z^{-1}) \times \mathbf{B}_{1,1}^{(1)}(z^{-3}) \times \begin{bmatrix} 1 \\ 1 \end{bmatrix} \\ &= \mathbf{G}_{26}^{(1)}\left(z^{-1}\right) \times \begin{bmatrix} 1 \\ 1 \end{bmatrix} \end{aligned} \tag{4.17}$$

Table 4.1 depicts all the stages of the generation process of the Golay kernel 26 by means of the decomposition presented here, whereas Figure 4.1 represents a diagram of the Golay kernels decomposition, where the blocks $\mathbf{B}_{A^{(1,q)},W^{(1,q)}}^{(1)}(z^{-D^{(q)}})$ represent the basic building block at iteration $q$.

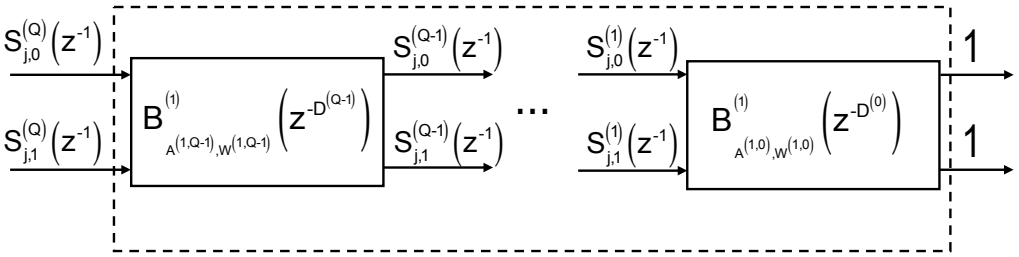


Figure 4.1: Block diagram of the decomposition of the Golay kernels.

| INITIAL SEQUENCES | |
|---|---|
| $s_{1,0}^{(0)}[l]$ | $\{1,0,0,0,0,0,0,0,0,0,0,0,0,0,0,0,0,0,0,0,0,0,0,0,0,0\}$ |
| $s_{1,1}^{(0)}[l]$ | $\{1,0,0,0,0,0,0,0,0,0,0,0,0,0,0,0,0,0,0,0,0,0,0,0,0,0\}$ |
| ZERO STAGE: $\mathbf{B}_{1,1}^{(1)}(z^{-3})$ | |
| $s_{1,0}^{(1)}[l]$ | $\{1,0,0,1,0,0,0,0,0,0,0,0,0,0,0,0,0,0,0,0,0,0,0,0,0,0\}$ |
| $s_{1,1}^{(1)}[l]$ | $\{1,0,0,-1,0,0,0,0,0,0,0,0,0,0,0,0,0,0,0,0,0,0,0,0,0,0\}$ |
| FIRST STAGE: $\mathbf{B}_{1/2,1}^{(1)}(z^{-1})$ | |
| $s_{1,0}^{(2)}[l]$ | $\{1,\frac{1}{2},0,1,-\frac{1}{2},0,0,0,0,0,0,0,0,0,0,0,0,0,0,0,0,0,0,0,0,0,0\}$ |
| $s_{1,1}^{(2)}[l]$ | $\{\frac{1}{2},-1,0,\frac{1}{2},0,0,0,0,0,0,0,0,0,0,0,0,0,0,0,0,0,0,0,0,0,0\}$ |
| SECOND STAGE: $\mathbf{B}_{1/5,-1}^{(1)}(z^{-1})$ | |
| $s_{1,0}^{(3)}[l]$ | $\{1,\frac{2}{5},\frac{1}{5},1,-\frac{3}{5},-\frac{1}{5},0,0,0,0,0,0,0,0,0,0,0,0,0,0,0,0,0,0,0,0\}$ |
| $s_{1,1}^{(3)}[l]$ | $\{\frac{1}{5},\frac{3}{5},-1,\frac{1}{5},\frac{2}{5},1,0,0,0,0,0,0,0,0,0,0,0,0,0,0,0,0,0,0,0,0\}$ |
| THIRD STAGE: $\mathbf{B}_{4/13,1}^{(1)}(z^{-1})$ | |
| $s_{1,0}^{(4)}[l]$ | $\{1,\frac{6}{13},\frac{5}{13},\frac{9}{13},-\frac{7}{13},-\frac{1}{13},\frac{4}{13},0,0,0,0,0,0,0,0,0,0,0,0,0,0,0,0,0,0,0\}$ |
| $s_{1,1}^{(4)}[l]$ | $\{\frac{4}{13},-\frac{1}{13},-\frac{7}{13},\frac{17}{13},-\frac{5}{13},-\frac{6}{13},-1,0,0,0,0,0,0,0,0,0,0,0,0,0,0,0,0,0,0\}$ |
| FOURTH STAGE: $\mathbf{B}_{3/37,1}^{(1)}(z^{-1})$ | |
| $s_{1,0}^{(5)}[l]$ | $\{1,\frac{18}{37},\frac{14}{37},\frac{24}{37},-\frac{16}{37},-\frac{4}{37},\frac{10}{37},-\frac{3}{37},0,0,0,0,0,0,0,0,0,0,0,0,0,0,0,0,0,0\}$ |
| $s_{1,1}^{(5)}[l]$ | $\{\frac{3}{37},-\frac{10}{37},\frac{4}{37},\frac{22}{37},-\frac{50}{37},\frac{14}{37},\frac{18}{37},1,0,0,0,0,0,0,0,0,0,0,0,0,0,0,0,0,0,0\}$ |
| FIFTH STAGE: $\mathbf{B}_{81/106,-1}^{(1)}(z^{-1})$ | |
| $s_{1,0}^{(6)}[l]$ | $\{1,\frac{45}{106},\frac{31}{53},\frac{30}{56},-\frac{47}{53},\frac{49}{53},-\frac{1}{53},-\frac{24}{53},-\frac{81}{106},0,0,0,0,0,0,0,0,0,0,0,0,0,0,0,0,0\}$ |
| $s_{1,1}^{(6)}[l]$ | $\{\frac{81}{106},\frac{24}{53},\frac{1}{53},\frac{32}{53},\frac{14}{53},-\frac{76}{53},\frac{31}{53},\frac{45}{106},1,0,0,0,0,0,0,0,0,0,0,0,0,0,0,0,0,0,0\}$ |
| SIXTH STAGE: $\mathbf{B}_{3/37,1}^{(1)}(z^{-1})$ | |
| $s_{1,0}^{(7)}[l]$ | $\{1,\frac{18}{37},\frac{23}{37},\frac{21}{37},-\frac{31}{37},\frac{35}{37},-\frac{5}{37},-\frac{15}{37},-\frac{27}{37},\frac{3}{37},0,0,0,0,0,0,0,0,0,0,0,0,0,0,0,0\}$ |
| $s_{1,1}^{(7)}[l]$ | $\{\frac{3}{37},-\frac{27}{37},-\frac{15}{37},\frac{1}{37},-\frac{25}{37},-\frac{7}{37},\frac{53}{37},-\frac{23}{37},-\frac{18}{37},1,0,0,0,0,0,0,0,0,0,0,0,0,0,0,0,0,0\}$ |
| SEVENTH STAGE: $\mathbf{B}_{4/13,-1}^{(1)}(z^{-1})$ | |
| $s_{1,0}^{(8)}[l]$ | $\{1,\frac{6}{13},\frac{11}{13},\frac{9}{13},-\frac{11}{13},\frac{15}{13},-\frac{1}{13},-\frac{11}{13},-\frac{7}{13},\frac{3}{13},\frac{4}{13},0,0,0,0,0,0,0,0,0,0,0,0,0,0,0\}$ |
| $s_{1,1}^{(8)}[l]$ | $\{\frac{4}{13},\frac{3}{13},-\frac{7}{13},-\frac{3}{13},-\frac{3}{13},-\frac{5}{13},-\frac{3}{13},\frac{17}{13},-\frac{11}{13},-\frac{6}{13},-1,0,0,0,0,0,0,0,0,0,0,0,0,0,0,0\}$ |
| EIGHTH STAGE: $\mathbf{B}_{1/5,-1}^{(1)}(z^{-1})$ | |
| $s_{1,0}^{(9)}[l]$ | $\{1,\frac{2}{5},\frac{4}{5},\frac{4}{5},-\frac{4}{5},\frac{6}{5},0,-\frac{4}{5},-\frac{4}{5},\frac{2}{5},\frac{2}{5},\frac{1}{5},0,0,0,0,0,0,0,0,0,0,0,0,0,0\}$ |
| $s_{1,1}^{(9)}[l]$ | $\{\frac{1}{5},\frac{2}{5},\frac{2}{5},-\frac{2}{5},-\frac{2}{5},0,-\frac{3}{5},-\frac{2}{5},\frac{6}{5},-\frac{4}{5},-\frac{2}{5},1,0,0,0,0,0,0,0,0,0,0,0,0,0,0\}$ |
| NINTH STAGE: $\mathbf{B}_{1/2,1}^{(1)}(z^{-1})$ | |
| $s_{1,0}^{(10)}[l]$ | $\{1,\frac{1}{2},1,1,-1,1,0,-1,-1,1,0,0,-\frac{1}{2},0,0,0,0,0,0,0,0,0,0,0,0,0,0\}$ |
| $s_{1,1}^{(10)}[l]$ | $\{\frac{1}{2},0,0,0,0,1,0,0,0,-1,1,\frac{1}{2},1,0,0,0,0,0,0,0,0,0,0,0,0,0,0\}$ |
| TENTH STAGE: $\mathbf{B}_{1,1}^{(1)}(z^{-1})$ | |
| $s_{1,0}^{(11)}[l]$ | $\{1,1,1,1,-1,1,1,-1,-1,1,-1,1,0,1,0,0,0,0,0,0,0,0,0,0,0,0\}$ |
| $s_{1,1}^{(11)}[l]$ | $\{1,0,1,1,-1,1,-1,-1,-1,1,1,-1,-1,-1,0,0,0,0,0,0,0,0,0,0,0,0\}$ |
| ELEVENTH STAGE: $\mathbf{B}_{1,-1}^{(1)}(z^{-12})$ | |
| $s_{1,0}^{(12)}[l]$ | $\{1,1,1,1,-1,1,1,-1,-1,1,-1,1,-1,1,-1,-1,1,-1,1,1,1,-1,-1,1,1,1\}$ |
| $s_{1,1}^{(12)}[l]$ | $\{1,1,1,1,-1,1,1,-1,-1,1,-1,1,-1,1,-1,-1,1,-1,1,1,1,-1,-1,1,1,1\}$ |

Table 4.1: Generation of a Golay binary pair of length 26 by means of the proposed decomposition.

## 4.2 Generation of 2-CSS

Following the Turyn's construction [Turyn 74], the previous generation matrices can be cascaded in any order and number to generate Golay binary sequence pairs (2-CSS) of length $L_{|Gol} = 2^N \cdot 10^M \cdot 26^P$. Thanks to the Golay kernels decomposition, this is carried out in $Q = N + 4 \cdot M + 12 \cdot P$ stages, as depicted in Figure 4.2. Notice that the building blocks are cascaded in the reverse order of Figure 4.1. A more detailed representation of the generation algorithm is depicted in Figure 4.3 where each building block is highlighted with a dashed square.

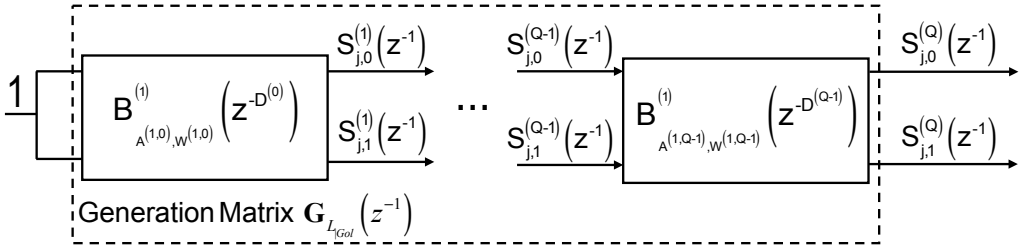


Figure 4.2: Diagram of the generation of a 2-CSS by cascading $Q$ building blocks.

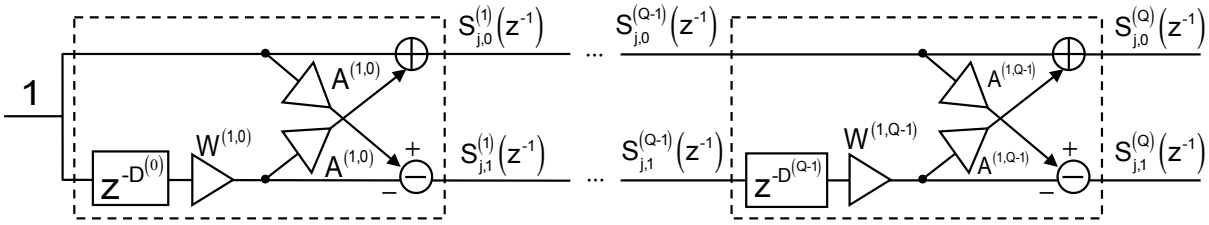


Figure 4.3: Modular generator of Golay sequence pairs of length $L_{|Gol} = 2^N \cdot 10^M \cdot 26^P$. The delay values $D^{(q)}$ confers an efficient implementation.

The delays of the generation matrices should be chosen so as to avoid overlaps between the Golay kernels. Here, firstly $N$ basic building blocks $\mathbf{B}^{(1)}_{A^{(1,q)},W^{(1,q)}}(z^{-D^{(q)}})$ are used to generate the lengths $2^N$; secondly, $M$ generation matrices $\mathbf{G}^{(1)}_{10}(z^{-1})$ are used to construct the lengths $2^N \cdot 10^M$; and finally, $P$ generation matrices $\mathbf{G}^{(1)}_{26}(z^{-1})$ are used to generate the lengths $2^N \cdot 10^M \cdot 26^P$. Therefore, the final sequence set after the iteration $Q-1$, can

be expressed as

$$\mathbf{S}_j^{(1,Q)}\left(z^{-1}\right) = \left\{\prod_{p=P-1}^{0} \mathbf{G}_{26}^{(1)}\left(z^{-2^N\cdot 10^M\cdot 26^p}\right)\right\} \times \left\{\prod_{m=M-1}^{0} \mathbf{G}_{10}^{(1)}\left(z^{-2^N\cdot 10^m}\right)\right\} \times \left\{\prod_{n=N-1}^{0} \mathbf{B}_{A^{(1,n)},W^{(1,n)}}^{(1)}\left(z^{-2^n}\right)\right\} \times \begin{bmatrix} 1 \\ 1 \end{bmatrix} \tag{4.18}$$

If other cascading orders are selected in equation 4.18, they will generate different complementary pairs.

As we shown in Chapter 3, in order to generate two uncorrelated CSS, i.e. the set $\mathbf{S}_0^{(1,Q)}(z^{-1})$ and the set $\mathbf{S}_1^{(1,Q)}(z^{-1})$, it is only needed to change the sign of the seed at the first stage ($W^{(1,0)}$), and to maintain the same values for both pairs at other stages. For example, set $W^{(1,0)} = +1$ for the generation of the complementary pair $\mathbf{S}_0^{(1,Q)}(z^{-1})$ and $W^{(1,0)} = -1$ for the complementary pair $\mathbf{S}_1^{(1,Q)}(z^{-1})$.

## 4.3 Generation of $K_{|CSS}$-CSS

In this section, the previous generation algorithm for 2-CSS will be expanded to $K_{|CSS}$-CSS, with $K_{|CSS} = 2^k$.

Among the generation algorithms of CSS shown in Table 2.4 of Chapter 2, we will use the interleaving method proposed by Tseng and Liu [Tseng 72] to expand the generation algorithm from 2-CSS of length $L_{|Gol} = 2^N \cdot 10^M \cdot 26^P$ to $K_{|CSS}$-CSS of length $\frac{K_{|CSS}}{2} \cdot (2^N \cdot 10^M \cdot 26^P)$. For each expansion factor $k$, $2 \cdot K_{|CSS}$ uncorrelated CSS of length $K_{|CSS} \cdot L_{|Gol}$ are obtained from $K_{|CSS}$ uncorrelated CSS of length $\frac{K_{|CSS}}{2} \cdot L_{|Gol}$. The generation matrices are expanded following this method in $Z$-domain:

$$\begin{aligned}
\mathbf{G}_{K_{|CSS}\cdot L_{|CSS}}^{(k+1)}\left(z^{-1}\right) &= \begin{bmatrix} \boldsymbol{\Delta}_{left}^{(k+1)} & \boldsymbol{\Delta}_{right}^{(k+1)} \end{bmatrix};\ k \in \mathbb{N} - \{0\} \\
\boldsymbol{\Delta}_{left}^{(k+1)} &= \begin{bmatrix} \mathbf{G}_{\frac{K_{|CSS}}{2}\cdot L_{|CSS}}^{(k)}\left(z^{-2}\right) & +z^{-1}\cdot \mathbf{G}_{\frac{K_{|CSS}}{2}\cdot L_{|CSS}}^{(k)}\left(z^{-2}\right) \\ \mathbf{G}_{\frac{K_{|CSS}}{2}\cdot L_{|CSS}}^{(k)}\left(z^{-2}\right) & -z^{-1}\cdot \mathbf{G}_{\frac{K_{|CSS}}{2}\cdot L_{|CSS}}^{(k)}\left(z^{-2}\right) \end{bmatrix} \\
\boldsymbol{\Delta}_{right}^{(k+1)} &= \begin{bmatrix} \mathbf{G}_{\frac{K_{|CSS}}{2}\cdot L_{|CSS}}^{(k)}\left(z^{-2}\right) & -z^{-1}\cdot \mathbf{G}_{\frac{K_{|CSS}}{2}\cdot L_{|CSS}}^{(k)}\left(z^{-2}\right) \\ \mathbf{G}_{\frac{K_{|CSS}}{2}\cdot L_{|CSS}}^{(k)}\left(z^{-2}\right) & +z^{-1}\cdot \mathbf{G}_{\frac{K_{|CSS}}{2}\cdot L_{|CSS}}^{(k)}\left(z^{-2}\right) \end{bmatrix}
\end{aligned} \tag{4.19}$$

This expansion method, can be unified and expressed by using the Kronecker product as follows:

$$\mathbf{G}^{(k+1)}_{K_{|CSS}\cdot L_{|CSS}}\left(z^{-1}\right) = \begin{bmatrix} \mathbf{G}^{(k)}_{\frac{K_{|CSS}}{2}\cdot L_{|CSS}}\left(z^{-2}\right) & +W^{(k+1,0)}\cdot \mathbf{G}^{(k)}_{\frac{K_{|CSS}}{2}\cdot L_{|CSS}}\left(z^{-2}\right)\cdot z^{-1} \\ \mathbf{G}^{(k)}_{\frac{K_{|CSS}}{2}\cdot L_{|CSS}}\left(z^{-2}\right) & -W^{(k+1,0)}\cdot \mathbf{G}^{(k)}_{\frac{K_{|CSS}}{2}\cdot L_{|CSS}}\left(z^{-2}\right)\cdot z^{-1} \end{bmatrix}$$
$$= \mathbf{G}^{(k)}_{\frac{K_{|CSS}}{2}\cdot L_{|CSS}}\left(z^{-2}\right)\otimes \mathbf{H}^{(k+1)}_{2}\left(z^{-1}\right);\ k\in\mathbb{N}-\{0\} \tag{4.20}$$

where the left and the right matrices in equation 4.19 are obtained by changing the values $\{+1,-1\}$ of $W^{(k+1,0)}$, and the paraunitary matrix $\mathbf{H}^{(k+1)}_{2}$ is determined by the next expression:

$$\mathbf{H}^{(k+1)}_{2}\left(z^{-1}\right) = \begin{bmatrix} 1 & W^{(k+1,0)}\cdot z^{-1} \\ 1 & -W^{(k+1,0)}\cdot z^{-1} \end{bmatrix} \tag{4.21}$$

Notice that $W^{(1,0)}$ was used in 4.8 to generate $K_{|CSS}=2$ uncorrelated CSS. Now the paraunitary matrix $\mathbf{H}^{(k+1)}_{2}(z^{-1})$ is expressed as the product of $Q$ Hadamard matrices as follows:

$$\mathbf{H}^{(k+1)}_{2}\left(z^{-1}\right) = \alpha\cdot\left\{\prod_{q=Q-1}^{1}\boldsymbol{\Upsilon}^{(q)}\left(z^{-1}\right)\right\}\times\boldsymbol{\Upsilon}^{(0)}\left(z^{-1}\right);\ \alpha\in\mathbb{R}-\{0\} \tag{4.22}$$

where

$$\boldsymbol{\Upsilon}^{(q)}\left(z^{-1}\right) = \begin{cases} \begin{bmatrix} 1 & A^{(k+1,q)}\cdot W^{(k+1,q)} \\ A^{(k+1,q)} & -W^{(k+1,q)} \end{bmatrix} & \text{if } 1\le q\le Q-1 \\ \begin{bmatrix} 1 & A^{(k+1,0)}\cdot W^{(k+1,0)}\cdot z^{-1} \\ A^{(k+1,0)} & -W^{(k+1,0)}\cdot z^{-1} \end{bmatrix}; & \text{if } q=0 \end{cases} \tag{4.23}$$

In this way, the recursive algorithm for the generation matrix of $2\cdot K_{|CSS}$ CSS (equation 4.20) is expressed as

$$\mathbf{G}^{(k+1)}_{K_{|CSS}\cdot L_{|CSS}}\left(z^{-1}\right) = \mathbf{G}^{(k)}_{\frac{K_{|CSS}}{2}\cdot L_{|CSS}}\left(z^{-2}\right)\otimes\left\{\prod_{q=Q-1}^{0}\boldsymbol{\Upsilon}^{(q)}\left(z^{-1}\right)\right\} \tag{4.24}$$

Equation 4.8 is now generalized to $K_{|CSS}$-CSS of length $\frac{K_{|CSS}}{2} \cdot L_{|Gol}$, so the complementary set is generated as

$$\mathbf{S}_j^{(k,Q)}\left(z^{-1}\right) = \mathbf{G}^{(k)}_{\frac{K_{|CSS}}{2} \cdot L_{|CSS}}\left(z^{-1}\right) \times \left[\begin{array}{ccc} 1 & \cdots & 1 \end{array}\right]^T_{K_{|CSS} \times 1} \tag{4.25}$$

Therefore, the set $j$ at the expansion step $k+1$ is equal to:

$$\begin{aligned} \mathbf{S}_j^{(k+1,Q)}\left(z^{-1}\right) = &\left(\mathbf{G}^{(k)}_{\frac{K_{|CSS}}{2} \cdot L_{|CSS}}\left(z^{-2}\right) \times \left[\begin{array}{ccc} 1 & \cdots & 1 \end{array}\right]^T_{K_{|CSS} \times 1}\right) \\ &\otimes \left(\mathbf{H}_2^{(k+1)}\left(z^{-1}\right) \times \left[\begin{array}{cc} 1 & 1 \end{array}\right]^T\right) \end{aligned} \tag{4.26}$$

In the following sections, the generation of $2 \cdot K_{|CSS}$ uncorrelated CSS of length $K_{|CSS} \cdot L_{|Gol}$ with equation 4.26 is analyzed for each kernel.

### 4.3.1 Golay Kernel 2

The generation matrix of equation 4.24 particularized to $2 \cdot K_{|CSS}$ of length $K_{|CSS} \cdot 2^N$ in $Q = N$ stages (as $M = 0$ and $P = 0$) is equal to:

$$\begin{aligned} \mathbf{G}^{(k+1)}_{K_{|CSS} \cdot 2^N}\left(z^{-1}\right) &= \mathbf{G}^{(k)}_{\frac{K_{|CSS}}{2} \cdot 2^N}\left(z^{-2}\right) \otimes \left\{\prod_{n=N-1}^{0} \boldsymbol{\Upsilon}^{(n)}\left(z^{-1}\right)\right\} \\ &= \left\{\prod_{n=N-1}^{0} \mathbf{B}^{(k)}_{A^{(k,n)},W^{(k,n)}}\left(z^{-2 \cdot D^{(n)}}\right)\right\} \otimes \left\{\prod_{n=N-1}^{0} \boldsymbol{\Upsilon}^{(n)}\left(z^{-1}\right)\right\} \end{aligned} \tag{4.27}$$

By using the property of the mixed product[1], the generation matrix is finally obtained with the expression

$$\mathbf{G}^{(k+1)}_{K_{|CSS} \cdot 2^N}\left(z^{-1}\right) = \prod_{n=N-1}^{0} \left(\mathbf{B}^{(k)}_{A^{(k,n)},W^{(k,n)}}\left(z^{-2 \cdot D^{(n)}}\right) \otimes \boldsymbol{\Upsilon}^{(n)}\left(z^{-1}\right)\right) \tag{4.28}$$

The basic building block $\mathbf{B}^{(k+1)}_{A^{(k+1,n)},W^{(k+1,n)}}(z^{-2 \cdot D^{(n)}})$ is now defined as

$$\mathbf{B}^{(k+1)}_{A^{(k+1,n)},W^{(k+1,n)}}\left(z^{-2 \cdot D^{(n)}}\right) = \mathbf{B}^{(k)}_{A^{(k,n)},W^{(k,n)}}\left(z^{-2 \cdot D^{(n)}}\right) \otimes \boldsymbol{\Upsilon}^{(n)}\left(z^{-1}\right) \tag{4.29}$$

[1]Given two sets of arrays $\{\boldsymbol{\mathcal{U}}_0, \boldsymbol{\mathcal{U}}_1, \ldots, \boldsymbol{\mathcal{U}}_{Q-1}\}$ and $\{\boldsymbol{\mathcal{V}}_0, \boldsymbol{\mathcal{V}}_1, \ldots, \boldsymbol{\mathcal{V}}_{Q-1}\}$ the following property holds: $(\boldsymbol{\mathcal{U}}_0 \otimes \boldsymbol{\mathcal{V}}_0) \times (\boldsymbol{\mathcal{U}}_1 \otimes \boldsymbol{\mathcal{V}}_1) \times \cdots \times (\boldsymbol{\mathcal{U}}_{Q-1} \otimes \boldsymbol{\mathcal{V}}_{Q-1}) = (\boldsymbol{\mathcal{U}}_0 \times \boldsymbol{\mathcal{U}}_1 \times \cdots \times \boldsymbol{\mathcal{U}}_{Q-1}) \otimes (\boldsymbol{\mathcal{V}}_0 \times \boldsymbol{\mathcal{V}}_1 \times \cdots \times \boldsymbol{\mathcal{V}}_{Q-1})$.

In order to define the basic building blocks for generating $2{\cdot}K_{|CSS}$ CSS of length $K_{|CSS}{\cdot}2^N$, the entries of the matrices $\boldsymbol{\Upsilon}^{(n)}(z^{-1})$ must be derived by solving the expression shown in equation 4.22. Depending on the parity of $Q$ (in this case $Q = N$), it has different solutions, as it is developed below.

#### 4.3.1.1 $Q$ is an Even Number

Recalling the definition of Hadamard matrix (refer to Chapter 2, section 2.3.1), to solve equation 4.22, the products of $Q$ matrices $\boldsymbol{\Upsilon}^{(q)}(z^{-1})$ can be arranged as

$$\alpha_1 \cdot \alpha_2 \cdot \left\{ \prod_{q=Q-1}^{2} \boldsymbol{\Upsilon}^{(q)}\left(z^{-1}\right) \right\} \times \boldsymbol{\Upsilon}^{(1)}\left(z^{-1}\right) \times \boldsymbol{\Upsilon}^{(0)}\left(z^{-1}\right) = \mathbf{H}_2^{(k+1)}\left(z^{-1}\right) \tag{4.30}$$

where $\alpha_1$ and $\alpha_2$ are constant real numbers different from zero and $\alpha_1 \cdot \alpha_2 = \alpha$. If $Q$ is an even number, $Q-2$ is also an even number. So setting the first $Q-2$ matrices $\boldsymbol{\Upsilon}^{(q)}(z^{-1})$ to $\boldsymbol{\mathcal{H}}_2$ and then using the definition of orthogonal matrix, the product of $Q-2$ matrices is equal to:

$$\alpha_1 \cdot \prod_{q=Q-1}^{2} \boldsymbol{\Upsilon}^{(q)}\left(z^{-1}\right) = \alpha_1 \cdot 2^{\frac{Q-2}{2}} \cdot \mathbf{I}_2 \tag{4.31}$$

In order to normalize equation 4.31, the value of $\alpha_1$ is set to $\alpha_1 = 2^{-(Q/2-1)}$, so the product $\alpha_1 \cdot 2^{(Q/2-1)}$ is equal to 1. Therefore, the product of the matrices $\boldsymbol{\Upsilon}^{(1)}(z^{-1})$ and $\boldsymbol{\Upsilon}^{(0)}(z^{-1})$ should be equal to:

$$\alpha_2 \cdot \boldsymbol{\Upsilon}^{(1)}\left(z^{-1}\right) \times \boldsymbol{\Upsilon}^{(0)}\left(z^{-1}\right) = \begin{bmatrix} 1 & W^{(k+1,0)} \cdot z^{-1} \\ 1 & -W^{(k+1,0)} \cdot z^{-1} \end{bmatrix} \tag{4.32}$$

By using the definition of the matrices $\boldsymbol{\Upsilon}^{(q)}(z^{-1})$ stated in the previous equation 4.23, the expression 4.32 can be rewritten as

$$\begin{aligned} \alpha_2 \cdot \begin{bmatrix} 1 & A^{(k+1,1)} \cdot W^{(k+1,1)} \\ A^{(k+1,1)} & -W^{(k+1,1)} \end{bmatrix} \times \begin{bmatrix} 1 & A^{(k+1,0)} \cdot W^{(k+1,0)} \cdot z^{-1} \\ A^{(k+1,0)} & -W^{(k+1,0)} \cdot z^{-1} \end{bmatrix} \\ = \begin{bmatrix} 1 & W^{(k+1,0)} \cdot z^{-1} \\ 1 & -W^{(k+1,0)} \cdot z^{-1} \end{bmatrix} \end{aligned} \tag{4.33}$$

Knowing that $W^{(k+1,0)} \in \{+1, -1\}$, the system of equations has the following valid solutions:

$$A^{(k+1,0)} = -\frac{A^{(k+1,1)} - 1}{A^{(k+1,1)} + 1};\ \alpha_2 = \frac{A^{(k+1,1)} + 1}{\left(A^{(k+1,1)}\right)^2 + 1};\ W^{(k+1,1)} = -1 \tag{4.34}$$

Where $A^{(k+1,1)}$ is an arbitrary real number and $W^{(k+1,0)}$ permits to choose the set that is generated. For convenience, $A^{(k+1,1)}$ is set to $A^{(k+1,1)} = 3$, so the values of $A^{(k+1,0)}$ and $\alpha_2$ are equal to $-\frac{1}{2}$ and $\frac{2}{5}$ respectively; therefore the constant $\alpha = \alpha_1 \cdot \alpha_2$ must be equal to $2^{(2-Q/2)}/5$.

The parameter values for the other stages, i.e $\{W^{(k+1,2)}, \ldots, W^{(k+1,Q-1)}\}$ and $\{A^{(k+1,2)}, \ldots, A^{(k+1,Q-1)}\}$, $k \geq 1$, must be equal to $\{\pm 1, \ldots, \pm 1\}$ for all of them.

#### 4.3.1.2 $Q$ is an Odd Number

If $Q$ is an odd number, the product of the $Q$ matrices $\boldsymbol{\Upsilon}^{(q)}(z^{-1})$ can be arranged as follows:

$$\alpha \cdot \left\{ \prod_{q=Q-1}^{1} \boldsymbol{\Upsilon}^{(q)}\left(z^{-1}\right) \right\} \times \boldsymbol{\Upsilon}^{(0)}\left(z^{-1}\right) = \mathbf{H}_2^{(k+1)}\left(z^{-1}\right) \tag{4.35}$$

Now $Q-1$ is an even number and then, if each of the $Q-1$ matrices $\boldsymbol{\Upsilon}^{(q)}(z^{-1})$ is set to $\boldsymbol{\mathcal{H}}_2$, their product is equal to:

$$\begin{aligned} \alpha \cdot \prod_{q=Q-1}^{1} \boldsymbol{\Upsilon}^{(q)}\left(z^{-1}\right) &= \alpha \cdot 2^{\frac{Q-1}{2}} \cdot \mathbf{I}_2 \\ &= \mathbf{I}_2 \Leftrightarrow \alpha = 2^{\frac{1-Q}{2}} \end{aligned} \tag{4.36}$$

Therefore, each of the parameter values $\{A^{(k+1,0)}, \ldots, A^{(k+1,Q-1)}\}$ and $\{W^{(k+1,0)}, \ldots, W^{(k+1,Q-1)}\}$ must be equal to $\{\pm 1, \ldots, \pm 1\}$.

### 4.3.2 Golay Kernels 10 and 26

As shown previously, the Golay kernels 10 and 26 can be decomposed as the product of four and twelve basic building blocks $\mathbf{B}^{(1)}_{A^{(1,q)},W^{(1,q)}}(z^{-D^{(q)}})$, respectively. In both cases, the number of building blocks involved is an even number, so the decomposition of equation 4.30 is the same that was done for Golay kernel 2 when $Q$ is an even number.

In general, the generation matrix for $2 \cdot K_{|CSS}$ CSS of length $L_{|CSS} = K_{|CSS} \cdot 10^M$ is defined as

$$\mathbf{G}^{(k+1)}_{K_{|CSS} \cdot 10^M}\left(z^{-1}\right) = \left\{ \prod_{m=M-1}^{0} \mathbf{G}^{(k)}_{\frac{K_{|CSS}}{2} \cdot 10}\left(z^{-2}\right) \right\} \otimes \left\{ \alpha \cdot \prod_{m=4 \cdot M-1}^{0} \boldsymbol{\Upsilon}^{(m)}\left(z^{-1}\right) \right\} \tag{4.37}$$

In the same form, the generation matrix for $2 \cdot K_{|CSS}$ CSS of length $L_{|CSS} = K_{|CSS} \cdot 26^P$ can be expressed as

$$\mathbf{G}^{(k+1)}_{K_{|CSS} \cdot 26^P}\left(z^{-1}\right) = \left\{ \prod_{p=P-1}^{0} \mathbf{G}^{(k)}_{\frac{K_{|CSS}}{2} \cdot 26}\left(z^{-2}\right) \right\} \otimes \left\{ \alpha \cdot \prod_{p=12 \cdot P-1}^{0} \boldsymbol{\Upsilon}^{(p)}\left(z^{-1}\right) \right\} \tag{4.38}$$

where the generation matrix of the Golay kernel 26, $\mathbf{G}^{(1)}_{26}(z^{-1})$, is defined in equation 4.17, and the interleaving matrices $\boldsymbol{\Upsilon}^{(p)}(z^{-1})$ are decomposed as stated from equation 4.30 to equation 4.34.

**Example.** Consider the generation of a CSS composed of $2 \cdot K_{|CSS} = 2 \cdot 2^k = 4$ sequences of length $L_{|CSS} = K_{|CSS} \cdot 10^M = 20$ (i.e. $k = 1$, $N = 0$, $M = 1$ and $P = 0$) in $Q = 4$ stages. Hence, the matrix $\mathbf{H}^{(k+1)}_2(z^{-1})$ is expressed as follows:

$$\begin{aligned}
\mathbf{H}^{(k+1)}_2\left(z^{-1}\right) &= \alpha \cdot \boldsymbol{\Upsilon}^{(3)}\left(z^{-1}\right) \times \boldsymbol{\Upsilon}^{(2)}\left(z^{-1}\right) \times \boldsymbol{\Upsilon}^{(1)}\left(z^{-1}\right) \times \boldsymbol{\Upsilon}^{(0)}\left(z^{-1}\right) \\
&= \alpha \cdot \begin{bmatrix} 1 & A^{(k+1,3)} \cdot W^{(k+1,3)} \\ A^{(k+1,3)} & -W^{(k+1,3)} \end{bmatrix} \times \begin{bmatrix} 1 & A^{(k+1,2)} \cdot W^{(k+1,2)} \\ A^{(k+1,2)} & -W^{(k+1,2)} \end{bmatrix} \\
&\times \begin{bmatrix} 1 & A^{(k+1,1)} \cdot W^{(k+1,1)} \\ A^{(k+1,1)} & -W^{(k+1,1)} \end{bmatrix} \times \begin{bmatrix} 1 & A^{(k+1,0)} \cdot W^{(k+1,0)} \cdot z^{-1} \\ A^{(k+1,0)} & -W^{(k+1,0)} \cdot z^{-1} \end{bmatrix} \\
&= \begin{bmatrix} 1 & W^{(k+1,0)} \cdot z^{-1} \\ 1 & -W^{(k+1,0)} \cdot z^{-1} \end{bmatrix}
\end{aligned}$$

Following the procedure indicated from equation 4.30 to equation 4.34, the matrix $\mathbf{H}_2^{(k+1)}(z^{-1})$ is equal to:

$$\begin{aligned}\mathbf{H}_2^{(k+1)}\left(z^{-1}\right) = \frac{1}{5}\cdot\begin{bmatrix}1 & 1\\ 1 & -1\end{bmatrix}\times\begin{bmatrix}1 & 1\\ 1 & -1\end{bmatrix}\\ \times\begin{bmatrix}1 & -3\\ 3 & 1\end{bmatrix}\times\begin{bmatrix}1 & -\frac{1}{2}\cdot W^{(k+1,0)}\cdot z^{-1}\\ -\frac{1}{2} & -W^{(k+1,0)}\cdot z^{-1}\end{bmatrix}\\ = \begin{bmatrix}1 & W^{(k+1,0)}\cdot z^{-1}\\ 1 & -W^{(k+1,0)}\cdot z^{-1}\end{bmatrix}\end{aligned}$$

Due to $M = 1$, we must use the basic building blocks of the Golay kernel 10 decomposition (refer to equation 4.15) and equation 4.37 for the generation of the matrix $\mathbf{G}_{20}^{(2)}(z^{-1})$. Therefore, the generation matrix for 4 CSS of length $L_{|CSS} = 20$ is as follows:

$$\begin{aligned}\mathbf{G}_{20}^{(2)}\left(z^{-1}\right) = \frac{1}{5}\cdot\left(\mathbf{B}_{1,1}^{(1)}\left(z^{-6}\right)\otimes\boldsymbol{\Upsilon}^{(3)}\left(z^{-1}\right)\right)\times\left(\mathbf{B}_{1,-1}^{(1)}\left(z^{-2}\right)\otimes\boldsymbol{\Upsilon}^{(2)}\left(z^{-1}\right)\right)\\ \times\left(\mathbf{B}_{1/2,-1}^{(1)}\left(z^{-2}\right)\otimes\boldsymbol{\Upsilon}^{(1)}\left(z^{-1}\right)\right)\times\left(\mathbf{B}_{1,1}^{(1)}\left(z^{-8}\right)\otimes\boldsymbol{\Upsilon}^{(0)}\left(z^{-1}\right)\right)\end{aligned}$$

By doing the Kronecker product in the previous equation and considering only the generation of the CSS with $W^{(k+1,0)} = 1$, the generation matrix is defined as

$$\begin{aligned}\mathbf{G}_{20}^{(2)}(z^{-1}) = \frac{1}{5}\cdot\begin{bmatrix}1 & 1 & z^{-6} & z^{-6}\\ 1 & -1 & z^{-6} & -z^{-6}\\ 1 & 1 & -z^{-6} & -z^{-6}\\ 1 & -1 & -z^{-6} & z^{-6}\end{bmatrix}\times\begin{bmatrix}1 & 1 & -z^{-2} & -z^{-2}\\ 1 & -1 & -z^{-2} & z^{-2}\\ 1 & 1 & z^{-2} & z^{-2}\\ 1 & -1 & z^{-2} & -z^{-2}\end{bmatrix}\\ \times\begin{bmatrix}1 & -3 & -\frac{1}{2}\cdot z^{-2} & \frac{3}{2}\cdot z^{-2}\\ 3 & 1 & -\frac{3}{2}\cdot z^{-2} & -\frac{1}{2}\cdot z^{-2}\\ \frac{1}{2} & -\frac{3}{2} & z^{-2} & -3\cdot z^{-2}\\ \frac{3}{2} & \frac{1}{2} & 3\cdot z^{-2} & z^{-2}\end{bmatrix}\times\begin{bmatrix}1 & -\frac{1}{2}\cdot z^{-1} & z^{-8} & -\frac{1}{2}\cdot z^{-9}\\ -\frac{1}{2} & -1\cdot z^{-1} & -\frac{1}{2}\cdot z^{-8} & -z^{-9}\\ 1 & -\frac{1}{2}\cdot z^{-1} & -z^{-8} & \frac{1}{2}\cdot z^{-9}\\ -\frac{1}{2} & -1\cdot z^{-1} & \frac{1}{2}\cdot z^{-8} & z^{-9}\end{bmatrix}\end{aligned}$$

Finally, by developing the products in the previous equation and by using equation 4.25, the binary CSS composed of $K_{|CSS} = 4$ sequences of length $L_{|CSS} = 20$ is as follows:

$$\mathbf{S}_j^{(2,4)}\left(z^{-1}\right) = \begin{bmatrix} S_{j,0}^{(4)}(z^{-1}) \\ S_{j,1}^{(4)}(z^{-1}) \\ S_{j,2}^{(4)}(z^{-1}) \\ S_{j,3}^{(4)}(z^{-1}) \end{bmatrix} = \begin{bmatrix} \sum_{l=0}^{19} s_{j,0}^{(4)}[l] \cdot z^{-l} \\ \sum_{l=0}^{19} s_{j,1}^{(4)}[l] \cdot z^{-l} \\ \sum_{l=0}^{19} s_{j,2}^{(4)}[l] \cdot z^{-l} \\ \sum_{l=0}^{19} s_{j,3}^{(4)}[l] \cdot z^{-l} \end{bmatrix}$$

where $j$ can be any value belonging to $0 \leq j \leq K_{|CSS} - 1$. The set $\{s_{j,0}^{(4)}[l], s_{j,1}^{(4)}[l], s_{j,2}^{(4)}[l], s_{j,3}^{(4)}[l]\}$ is equal to:

$$\begin{aligned}
s_{j,0}^{(4)}[l] &= \{+1,+1,-1,-1,-1,-1,+1,+1,+1,+1,+1,+1,+1,+1,+1,+1,+1,-1,-1\} \\
s_{j,1}^{(4)}[l] &= \{+1,-1,-1,+1,-1,+1,+1,-1,+1,-1,+1,-1,+1,-1,+1,-1,+1,-1,-1,+1\} \\
s_{j,2}^{(4)}[l] &= \{+1,+1,-1,-1,-1,-1,-1,-1,+1,+1,-1,-1,+1,+1,-1,-1,-1,-1,+1,+1\} \\
s_{j,3}^{(4)}[l] &= \{+1,-1,-1,+1,-1,+1,-1,+1,+1,-1,-1,+1,+1,-1,-1,+1,-1,+1,+1,-1\}
\end{aligned}$$

If we carry out the SACF of this set of sequences, it can be demonstrated that it is a CSS.

▲

Now, by using the property of the mixed product and the Turyn's construction [Turyn 74], the generation matrices of equations 4.28, 4.37 and 4.38 can be cascaded to build the generation matrix for $2 \cdot K_{|CSS}$ CSS of length $L_{|CSS} = K_{|CSS} \cdot \left(2^N \cdot 10^M \cdot 26^P\right)$ in $Q$ stages as

$$\begin{aligned}
\mathbf{G}_{K_{|CSS} \cdot 2^N \cdot 10^M \cdot 26^P}^{(k+1)}\left(z^{-1}\right) = &\left\{ \prod_{p=P-1}^{0} \mathbf{G}_{K_{|CSS} \cdot 26}^{(k+1)}\left(z^{-K_{|CSS} \cdot 2^N \cdot 10^M \cdot 26^p}\right) \right\} \\
&\times \left\{ \prod_{m=M-1}^{0} \mathbf{G}_{K_{|CSS} \cdot 10}^{(k+1)}\left(z^{-K_{|CSS} \cdot 2^N \cdot 10^m}\right) \right\} \\
&\times \left\{ \prod_{n=N-1}^{0} \mathbf{G}_{K_{|CSS} \cdot 2}^{(k+1)}\left(z^{-K_{|CSS} \cdot 2^n}\right) \right\}
\end{aligned} \tag{4.39}$$

This generation matrix can be expressed in terms of the Kronecker product as stated in the next equation:

$$\begin{aligned}\mathbf{G}^{(k+1)}_{K_{|CSS}\cdot 2^N\cdot 10^M\cdot 26^P}\left(z^{-1}\right) = &\left\{\left[\prod_{p=P-1}^{0}\mathbf{G}^{(k)}_{\frac{K_{|CSS}}{2}\cdot 26}\left(z^{-2^{(N+1)}\cdot 10^M\cdot 26^p}\right)\right]\otimes\left[\prod_{p=Q-1}^{Q-12\cdot P}\boldsymbol{\Upsilon}^{(p)}\left(z^{-1}\right)\right]\right\}\\ &\times\left\{\left[\prod_{m=M-1}^{0}\mathbf{G}^{(k)}_{\frac{K_{|CSS}}{2}\cdot 10}\left(z^{-2^{(N+1)}\cdot 10^m}\right)\right]\otimes\left[\prod_{m=Q-12\cdot P-1}^{N}\boldsymbol{\Upsilon}^{(m)}\left(z^{-1}\right)\right]\right\}\\ &\times\left\{\left[\prod_{n=N-1}^{0}\mathbf{B}^{(k)}_{A^{(k,n)},W^{(k,n)}}\left(z^{-2^{(n+1)}}\right)\right]\otimes\left[\prod_{n=N-1}^{0}\boldsymbol{\Upsilon}^{(n)}\left(z^{-1}\right)\right]\right\}\end{aligned} \tag{4.40}$$

Figure 4.4 depicts the stage $q = 0$ and the $q$-th stage of the lattice filter for the generation of 4 CSS of length $L_{|CSS} = 2^{(N+1)}\cdot 10^M\cdot 26^P$, whereas Figure 4.5 shows the stage $q = 0$ and the $q$-th stage for the generation of $K_{|CSS}$-CSS[2] of lengths $L_{|CSS} = \frac{K_{|CSS}}{2}\cdot 2^N\cdot 10^M\cdot 26^P$.

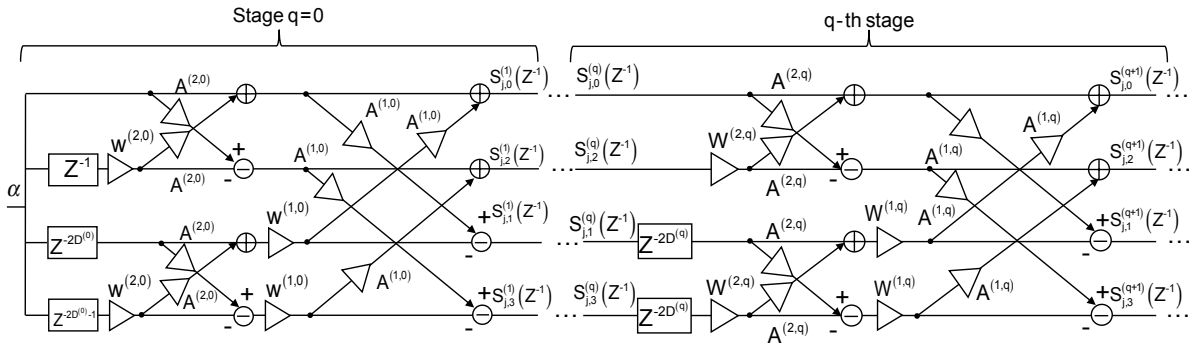


Figure 4.4: Stage $q = 0$ and $q$-th stage ($1 \leq q \leq Q-1$) of a modular generator of 4 CSS of length $L_{|CSS} = 2^{(N+1)}\cdot 10^M\cdot 26^P$.

To generate $K_{|CSS}$ uncorrelated CSS, the variations with repetition of the seeds $\{W^{(1,0)}, W^{(2,0)},\ldots,W^{(k,0)}\} \in \{-1,+1\}$ establish the set that is generated. The number of variations with repetition of the two feasible seed values $\{-1,+1\}$, taken from $k$ in $k$ is equal to $K_{|CSS} = 2^k$. So the variations of the seed values generate up to $K_{|CSS}$ uncorrelated CSS. For example, if $K_{|CSS} = 4$ CSS of length $L_{|CSS} = 4$ is going to be generated by using equation 4.28 (where $\boldsymbol{\Upsilon}^{(0)}(z^{-1}) = \mathbf{H}_2^{(2)}(z^{-1})$, $A^{(1,0)} = 1$ and $\alpha = 1$), the generation

[2]Notice that for generating $K_{|CSS}$ CSS of length $L_{|CSS} = \frac{K_{|CSS}}{2}\cdot 2^N\cdot 10^M\cdot 26^P$ we have to carry out one iteration less in equation 4.19 than for generating $2\cdot K_{|CSS}$ CSS of length $L_{|CSS} = K_{|CSS}\cdot 2^N\cdot 10^M\cdot 26^P$.

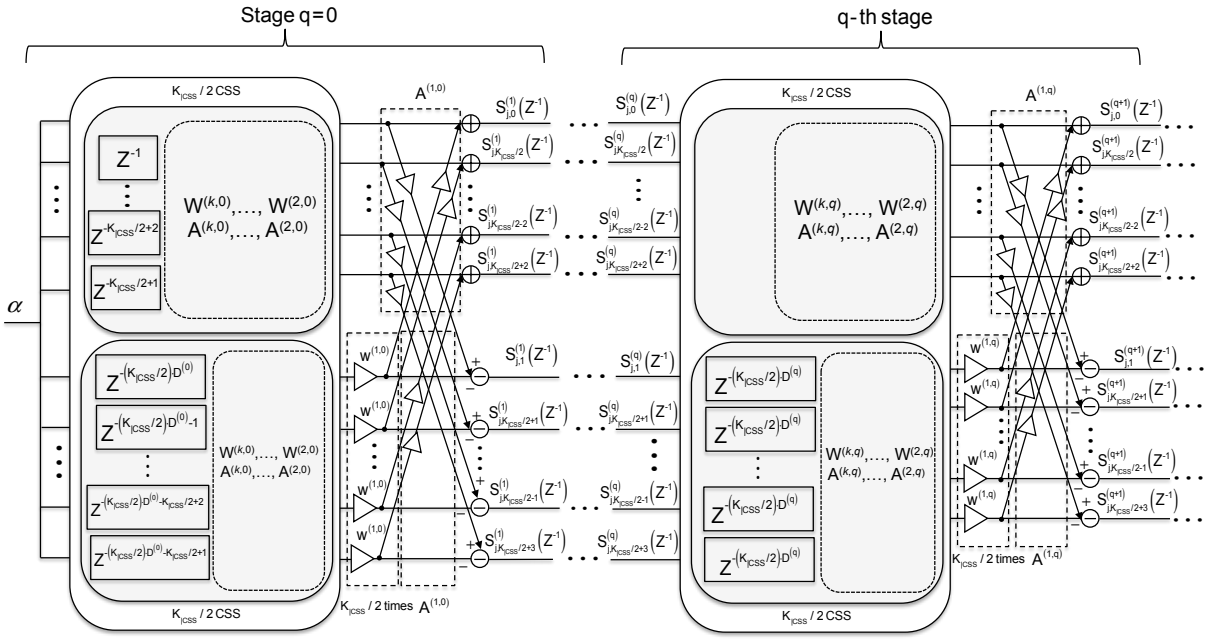


Figure 4.5: Stage $q = 0$ and $q$-th stage ($1 \leq q \leq Q-1$) of a modular generator of $K_{|CSS}$ CSS of length $L_{|CSS} = \frac{K_{|CSS}}{2} \cdot 2^N \cdot 10^M \cdot 26^P$.

matrix is equal to:

$$\mathbf{G}_4^{(2)}\left(z^{-1}\right) = \begin{bmatrix} 1 & A^{(1,0)} \cdot W^{(1,0)} \cdot z^{-2} \\ A^{(1,0)} & -W^{(1,0)} \cdot z^{-2} \end{bmatrix} \otimes \begin{bmatrix} 1 & W^{(2,0)} \cdot z^{-1} \\ 1 & -W^{(2,0)} \cdot z^{-1} \end{bmatrix}$$

$$= \begin{bmatrix} 1 & A^{(1,0)} \cdot W^{(1,0)} \cdot z^{-2} & W^{(2,0)} \cdot z^{-1} & A^{(1,0)} \cdot W^{(1,0)} \cdot W^{(2,0)} \cdot z^{-3} \\ A^{(1,0)} & -W^{(1,0)} \cdot z^{-2} & A^{(1,0)} \cdot W^{(2,0)} \cdot z^{-1} & -W^{(1,0)} \cdot W^{(2,0)} \cdot z^{-3} \\ 1 & A^{(1,0)} \cdot W^{(1,0)} \cdot z^{-2} & -W^{(2,0)} \cdot z^{-1} & -A^{(1,0)} \cdot W^{(1,0)} \cdot W^{(2,0)} \cdot z^{-3} \\ A^{(1,0)} & -W^{(1,0)} \cdot z^{-2} & -A^{(1,0)} \cdot W^{(2,0)} \cdot z^{-1} & W^{(1,0)} \cdot W^{(2,0)} \cdot z^{-3} \end{bmatrix} \tag{4.41}$$

For the sake of clarity, the generation of $K_{|CSS} = 4$ CSS of length $L_{|CSS} = 4$ ($N = 1$), for different seed values, is included in Table 4.2.

## 4.4 Correlation of $K_{|CSS}$-CSS

The previous generation algorithm for $K_{|CSS}$ represents a lattice filter with an impulse response equal to the $K_{|CSS}$-CSS. So, if it is modified to generate the reversed CSS, the architecture will be equivalent to a filter matched to the direct sequences. Therefore, the

| $W^{(1,0)}=+1,\ W^{(2,0)}=+1$ | $W^{(1,0)}=-1,\ W^{(2,0)}=+1$ |
|---|---|
| $\begin{bmatrix} 1 & z^{-2} & z^{-1} & z^{-3} \\ 1 & z^{-2} & -z^{-1} & -z^{-3} \\ 1 & -z^{-2} & z^{-1} & -z^{-3} \\ 1 & -z^{-2} & -z^{-1} & z^{-3} \end{bmatrix}$ | $\begin{bmatrix} 1 & z^{-2} & -z^{-1} & -z^{-3} \\ 1 & z^{-2} & z^{-1} & z^{-3} \\ 1 & -z^{-2} & -z^{-1} & z^{-3} \\ 1 & -z^{-2} & z^{-1} & -z^{-3} \end{bmatrix}$ |
| $W^{(1,0)}=+1,\ W^{(2,0)}=-1$ | $W^{(1,0)}=-1,\ W^{(2,0)}=+-1$ |
| $\begin{bmatrix} 1 & -z^{-2} & z^{-1} & -z^{-3} \\ 1 & -z^{-2} & -z^{-1} & z^{-3} \\ 1 & z^{-2} & z^{-1} & z^{-3} \\ 1 & z^{-2} & -z^{-1} & -z^{-3} \end{bmatrix}$ | $\begin{bmatrix} 1 & -z^{-2} & -z^{-1} & z^{-3} \\ 1 & -z^{-2} & z^{-1} & -z^{-3} \\ 1 & z^{-2} & -z^{-1} & -z^{-3} \\ 1 & z^{-2} & z^{-1} & z^{-3} \end{bmatrix}$ |

Table 4.2: Generation matrices of 4 CSS obtained as a combination of the seed values at the first stage.

correlator is designed by reversing the delays in each stage of the previous generation algorithm.

Figure 4.6 and Figure 4.7 show the correlator for 2 CSS and 4 CSS respectively. In this case, the delay elements are placed now in the upper branch when compared to the generators of Figure 4.3 and Figure 4.4. Moreover, the stage $q = 0$ has a different delay arrangement compared to the other stages ($1 \leq q \leq Q-1$). This is due to the interleaving operation carried out to increase the set size. The terms $\phi_{R,S_{j,i}^{(q)}}(z^{-1})$ are intermediate results different from the aperiodic correlation function, which only appears at the end of the final stage.

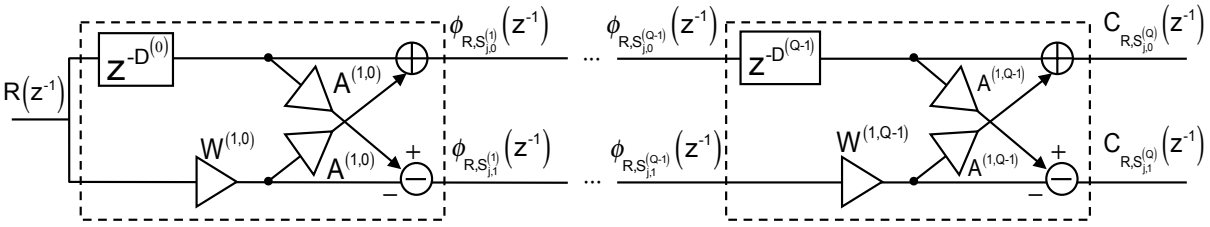


Figure 4.6: Modular correlator of Golay pairs of sequences of length $L_{|Gol} = 2^N \cdot 10^M \cdot 26^P$.

This can be carried out for $K_{|CSS}$-CSS in the same form, as depicted in Figure 4.8, which is the reversed version of the generator of Figure 4.5.

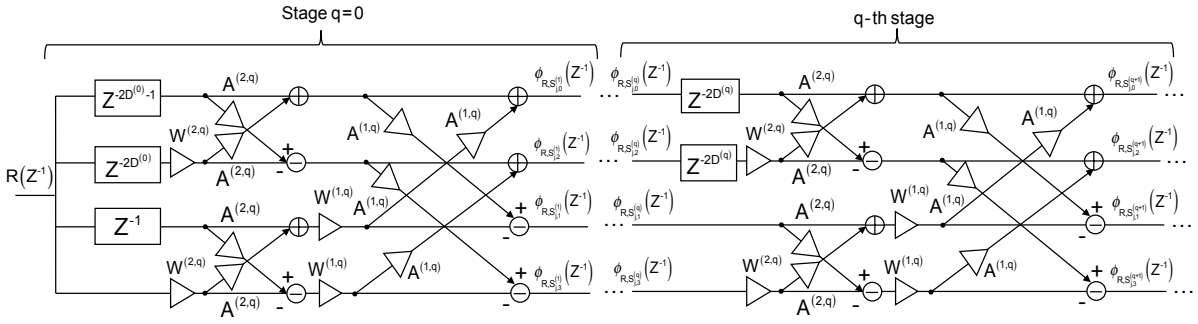


Figure 4.7: Stage $q = 0$ and $q$-th stage ($1 \leq q \leq Q-1$) of a modular correlator of 4 CSS of length $L_{|CSS} = 2^{(N+1)} \cdot 10^M \cdot 26^P$.

## 4.5 Implementation Issues

According to the previous figures, in each $k$-th expansion step, new seed values $W^{(k,q)}$ appear at the beginning of the blocks and the seeds of the previous expansions steps $(W^{(k-1,q)}, \ldots, W^{(1,q)})$ are shifted to the right. Additionally, the delays of the first stage for the generation algorithm will be arranged as

$$\left\{1, z^{-1}, z^{-2}, \ldots, z^{-\frac{K_{|CSS}}{2}+1}, z^{-\frac{K_{|CSS}}{2}\cdot D^{(0)}}, z^{-\frac{K_{|CSS}}{2}\cdot D^{(0)}-1}, \ldots, z^{-\frac{K_{|CSS}}{2}\cdot D^{(0)}-\frac{K_{|CSS}}{2}+1}\right\} \tag{4.42}$$

while in the other stages, half of the branches will have delays equal to $(\frac{K_{|CSS}}{2}) \cdot D^{(q)}$, $q > 0$. Table 4.3 shows the number of products and additions needed to perform the generation/correlation of a complementary sequence with the proposed algorithm and with a straightforward architecture. To perform the sum of aperiodic correlations functions, it is necessary to replicate the architectures (both the straightforward and the proposed one) $K_{|CSS} - 1$ times more and to carry out an extra addition. Additionally, Table 4.4 includes some examples of the operations required for the generation/correlation of a complementary sequence for several lengths. Notice that many of the products involved in the correlations are by 1/2, and they can be implemented by shifting.

Notice that although for certain sequence lengths, the proposed architecture would require more number of operations than the straightforward one, the proposal computes $K_{|CSS}$ simultaneous correlations (although only one is used for a given data input). Therefore, the proposal could be more efficient by transposing it in a similar way as was done in [De Ma 11]. Then, the architecture would carry out simultaneously the $K_{|CSS}$ aperiodic correlations needed to perform the sum of aperiodic correlations.

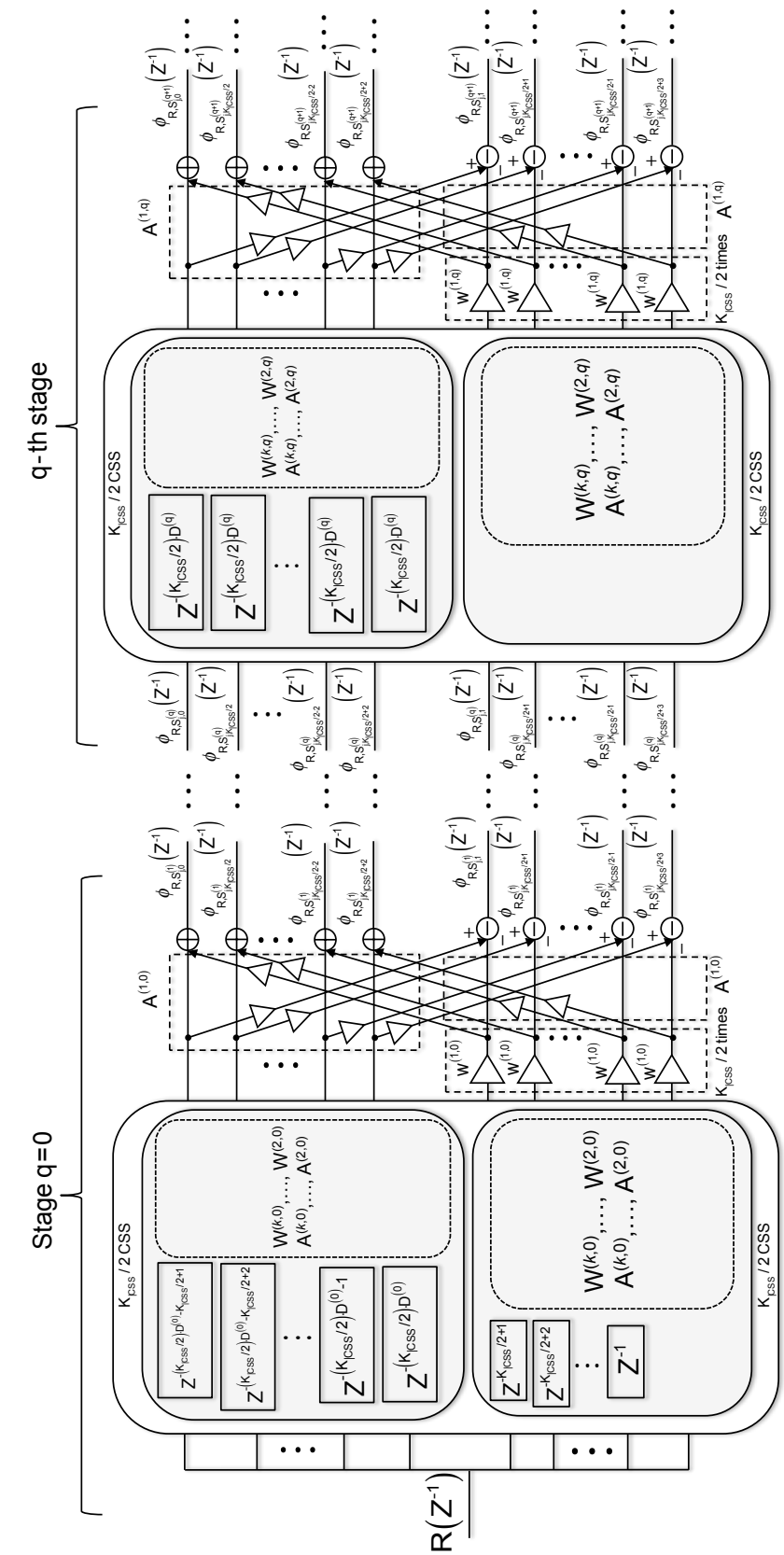


Figure 4.8: Stage $q = 0$ and $q$-th stage ($1 \leq q \leq Q-1$) of a modular correlator of $K_{|CSS}$-CSS of length $L_{|CSS} = \frac{K_{|CSS}}{2} \cdot 2^N \cdot 10^M \cdot 26^P$.

| | | Proposed |
|---|---|---|
| Additions | $2^N$ | $N \cdot K_{\|CSS} \cdot log_2(K_{\|CSS})$ |
| | $10^M$ | $4 \cdot M \cdot K_{\|CSS} \cdot log_2(K_{\|CSS})$ |
| | $26^P$ | $12 \cdot P \cdot K_{\|CSS} \cdot log_2(K_{\|CSS})$ |
| Products | $2^N$ | $\begin{cases} 2 \cdot K_{\|CSS} \cdot [log_2(K_{\|CSS}) - 1] & \text{if } N \text{ even} \cap K_{\|CSS} > 2 \\ 0 & \text{if } N \text{ odd} \cup K_{\|CSS} = 2 \end{cases}$ |
| | $10^M$ | $\begin{cases} 2 \cdot K_{\|CSS} \cdot [log_2(K_{\|CSS}) - 1] + M \cdot K_{\|CSS} & \text{if } N = 0 \cap K_{\|CSS} > 2 \\ M \cdot K_{\|CSS} & \text{if } N \neq 0 \cup K_{\|CSS} = 2 \end{cases}$ |
| | $26^P$ | $\begin{cases} 2 \cdot K_{\|CSS} \cdot [log_2(K_{\|CSS}) - 1] + 9 \cdot P \cdot K_{\|CSS} & \text{if } N = 0 \cap M = 0 \cap K_{\|CSS} > 2 \\ 9 \cdot P \cdot K_{\|CSS} & \text{if } N \neq 0 \cup M \neq 0 \cup K_{\|CSS} = 2 \end{cases}$ |
| Straightforward | | |
| Additions | $\frac{K_{\|CSS}}{2} \cdot (2^N \cdot 10^M \cdot 26^P) - 1$ | |
| Products | 0 | |

Table 4.3: Operations needed for the generation/correlation of $K_{|CSS}$-CSS as a function of $K_{|CSS}$, $N$, $M$ and $P$ (considering only one sequence for the straightforward architecture).

As stated in Chapter 3 for the generation/correlation architectures of multilevel CSS, in order to avoid quantization effects, the data bus width has to be increased in each stage. Fortunately, lattice architectures, as the one proposed are robust to severe quantization effects [Vaidy 93]. In fact, the efficient architecture for $K_{|Gol} = 2$ Golay binary sequence pairs of length $L_{|Gol} = 2^N \cdot 10^M \cdot 26^P$ has been satisfactorily implemented in [Casti 13] by using a FPGA Virtex 5 (XC5VLX50T) [Xilin 12a]. The maximum Sidelobe-to-Mainlobe Ratio (SMR) in the SACF due to quantization errors is equal to 0.422% for a length $L_{|Gol} = 26$, by using the following configuration: an input data bus width of 10 bits, an output data bus width of 24 bits and the Golay kernels coefficients represented by means of the SPT decomposition [Lim 99]. For clarity we include the Table 4.5, that shows the SMR in the SACF for different lengths of Golay binary sequence pairs obtained with the implementation of [Casti 13].

## 4.6 Conclusions

In this chapter we have presented the Golay kernel 26 decomposition in twelve stages of a lattice filter, by iterating backwards the generation algorithm for pairs of multilevel complementary sequences. Then, by using the Golay kernel 10 decomposition proposed by Budišin [Budis 11] we have proposed an efficient generator/correlator for Golay binary

| $K_{\|CSS}$, $N$, $M$, $P$, $L$ | Straightforward | | Proposed | |
|---|---|---|---|---|
| | Additions | Products | Additions | Products |
| $K_{\|CSS}=2$, $N=0$, $M=1$, $P=1$, $L_{\|CSS}=260$ | 259 | 0 | 32 | 20 |
| $K_{\|CSS}=4$, $N=3$, $M=1$, $P=0$, $L_{\|CSS}=160$ | 159 | 0 | 56 | 4 |
| $K_{\|CSS}=8$, $N=1$, $M=2$, $P=0$, $L_{\|CSS}=400$ | 399 | 0 | 216 | 16 |
| $K_{\|CSS}=8$, $N=4$, $M=0$, $P=1$, $L_{\|CSS}=1664$ | 1663 | 0 | 384 | 104 |

Table 4.4: Number of operations needed for the generation/correlation of $K_{|CSS}$-CSS for several lengths (considering only one sequence for the straightforward architecture).

| $N$ | $M$ | $P$ | $L_{\|Gol}$ | SMR(%) |
|---|---|---|---|---|
| 0 | 0 | 1 | 26 | 0.42 |
| 2 | 2 | 0 | 400 | 0 |
| 4 | 0 | 1 | 416 | 0.15 |
| 9 | 0 | 0 | 512 | 0 |
| 1 | 1 | 1 | 520 | 0.18 |
| 3 | 2 | 0 | 800 | 0 |
| 0 | 3 | 0 | 1000 | 0 |

Table 4.5: SMR in the SACF for different lengths of Golay binary sequence pairs.

sequence pairs of length $L_{|Gol} = 2^N \cdot 10^M \cdot 26^P$ (with $P > 0$) composed of $Q = N + 4 \cdot M + 12 \cdot P$ stages of a lattice filter.

Finally, we have generalized the previous efficient architectures [Worne 95, Alvar 04, De Ma 07] to $K_{|CSS} = 2^k$ binary CSS of length $L_{|CSS} = \frac{K_{|CSS}}{2} \cdot 2^N \cdot 10^M \cdot 26^P$. These architectures could be improved further by using their transposed version as was done in [De Ma 11].

The contributions of this chapter allows to increase the versatility of previous efficient architectures reported in the literature. Moreover, as the CSS are used as basic blocks for the generation and correlation of several families of GO sequences used in QS-CDMA, the architectures presented in this chapter also contribute to improve the versatility of the

efficient generation/correlation algorithms for those GO sequences. This will be shown in the following chapter.

# Chapter 5

# Novel Algorithms for the Generation and Correlation of Generalized Orthogonal Sequences

As stated in Chapter 2, section 2.3.5, the interest for QS-CDMA systems has boosted [Suehi 94, Fan 03, Li 03] in the last years. GO spreading sequences are used in many fields as ranging applications [Perez 09c], channel identification [Kim 06] or MIMO OFDM communication systems [Jian 07]. These applications demand spreading sequences whose number, length, and ZCZ can be adapted without constraints. Furthermore, it is also required to generate and correlate the spreading sequences with a reduced hardware complexity. This is an active field of research with a large number of proposals in the last decade.

Here, the modular architectures presented in previous chapters are used to improve the properties of two families of GO sequences: LS and GPC sequences. This chapter presents three main contributions:

- Firstly, the generation of multilevel LS sequences with flexible ZCZ length.
- Secondly, we introduce an efficient algorithm for the generation and correlation of GPC sequences.
- Finally, we show the theoretical link between LS and the proposed efficient generator/correlator for GPC sequences. This relationship permits to propose a novel efficient algorithm for the generation/correlation of LS sequences which requires almost the same hardware resources than a previous efficient architecture [Perez 10].

## 5.1 Generation Algorithm of LS Sequences

Daoben Li introduced Large Area Synchronized (LAS) CDMA sequences as a candidate for the 3G standard in 2000 [Li 00, Li 02], and later it was proposed for the novel 4G standard [Li 03]. LAS codes are generated as a combination of LS sequences and LA (Large Area) sequences. A set of $K_{|LS}$ ternary sequences of length $L_{|LS}$, $\{\mathbf{V}[l] = \{v_k[l]\}; 0 \leq k \leq K_{|LS} - 1; 0 \leq l \leq L_{|LS} - 1\}$ ; $v_k \in \{-1, 0, +1\}$ are called LS sequences if their aperiodic correlation functions are as follows:

$$C_{v_i,v_j}[\tau] = \sum_{l=0}^{L_{|LS}-1-\tau} v_i[l] \cdot v_j[l+\tau] = \begin{cases} C_p, & \text{for } \tau = 0, \quad i = j \\ 0, & \text{for } 1 \leq |\tau| \leq W_{ZCZ}, \quad i = j \\ 0, & \text{for } 0 \leq |\tau| \leq W_{ZCZ}, \quad i \neq j \end{cases} \tag{5.1}$$

Where $v_i$, $v_j$ are two LS sequences of length $L_{|LS}$, $C_p$ is the correlation peak value, i.e. the energy of the sequence, obtained for the time shift $\tau = 0$, and $W_{ZCZ}$ is the ZCZ length of the LS sequence.

### 5.1.1 Generation of LS Sequences from Golay Binary Sequence Pairs

Given a Golay binary sequence pair of length $L_{|Gol} = 2^N \cdot 10^M \cdot 26^P$ in $Z$-domain: $\{S^{(Q)}_{0,0}(z^{-1}), S^{(Q)}_{0,1}(z^{-1})\}$ and its mate $\{S^{(Q)}_{1,0}(z^{-1}), S^{(Q)}_{1,1}(z^{-1})\}$, $K_{|LS}/2 = 2^{a-1}; a \in \mathbb{N} - \{0\}$ LS sequences $\{V_0(z^{-1}), V_1(z^{-1}), \ldots, V_{K_{|LS}/2}(z^{-1})\}$ of length $L_{|LS} = K_{|LS} \cdot L_{|Gol} + W_{|LS}$ are generated as stated in equation (5.2) [Stanc 01]:

$$V_k\left(z^{-1}\right) = \sum_{i=0}^{K_{|LS}/2-1} h_{k,i} \cdot z^{-i \cdot L_{|Gol}} \cdot \left[ S^{(Q)}_{\pi_i,0}\left(z^{-1}\right) + z^{-\left(\frac{K_{|LS}}{2} L_{|Gol} + W_{|LS}\right)} S^{(Q)}_{\pi_i,1}\left(z^{-1}\right) \right] \tag{5.2}$$

The notation $h_{k,i}$ refers to the row $k$ and column $i$ of a Hadamard matrix of order $K_{|LS}/2$ and $\pi_i$ is the element $i$ of a vector $\boldsymbol{\pi} = [\pi_0, \pi_1, \ldots, \pi_{K_{|LS}/2-1}], \pi_i \in \{0, 1\}$. The vector $\boldsymbol{\pi}$ represents the binary expansion of an arbitrary integer $p$, $0 \leq p \leq 2^{K_{|LS}/2-1}$, so as to $p = \sum_{i=0}^{K_{|LS}/2-1} \pi_i 2^i$ [Stanc 01].

Another group of $K_{|LS}/2$ LS sequences $\{V_{K_{|LS}/2}(z^{-1}), V_{K_{|LS}/2+1}(z^{-1}), \ldots, V_{K_{|LS}-1}(z^{-1})\}$ is generated if in the previous equation (5.2) the vector $\boldsymbol{\pi}$ is changed by its complementary: $\boldsymbol{\pi}^* = [\pi_0^*, \pi_1^*, \ldots, \pi_{K_{|LS}/2-1}^*]$, with $\pi_i^* = \pi_i + 1(mod\,2)$.

In order to avoid the overlapping of the Golay sequences $S_{\pi_i,0}^{(Q)}(z^{-1})$ and $S_{\pi_{i'},1}^{(Q)}(z^{-1})$, $(i \neq i',\, 0 \leq i, i' \leq \frac{K_{|LS}}{2} - 1)$ a chain of zeros of length $W_{|LS}$ is introduced. The length of this chain is equal to the ZCZ length if and only if $W_{|LS} \leq L_{|Gol} - 1$. This implies that for a given set size of $K_{|LS}$ LS sequences, the maximum ZCZ length[1] is equal to $L_{|Gol} - 1$. Moreover, despite of the fact that there is a trade-off between $W_{|LS}$ and the energy efficiency, $W_{|LS}$ is commonly chosen as $W_{|LS} = L_{|Gol} - 1$.

**Example.** Figure 5.1 shows a scheme of the generation of $K_{|LS} = 4$ LS sequences of length $L_{|LS} = K_{|LS} \cdot L_{|Gol} + W_{|LS} = 5 \cdot L_{|Gol} - 1$, according to [Stanc 01]. The vectors $\boldsymbol{\pi}$ and $\boldsymbol{\pi}^*$ determine the concatenation order.

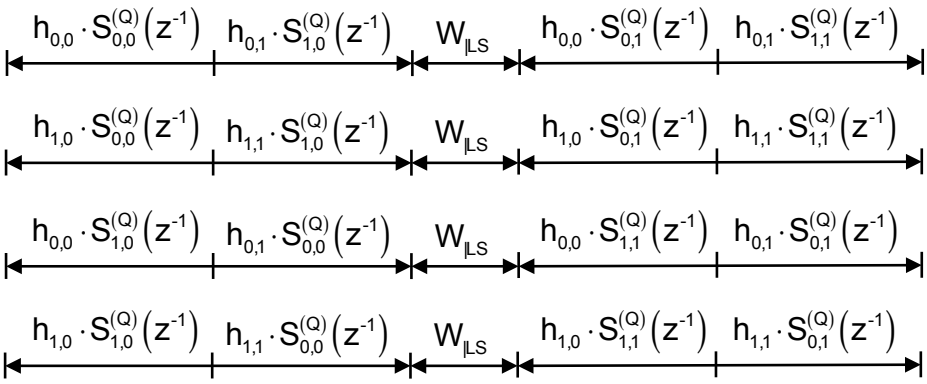


Figure 5.1: Scheme of the generation algorithm of 4 LS sequences with $\boldsymbol{\pi} = [0, 1]$ and $\boldsymbol{\pi}^* = [1, 0]$, according to [Stanc 01].

To clarify that the maximum ZCZ length for a given set size $K_{|LS}$ is equal to $W_{ZCZ} = W_{|LS} = L_{|Gol} - 1$, consider the generation of $K_{|LS} = 4$ LS sequences $\{V_0(z^{-1}), \ldots, V_3(z^{-1})\}$ of length $L_{|LS} = 30$ bits, generated from Golay binary sequence pairs of length $L_{|Gol} = 4$ bits and a chain of zeros of length 14 bits. The maximum ZCZ length of this set of LS sequences is equal to 3 bits, despite of having inserted a chain of 14 zeros.

If we carry out the aperiodic cross-correlation function between any sequence from the first $K_{|LS}/2$ sequences of the set (i.e $V_0(z^{-1})$ or $V_1(z^{-1})$) with any other sequence of the second half of the set ($V_2(z^{-1})$ or $V_3(z^{-1})$), we can check that the maximum ZCZ

[1] In what follows, we assume that the ZCZ length is equal to $W_{|LS} = L_{|Gol} - 1$

length is equal to 3 bits. Figure 5.2 shows sequences $V_0(z^{-1})$, $V_2(z^{-1})$ and the aperiodic cross-correlation function among them, i.e. $V_0(z^{-1}) \cdot V_2(z)$ where $l$ is the time index of the sequences $0 \leq l \leq L_{|LS} - 1$; as depicted, the ZCZ length is limited by the length of the Golay binary sequence pairs used for the generation of the LS sequences and the insertion of more zeros than $L_{|Gol} - 1$ does not increase the ZCZ.

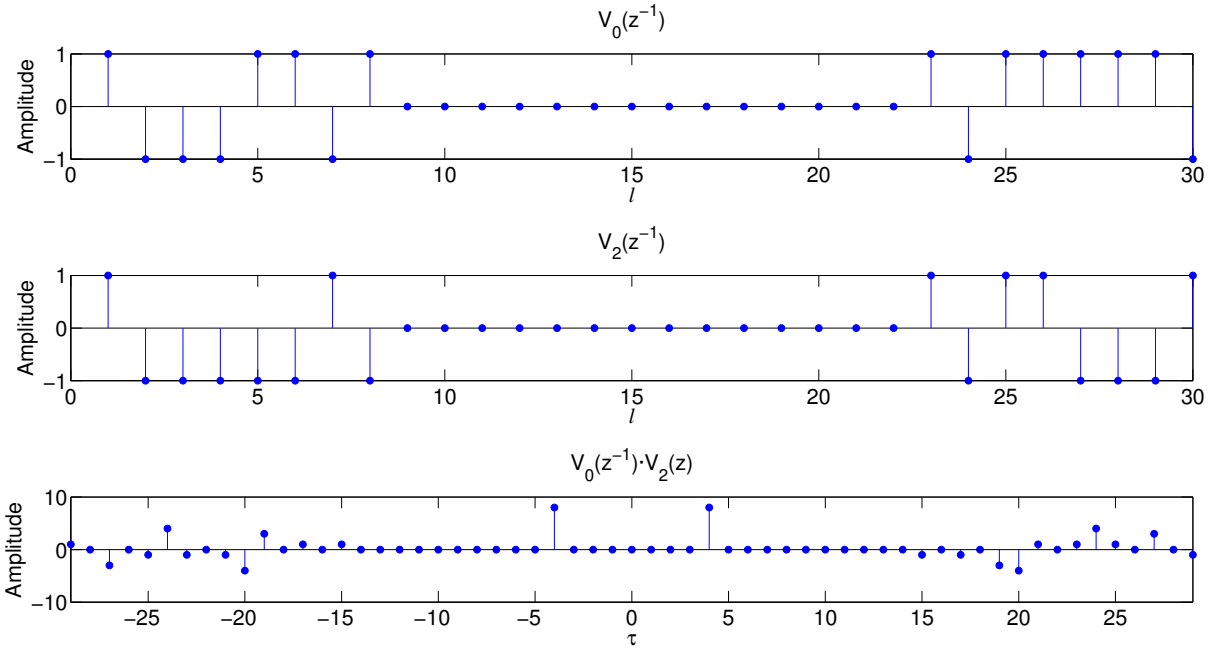


Figure 5.2: LS sequences of 30 bits with a chain of zeros of 14 bits and their aperiodic cross-correlation. The ZCZ length is limited by the length of the Golay binary sequence pairs used for their generation.

▲

LS sequences have been used in numerous applications due to their simplified architectures for their correlation and because they can be transmitted with a simple modulation scheme, as BPSK [Wei 05, Ullah 10, Perez 11].

## 5.2 Multilevel LS Sequences with Flexible ZCZ Length

The generation algorithm of LS sequences of equation 5.2 can be generalized to $K_{|MultLS} = K_{|LS}$ multilevel LS sequences with flexible ZCZ length if the sequences $S^{(Q)}_{\pi_i,0}(z^{-1})$ and $S^{(Q)}_{\pi_i,1}(z^{-1})$ are multilevel, i.e. if it is used the generation algorithm of equation 3.5 (refer to Chapter 3, section 3.1). This is mainly due to two factors:

1. There are no constraints on the length of the Pairs of Multilevel Complementary Sequences (PMCS), i.e. on the lengths of multilevel CSS of $K_{|MultCSS} = 2$ sequences.

2. The ZCZ length is equal to the length of the chain of zeros $W_{|LS}$ if and only if $W_{|LS} \leq L_{|Gol} - 1$. As stated previously it is assumed to be $W_{|LS} = L_{|Gol} - 1$.

The proposed generation algorithm for multilevel LS sequences uses as a basis the algorithm for generating power-of-two length complementary pairs of sequences (i.e. $M$ and $P$ are equal to zero). Nevertheless, it is possible to generate multilevel LS sequences with $M$ and $P$ larger than zero. This straightforward modification allows the generation of multilevel LS sequences of lengths $L_{|MultLS} = K_{|MultLS} \cdot L_{|MultLS} + W_{|MultLS}$; $W_{|MultLS} = L_{|PMCS} - 1$. Figure 5.3 shows a diagram block of the generation algorithm of multilevel LS sequences. This algorithm has the same stages as the one of [Stanc 01, Perez 08] for binary LS sequences.

In Chapter 3, section 3.4, we have determined the feasible lengths of the multilevel $K_{|MultCSS}$-CSS generated with the proposed algorithms. In order to generate PMCS without constraints on their lengths, the number of iterations of the algorithm, $Q$, is defined as was done in equation 3.47. And if it is particularized to $K_{|MultCSS} = 2$ is defined as

$$Q = \left\lceil log_2 \left( L_{|PMCS} \right) \right\rceil \tag{5.3}$$

The delay distribution is defined as was done in Chapter 3, section 3.4; particularized to PMCS it is equal to:

$$D^{(q)} = \begin{cases} \left\{ 2^0, \ldots, 2^{Q-2} \right\} & for\, 0 \leq q \leq Q-2 \\ L_{|PMCS} - 2^{Q-1} & for\, q = Q-1 \end{cases} \tag{5.4}$$

These parameters have been chosen accordingly for avoiding an excessive number of stages. In this way, the algorithm generates multilevel LS sequences with a power-of-two length in the stages $\{0, \ldots, Q-2\}$, by choosing any permutation of the delays $\left\{ 2^0, \ldots, 2^{Q-2} \right\}$. In the last iteration $Q-1$, the algorithm adjusts the delay $D^{(Q-1)}$ to generate PMCS of the desired length. The value of $D^{(Q-1)}$ is shown in equation 5.4, $A^{(q)}$ can be any real number and the seed values $W^{(1,q)}$ are the same as the ones for Golay binary sequence pairs for $0 \leq q \leq Q-1$.

By using this algorithm, there exist multilevel LS sequences for more lengths than for the binary LS ones. In fact, the length of binary LS sequences depends on the number of

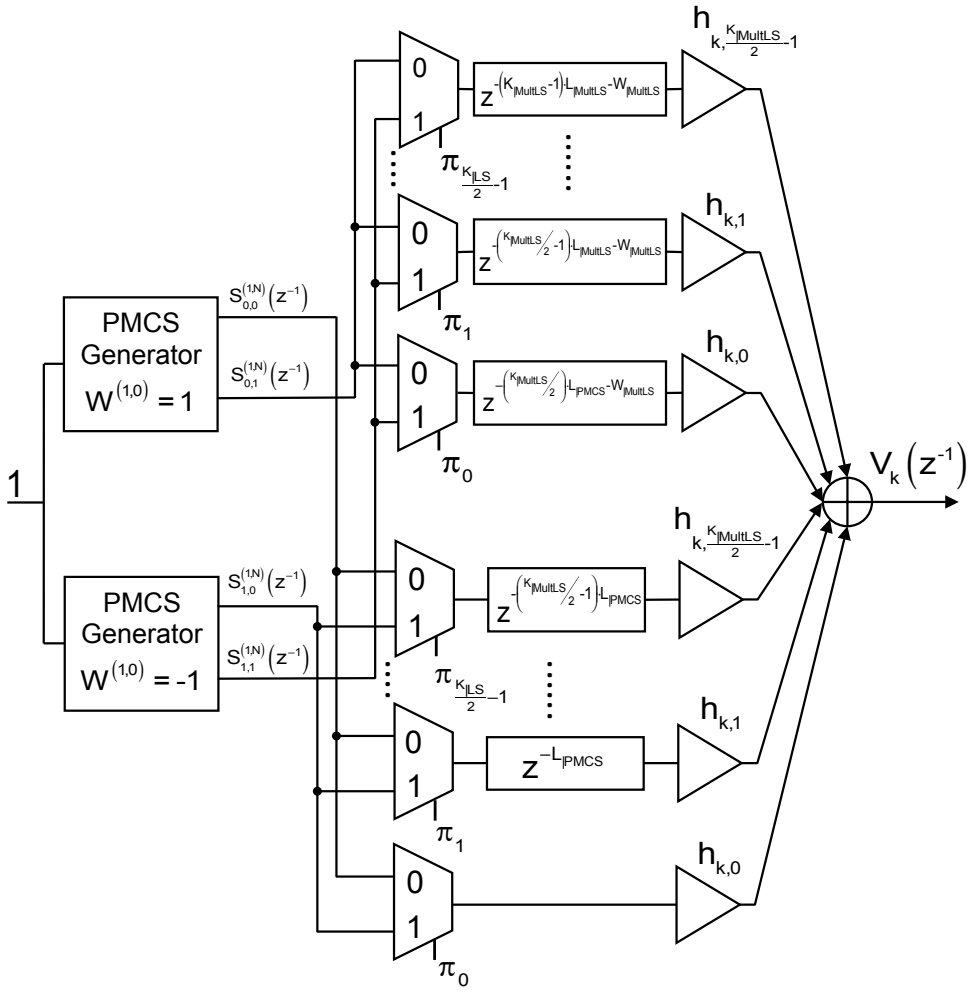


Figure 5.3: Diagram block of the generation of multilevel LS sequences.

LS sequences in the set, $K_{|LS}$, and on the known lengths of Golay binary sequence pairs, $L_{|Gol}$, whereas the length of multilevel LS sequences only depends on the set size $K_{|LS}$.

Figure 5.4 shows a multilevel LS sequence of length $L_{|MultLS} = 34$, generated from PMCS (equivalent to two multilevel CSS of $K_{|MultCSS} = 2$ sequences) in 3 stages with the parameters $A^{(q)} = \{1, 1, 2\}$, $D^{(q)} = \{1, 2, 3\}$ and $W^{(1,q)} = \{1, 1, 1\}$.

For the sake of better understanding the advantages of this new construction, consider the example of having a LPS working with four LS sequences, i.e. $K_{|LS} = 4$, and with maximum differences in the time of arrival between users (in sequence bits) of 85 bits. Therefore, to minimize ISI and MAI, the ZCZ length must be ZCZ $\geq$ 86 bits and the length of Golay pairs, $L_{|Gol}$, should be $W_{|LS} + 1 = 87$ bits. As there no exist Golay binary pairs of length 87 bits, it is needed complementary pairs of sequences of length 100

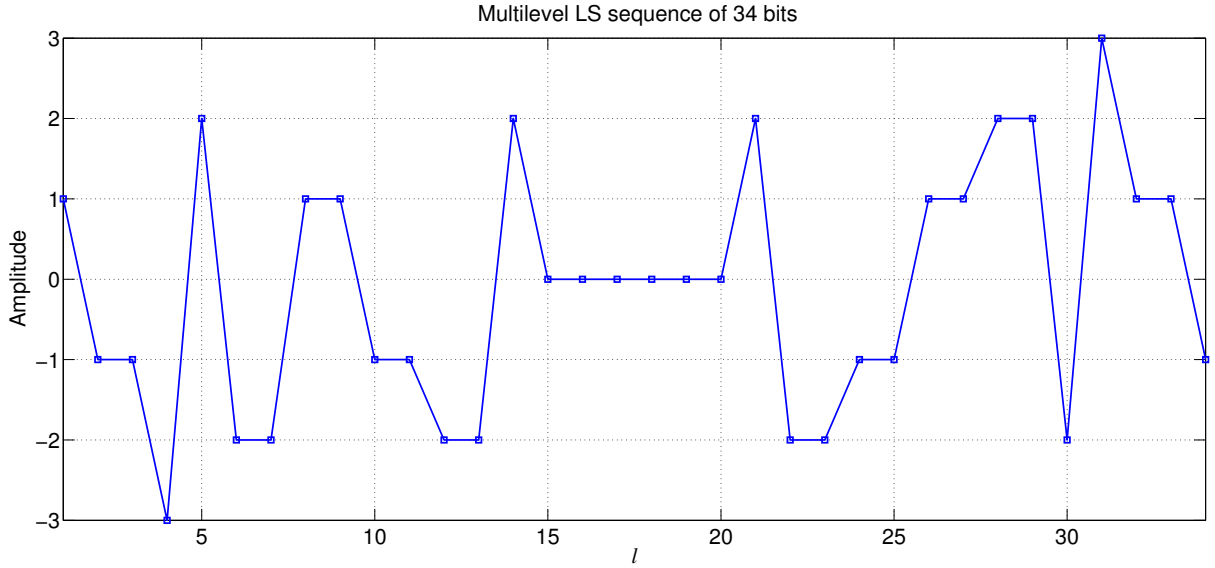


Figure 5.4: Multilevel LS sequence of length $L_{|MultLS} = 34$, generated with $A^{(q)} = \{1, 1, 2\}$, $D^{(q)} = \{1, 2, 3\}$ and $W^{(1,q)} = \{1, 1, 1\}$.

bits, as this is the next available length greater than 87 that can be obtained with the efficient generation algorithm of [Budis 11]; therefore, the shortest binary LS sequence which accomplishes the condition ZCZ $\geq 86$ is $L_{|LS} = 4 \cdot 100 + 127 = 527$ bits.

If we use multilevel LS sequences instead, as there are no limitations in the length of the PMCS, we can generate two PMCS of length $L_{|PMCS} = 87$. Consequently, the multilevel LS sequences will have a length of $L_{|MultLS} = 4 \cdot 87 + 86 = 434$ bits. So we can construct the shortest multilevel LS sequence which accomplishes the system requirements.

This reduction in the sequence length to meet the systems requirements implies a shorter emission time. This is of great importance when there are significant Doppler shifts [Pared 11].

In practice, the spreading sequences should be modulated and fed into independent power amplifiers to transmit them through the channel. If the modulated signals do not have a constant envelope, the power amplifier will not work efficiently, as it will radiate less power to avoid the distortion of the signal. As stated in Chapter 3, section 3.5, a common parameter used to evaluate the envelope of the signal is the PAPR [Popov 99b], which depends on the modulation scheme and, for multilevel LS sequences, on the values of $A^{(q)}$, $W^{(1,q)}$ and $D^{(q)}$. If DS-CDMA is used to transmit them, the use of multilevel sequences implies an increase in the PAPR. For example, for $K_{|LS} = 4$ binary LS sequences of length $L_{|LS} = 639$ bits, the PAPR is equal to 1.25, while for $K_{|MultLS} = 4$ multilevel LS

sequences of the same length it is equal to 1.99 (for $A^{(q)} = \{1, 1, 1, 1, 1, 1, 2\}$, seeds $W^{(1,q)} = \{\pm 1, -1, \ldots, -1\}$ and delays $D^{(q)} = \{64, 32, \ldots, 1\}$). So sequences with flexible ZCZ are obtained at the cost of an increase in the PAPR. Different delays $D^{(q)}$, seeds $W^{(1,q)}$ and weight values $A^{(q)}$, generate multilevel LS sequences with different amplitude distributions and PAPR. By selecting the previous parameters, the computational complexity is reduced in spite of not having the lowest PAPR.

If we use the optimal ternary complementary pairs generated in the previous Chapter 3, section 3.5, the obtained LS sequences will have a lower PAPR and then, will have more energy efficiency. Figure 5.5 shows a LS sequence of length $L_{|MultLS} = 89$, generated with the values $A^{(q)} = \{1, 1, 1, 1\}$, seeds $W^{(1,q)} = \{1, 1, 1, 1\}$ and delays distribution $D^{(q)} = \{9, 1, 2, 5\}$. The PAPR of this LS sequence is equal to 1.39.

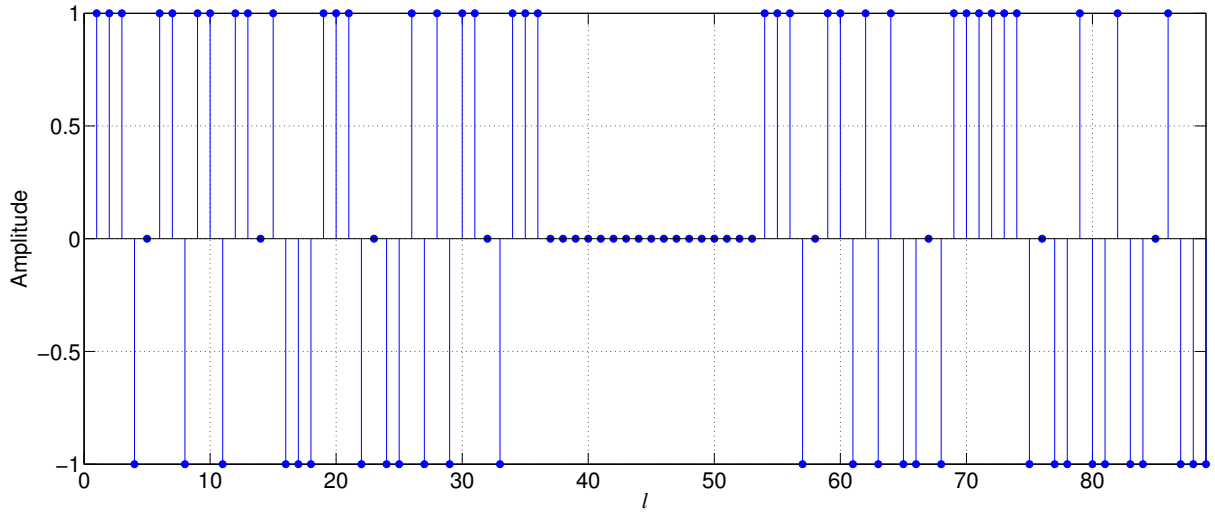


Figure 5.5: LS sequence generated from optimal ternary complementary pairs of length 9.

Another alternative is to increase the lineal region of the power amplifier to transmit more power and to have the same processing gain as the binary sequence.

An energy efficient solution is the use of MC-CDMA, where each level is assigned to an specific carrier. Nevertheless, this solution requires a larger bandwidth (i.e. less spectral efficiency), which could not be feasible and it introduces more complexity in the system. Figure 5.6 shows the diagram blocks of the MC-CDMA solution when the weight values are $A^{(q)} = \{1, 1, \ldots, 1\}$ for $0 \leq q \leq Q - 2$ and $A^{(q)} = 2$ for $q = Q - 1$ and the delay distribution is the one shown in equation 5.4.

Consequently, there is a trade-off between system complexity, energy efficiency and spectral efficiency.

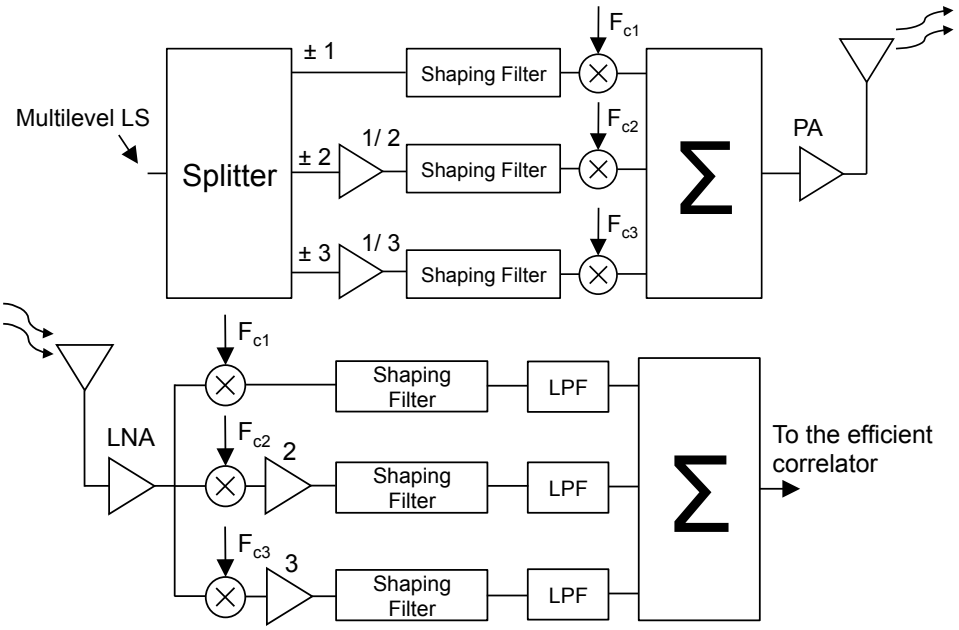


Figure 5.6: MC-CDMA scheme to avoid an increase in the PAPR.

## 5.3 Generation Algorithm of GPC Sequences

Chen *et al.* proposed GPC sequences to improve the correlation properties of LS and T-ZCZ sequences [Chen 06]. $T_{|GPC}$ pairs of sequences of length $L_{|GPC}$, $\mathbf{U}^{(j)}[l] = \{u_{k,0}^{(j)}[l], u_{k,1}^{(j)}[l]\}$; $0 \leq l \leq L_{|GPC} - 1$; $0 \leq k \leq G - 1$, with $Z$-transforms $\{U_{k,0}^{(j)}(z^{-1}), U_{k,1}^{(j)}(z^{-1})\}$, are a family of GPC sequences if their SACF and their SCCF hold the properties shown in equation 5.5 and equation 5.6 respectively. The term $j \in \{0, 1\}$ represents the group of the family set $\{\mathbf{U}^{(0)}[l], \mathbf{U}^{(1)}[l]\}$; $T_{|GPC} = 2 \cdot G$ and $G = 2^a$; $a \in \mathbb{N} - \{0\}$.

$$SACF[\tau] = \sum_{l=0}^{L_{|GPC}-1-\tau} u_{k,0}^{(j)}[l] \cdot u_{k,0}^{(j)}[l+\tau] + \sum_{l=0}^{L_{|GPC}-1-\tau} u_{k,1}^{(j)}[l] \cdot u_{k,1}^{(j)}[l+\tau]$$

$$= \begin{cases} C_p & \text{if } \tau = 0 \\ 0 & \text{if } 1 \leq |\tau| \leq W_{|GPC} \end{cases} \qquad 0 \leq k \leq G-1; j \in \{0,1\} \tag{5.5}$$

$$SCCF[\tau] = \sum_{l=0}^{L_{|GPC}-1-\tau} u_{k,0}^{(j)}[l] \cdot u_{k',0}^{(j')}[l+\tau] + \sum_{l=0}^{L_{|GPC}-1-\tau} u_{k,1}^{(j)}[l] \cdot u_{k',1}^{(j')}[l+\tau]$$
$$= \begin{cases} 0 & \text{if } 0 \leq |\tau| \leq W_{|GPC}; j = j' \\ 0 & \text{if } j \neq j'; \forall \tau \end{cases} \quad 0 \leq k, k' \leq G-1; k \neq k'; j, j' \in \{0,1\} \tag{5.6}$$

Where $C_p$ is the energy of the pair of GPC sequences; $W_{|GPC} = 4 \cdot L_{|CC} - 1$ is the ZCZ length and $L_{|GPC} = 4 \cdot G \cdot L_{|CC}$ is the length of the GPC sequences. The double-sided ZCZ, (IFW) is $2 \cdot W_{|GPC} + 1 = 8 \cdot L_{|CC} - 1$ and the number of sequence pairs is $T_{|GPC} = 2 \cdot G$. Therefore, a family of GPC sequences can be defined as GPC($T_{|GPC}$, $L_{|GPC}$, IFW), i.e. GPC($2 \cdot G$, $2 \cdot T_{|GPC} \cdot L_{|CC}$, $8 \cdot L_{|CC} - 1$). Figure 5.7 shows the SACF and the SCCF of a set GPC(4,32,31). The sidelobes of the SACF are sparsely distributed and located at shifts $|\tau| = 4 \cdot L_{|CC} \cdot \Phi_1$, with $\Phi_1 \in \{1, \ldots, 2^a - 1\}$, while the sidelobes of the intra-group SCCF ($j = j$'), are distributed at shifts $|\tau| = 4 \cdot L_{|CC} \cdot \Phi_2$ with $\Phi_2 \in \mathbb{N} - \{0\}$ [Chen 06]. Therefore, the larger number of available GPC sequences ($T_{|GPC}$), the larger number of sidelobes will appear in the correlation functions.

In the case of inter-group SCCF, the sum of aperiodic cross-correlation functions is zero for all shifts $\tau$.

GPC sequences can be combined in the emitter by means of any orthogonal modulation scheme. For example, Figure 5.8 shows a generic block diagram where a GPC pair is transmitted by using an I/Q modulation. At the receiver front-end, each demodulated sequence is fed into a Matched Filter (MF). If an ideal channel with AGWN is considered, where $N(z^{-1})$ is the AWGN term, the output $\sum C(z^{-1})$ is as follows:

$$\sum C\left(z^{-1}\right) = O_I\left(z^{-1}\right) + O_Q\left(z^{-1}\right) \tag{5.7}$$

Where $O_I\left(z^{-1}\right)$ and $O_Q\left(z^{-1}\right)$ are defined as

$$O_I\left(z^{-1}\right) = C_{R_I, U_{k,0}^{(j)}}\left(z^{-1}\right) + C_{N,R_I}\left(z^{-1}\right)$$
$$O_Q\left(z^{-1}\right) = C_{R_Q, U_{k,1}^{(j)}}\left(z^{-1}\right) + C_{N,R_Q}\left(z^{-1}\right) \tag{5.8}$$

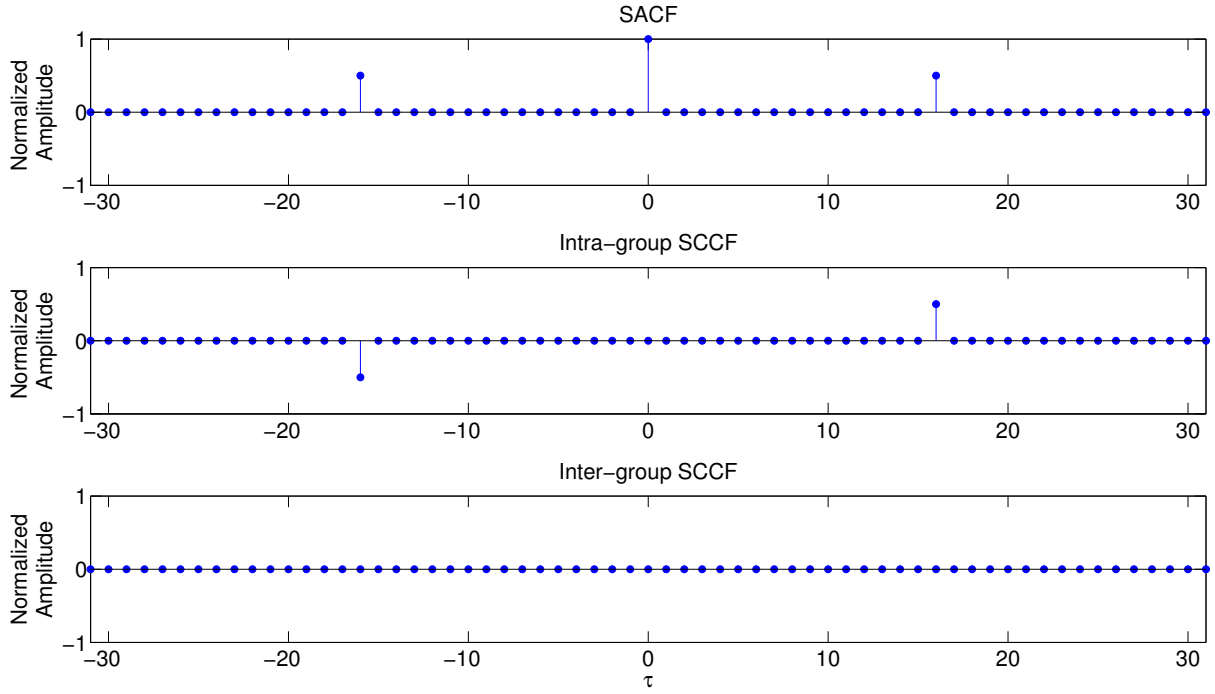


Figure 5.7: Aperiodic correlation functions of GPC(4,32,31) sequences.

The terms $C_{N,R_I}(z^{-1})$ and $C_{N,R_Q}(z^{-1})$ represents the noise factor due to the AWGN. As it has been shown from the matched filter theory [Proak 00, Leave 09] and from its application to pairs of sequences [White 92, Diaz 02], in this kind of systems, the SNR is improved by a factor twice the sequence length at the final output, with the addition of the corresponding output of both correlators.

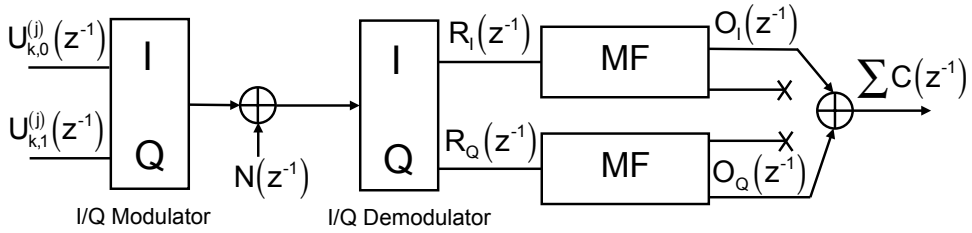


Figure 5.8: Block diagram of a QS-CDMA link using GPC sequences with an I/Q modem and two matched filters.

The generation algorithm of GPC sequences [Chen 06] is based on the properties of Generalized Even-Shift Orthogonal (GESO) sequences, constructed from Complete Complementary sequences (CC) [Suehi 88, Chen 01]. The CC sequences used in [Chen 06]

are in fact $K_{|CC} = \sqrt{L_{|CC}}$ uncorrelated CSS[2] of length $L_{|CC} = 4^b$; $b \in \mathbb{N} - \{0\}$ generated by means of non-recursive methods [Chen 07]. The generation algorithm of GPC sequences can be divided into three steps:

*Step 1*: Generation of GESO sequences. Without loss of generality, the generation of GESO sequences is explained here for $K_{|CC} = 2$ CC sequences of length $L_{|CC} = 4$, $\mathbf{Sc}_j(z^{-1}) = \{Sc_{j,0}(z^{-1}), Sc_{j,1}(z^{-1})\}$, being $\mathbf{Sc}_j(z^{-1})$ the $j$-th CC set, formed of the sequences $\{Sc_{j,0}(z^{-1}), Sc_{j,1}(z^{-1})\}$. The CC sequences $Sc_{j,i}(z^{-1})$, $0 \leq i \leq 1$, in $Z$-domain are defined as

$$Sc_{j,i}\left(z^{-1}\right) = \sum_{l=0}^{L_{|CC}-1} sc_{j,i}\left[l\right] \cdot z^{-l} \tag{5.9}$$

Consider a Hadamard matrix of order $K_{|CC} = 2$, $\boldsymbol{\mathcal{H}}_2 = [\mathbf{h}_1 \ \mathbf{h}_2]^T$ ($\mathbf{h}_i$ is the $i$-th row of the matrix), and generated from any known construction method [Seber 92], then the GESO sequences, $\mathcal{E}_j\left(z^{-1}\right)$; $0 \leq j \leq 1$, are generated as follows:

$$\mathcal{E}_j\left(z^{-1}\right) = \sum_{i=0}^{1} \sum_{l=0}^{L_{|CC}-1} \left(sc_{j,i}\left[l\right] \cdot z^{-l} \otimes \mathbf{h}_i\right) \cdot z^{-i \cdot 2 \cdot L_{|CC}} \tag{5.10}$$

The GESO sequences $\mathcal{E}_j(z^{-1})$ generated in this form, have aperiodic correlation functions with zero sidelobes at even shifts and a length $L_{|GESO} = 4 \cdot L_{|Gol}$. Figure 5.9 depicts the correlation functions of $K_{|GESO} = 2$ GESO sequences of length $L_{|GESO} = 16$.

*Step* 2: In order to enlarge the sequence set, the Walsh-Hadamard expansion of order $G$, $G = 2^a$; $\forall a \in \mathbb{N} - \{0\}$, is used. The recursive method for the generation of the Hadamard matrix is the same as the explained in Chapter 2, section 2.3.1 for the generation of OVSF sequences and it is expressed as

$$\begin{aligned} \boldsymbol{\mathcal{H}}_1 &= [1] \\ \boldsymbol{\mathcal{H}}_{2^{\Psi+1}} &= \begin{bmatrix} \boldsymbol{\mathcal{H}}_{2^\Psi} & \boldsymbol{\mathcal{H}}_{2^\Psi} \\ \boldsymbol{\mathcal{H}}_{2^\Psi} & -\boldsymbol{\mathcal{H}}_{2^\Psi} \end{bmatrix}; \Psi \in \{0, 1, \ldots, a-1\} \end{aligned} \tag{5.11}$$

Then the Walsh-Hadamard expansion is carried out as follows:

[2]Observe that the number of CSS, $T_{|CSS}$, and the number of sequences in each set, $K_{|CSS}$, are the same.

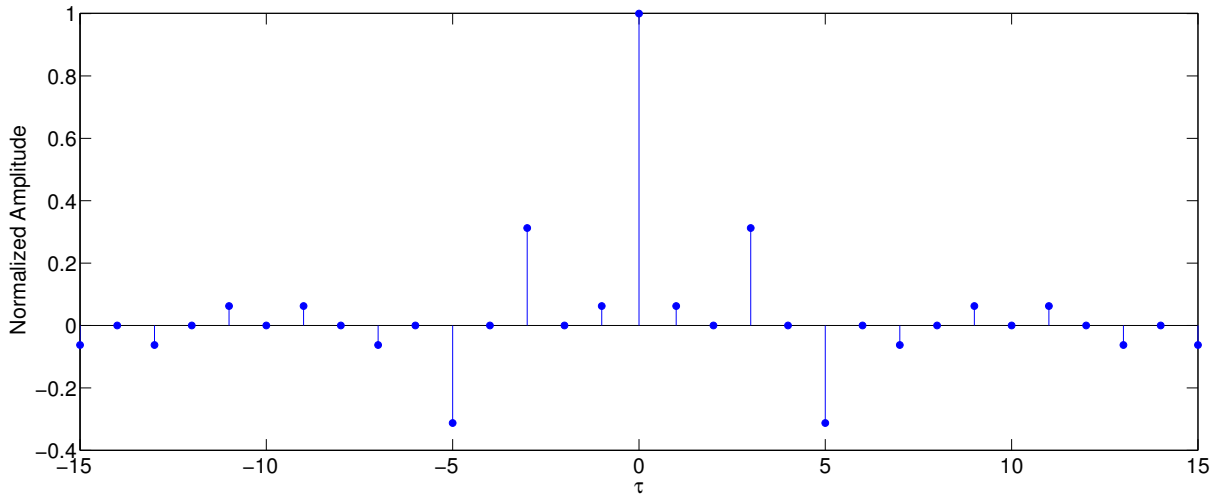


Figure 5.9: Aperiodic correlation function of a GESO sequence of length $L_{|GESO} = 16$.

$$U_{k,0}^{(j)}(z^{-1}) = \sum_{i=0}^{G-1} h_{k,i} \cdot z^{-i \cdot 4 \cdot L_{|CC}} \cdot \mathcal{E}_j(z^{-1}) \tag{5.12}$$

Where $h_{k,i}$ are the entries of the Hadamard matrix $\boldsymbol{\mathcal{H}}_G$ and $U_{k,0}^{(j)}(z^{-1})$; $0 \leq k \leq G-1$ is the first GPC sequence of the pair $k$, which belongs to the subgroup $j$. The length of the GPC sequence is equal to $L_{|GPC} = 4 \cdot G \cdot L_{|CC}$, so both the length of the GPC sequence and the number of them are increased in a factor $G$ with the Walsh-Hadamard expansion. The sequences are divided into two groups $\{\mathbf{U}^{(0)}(z^{-1}), \mathbf{U}^{(1)}(z^{-1})\}$, each of them composed of $G$ sequences. Figure 5.10 shows the aperiodic correlation function of the sequence $U_{0,0}^{(0)}(z^{-1})$ of length $L_{|GPC} = 32$, i.e. $G = 2$ and $L_{|CC} = 4$. As depicted, the aperiodic auto-correlation of the sequence $U_{0,0}^{(0)}(z^{-1})$ is zero at even shifts except at shifts $|\tau| = 4 \cdot L_{|CC} \cdot \Phi_1$, with $\Phi_1 \in \{1, \ldots, 2^a - 1\}$, due to the Walsh-Hadamard expansion.

*Step* 3: Elimination of odd shift interferences. To eliminate the interferences at odd shifts, the second GPC sequence of the pair $k$ is generated as follows:

$$U_{k,1}^{(j)}(z^{-1}) = \sum_{l=0}^{L_{|GPC}-1} (-1)^l \cdot u_{k,0}^{(j)}[l] \cdot z^{-l} \tag{5.13}$$

Notice that with this construction, the GPC sequences have interferences sparsely distributed and the ZCZ length is equal to $4 \cdot L_{|CC} - 1$ [Chen 06]. Figure 5.11 shows the aperiodic correlation function of the sequence $U_{0,1}^{(0)}(z^{-1})$ of length $L_{|GPC} = 32$. This sequence has been generated by negating the even bits of $U_{0,0}^{(0)}(z^{-1})$. If we carry out the

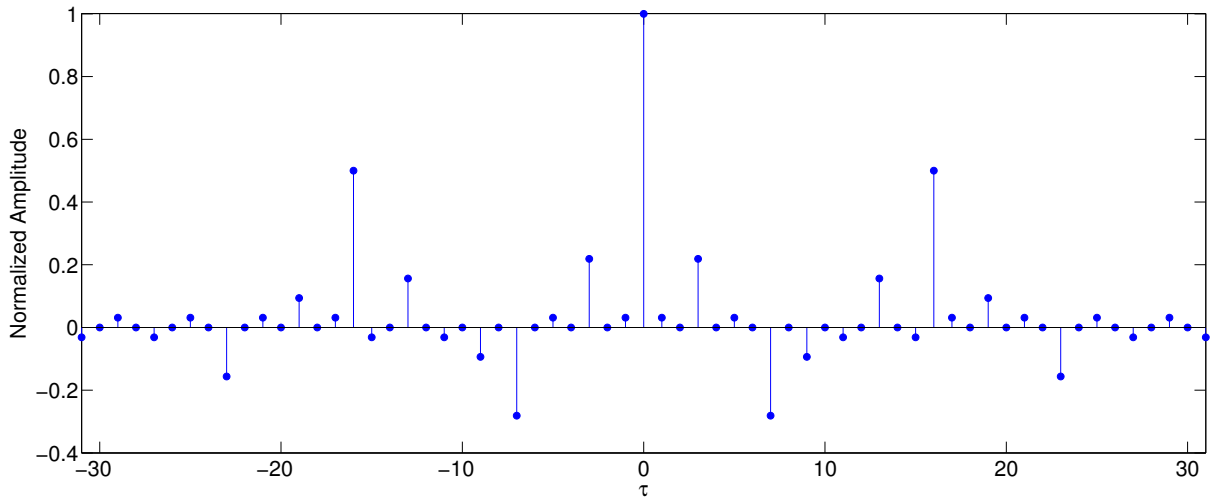


Figure 5.10: Aperiodic auto-correlation function of the sequence $U_{0,0}^{(0)}(z^{-1})$ of length $L_{|GPC} = 32$.

sum of the aperiodic correlation function of the sequences $U_{0,0}^{(0)}(z^{-1})$ (Figure 5.10) and $U_{0,1}^{(0)}(z^{-1})$ (Figure 5.11), we obtain the SACF depicted in Figure 5.7.

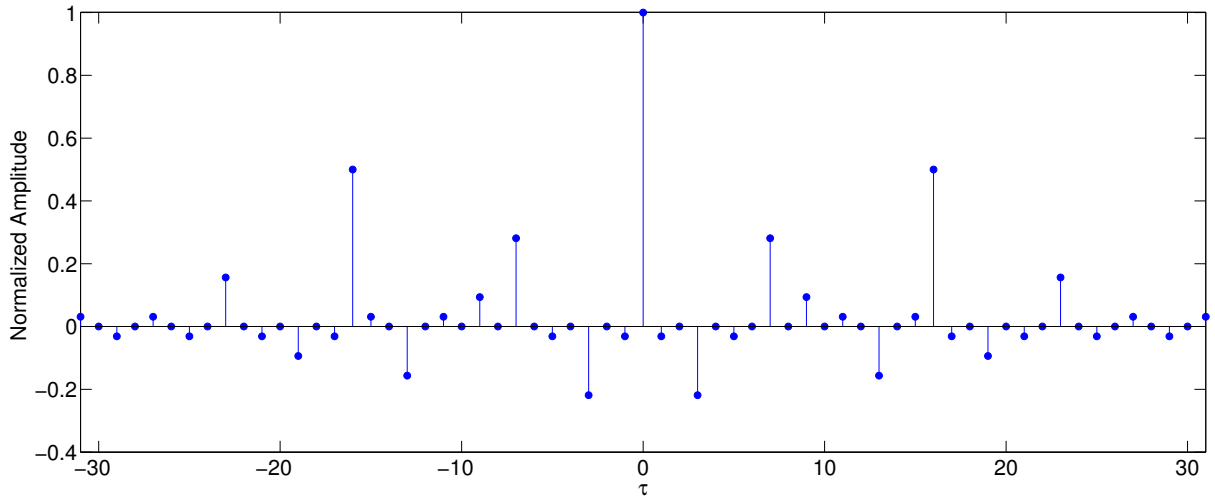


Figure 5.11: Aperiodic auto-correlation function of the sequence $U_{0,1}^{(0)}(z^{-1})$ of length $L_{|GPC} = 32$.

## 5.4 Efficient Generation Algorithm of GPC Sequences

The properties of the $T_{|GPC} = 2{\cdot}G$ GPC sequences generated with the proposed generation algorithm are: IFW $= 4 \cdot L_{|Gol} - 1$; $L_{|GPC} = 2 \cdot G \cdot L_{|Gol}$, i.e. now the GPC set is defined as GPC($2{\cdot}G$, $T_{|GPC}{\cdot}L_{|Gol}$, $4{\cdot}L_{|Gol}-1$). Notice that the generation algorithm of [Chen 06] and the proposed here, are equivalent as they have the same $L_{|GPC}$/IFW relationship. The algorithm is based on the properties of $E$-sequences [Taki 69], $e_j[l]$, with $Z$-transform equal to $E_j\,(z^{-1})$, obtained from Golay pairs of sequences instead of GESO sequences, $\mathcal{E}_j(z^{-1})$, generated from CC sequences.

The proposed generation algorithm for GPC sequences, expressed in $Z$-domain, is as follows:

$$\begin{aligned} U_{k,0}^{(j)}(z^{-1}) &= \sum_{i=0}^{G-1} h_{k,i}{\cdot}z^{-i\cdot 2\cdot L_{|Gol}}{\cdot}E_j(z^{-1}) \\ U_{k,1}^{(j)}(z^{-1}) &= \sum_{l=0}^{L_{|GPC}-1} (-1)^l \cdot u_{k,0}^{(j)}[l] \cdot z^{-l} \end{aligned} \tag{5.14}$$

Where $U_{k,\rho}^{(j)}(z^{-1})$ with $\rho$, $j \in \{0,1\}$ and $0 \le k \le G-1$ refers to the sequence $\rho$ of the pair $k$ belonging to the subgroup $j$; $h_{k,i}$ are the entries of a Hadamard matrix of order $G$; $L_{|Gol}$ is the length of the Golay sequences pairs and $E_j(z^{-1})$ is an $E$-sequence obtained by interleaving the Golay pair $j$.

An efficient generator for GPC sequences is obtained by following the steps indicated below. The first step includes the modifications to the original algorithm of [Chen 06].

*Step 1*: For generating the $E$-sequences it is necessary to interleave the Golay sequence pairs of length $L_{|Gol} = 2^N \cdot 10^M \cdot 26^P$, with $N$, $M$, $P$ non-negative integers. To accomplish that, three sub-steps are required: First, we use the efficient generation algorithm presented in Chapter 4 for the Golay pairs $\mathbf{S}_j^{(1,Q)}(z^{-1}) = \{S_{j,0}^{(Q)}(z^{-1}), S_{j,1}^{(Q)}(z^{-1})\}$ in $Q$ iterations, $Q = N + 4 \cdot M + 12 \cdot P$. Later, the Golay pairs must be zero-padded by inserting one zero between every two bits of both sequences, obtaining the sequence pairs of length $2 \cdot L_{|Gol}$, ${}^d\mathbf{S}_j^{(1,Q)}(z^{-1}) = \{{}^dS_{j,0}^{(Q)}(z^{-1}), {}^dS_{j,1}^{(Q)}(z^{-1})\}$. Finally, we have to delay one bit the sequence ${}^dS_{j,1}^{(Q)}(z^{-1})$ and add it with the sequence ${}^dS_{j,0}^{(Q)}(z^{-1})$ to obtain the $E$-sequence $E_j(z^{-1})$.

Fig. 5.12 depicts a block diagram of the Efficient Golay Generator (EGG). In order to generate the pairs ${}^d\mathbf{S}_j^{(1,Q)}(z^{-1}) = \{{}^dS_{j,0}^{(Q)}(z^{-1}), {}^dS_{j,1}^{(Q)}(z^{-1})\}$ with the architecture of Figure

5.12, the delays $D^{(q)}$ of each stage have to be multiplied by two. This is a straightforward modification and it does not affect to the architecture of the EGG.

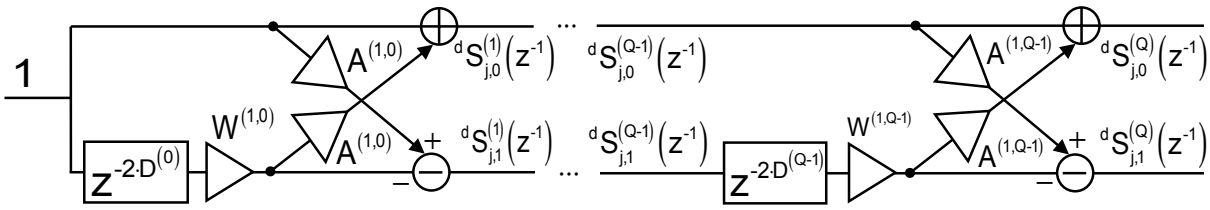


Figure 5.12: Efficient Golay Generator for the sequence pairs in $Z$-domain $\{{}^dS_{j,0}^{(Q)}(z^{-1}), {}^dS_{j,1}^{(Q)}(z^{-1})\}$.

Therefore, the Golay pairs $\{{}^dS_{j,0}^{(Q)}(z^{-1}), {}^dS_{j,1}^{(Q)}(z^{-1})\}$ are generated by duplicating the EGG memory elements in each stage and they are equal to:

$$\sum_{l=0}^{2\cdot L_{|Gol}-1} {}^d s_{j,\rho}^{(Q)}[l] \cdot z^{-l} = 0;\ for\, l\, even;\ \rho \in \{0,1\} \tag{5.15}$$

The pairs of sequences ${}^d\mathbf{S}_j^{(1,Q)}(z^{-1}) = \{{}^dS_{j,0}^{(Q)}(z^{-1}), {}^dS_{j,1}^{(Q)}(z^{-1})\}$ are interleaved by delaying one bit the sequence ${}^dS_{j,1}^{(Q)}(z^{-1})$ and then adding both sequences of the pair $j$ as follows:

$$E_j(z^{-1}) = {}^dS_{j,0}^{(Q)}(z^{-1}) + z^{-1} \cdot {}^dS_{j,1}^{(Q)}(z^{-1}) \tag{5.16}$$

The sequences generated in this form, for $j = 0$ and $j = 1$, are $E$-sequences of length $2 \cdot L_{|Gol}$ and their correlation functions are zero for all even shifts [Taki 69].

As stated in Chapter 4, the pairs of sequences can be matched to the 8-QAM alphabet $\{a + i \cdot b; (a,b) \in (\pm 1, \pm 3) \times (\pm 1, \pm 3\})\}$ by setting all the multipliers $A^{(n)}$ to 1 except one of them, which is arbitrarily selected, in this case with the value 3. In the case that all the multipliers $A^{(n)}$ were fixed to $A^{(n)} = 1$, the Golay pairs of sequences would be binary.

*Step 2*: The same Walsh-Hadamard expansion as the proposed in [Chen 06] has to be carried out to enlarge the set size:

$$U_{k,0}^{(j)}(z^{-1}) = \sum_{i=0}^{G-1} h_{k,i} \cdot z^{-i\cdot 2\cdot L_{|Gol}} \cdot E_j(z^{-1}) \tag{5.17}$$

Where $h_{k,i}$ are the entries of a Hadamard matrix of order $G$, $G = 2^a$; $\forall a \in \mathbb{N} - \{0\}$, obtained by using the Sylvester's construction, stated in equation 5.11. Notice that the entries $h_{k,0}$, $0 \leq k \leq G-1$, are equal to $+1$ when the Sylvester's construction is used.

*Step 3*: Finally, to generate the sequence $U_{k,1}^{(j)}(z^{-1})$, the sign of the even bits of $U_{k,0}^{(j)}(z^{-1})$, [Chen 06] must be changed i.e.:

$$U_{k,1}^{(j)}(z^{-1}) = \sum_{l=0}^{L_{|GPC}-1} (-1)^l \cdot u_{k,0}^{(j)}[l] \cdot z^{-l} \tag{5.18}$$

Figure 5.13 shows the described steps in a block diagram. As depicted, the change of sign at the even bits of $U_{k,0}^{(j)}(z^{-1})$ is managed by the signal CLK/2 (the half of frequency of the system clock).

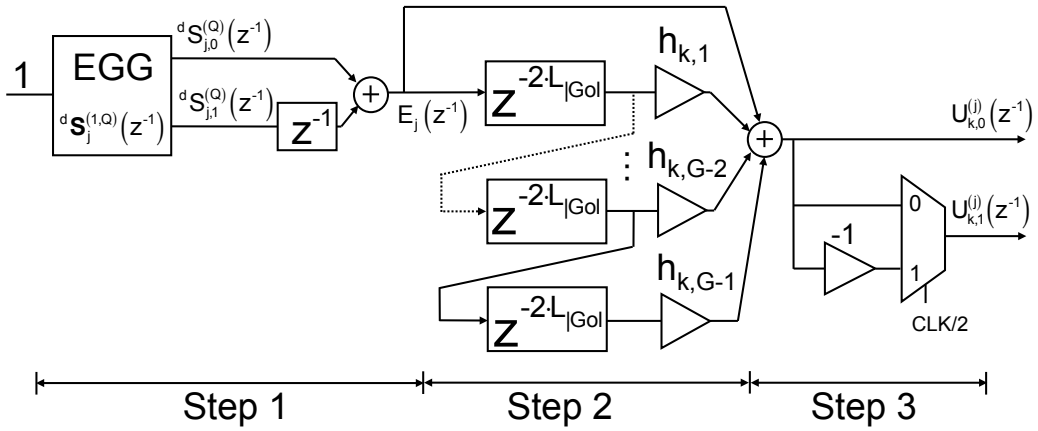


Figure 5.13: Efficient generator for GPC sequences in $Z$-domain.

Notice that the main contribution of the efficient generator is the *Step 1*, where $E$-sequences are used instead of GESO sequences. This modification permits to use the efficient generator of Golay pairs of sequences of length $L_{|Gol} = 2^N \cdot 10^M \cdot 26^P$ instead of the CC sequences which have a reduced flexibility in the sequence length, and therefore in the ZCZ length.

## 5.5 Efficient Correlator of GPC Sequences

Due to the relationship between convolution and correlation, if the generation algorithm is modified to build the reversed sequences, it will be equivalent to a correlator matched to the sequences $\{U_{k,0}^{(j)}(z^{-1}), U_{k,1}^{(j)}(z^{-1})\}$ that has the same impulse response as the straightforward correlator. To accomplish this, it is necessary to carry out the modifications to the generation algorithm for GPC sequences pointed out in the following steps:

*Step 1*: The Walsh-Hadamard expansion of the input signal $R(z^{-1})$, must be performed by reversing the delay orders to generate the signal $R_e(z^{-1})$ as follows:

$$R_e(z^{-1}) = R(z^{-1}) \cdot \left[ z^{-(G-1)2L_{|Gol}} + \sum_{i=1}^{G-1} h_{k,i} \cdot z^{-(G-1-i)\cdot 2\cdot L_{|Gol}} \right] \tag{5.19}$$

As all the entries $h_{k,0}$ are equal to +1 when using the Sylvester's construction, they have been omitted in equation 5.19.

*Step 2*: The order of the delays in the EGG must be reversed to correlate the signal $R_e(z^{-1})$ with the zero-padded Golay pairs ${}^d\mathbf{S}_j^{(1,Q)}(z^{-1}) = \{{}^dS_{j,0}^{(Q)}(z^{-1}), {}^dS_{j,1}^{(Q)}(z^{-1})\}$. Figure 5.14 shows a block diagram of the Efficient Golay Correlator (EGC) for zero-padded Golay pairs.

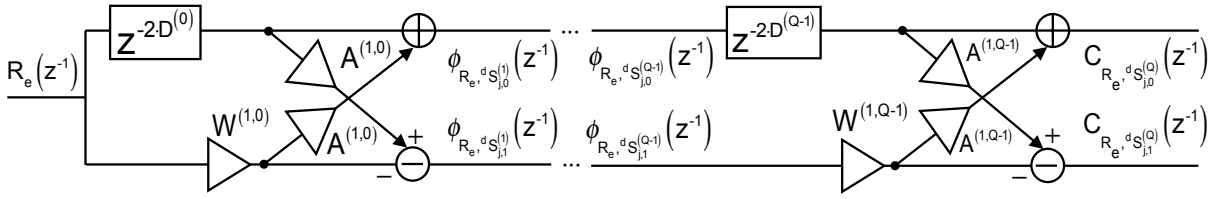


Figure 5.14: Efficient Golay Correlator (EGC) for zero-padded Golay pairs in $Z$-domain.

*Step 3*: Finally, the delay $z^{-1}$ at the output of the EGG for the zero-padded Golay pairs must be applied to $C_{R_e,{}^dS_{j,0}^{(Q)}}(z^{-1})$ to obtain the aperiodic correlation between the input signal, $R(z^{-1})$, and the sequence $U_{k,0}^{(j)}(z^{-1})$:

$$C_{R,U_{k,0}^{(j)}}(z^{-1}) = z^{-1} \cdot C_{R_e,{}^dS_{j,0}^{(Q)}}(z^{-1}) + C_{R_e,{}^dS_{j,1}^{(Q)}}(z^{-1}) \tag{5.20}$$

And the aperiodic correlation between the signal $R(z^{-1})$ and the sequence $U_{k,1}^{(j)}(z^{-1})$ is:

$$C_{R,U_{k,1}^{(j)}}(z^{-1}) = z^{-1} \cdot C_{R_e,{}^dS_{j,0}^{(Q)}}(z^{-1}) - C_{R_e,{}^dS_{j,1}^{(Q)}}(z^{-1}) \tag{5.21}$$

Figure 5.15 shows a block diagram of the efficient correlator for GPC sequences, obtained by following the previous steps.

### 5.5.1 Implementation Aspects

Table 5.1 shows a comparison of the necessary resources for the efficient generator/correlator for binary GPC sequences proposed here, and for a straightforward correlator that can be used for implementing the generator proposed in [Chen 06], as in this case an efficient generator is not known. Notice that the resources needed for the efficient generator

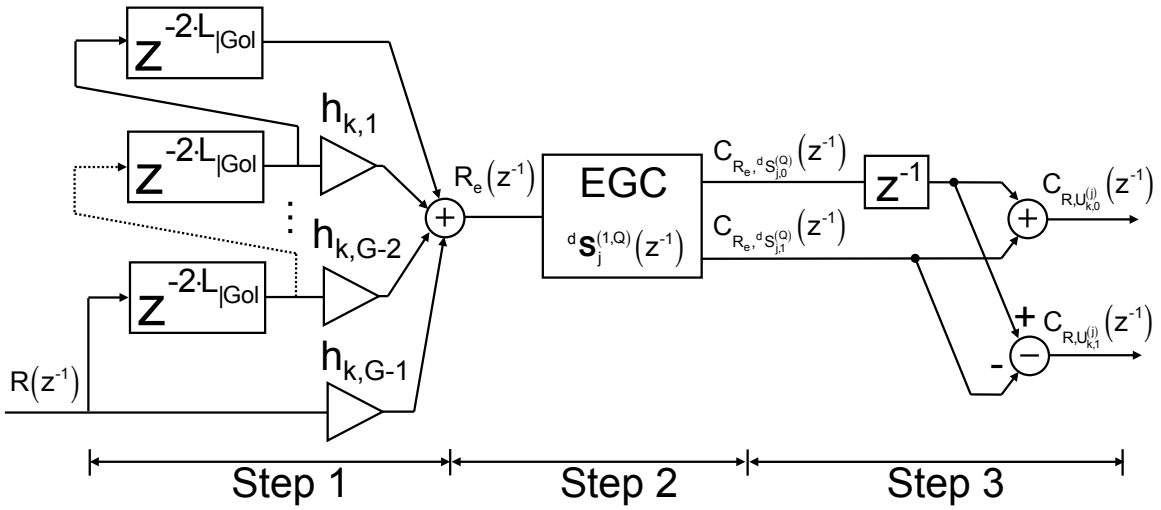


Figure 5.15: Efficient correlator for GPC sequences in $Z$-domain.

are the same as those needed for the efficient correlator (each one is the time reversed version of the other). An important difference between the generator and the correlator in a real implementation is related to the data bus width needed: in the generator the input is just a bit while in the correlator the input is normally the output of an ADC (e. g. 8 bits).

| Resources | Straightforward Generator/Correlator | Efficient Generator/Correlator |
|---|---|---|
| Products | – | $2 \cdot (M + 9 \cdot P)$ |
| Additions | $T_{\|GPC} \cdot L_{\|Gol} - 1$ | $2 \cdot Q + T_{\|GPC}/2$ |
| Delays | $T_{\|GPC} \cdot L_{\|Gol} - 1$ | $T_{\|GPC} \cdot L_{\|Gol} - 1$ |

Table 5.1: Resources Required for the Proposed Generator/Correlator and for the Straightforward Generator/Correlator (considering only one sequence).

For example, consider a set of $T_{|GPC} = 8$ pairs of GPC sequences of length $L_{|GPC} = 4096$, generated from two uncorrelated Golay pairs of length $L_{|Gol} = 512$, GPC(8, 4096, 2047), with $N = 9$, $M = 0$ and $P = 0$, i.e. $Q = 9$. In that case, the architecture only needs 22 additions to carry out the correlation of a GPC of the pair. For the case of the straightforward correlator, the number of additions is 4095. Regarding the number of delays needed to carry out the aperiodic correlations for both cases is 4095. Nonetheless, in the proposed correlator, the data bus width is larger than the case of the straightforward correlator. So, the number of operations in the proposed correlator is reduced at the expense of increasing the number of memory bits.

The reduction in the number of operations with the correlator proposed here, in comparison with the straightforward one, allows real-time implementation (using reconfigurable hardware) in cases in which high frequencies or long sequences are involved. Furthermore, the use of long sequences can benefit from larger IFW and set size.

## 5.6 Theoretical Relationship between GPC and LS Sequences

GPC sequences and LS sequences are closely related to each other. In fact the efficient generation algorithm of GPC sequences introduced previously can be used, with minor modifications, for the generation of a set of $K_{|LS}$ LS sequences. Given $T_{|GPC}$ sets of GPC sequences $\{\mathbf{U}^{(j)}[l] = \{u_{k,0}^{(j)}[l], u_{k,1}^{(j)}[l]\}; 0 \leq l \leq L_{|GPC}-1; 0 \leq k \leq G-1\}$, $j \in \{0,1\}$, with $Z$-transform $\{U_{k,0}^{(j)}(z^{-1}), U_{k,1}^{(j)}(z^{-1})\}$ it is possible to generate a set of $K_{|LS} = 2{\cdot}G$ LS sequences $\{\mathbf{V}[l] = \{v_k\,[l]\}; 0 \leq l \leq L_{|LS}-1;\ 0 \leq k \leq K_{|LS}\}$ of length $L_{|LS} = 2 \cdot L_{|Gol} \cdot (2 \cdot G + 1) - 1$ by concatenating the pairs of GPC sequences, which expressed in the $Z$-domain, is as follows:

$$V_k\left(z^{-1}\right) = U_{k,0}^{(j)}\left(z^{-1}\right) + U_{k,1}^{(j)}\left(z^{-1}\right) \cdot z^{-\left(2 \cdot L_{|Gol} \cdot G + W_{|LS}\right)} \tag{5.22}$$

where $W_{|LS}$ is now $W_{|LS} = 2 \cdot L_{|Gol} - 1$. Figure 5.16 shows a scheme of the generation algorithm of a set of $K_{|LS} = 4$ LS sequences. Notice that in the generation algorithm of Stanczak [Stanc 01], Golay binary sequence pairs are concatenated with different polarities (see Figure 5.1). In the proposed generation algorithm, it is used $E$-sequences instead.

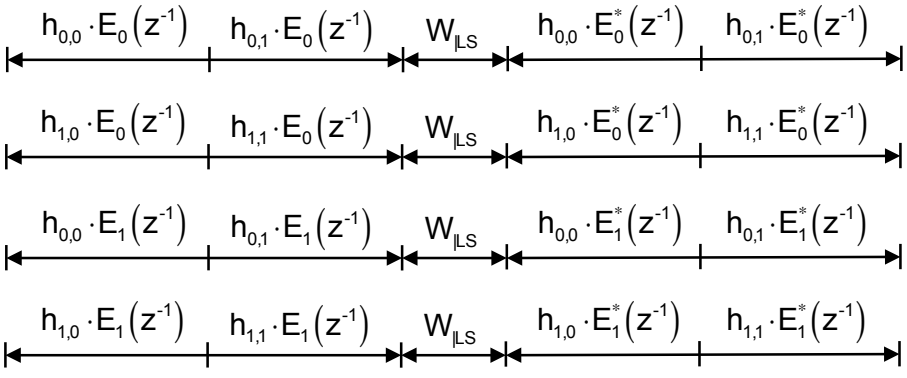


Figure 5.16: Scheme of the proposed generation method of a set of $K_{|LS} = 4$ LS sequences.

*Claim.* The LS sequences generated with equation 5.22 have a length $L_{|LS} = 2 \cdot L_{|Gol} \cdot K_{|LS} + W_{|LS}$; $W_{|LS} = 2 \cdot L_{|Gol} - 1$ and an IFW $= 2 \cdot W_{|LS} + 1 = 4 \cdot L_{|Gol} - 1$. Also they have the same $L_{|LS}$/IFW relationship as the LS sequences generated with the algorithm of [Stanc 01].

*Proof.* From the properties of GPC sequences it is known that $C_{U_{k,0}^{(j)},U_{k,0}^{(j)}}(z^{-1}) = -C_{U_{k,1}^{(j)},U_{k,1}^{(j)}}(z^{-1})$ except for $|\tau| = 2 \cdot L_{|Gol} \cdot \Phi_1$; $\Phi_1 \in \{0, \ldots, 2^a - 1\}$; $a = \log_2 G$ [Chen 06]. Also from the properties of the $E$-sequences, the following equations hold:

$$C_{E_j,E_j}\left(z^{-1}\right) + C_{E_j^*,E_j^*}\left(z^{-1}\right) = 4 \cdot L_{|Gol} \tag{5.23}$$

$$C_{E_j,E_{j'}}\left(z^{-1}\right) + C_{E_j^*,E_{j'}^*}\left(z^{-1}\right) = 0;\ j \neq j' \tag{5.24}$$

where $E_j^*\left(z^{-1}\right)$ is equal to $E_j^*(z^{-1}) = \sum_{l=0}^{2 \cdot L_{|Gol}-1} e_j[l] \cdot z^{-l} \cdot (-1)^{-l}$, which implies that the $E$-sequence $E_j^*(z^{-1})$ is equal to the $E$-sequence $E_j(z^{-1})$ with the even bits negated. Notice that this is the same operation carried out for obtaining the sequence $U_{k,1}^{(j)}(z^{-1})$ (refer to equations 5.14 and 5.18). So the generation algorithm stated in equation 5.22 can be expressed as

$$V_k\left(z^{-1}\right) = \sum_{i=0}^{G-1} h_{k,i} \cdot z^{-i \cdot 2 \cdot L_{|Gol}} \cdot E_j(z^{-1}) + \left( \sum_{i=0}^{G-1} h_{k,i} \cdot z^{-i \cdot 2 \cdot L_{|Gol}} \cdot E_j^*(z^{-1}) \right) \cdot z^{-\left(2 \cdot L_{|Gol} \cdot G + W_{|LS}\right)} \tag{5.25}$$

Consider now the aperiodic auto-correlation function for $0 \leq \tau \leq 2 \cdot L_{|Gol} - 1$; due to the chain of zeros $W_{|LS}$ of length $2 \cdot L_{|Gol} - 1$, the left part of the sequence $(U_{k,0}^{(j)}(z^{-1}))$ and the right one $(U_{k,1}^{(j)}(z^{-1}))$ do not overlap for displacements $0 \leq \tau \leq 2 \cdot L_{|Gol} - 1$, consequently the aperiodic auto-correlation for $0 \leq \tau \leq 2 \cdot L_{|Gol} - 1$ is

$$\begin{aligned} V_k\left(z^{-1}\right) \cdot V_k\left(z\right) &= \sum_{i=0}^{G-1} h_{k,i} \cdot E_j\left(z^{-1}\right) \cdot z^{-i \cdot 2 \cdot L_{|Gol}} \cdot \sum_{i'=0}^{G-1} h_{k,i'} \cdot E_j\left(z\right) \cdot z^{i' \cdot 2 \cdot L_{|Gol}} \\ &+ \sum_{i=0}^{G-1} h_{k,i} \cdot E_j^*\left(z^{-1}\right) \cdot z^{-i \cdot 2 \cdot L_{|Gol}} \cdot \sum_{i'=0}^{G-1} h_{k,i'} \cdot E_j^*\left(z\right) \cdot z^{i' \cdot 2 \cdot L_{|Gol}} \\ &= \left( C_{E_j,E_j}\left(z^{-1}\right) + C_{E_j^*,E_j^*}\left(z^{-1}\right) \right) \cdot \sum_{i=0}^{G-1} h_{k,i} \cdot z^{-i \cdot 2 \cdot L_{|Gol}} \cdot \sum_{i'=0}^{G-1} h_{k,i'} \cdot z^{i' \cdot 2 \cdot L_{|Gol}} \\ &\text{for } 0 \leq \tau \leq 2 \cdot L_{|Gol} - 1 \end{aligned} \tag{5.26}$$

Due to the window of interest is defined by $0 \leq \tau \leq 2 \cdot L_{|Gol} - 1$, the term $z^{(-i+i') \cdot 2 \cdot L_{|Gol}}$ must be equal to $+1$, so $i = i'$. This implies that the aperiodic auto-correlation function within the window of interest is equal to:

$$V_k\left(z^{-1}\right) \cdot V_k\left(z\right) = \left(C_{E_j,E_j}\left(z^{-1}\right) + C_{E_j^*,E_j^*}\left(z^{-1}\right)\right) \cdot \left(h_{k,0}^2 + \cdots + h_{k,G-1}^2\right)$$
$$\text{for } 0 \leq \tau \leq 2 \cdot L_{|Gol} - 1 \tag{5.27}$$

By using the property of equation 5.23 and knowing that the order of the Hadamard matrix is $G$, the aperiodic auto-correlation of the LS sequence $V_k(z^{-1})$ for $0 \leq \tau \leq 2 \cdot L_{|Gol} - 1$ is equal to:

$$V_k\left(z^{-1}\right) \cdot V_k\left(z\right) = 4 \cdot L_{|Gol} \cdot G; \text{ for } 0 \leq \tau \leq 2 \cdot L_{|Gol} - 1 \tag{5.28}$$

Due to the symmetry properties of the correlation function, the IFW is equal to IFW $= 4 \cdot L_{|Gol} - 1$. Analysing now the aperiodic cross-correlation of the LS sequences $V_k(z^{-1})$ and $V_{k'}(z^{-1})$, $k \neq k'$ for $0 \leq \tau \leq 2 \cdot L_{|Gol} - 1$ it is shown that

$$\begin{aligned} V_k\left(z^{-1}\right) \cdot V_{k'}\left(z\right) &= \sum_{i=0}^{G-1} h_{k,i} \cdot E_j\left(z^{-1}\right) \cdot z^{-i \cdot 2 \cdot L_{|Gol}} \cdot \sum_{i'=0}^{G-1} h_{k',i'} \cdot E_j\left(z\right) \cdot z^{i' \cdot 2 \cdot L_{|Gol}} \\ &+ \sum_{i=0}^{G-1} h_{k,i} \cdot E_j^*\left(z^{-1}\right) \cdot z^{-i \cdot 2 \cdot L_{|Gol}} \cdot \sum_{i'=0}^{G-1} h_{k',i'} \cdot E_j^*\left(z\right) \cdot z^{i' \cdot 2 \cdot L_{|Gol}} \\ &= \left(C_{E_j,E_j}\left(z^{-1}\right) + C_{E_j^*,E_j^*}\left(z^{-1}\right)\right) \cdot \sum_{i=0}^{G-1} h_{k,i} \cdot z^{-i \cdot 2 \cdot L_{|Gol}} \sum_{i'=0}^{G-1} h_{k',i'} \cdot z^{i' \cdot 2 \cdot L_{|Gol}} \\ &\text{for } 0 \leq \tau \leq 2 \cdot L_{|Gol} - 1;\ k \neq k' \end{aligned} \tag{5.29}$$

Again, the term $z^{(-i+i') \cdot 2 \cdot L_{|Gol}}$ must be equal to $+1$, as the window of interest is $0 \leq \tau \leq 2 \cdot L_{|Gol} - 1$. Hence, the aperiodic cross-correlation function within the IFW is equal to:

$$V_k\left(z^{-1}\right) \cdot V_{k'}\left(z\right) = \left(C_{E_j,E_j}\left(z^{-1}\right) + C_{E_j^*,E_j^*}\left(z^{-1}\right)\right) \cdot \left(h_{k,0} \cdot h_{k',0} + \cdots + h_{k,G-1} \cdot h_{k',G-1}\right)$$
$$\text{for } 0 \leq \tau \leq 2 \cdot L_{|Gol} - 1;\ k \neq k' \tag{5.30}$$

Due to the rows $\mathbf{h}_k$ of the Hadamard matrix $\boldsymbol{\mathcal{H}}_G$ are pairwise orthogonal, i.e. $C_{\mathbf{h}_k,\mathbf{h}_{k'}} = 0$; for $\tau = 0$, and because of the property of equation 5.23, the aperiodic cross-correlation function within the window of interest is

$$V_k\left(z^{-1}\right)\cdot V_{k'}\left(z\right)=0;\ \text{for}\ 0\leq\tau\leq 2\cdot L_{|Gol}-1;\ k\neq k' \tag{5.31}$$

Now, if the aperiodic cross-correlation among LS sequences of different subgroups $j$ is considered, we have:

$$\begin{aligned}V_k\left(z^{-1}\right)\cdot V_{k'}\left(z\right)&=\sum_{i=0}^{G-1}h_{k,i}\cdot E_j\left(z^{-1}\right)\cdot z^{-i\cdot 2\cdot L_{|Gol}}\cdot\sum_{i'=0}^{G-1}h_{k',i'}\cdot E_{j'}\left(z\right)\cdot z^{i'\cdot 2\cdot L_{|Gol}}\\&+\sum_{i=0}^{G-1}h_{k,i}\cdot E_j^{*}\left(z^{-1}\right)\cdot z^{-i\cdot 2\cdot L_{|Gol}}\cdot\sum_{i'=0}^{G-1}h_{k',i'}\cdot E_{j'}^{*}\left(z\right)\cdot z^{i'\cdot 2\cdot L_{|Gol}}\\&=\left(C_{E_j,E_{j'}}\left(z^{-1}\right)+C_{E_j^{*},E_{j'}^{*}}\left(z^{-1}\right)\right)\cdot\sum_{i=0}^{G-1}h_{k,i}\cdot z^{i'\cdot 2\cdot L_{|Gol}}\cdot\sum_{i'=0}^{G-1}h_{k',i'}\cdot z^{i'\cdot 2\cdot L_{|Gol}}\\&\text{for}\ 0\leq\tau\leq 2\cdot L_{|Gol}-1;\ k\neq k'\ j\neq j'\end{aligned} \tag{5.32}$$

Within the IFW, the aperiodic cross-correlation is equal to:

$$\begin{aligned}V_k\left(z^{-1}\right)\cdot V_{k'}\left(z\right)&=\left(C_{E_j,E_{j'}}\left(z^{-1}\right)+C_{E_j^{*},E_{j'}^{*}}\left(z^{-1}\right)\right)\cdot\left(h_{k,0}\cdot h_{k',0}+\cdots+h_{k,G-1}\cdot h_{k',G-1}\right)\\&=0\,\text{for}\ 0\leq\tau\leq 2\cdot L_{|Gol}-1;\ k\neq k'\end{aligned} \tag{5.33}$$

As the terms $C_{E_j,E_{j'}}\left(z^{-1}\right)+C_{E_j^{*},E_{j'}^{*}}\left(z^{-1}\right)$ are equal to zero (refer to equation 5.24) and the rows of the Hadamard matrix $\boldsymbol{\mathcal{H}}_G$ are pairwise orthogonal.

The $L_{|LS}$/IFW relationship of the proposed LS sequences is equal to $\frac{2\cdot L_{|Gol}\cdot\left(K_{|LS}+1\right)-1}{4\cdot L_{|Gol}-1}$, which is the same of the LS generated with the algorithm of [Stanc 01]. ■

The novel approach for the generation of LS sequences is represented in the diagram block of Figure 5.17. The correlator of these sequences is equivalent to the generator with the delays arranged in a reversed order, as depicted in Figure 5.18. Interestingly, the proposed correlator for binary LS sequences requires similar hardware resources than the previous optimised architecture of [Perez 10] as stated in Table 5.2. Notice that for comparison purposes only has been considered binary LS sequences generated from power-of-two Golay binary pairs (i.e. $M$ and $P$ are zero).

The proposed generation/correlation architecture can be optimized further if the Walsh-Hadamard Expansion (WHE) block (*Step 4* in the diagram blocks) is replaced by one of the butterfly architectures shown in [Regal 89]. These structures allow the sim-

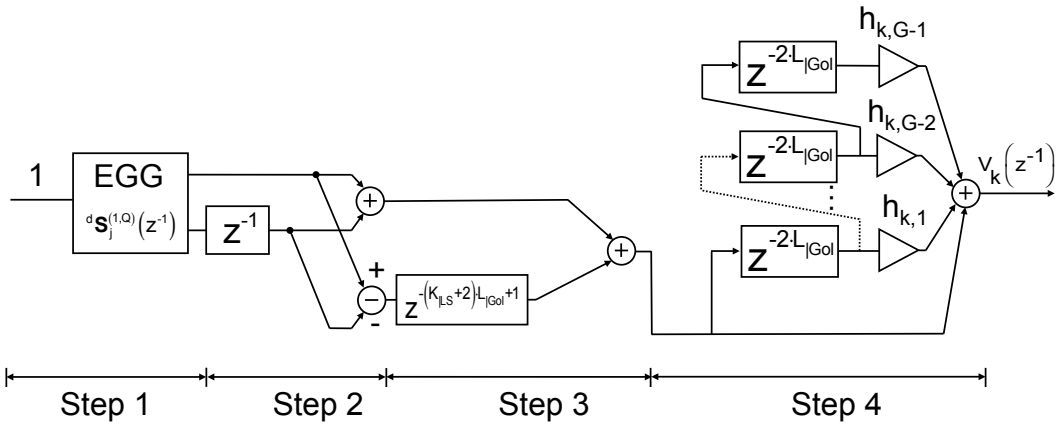


Figure 5.17: Diagram block of the efficient generator of LS sequences obtained from GPC sequences.

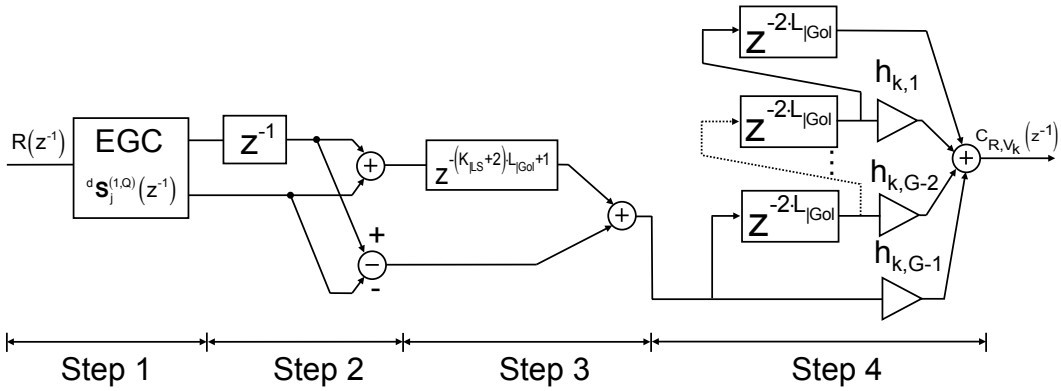


Figure 5.18: Diagram block of the proposed LS sequences correlator.

ultaneous generation/correlation of the first of $\frac{K_{|LS}}{2}$ LS sequences. In order to correlate a complete set of $K_{|LS}$ sequences with the proposed architecture, two EGC are needed. Figure 5.19 shows the complete architecture for the correlation of a set of $K_{|LS}$ LS sequences. The upper branch, (which uses the EGC for $^{d}\mathbf{S}_{0}^{(1,Q)}(z^{-1})$) correlates the first $\frac{K_{|LS}}{2}$ sequences and the lower one (which uses the EGC for $^{d}\mathbf{S}_{1}^{(1,Q)}(z^{-1})$), the remaining $\frac{K_{|LS}}{2}$ sequences. Further optimizations of this proposal may be accomplished by using the EGC architecture of [Donat 09a].

## 5.7 Conclusions

In this Chapter we took advantage of the efficient architectures proposed in Chapter 3 and Chapter 4 for CSS for introducing multilevel LS sequences, which allow the selection

| Resources | Products | Additions | Delays |
|---|---|---|---|
| Straightforward | – | $K_{\|LS} \cdot 2 \cdot L_{\|Gol} - 1$ | $2 \cdot (K_{\|LS} \cdot L_{\|Gol} + L_{\|Gol}) - 1$ |
| ELSC [Perez 07b] | – | $4 \cdot \log_2(L_{\|Gol}) + K_{\|LS} + 3$ | $4 \cdot L_{\|Gol} - 2 + \frac{K_{\|LS}}{2} \cdot (K_{\|LS} \cdot 2 \cdot L_{\|Gol} - 1)$ |
| VELSC [Perez 10] | – | $2 \cdot \log_2(L_{\|Gol}) + K_{\|LS} + 1$ | $2 \cdot (K_{\|LS} \cdot L_{\|Gol} + L_{\|Gol}) - 1$ |
| Proposed | – | $2 \cdot \log_2(L_{\|Gol}) + \frac{K_{\|LS}}{2} + 1$ | $2 \cdot (K_{\|LS} \cdot L_{\|Gol} + L_{\|Gol}) + 1$ |

Table 5.2: Comparison of hardware resources required for the generation/correlation of LS sequences for different methods (only one LS sequence is considered).

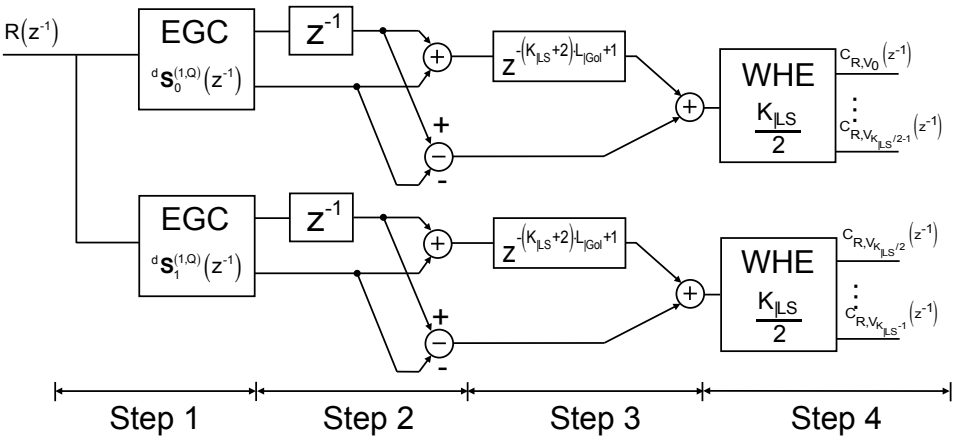


Figure 5.19: Complete architecture for the correlation of a set of $K_{|LS}$ LS sequences.

of the LS sequence length with less constraints than the binary ones. Due to the fact that there is no limitations on the length of the PMCS, the maximum ZCZ for a given LS sequence length can be adjusted to accomplish the particular system requirements.

Nonetheless, the use of multilevel LS sequences has the limitation of the energy efficiency. Depending on the values $A^{(q)}$, $W^{(1,q)}$ and $D^{(q)}$ of the PMCS generator, the resultant LS sequences can have a reduced energy efficiency. This can be coped with an appropriate encoding scheme as MC-CDMA or by using the values $A^{(q)}$, $W^{(1,q)}$ and $D^{(q)}$ that provide energy efficient LS sequences.

In this chapter we have also proposed a novel and efficient correlator for GPC sequences, which have a very promising correlation properties. Finally, we have shown the theoretical link between GPC and LS sequences. This helps us to introduce a novel generation algorithm of LS sequences and to correlate them with a similar number of hardware resources than with previous efficient architectures.

# Chapter 6

# Application to Ultra-Wideband Ranging Systems

In this chapter, we propose a CDMA-based Ultra-Wideband (UWB) Local Positioning System (LPS) with Commercial Off-The-Shelf (COTS) components; also the performance of two spreading sequences in this LPS is evaluated. We have compared Kasami [Kasam 66] sequences (which are unitary sequences with good aperiodic correlation functions and used previously in several ultrasonic indoor positioning systems [Villa 13], refer to Appendix A) with LS sequences [Stanc 01]. These GO sequences, have been also employed satisfactorily in an ultrasonic LPS under the presence of near-far effect [Perez 09c]; also the use of LS sequences has the advantage of using the architectures presented previously. In contrast to other positioning systems as ultrasound-based LPS, UWB LPS has to cope with the following challenges:

1. As an electromagnetic wave, in LOS conditions it propagates at the speed of light, $c = 3 \cdot 10^8$ m/s (which is more than $877,000$ times faster than propagation speed of ultrasound in the air at 20°C); this requires high sampling frequencies to increase time resolution.

2. Due to the high propagation speed and the sampling frequency, the beacons must be separated enough to obtain TDOAs with significative values, and avoid indeterminations in the positioning algorithm. This accentuates the near-far effect.

3. Because of the severe restrictions on power emissions it is needed receivers with a high sensitivity. In CDMA-based systems, as the one used here, it implies the use of spreading sequences with high immunity to noise.

4. The frequency-dependent UWB channel introduces additional distortions to those caused by the antennas. This effect and the signal propagation characteristics make

very difficult the detection of the first arriving path in Non-Line-of-Sight (NLOS) conditions with the presence of multipath.

With the application of the spreading sequences to the UWB LPS we can determine firstly the goodness of LS sequences (and by extension of GO sequences) in harsh conditions and secondly, the importance in practice of the proposed length extensions for the efficients binary LS correlators.

This chapter is divided into five subsections: first the global structure of the experimental system is described; later the emitter architecture and the receiver platform are explained; then the results of the ranging test are shown and finally some conclusions from the results are derived.

## 6.1 Global Structure of the Experimental System

The design of the UWB experimental system is privacy-oriented, i.e. the mobile device computes its position. Also it is CDMA-based, which has important implications in the overall system. Typical UWB systems use TDMA in order to manage the multiple access and to avoid undesired phenomena's as MAI and near-far effect, but the developed UWB system uses DS-CDMA instead. In this way, the UWB channel is accessed simultaneously by the beacons, relying on the properties of the spreading sequences to cope with those undesired effects. It is important to consider that the signal acquisition of designed UWB-LPS is asynchronous, and consequently if TDMA is used, a very large buffer must be acquired to ensure at least the acquisition of a complete frame from each transmitted beacon. Furthermore, the buffer size increases with the number of the transmitting beacons. This makes difficult the UWB signal detection in digital domain for a large number of beacons. Fortunately, the use of CDMA requires a smaller input buffer size and it is independent of the number of beacons in the LPS.

The main features of the experimental system are:

- Four beacons placed in the positions shown in Table 6.1 and determined with a tape measure. Each of them transmit periodically a spreading sequence (Kasami or LS) with a measured bandwidth at $-10$ dB of 577 MHz and center frequency of 3.5 GHz. The sequences emitted by each beacon are spaced-out in time to avoid ISI of successive emissions, 2 $\mu$s when transmitting LS sequences and 2.02 $\mu$s when transmitting Kasami sequences. The repetition period is equal to 4.08 $\mu$s for both sequences.

| Beacon | $x$ | $y$ | $z$ |
|---|---|---|---|
| B1 | $-0.28$ | 4.19 | 2.80 |
| B2 | $-0.22$ | $-1.39$ | 2.80 |
| B3 | 7.14 | $-1.38$ | 2.81 |
| B4 | 5.84 | 2.09 | 2.82 |

Table 6.1: Beacon positions in the test area (in metres).

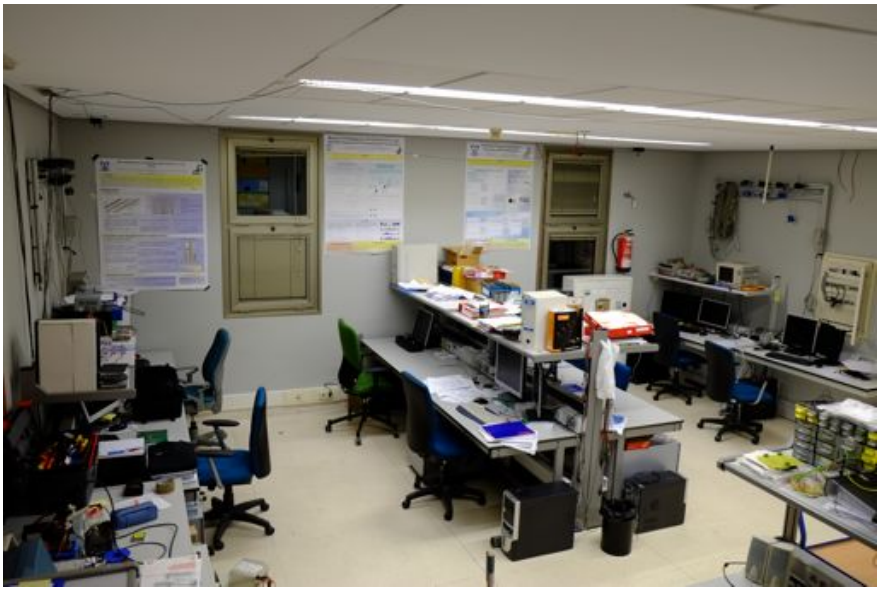

Figure 6.1: Environment used to perform the ranging test.

- The working area is approximately equal to 38 square metres. The ground truth is achieved thanks to the equally spaced floor tile of size 40 cm. Figure 6.1 shows the environment where the experimental system has been deployed.

- A receiver, placed in a known position acquires a signal frame that contains the signals from the four beacons, and determines the TDOAs.

Next subsections present a detailed description of the system components.

## 6.2 Emitter Module

The emitter of the UWB system is composed by the following elements:

- FPGA Virtex II-pro [Xilin 07]. It transmits the four sequences in base-band through dedicated differential ports RocketIO [Xilin 07] with a bit rate of 500 Mbps. The

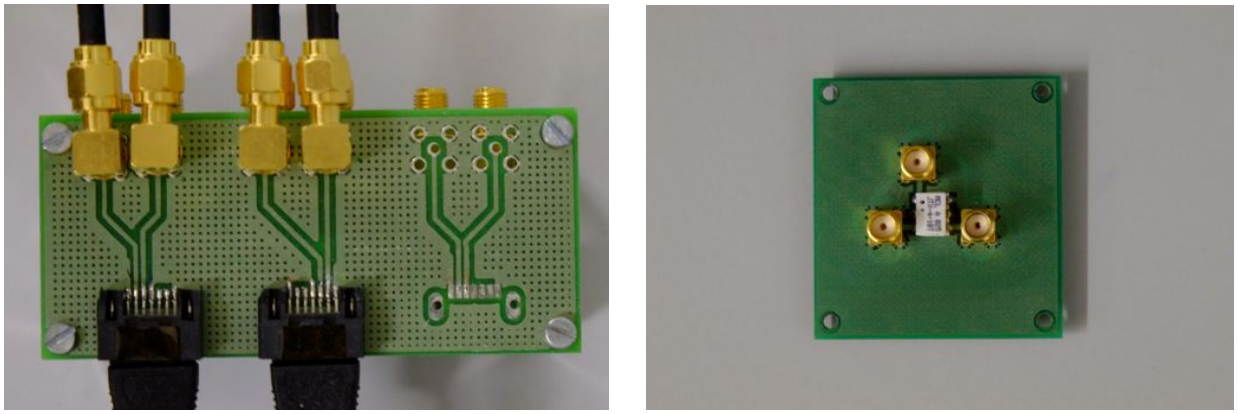

(a) (b)

Figure 6.2: PCB for referencing the RocketIO signals to ground: (a) PCB for SATA connectors (b) PCB for SMA connectors.

sampling frequency of the digital RocketIO ports are 1.5 Gsps, so each sequence bit is oversampled by a factor of 3. The FPGA has four accessible RocketIO ports: one through a pair of SMA connectors and the other three through SATA connectors.

- RF Transformers JTX-4-10T+ from Mini-circuits [Mini 13]. It has the task to convert the differential RocketIO signals to single-ended mode. Figure 6.2 shows the designed circuits with the RF transformer. Differences between PCBs traces and parasitic effects caused by soldadures make that, at the output of the PCB circuits, the coded signals are not synchronized. The relative delays among base-band signals have been quantified and compensated in the receiver. The relative delays, referred to the fourth RocketIO port, are equal to 1.8 ns for the first port, 0.6 ns for the second one and 0.2 ns for the third RocketIO port. Each port is assigned to a beacon that follows the same numeration.

- PLL Frequency synthesizer evaluation board EVAL-ADF4350 from Analog Devices [Analo 13]. It allows to configure the frequency of the Local Oscillator (LO) through a PC from 137.5 MHz to 4.4 GHz.

- Power splitter ZB4PD-42+ from Mini-circuits. It divides, with minimum power unbalance, the LO into four ports.

- Frequency mixers ZX05-43LH+ from Mini-circuits. They multiply each of the base-band signals coming from the RocketIO ports with the splitted LO to up-convert the base-band signals to 3.5 GHz.

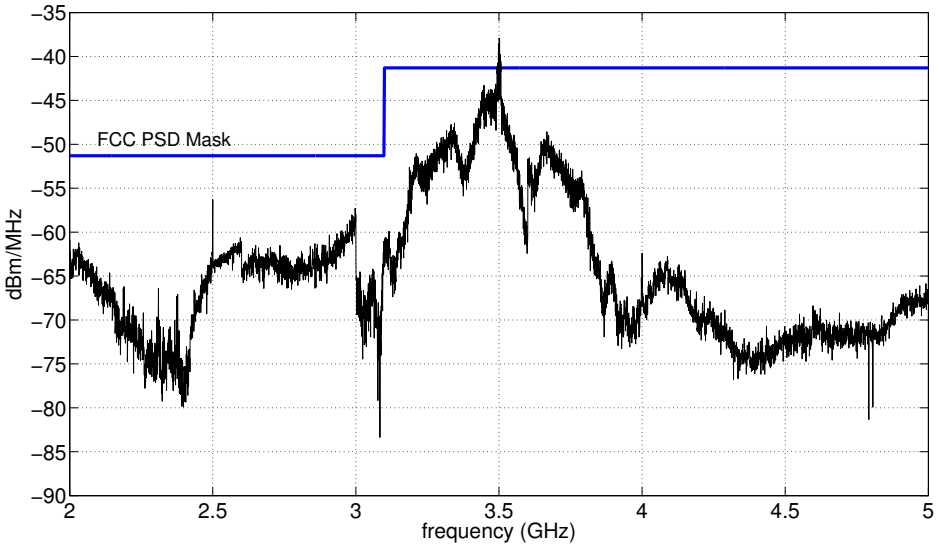


Figure 6.3: Power Spectral Density of the radiated signal measured with a spectrum analyzer.

- Wideband Power Amplifiers (PA) ZX60-V83+ from Mini-circuits. The four UWB RF signals coming from the frequency mixers are fed into the wideband amplifiers. They operates in the frequency range from 20 MHz to 4.7 GHz and have a gain of 15 dB at 3 GHz.

- RG-174 coaxial cables of length 30 feet. The cables introduce an estimated attenuation of 16 dB at 3.5 GHz [Times 13] that allows to be compliant with the FCC PSD mask.

- UWB Fractus planar antennas [Fract 13]. They have an operational frequency range from 3.1 GHz to 5 GHz with an average efficiency of 84%.

Figure 6.3 shows the PSD of the emitted UWB signals. The bandwidth measured at $-10$ dB is approximately equal to 577 MHz and centred in 3.5 GHz. Integrating over the available bandwidth, each emitter transmits approximately 13.1 $\mu$W. This is roughly 76 times lower than the maximum allowed output power for Bluetooth class 3 devices [p. 46, IEEE 05] and 763 times lower than the power output of UMTS class 5 [Europ 98].

The antennas have been characterized in a semi-anechoic chamber (Figure 6.4) resulting in the radiation patterns of Figure 6.5. As depicted, the planes $x-z$ and $z-y$ are not completely omnidirectional. Therefore, the transmitted power signal (and the received one) will depend on the relative angle between emitter and receiver. This is a fundamental

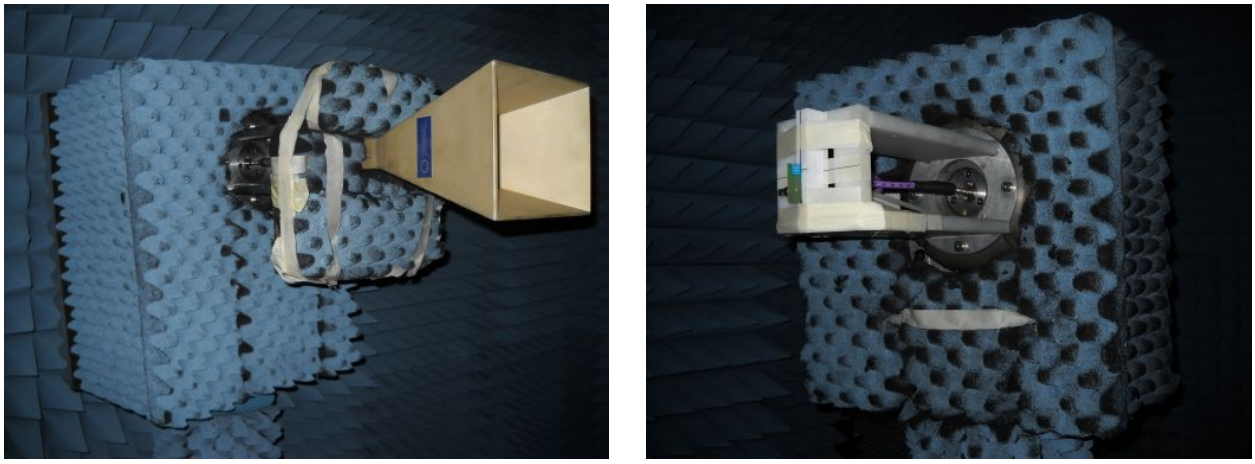

(a) (b)

Figure 6.4: Probe (a) measuring the radiation in the $z-x$ plane of the FRACTUS antenna (b).

issue in UWB ranging systems where the transmitted power is strictly limited to $-41.3$ dBm/MHz in the working frequency range of the UWB test-bed (refer to Figure 6.3).

Figure 6.6 shows a photograph of the UWB transmitter, while Figure 6.7 depicts the architecture of the emitter platform. Contrary to IR-UWB systems, which emit narrow pulses in base-band, without the necessity of up-conversion [Wentz 06], the employed UWB system uses a more complex homodyne architecture. Nevertheless, it confers more flexibility in the selection of both the center frequency and modulation [Segur 10].

## 6.3 Receiver Module

The receiver module has the following elements:

- UWB Fractus planar antenna. This antenna is the same as those used for the UWB signal transmission.
- Bandpass Filter (BPF) VBFZ-3590+ from Mini-circuits. It has a loss lower than 2 dB in the passband (3 GHz-4.3 GHz) and a rejection loss larger than 20 dB in the stopbands.
- Low Noise Amplifier (LNA) ZX60-3800LN+ from Mini-circuits. It has a noise figure of 0.9 dB and a bandwidth from 3.3 GHz to 3.8 GHz.

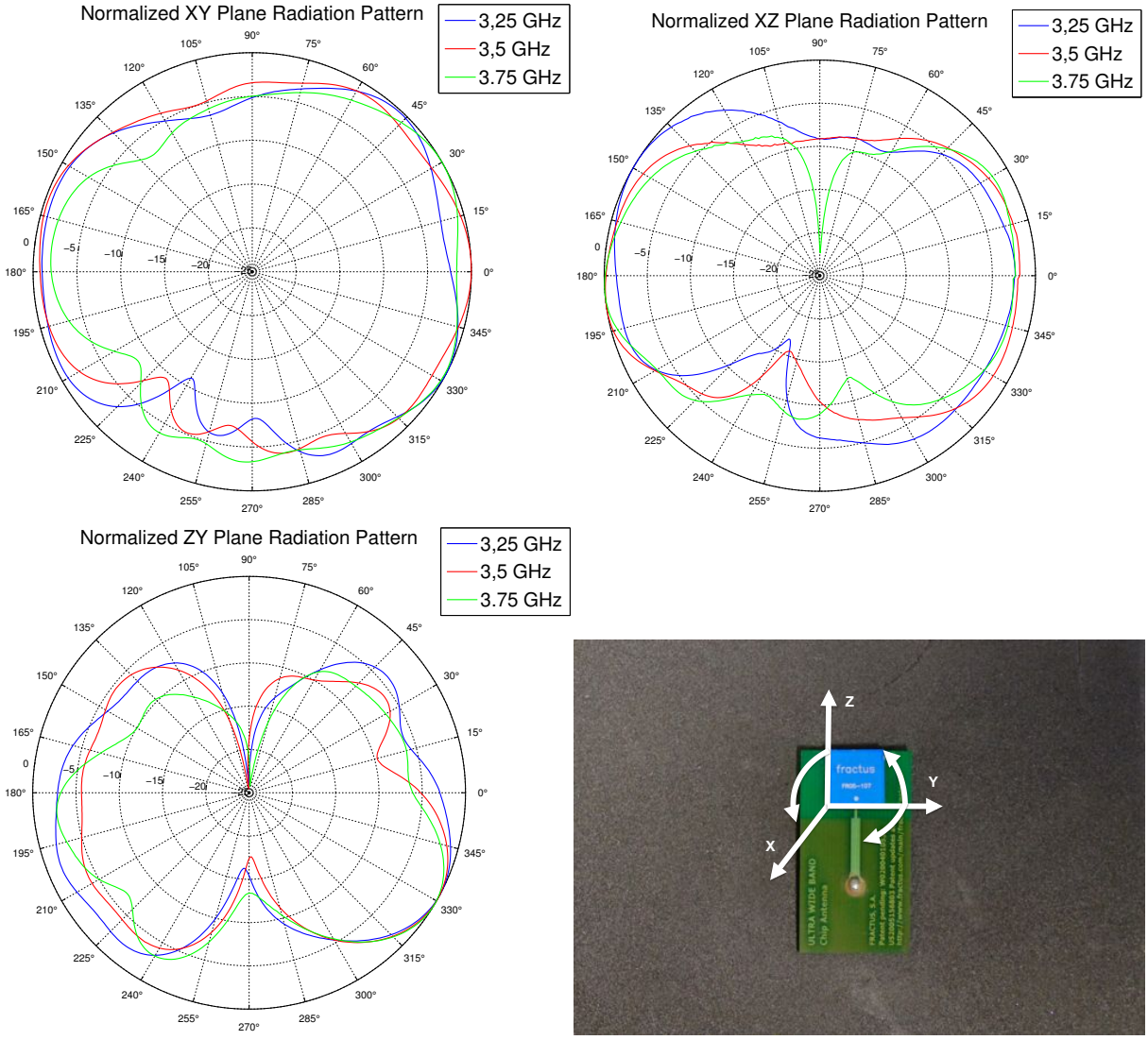


Figure 6.5: Radiation Pattern of the FRACTUS planar antennas measured on different planes.

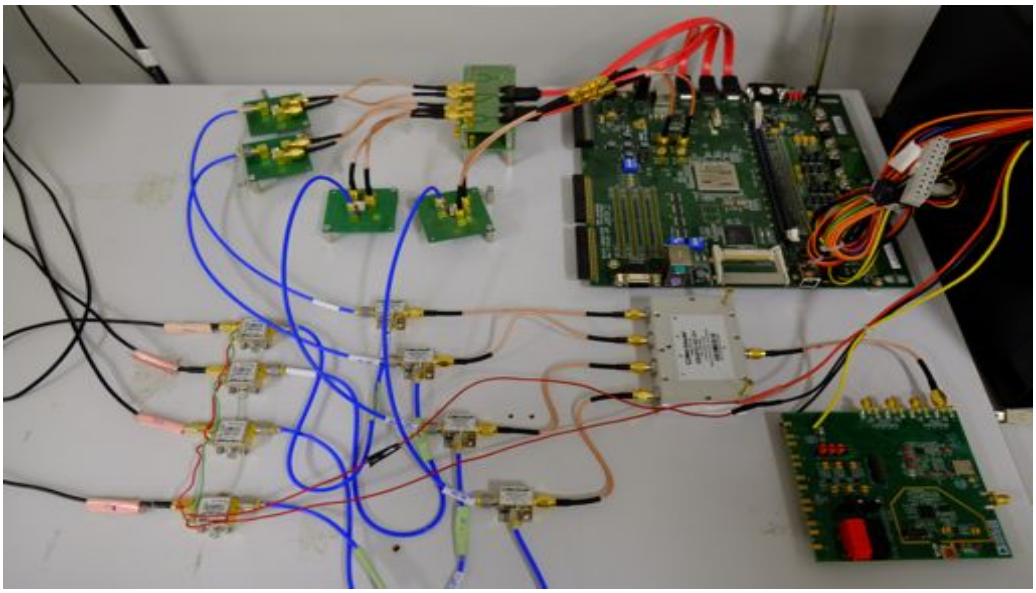

Figure 6.6: Complete UWB transmitter module.

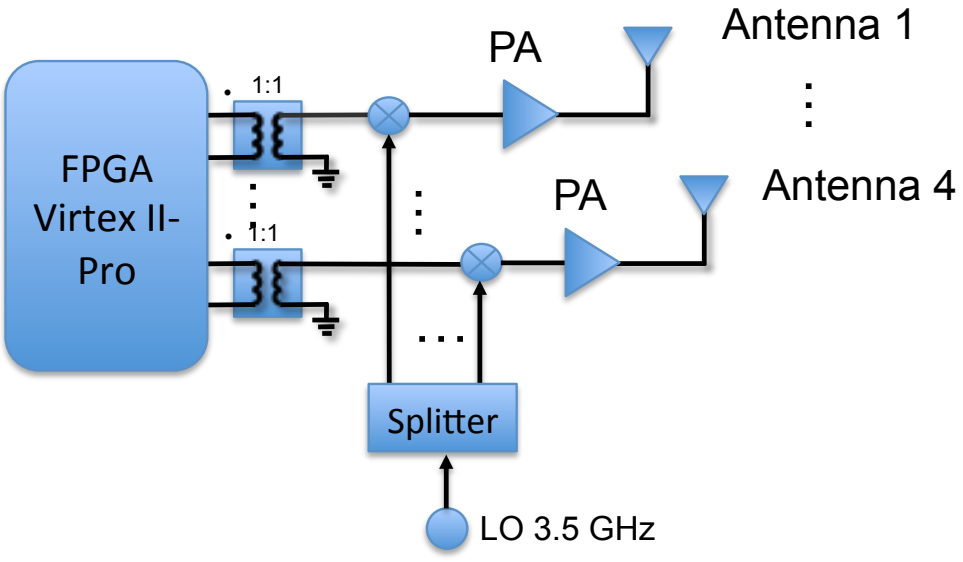


Figure 6.7: Diagram block of the UWB emitter.

- Quadrature demodulator ADL5375-05-EVALZ with an operating RF and LO frequency from 400 MHz to 6 GHz. This demodulator will permit in future versions of the UWB LPS to work with quadrature modulations, adequate for pair of sequences as GPC or T-ZCZ. In the following tests it is only used the in-phase (I) output.

- PLL Frequency synthesizer evaluation board EVAL-ADF4350 from Analog Devices. The same LO than the one employed in the emitter side has been used in the receiver.

- Low Pass Filter (LPF) VLF-1000+ from Mini-circuits. It has a loss lower than 1 dB in the passband (0-1 GHz) and a rejection loss of 30 dB in the stopband.

- Power Amplifier ZX60-3018G+ from Mini-circuits. This PA has a a noise figure of 2.7 dB and a wide bandwidth, 20 MHz-3 GHz.

- Digital Sampling Oscilloscope (DSO) DL9140L from Yokogawa [Yokog 13]. The main features of this oscilloscope are an input sampling frequency of 5 GSps, a bandwidth of 1 GHz and a large input buffer size of 6.25 mega-words. This implies that the oversampling factor is equal to 10 samples per sequence bit and that the ranging resolution is equal to 6 cm (i.e. one digital sample represents 6 cm). The UWB signal is acquired and stored in a USB flash memory stick to offline determine the TDOAs in a PC with MATLAB. In spite of using an oscilloscope for the signal acquisition in the tests carried out, the final version of the receiver uses a 5 GSps FMC126 10 bits resolution ADC, from 4DSP [4DSP 13] attached to a Virtex VI FPGA (with a 100 MHz frequency clock) [Xilin 12b] via a PCM bus for data acquisition. The use of an oscilloscope previously, allows the validation of the UWB system, for the later implementation of the signal processing techniques in the FPGA. This implementation has been successfully done recently, obtaining similar ranging errors than the ones presented here.

Figure 6.8 shows a diagram block of the UWB receiver. It is important to notice that the receiver is asynchronous, so neither the carrier phase nor the frequency is tracked.

Although longer sequences could be transmitted if the oscilloscope is used for acquisition purposes (it has a large input buffer size), it has been used sequences of the largest length lower than the input buffer size instantiated in the FPGA platform: Kasami sequences of length $L_{|Kasami} = 1023$ and LS sequences of length $L_{|LS} = 1039$. Notice that with this constraints, for binary LS sequences without the proposed generalization, the largest LS sequences length that could be used with an efficient correlator is $L_{|LS} = 639$.

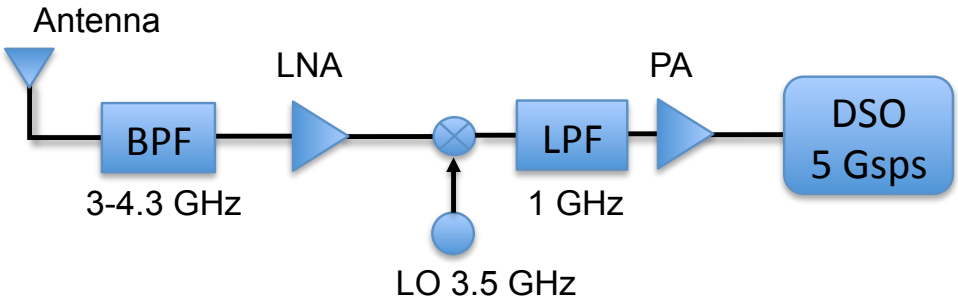


Figure 6.8: Diagram block of the UWB receiver.

The ZCZ length of the LS sequences used is equal to 207 bits which is larger than the maximum theoretical TDOA that can be obtained due to the geometrical configuration of the beacon and the coverage area (approximately 107 samples, and consequently the minimum theoretical IFW is equal to 215 samples).

An analysis of the link budget has been done resulting in an approximate maximum range (without considering body effects) of 9 metres. The receiver has a noise figure of 7.57 dB and a sensitivity of $-88.74$ dBm.

First arriving path detection for both types of spreading sequences is carried out as depicted in the algorithm 6.1. Notice that, in contrast to ultrasound ranging systems, in UWB systems the maximum correlation peak does not necessarily means that it is the TOA; as UWB signals can penetrate certain materials, the first arriving path can be more attenuated than multipath components.

Firstly, the detection algorithm computes the correlations between the received signal and the sequences transmitted by each beacon; later the absolute value of the correlation amplitudes is done; then the relative delays between the base-band signals are compensated by delaying individually each correlation; afterwards the absolute maximum of the correlations is worked out to determine an initial searching window, with length $SW$ equal to 300 samples for the four correlations centred around this maximum value. This value is larger than the minimum theoretical IFW to ensure that the correlation peaks are within the window of 300 samples. Later, for each correlation the algorithm searches the first arriving path in the 100 first samples that precede its maximum correlation value (an smaller window whose length we will call $ZCZleft$). This smaller window is the same for the four aperiodic correlations and it has been established to detect the first arriving path, that could be more attenuated than the maximum correlation value.

**Algorithm 6.1** MATLAB pseudo-code for first arriving path detection.

**Entry**: received: received signal; template: spreading sequences with zero padding

**for** i=1 **to** 4 **do**

corr(i,:)=absolute_value(correlation(received,template(i,:)));

correlations_adjusted(i,:)=Compensate_Delays(corr(i,:));

**end**

initial_position=(max(max(correlations_adjusted)));

left_margin=initial_position - $\frac{SW}{2}$;

right_margin=initial_position+ $\frac{SW}{2}$;

**for** i=1 **to** 4 **do**

large_SearchWindow(i,:)=correlations(i,left_margin : right_margin);

MaxValue_SearchWindow=max(large_SearchWindow(i,:));

threshold(i)=0.4*Max_Value_SearchWindow;

search_windowZCZleft=

correlations(i,MaxValue_SearchWindow-$ZCZleft$ : MaxValue_SearchWindow);

Leading_Edge(i)=find_first_sample(search_windowZCZleft(i,:)>=threshold(i));

FirstArrivingPath(i)=FindFirstPeak(Leading_Edge(i),search_windowZCZleft(i,:));

**end**

**Return**: FirstArrivingPath

For each correlation and within the previous window of length $ZCZleft$, the algorithm searches for the first correlation peak that exceeds a given threshold. This threshold is unique for each correlation and equal to the 40% of the maximum correlation peak, independently of the type of sequences used. The threshold values have been determined experimentally and are specific for the working environment.

Notice that there are more robust (but complex) UWB TOA detectors in the literature than can be applied instead [Guven 05, Falsi 06, Kuhn 10]. Nevertheless it is beyond the scope of this thesis.

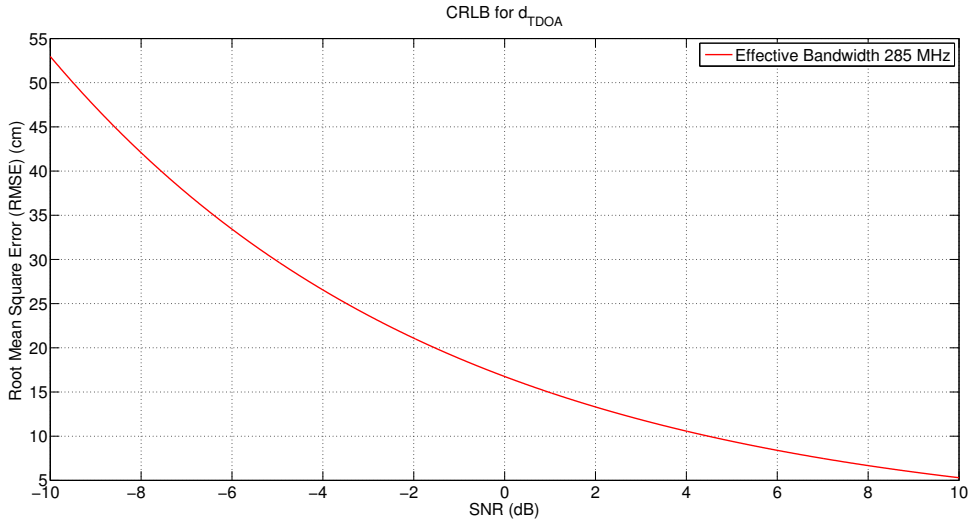


Figure 6.9: Cramér-Rao Lower Bound of the UWB LPS for different SNR.

## 6.4 Results

Recalling the Cramér-Rao Lower Bound (CRLB) for the estimation of TDOA in LOS conditions and without multipath, we have

$$\mathrm{RMS}E_{TDOA} \geq \frac{c}{2 \cdot \pi \cdot B \cdot \sqrt{\mathrm{SNR}}};\ B = \frac{\int_{-\infty}^{\infty} f^2 \cdot |S_t(f)|^2 \, df}{\int_{-\infty}^{\infty} |S_t(f)|^2 \, df} \tag{6.1}$$

where $B$ is the effective bandwidth and $S_t(f)$ is the spectrum of the transmitted signal. The CRLB will permit to compare the system precision with the best achievable in theory. Figure 6.9 shows the lowest Root Mean Square Error (RMSE) in centimetres that can be achieved with the described UWB LPS for different SNR conditions.

Where $\mathrm{d_{TDOA}}$ is defined as $\mathrm{d_{TDOA}} = TDOA/c$. The previous UWB LPS has been evaluated with two different spreading sequences: Kasami and LS sequences. In this section, a comparative analysis of the performance for both types of sequences is carried out. First, the ranging errors of the UWB LPS with Kasami sequences are obtained; then it is shown the improvements achieved when used LS sequences. The TDOA measurements could be used to position the receiver by using certain hyperbolic positioning algorithms as Gauss-Newton [Sirol 10] or Cayley-Menger [Ruiz 11].

### 6.4.1 Kasami Sequences

The received signal is processed by using the algorithm 6.1; once detected the first arriving path for each correlation, three measurements $d_{\text{TDOA}}$ are obtained: $d_{\text{TDOA}}$1-2, $d_{\text{TDOA}}$2-3 and $d_{\text{TDOA}}$3-4, where the term $d_{\text{TDOA}}i-j$ refers to the difference in the measured distances receiver-beacon $i$ and receiver-beacon $j$, i.e. $d_{TOA}\ i$ - $d_{TOA}\ j$. Figure 6.10 shows the RMSE values in each test position for the three $d_{\text{TDOA}}$ measurements (100 measurements have been carried out for each position and the RMSE values larger than 1 m have been clipped to that value). The low power transmissions and the near-far effect, make the first arriving path of the furthest beacon undetectable in positions close to other beacons. For example, this happens for beacon 1 in positions 8 to 16. This also happens with beacons 3 and 4 for positions 17 to 23, 29 and 30 and for beacons 2 and 3 for positions close to beacon 1.

For a more detailed information, Table 6.2 includes the RMSE values for each test position and the first (25%), second (50%) and the third (75%) quartiles, expressed as $Q_1 - Q_2 - Q_3$ in metres.

Firstly it is analyzed the ranging errors in the position $(3.20, 0.80, 1.57)$ (position number 2), which is located in the center of the coverage area. Figure 6.11 shows the Cumulative Distribution Function (CDF) in the test position $(3.20, 0.80, 1.57)$. The quartiles (in metres) are equal to $0.06 - 0.12 - 0.54$ for $d_{\text{TDOA}}$1-2, $0.12 - 0.24 - 3.18$ for $d_{\text{TDOA}}$2-3, and $0.18 - 0.24 - 3.36$ for $d_{\text{TDOA}}$3-4.

Figure 6.12 depicts the aperiodic correlation functions computed for a given measurement in this location, where the purple markers represent the estimated first arriving paths. Although there is a large amount of multipath components and the signals emitted by beacon 1 and beacon 4 are obstructed (i.e. there is NLOS), the algorithm 6.1 estimates the $d_{\text{TDOA}}$1-2, $d_{\text{TDOA}}$2-3 and $d_{\text{TDOA}}$3-4 in this particular measurement instance with errors (in samples) of 3, 4 and 3 samples respectively. Also it is noteworthy that the RMSE values of $d_{\text{TDOA}}$2-3 (2.78 metres) and $d_{\text{TDOA}}$3-4 (2.85 metres), are much larger than the RMSE value of $d_{\text{TDOA}}$1-2 (0.44 metres).

Now the test position 10, whose coordinates are $(5.20, 0.40, 1.57)$, is analyzed. This test position will illustrate both, near-far and radiation pattern effects. Figure 6.13 shows the CDF in this location. Quartiles (in metres) are equal to $3.18 - 3.90 - 4.68$ for $d_{\text{TDOA}}$1-2, $5.40 - 6.00 - 6.18$ for $d_{\text{TDOA}}$2-3, and $0.12 - 0.18 - 0.24$ for $d_{\text{TDOA}}$3-4. Notice that the $d_{\text{TDOA}}$1-2 and $d_{\text{TDOA}}$2-3 errors are much larger than the errors of $d_{\text{TDOA}}$3-4. The reasons of these errors become more clear, if we take a look into the aperiodic correlations functions.

Figure 6.14 shows the aperiodic correlation functions obtained in the location (5.20, 0.40, 1.57) for a given measurement instance. As depicted, the first arriving path of the signals emitted by beacons 1, 2 and 4 are undetectable. The highly attenuated signals emitted by beacons 1 and 2 are masked by MAI. Also, it is interesting to note the poor correlation values obtained for beacon 4. Although the analyzed position is close to it, the radiation pattern of the antennas makes that the received signal is severely attenuated for certain relative angles between emitter and receiver (refer to Figure 6.5) and thus being affected by near-far effect.

The large errors obtained with Kasami sequences are mainly due to near-far effect and MAI. Notice that algorithm 6.1, searches for the maximum peak value in each of the four correlations to determine a searching window. This peak does not have to be a first arriving path and it could be a large multipath component. When the algorithm searches $ZCZleft$ samples backwards for the first arriving path, it can lock into noise. Also the high propagation speed of the UWB signals makes that small errors in samples in the TOA estimation implies large errors in the distance estimation. In fact, with the frequency acquisition of 5 Gsps used in the tests, an error of one sample in the TOA estimation is translated to a ranging error of 6 centimetres.

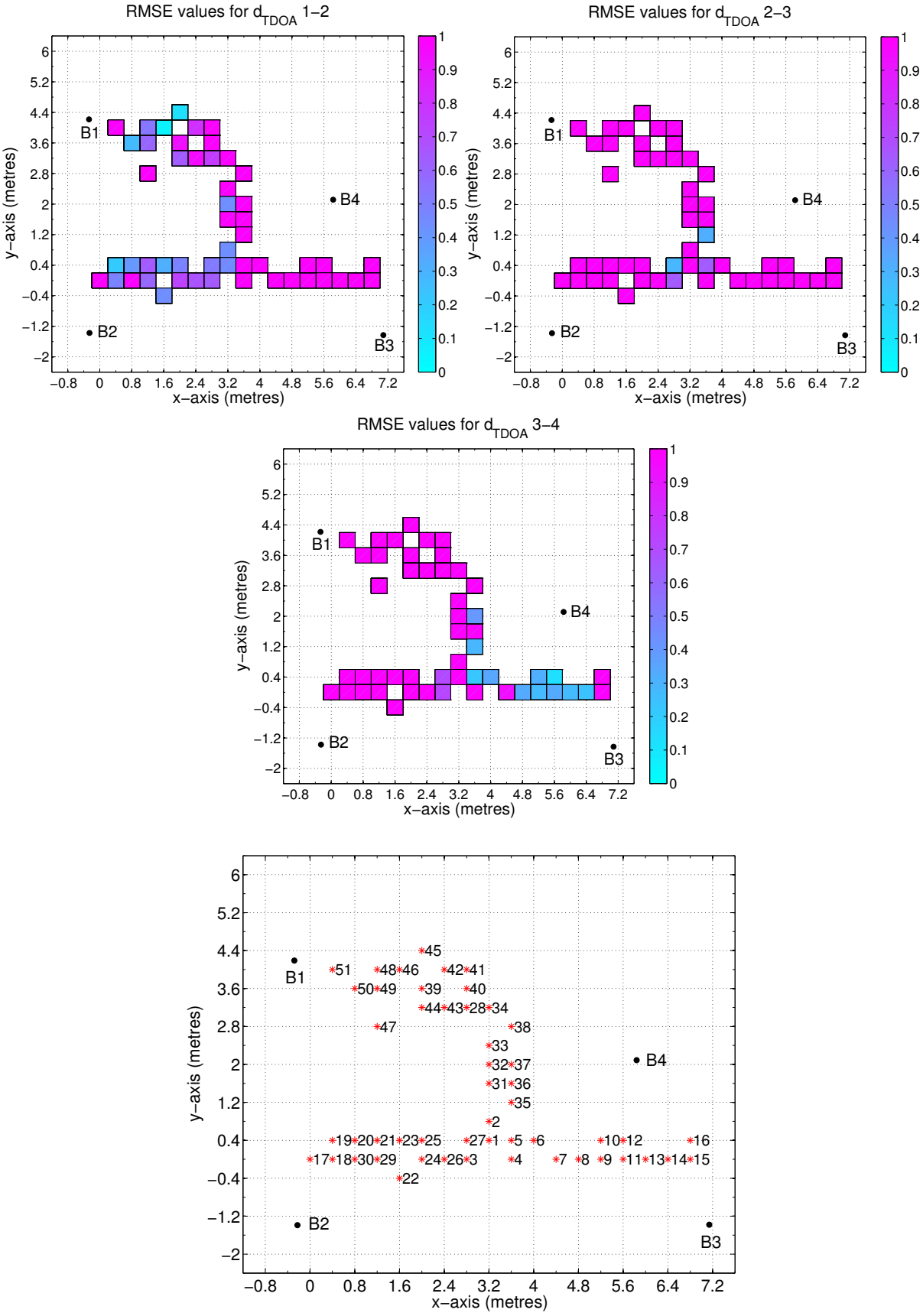


Figure 6.10: RMSE values in each test position for the three $d_{TDOA}$ measurements when using Kasami sequences.

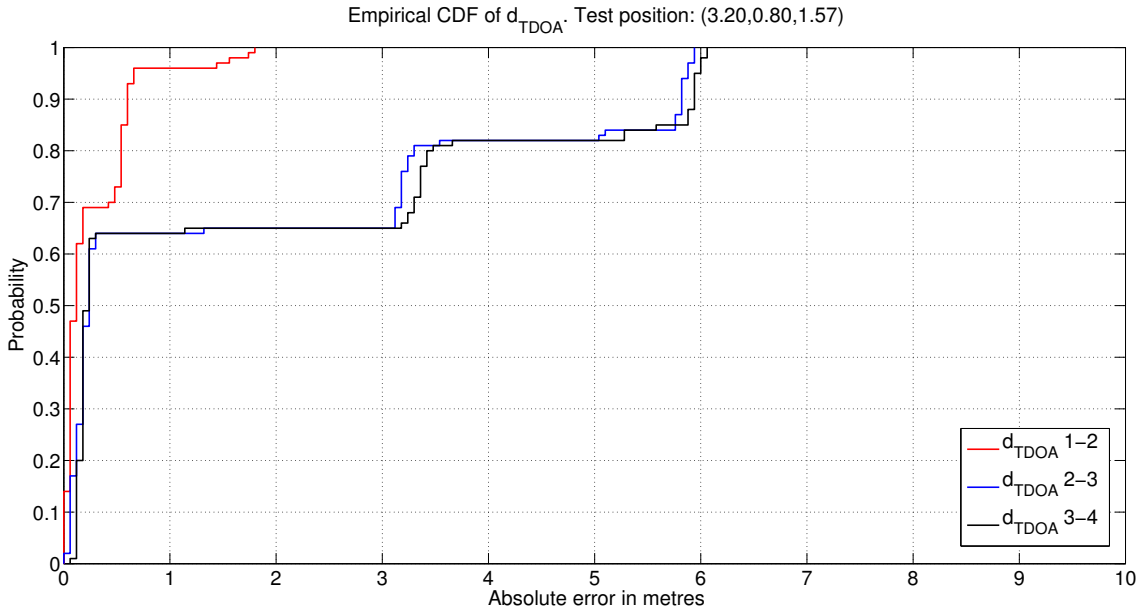


Figure 6.11: Empirical Cumulative Distribution Function for the test position (3.20, 0.80, 1.57).

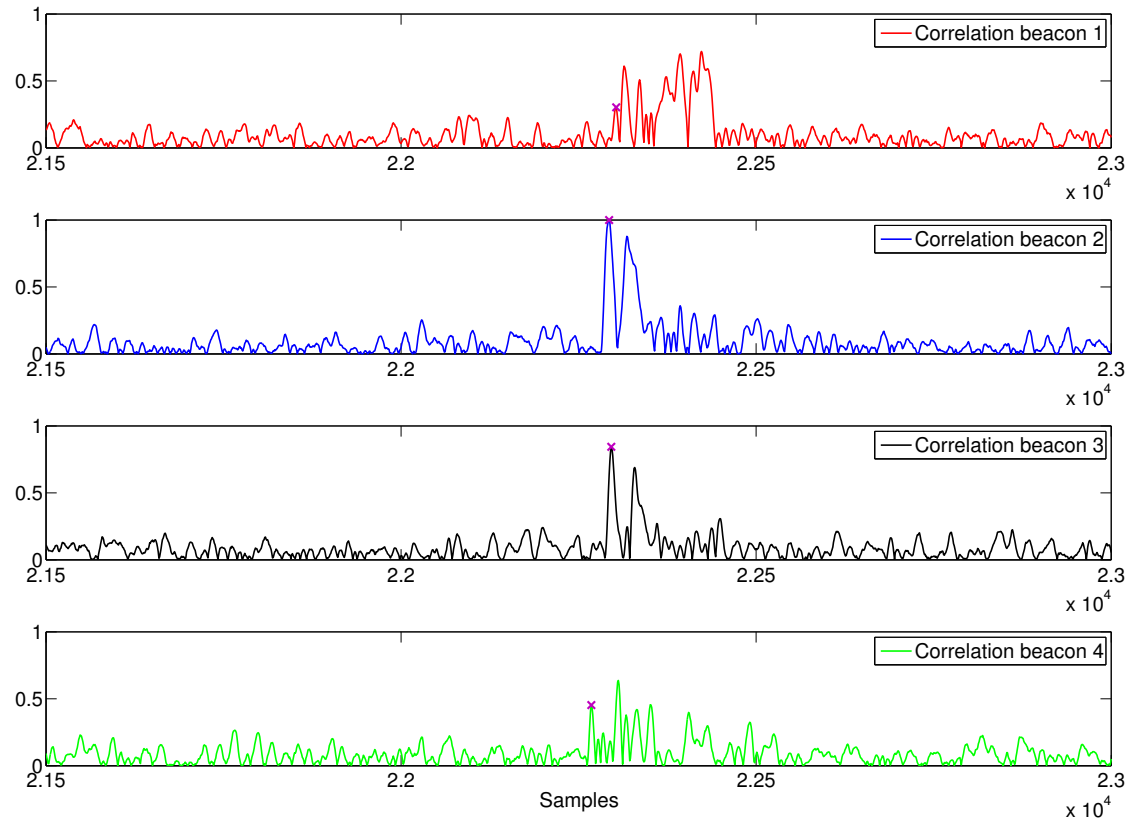


Figure 6.12: Aperiodic correlation functions in the test position (3.20, 0.80, 1.57).

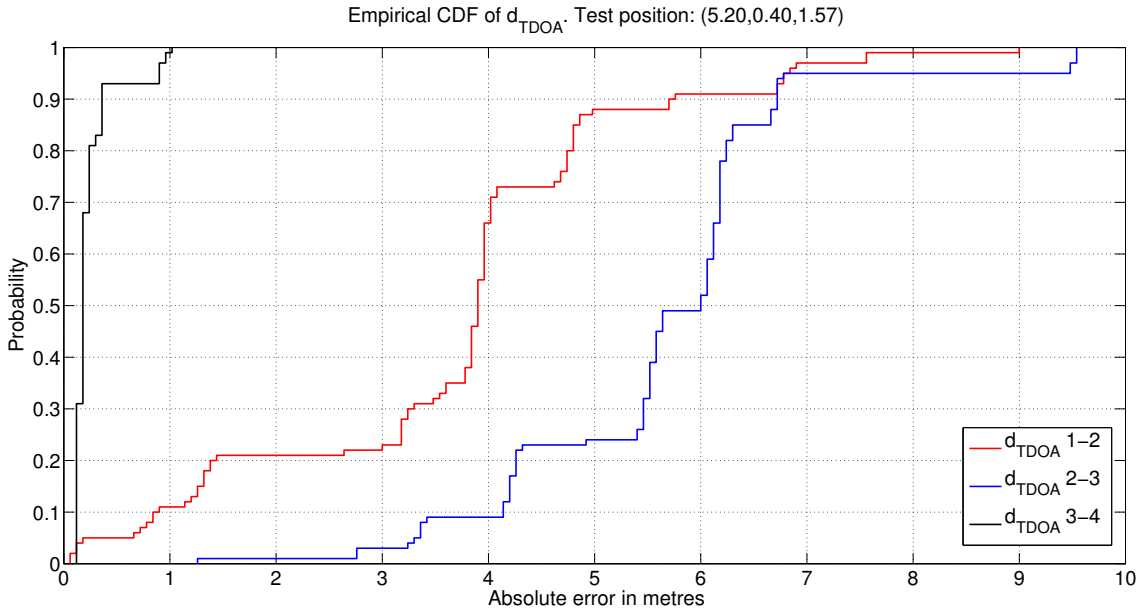


Figure 6.13: Empirical Cumulative Distribution Function for the test position (5.20, 0.40, 1.57).

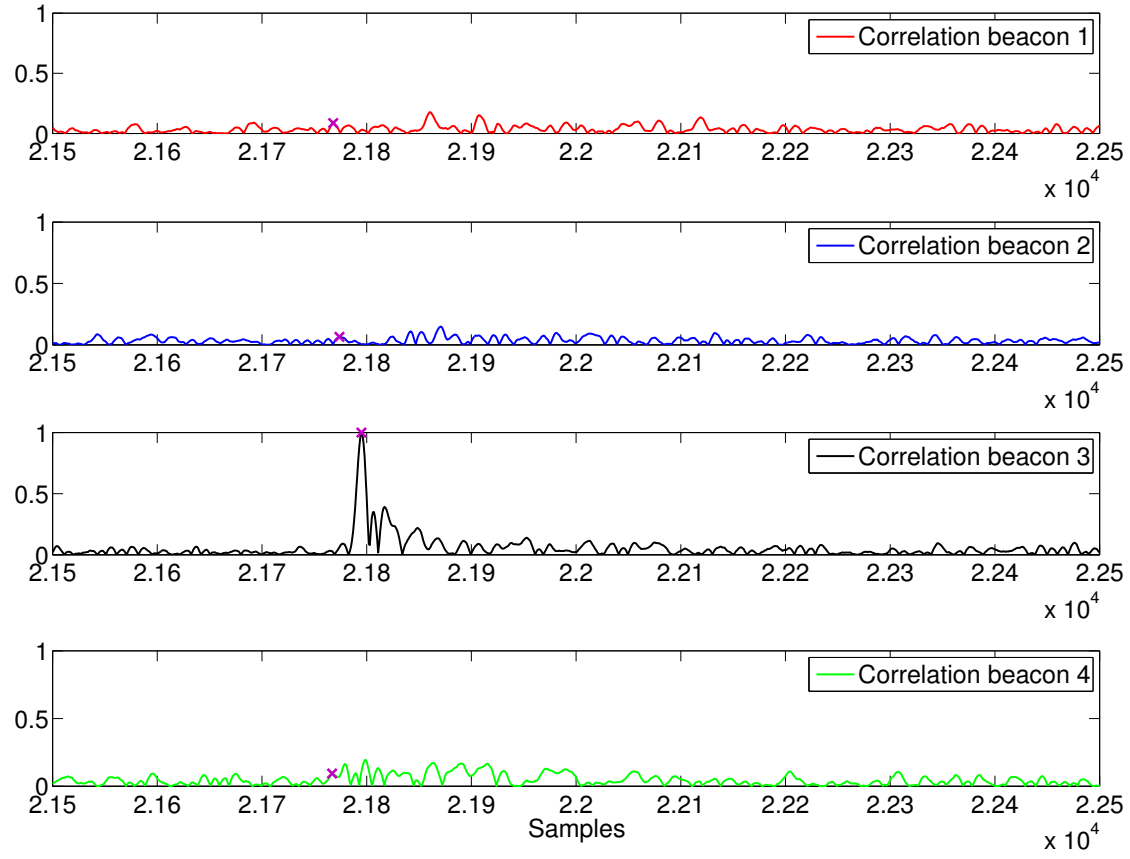


Figure 6.14: Aperiodic correlation functions in the test position (5.20, 0.40, 1.57).

### 6.4.2 LS Sequences

Figure 6.15 depicts the RMSE values (in metres) in each test position for the three $d_{TDOA}$ measurements. In the same form as was done for Kasami sequences, 100 measurements have been carried out in each position. Again, the RMSE values larger than 1 m have been clipped to that value. For a more detailed information, Table 6.3 includes the RMSE values for each test position and the first (25%), second (50%) and the third (75%) quartiles, expressed as $Q_1 - Q_2 - Q_3$ in metres.

Notice that now, ranging errors in positions susceptible to near-far effect, as positions 8 to 16, positions 17 to 23, position 29 or position 30 have lower ranging errors than in the previous case with Kasami sequences. The source of errors in those zones are due to the path loss.

We analyze in detail two test positions: position 2, which corresponds with the coordinates $(3.20, 0.80, 1.57)$ and the position 10, in the coordinates $(5.20, 0.40, 1.57)$. The first one, is approximately in the center of the coverage area; the CDF for each $d_{TDOA}$ measurement in the position $(3.20, 0.80, 1.57)$ is shown in Figure 6.16.

As Figure 6.16 depicts, the quartiles (in metres) are equal to $0.06 - 0.12 - 0.48$ for $d_{TDOA}$1-2, $0.06 - 0.06 - 0.21$ for $d_{TDOA}$2-3, and $0.12 - 0.18 - 0.24$ for $d_{TDOA}$3-4. Figure 6.17 shows the aperiodic correlation functions in the coordinates $(3.20, 0.80, 1.57)$ for a certain measurement instance. The purple markers depicts the first arriving path estimated by the peak detector algorithm. Observe in the correlation with the LS emitted by beacon 1 (which is the furthest beacon to the receiver) that in spite of being the first arriving path highly attenuated, i.e. there is NLOS, it is correctly detected. It is also noteworthy the large amount of multipath components in the received signal. This makes an idea of the complex environment in which the UWB system is deployed. The differences between the estimated and the theoretical $d_{TDOA}$ are mostly due to:

- Propagation through obstacles (NLOS condition), which reduces the propagation speed and consequently introduces a positive bias in the ranging estimation [Darda 09].
- Not having a strictly synchronization between beacons because of different hardware delays (refer to Figure 6.2).
- Discretization errors due to sampling.
- Errors in the measurement of the beacon positions.

Now we analyze thoroughly the test position 10. Figure 6.18 shows the CDF in this test position for the three $d_{TDOA}$ measurements. The quartiles (in metres) are equal to $1.20 - 1.26 - 2.25$ for $d_{TDOA}$1-2, $0.18 - 0.24 - 0.30$ for $d_{TDOA}$2-3, and $0.12 - 0.18 - 0.24$ for $d_{TDOA}$3-4. Notice from Table 6.3 that the RMSE value for the measurement $d_{TDOA}1 - 2$ is much larger than the other two. This will become clear by analyzing the aperiodic correlation functions.

Figure 6.19 shows the aperiodic correlation functions in the test position 10. As depicted, the correlation peaks of beacon 1 and beacon 2 are highly attenuated due to propagation loss, causing that the first arriving path estimator fails. Again, it is interesting to note that the correlation of beacon 4 is highly attenuated for the real distance to the receiver. This is because the radiation pattern of the antenna (refer to Figure 6.5).

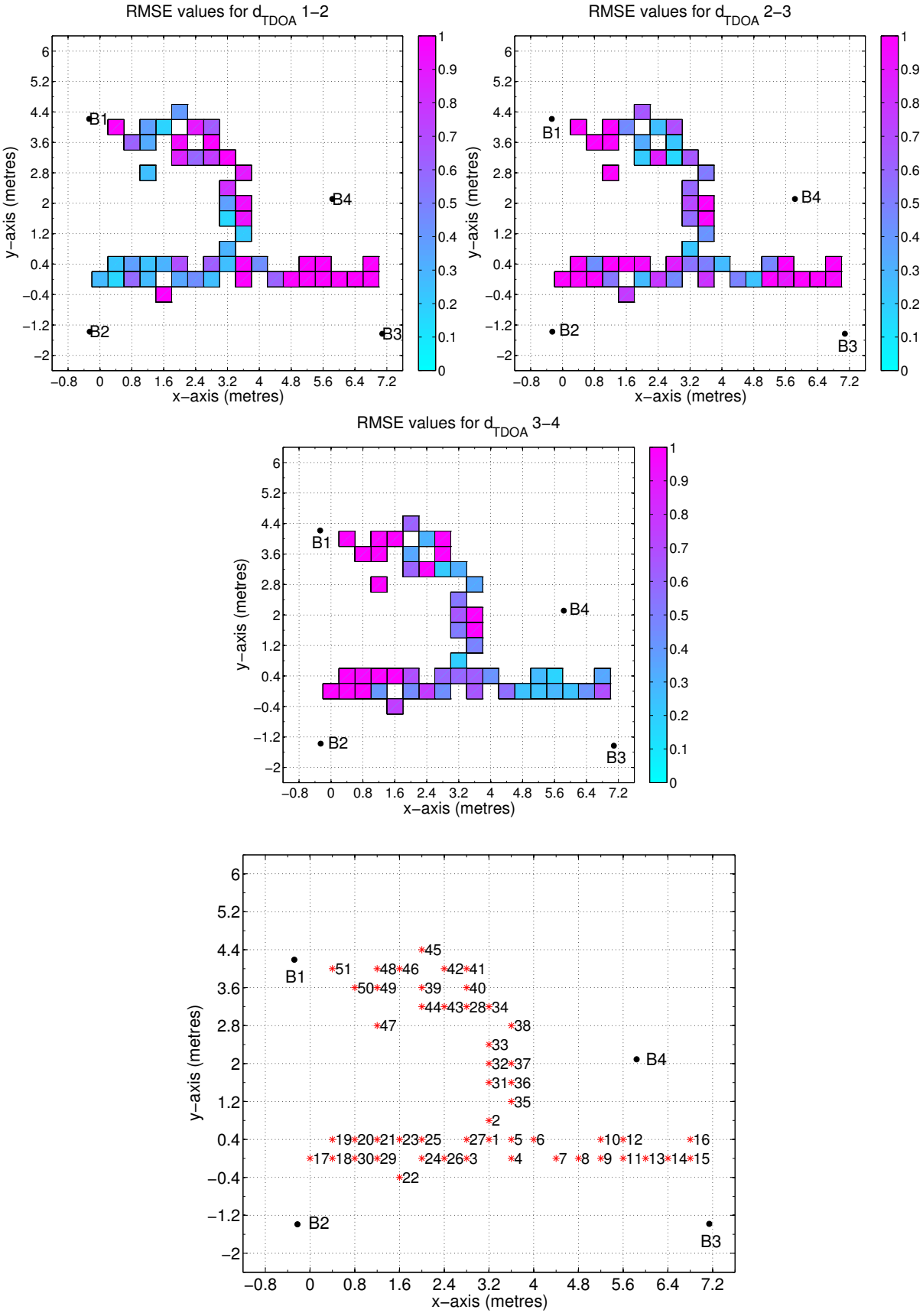


Figure 6.15: RMSE values in each test position for the three $d_{TDOA}$ measurements when using LS sequences.

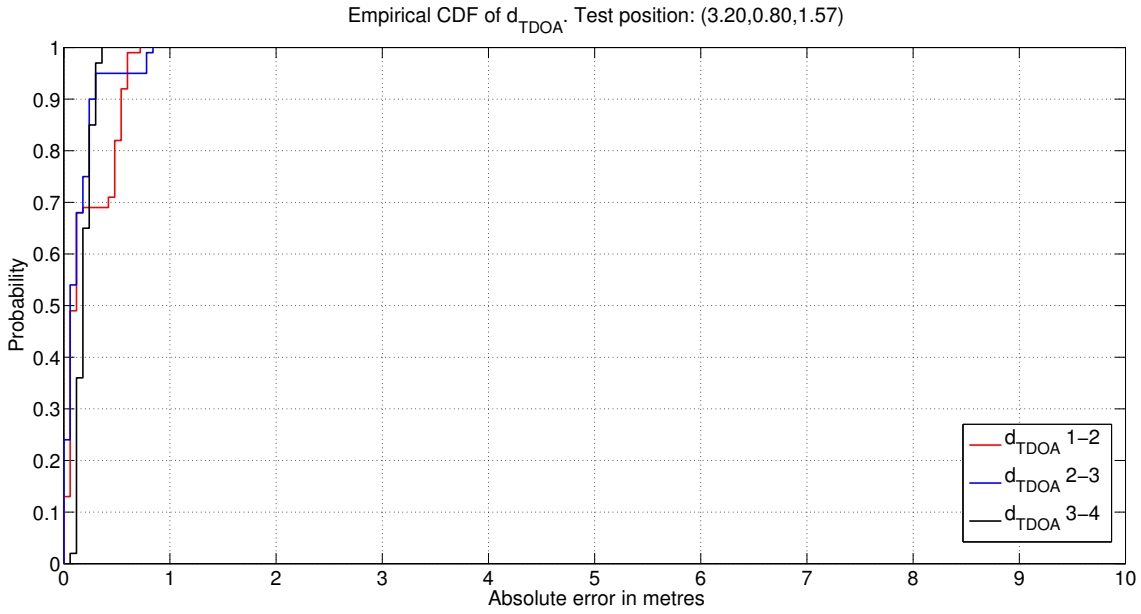


Figure 6.16: Empirical Cumulative Distribution Function for the test position (3.20, 0.80, 1.57).

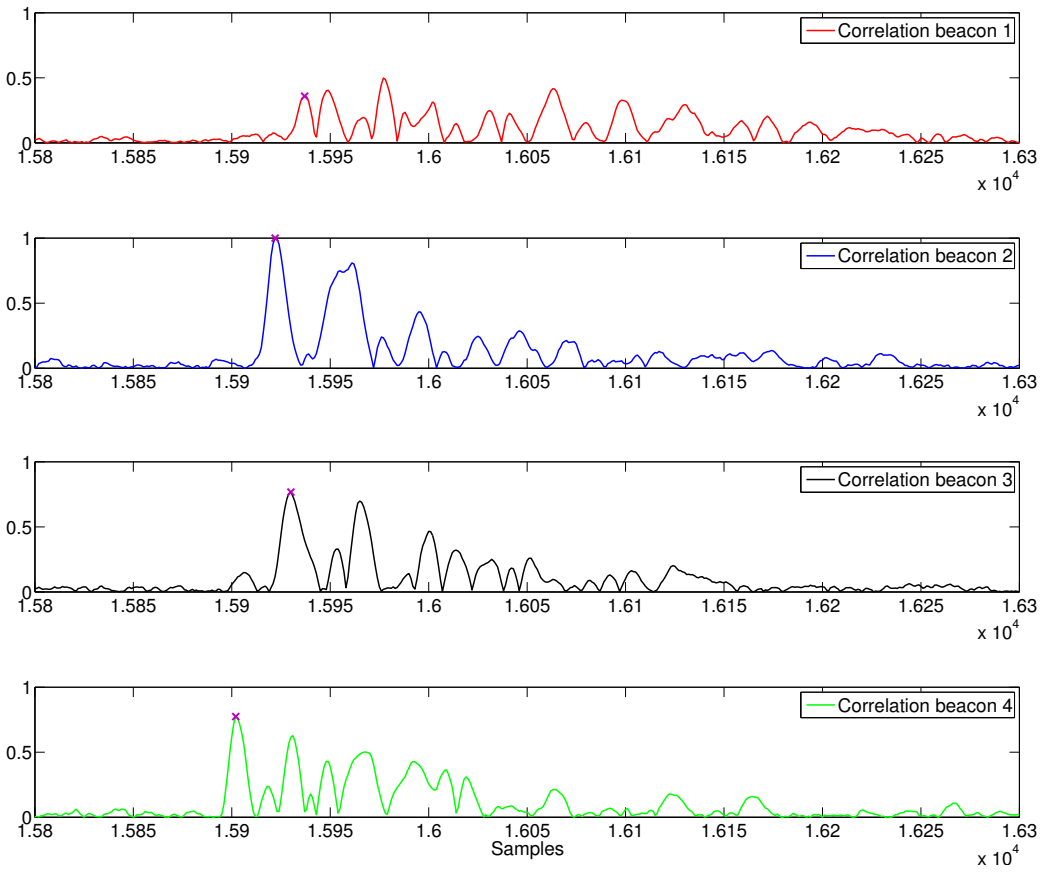


Figure 6.17: Aperiodic correlation functions in the test position (3.20, 0.80, 1.57).

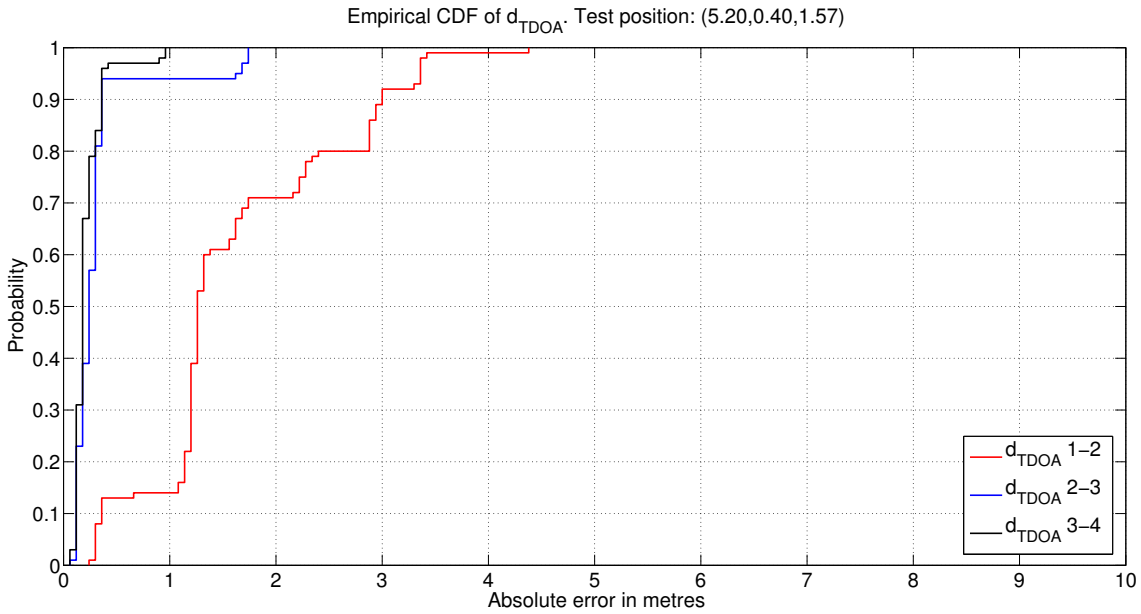


Figure 6.18: Empirical Cumulative Distribution Function for the test position (5.20, 0.40, 1.57).

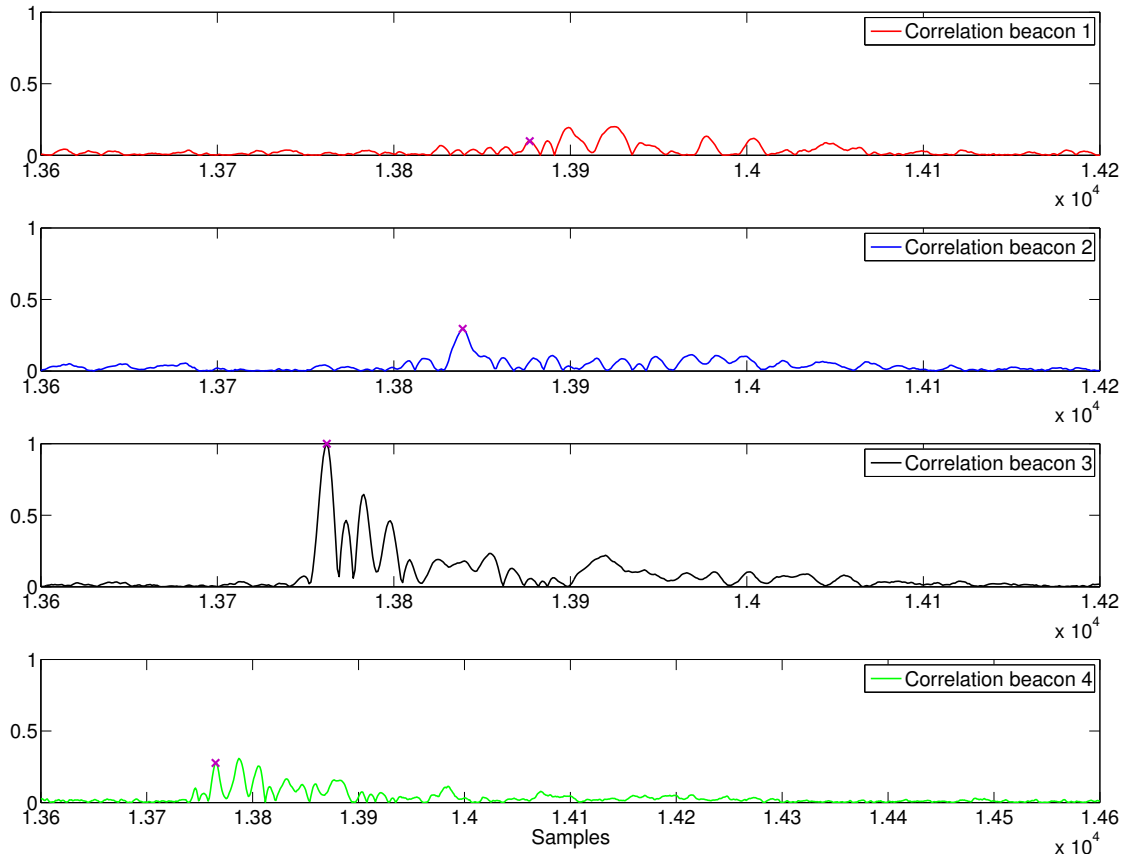


Figure 6.19: Aperiodic correlation functions in the test position (5.20, 0.40, 1.57).

## 6.5 Conclusions

We have proposed a CDMA-based UWB LPS with COTS components. This LPS has been used to analyzed the performance of two types of spreading sequences: Kasami and LS sequences. The ranging test previously shown demonstrates the accuracy and robustness improvement achieved by using LS sequences instead of Kasami sequences. The large separation needed between UWB beacons increases the importance of near-far effect. As Kasami sequences do not have a ZCZ, and due to there is no power control in the emissions, Kasami sequences are very vulnerable to this undesired effect in UWB systems.

If LS sequences are used instead, the ZCZ length is adapted to the maximum feasible TDOA in the working environment. Hence, the presence of a ZCZ in LS sequences and its length larger than the maximum theoretical TDOA, allows to effectively mitigate near-far effect and increases the system robustness in the coverage area.

Furthermore, the use of an adaptive first peak detector is fundamental in practical UWB systems. The UWB channel, the relative angle and the distance between beacons and mobile device, hardware constraints and limited power emissions make very challenging the accurate detection of UWB signals.

| | $d_{TDOA}$1-2 | | $d_{TDOA}$2-3 | | $d_{TDOA}$3-4 | |
|---|---|---|---|---|---|---|
| Test points | Quartiles | RMSE | Quartiles | RMSE | Quartiles | RMSE |
| 1 | 0.09 – 0.36 – 0.66 | 0.46 | 0.24 – 0.78 – 6.90 | 4.02 | 0.12 – 0.36 – 7.08 | 4.07 |
| 2 | 0.06 – 0.12 – 0.54 | 0.44 | 0.12 – 0.24 – 3.18 | 2.78 | 0.18 – 0.24 – 3.36 | 2.85 |
| 3 | 0.12 – 0.18 – 0.30 | 0.64 | 0.18 – 0.30 – 0.42 | 0.64 | 0.18 – 0.24 – 0.36 | 0.73 |
| 4 | 0.06 – 0.48 – 1.89 | 1.96 | 0.39 – 1.50 – 5.31 | 3.54 | 0.24 – 0.30 – 6.06 | 3.15 |
| 5 | 0.06 – 0.06 – 1.62 | 1.52 | 0.15 – 0.30 – 0.48 | 0.65 | 0.06 – 0.12 – 0.18 | 0.22 |
| 6 | 0.18 – 3.45 – 7.35 | 5.52 | 0.06 – 0.12 – 0.66 | 1.57 | 0.12 – 0.18 – 0.24 | 0.34 |
| 7 | 1.80 – 2.88 – 4.08 | 3.97 | 0.21 – 3.00 – 5.01 | 4.35 | 0.06 – 0.12 – 0.27 | 0.93 |
| 8 | 0.06 – 3.03 – 4.20 | 3.51 | 0.12 – 4.68 – 7.20 | 5.55 | 0.06 – 0.12 – 0.18 | 0.33 |
| 9 | 1.98 – 4.32 – 4.56 | 5.05 | 3.99 – 8.76 – 9.00 | 7.19 | 0.12 – 0.12 – 0.18 | 0.28 |
| 10 | 3.18 – 3.90 – 4.68 | 4.08 | 5.40 – 6.00 – 6.18 | 5.81 | 0.12 – 0.18 – 0.24 | 0.31 |
| 11 | 0.60 – 0.72 – 0.84 | 3.06 | 7.80 – 7.86 – 7.98 | 7.88 | 0.06 – 0.12 – 0.18 | 0.33 |
| 12 | 1.53 – 2.10 – 4.17 | 3.60 | 0.42 – 7.38 – 8.73 | 6.74 | 0.00 – 0.00 – 0.06 | 0.13 |
| 13 | 0.72 – 2.85 – 5.64 | 4.04 | 9.72 – 9.84 – 10.23 | 9.75 | 0.00 – 0.06 – 0.30 | 0.27 |
| 14 | 1.74 – 1.86 – 1.98 | 2.10 | 8.52 – 8.58 – 8.64 | 8.61 | 0.00 – 0.06 – 0.06 | 0.24 |
| 15 | 1.02 – 2.10 – 2.49 | 2.11 | 8.94 – 9.18 – 10.86 | 9.79 | 0.06 – 0.12 – 2.34 | 2.33 |
| 16 | 1.50 – 5.43 – 9.24 | 6.73 | 7.14 – 8.25 – 10.32 | 8.59 | 0.12 – 0.24 – 0.60 | 1.15 |
| 17 | 0.12 – 0.24 – 0.30 | 0.99 | 7.80 – 8.76 – 8.97 | 8.56 | 1.53 – 2.58 – 4.92 | 3.24 |
| 18 | 0.36 – 0.48 – 0.60 | 0.50 | 6.00 – 10.92 – 10.98 | 9.47 | 0.96 – 1.02 – 1.41 | 1.50 |
| 19 | 0.18 – 0.18 – 0.24 | 0.21 | 0.54 – 5.64 – 6.66 | 5.13 | 0.18 – 1.02 – 4.71 | 3.87 |
| 20 | 0.06 – 0.48 – 0.48 | 0.42 | 3.30 – 7.98 – 8.46 | 7.19 | 2.70 – 3.39 – 6.36 | 4.69 |
| 21 | 0.06 – 0.06 – 0.12 | 0.65 | 1.44 – 6.12 – 6.87 | 5.68 | 2.46 – 8.94 – 9.66 | 7.72 |
| 22 | 0.06 – 0.12 – 0.18 | 0.44 | 3.60 – 5.85 – 6.54 | 5.43 | 3.84 – 5.70 – 6.72 | 5.57 |
| 23 | 0.24 – 0.30 – 0.39 | 0.32 | 6.00 – 6.03 – 6.18 | 6.15 | 1.86 – 5.70 – 6.12 | 5.13 |
| 24 | 0.18 – 0.18 – 0.54 | 0.73 | 0.12 – 0.18 – 0.36 | 1.38 | 0.12 – 0.18 – 1.32 | 1.49 |
| 25 | 0.15 – 0.18 – 0.18 | 0.49 | 0.00 – 0.12 – 4.65 | 2.60 | 0.06 – 0.18 – 4.65 | 2.61 |

Table 6.2: Quartiles and RMSE values for each test position when using Kasami sequences.

| | $d_{TDOA}$1-2 | | $d_{TDOA}$2-3 | | $d_{TDOA}$3-4 | |
|---|---|---|---|---|---|---|
| Test points | Quartiles | RMSE | Quartiles | RMSE | Quartiles | RMSE |
| 26 | 0.06 – 0.06 – 0.12 | 0.68 | 0.00 – 0.06 – 0.75 | 1.18 | 0.06 – 0.12 – 0.42 | 1.15 |
| 27 | 0.06 – 0.12 – 0.78 | 0.52 | 0.12 – 0.18 – 0.24 | 0.28 | 0.06 – 0.12 – 0.48 | 0.71 |
| 28 | 0.06 – 0.06 – 0.12 | 0.77 | 0.18 – 0.24 – 0.78 | 1.81 | 0.12 – 0.39 – 2.40 | 1.84 |
| 29 | 0.06 – 0.18 – 0.36 | 0.61 | 0.6 – 0.78 – 7.56 | 5.36 | 0.90 – 0.96 – 4.20 | 3.88 |
| 30 | 0.66 – 0.72 – 0.78 | 1.04 | 1.92 – 2.67 – 4.98 | 4.70 | 2.55 – 2.76 – 4.38 | 4.05 |
| 31 | 0.30 – 0.36 – 0.60 | 1.13 | 0.18 – 0.24 – 4.02 | 3.19 | 0.06 – 0.42 – 5.70 | 3.38 |
| 32 | 0.12 – 0.18 – 0.60 | 0.44 | 0.18 – 0.36 – 3.45 | 3.57 | 0.06 – 0.06 – 3.90 | 3.74 |
| 33 | 0.54 – 1.14 – 1.56 | 1.17 | 0.06 – 1.02 – 1.68 | 2.40 | 0.06 – 0.18 – 0.78 | 2.37 |
| 34 | 0.66 – 4.86 – 5.22 | 4.23 | 1.02 – 4.62 – 5.52 | 4.55 | 1.68 – 4.74 – 7.77 | 5.31 |
| 35 | 0.12 – 0.24 – 0.30 | 1.08 | 0.12 – 0.18 – 0.42 | 0.31 | 0.00 – 0.06 – 0.42 | 0.29 |
| 36 | 1.02 – 4.38 – 4.44 | 4.54 | 0.06 – 0.06 – 3.87 | 3.59 | 0.00 – 0.06 – 7.14 | 3.98 |
| 37 | 2.01 – 2.10 – 5.61 | 3.85 | 0.00 – 0.06 – 1.08 | 3.99 | 0.00 – 0.06 – 0.36 | 0.41 |
| 38 | 0.66 – 0.72 – 1.08 | 1.08 | 0.24 – 0.30 – 0.36 | 1.43 | 0.06 – 0.06 – 0.12 | 1.32 |
| 39 | 0.06 – 0.24 – 1.32 | 0.95 | 0.06 – 0.09 – 3.57 | 2.94 | 0.09 – 3.00 – 3.84 | 3.42 |
| 40 | 0.00 – 0.06 – 2.10 | 1.30 | 0.18 – 5.88 – 6.00 | 5.05 | 0.72 – 5.10 – 5.28 | 4.42 |
| 41 | 0.30 – 0.36 – 0.42 | 1.38 | 1.32 – 2.13 – 2.34 | 2.45 | 1.35 – 2.22 – 2.46 | 2.96 |
| 42 | 0.06 – 0.06 – 0.33 | 0.82 | 1.02 – 4.02 – 6.81 | 4.68 | 3.21 – 5.19 – 6.69 | 5.13 |
| 43 | 0.12 – 0.18 – 1.68 | 0.96 | 1.20 – 1.74 – 3.75 | 3.28 | 1.38 – 1.56 – 4.05 | 3.38 |
| 44 | 0.06 – 0.42 – 0.48 | 0.64 | 0.12 – 5.88 – 6.18 | 4.62 | 2.52 – 4.83 – 6.00 | 4.57 |
| 45 | 0.12 – 0.12 – 0.12 | 0.13 | 5.76 – 8.64 – 8.70 | 7.38 | 1.98 – 2.61 – 3.24 | 3.53 |
| 46 | 0.06 – 0.06 – 0.06 | 0.06 | 1.50 – 6.78 – 11.46 | 8.04 | 4.65 – 6.87 – 7.14 | 6.97 |
| 47 | 0.24 – 0.51 – 0.78 | 2.08 | 1.32 – 4.11 – 5.16 | 4.78 | 2.58 – 4.05 – 5.01 | 4.61 |
| 48 | 0.18 – 0.24 – 0.24 | 0.53 | 1.68 – 10.74 – 10.80 | 8.35 | 3.42 – 7.71 – 9.12 | 7.08 |
| 49 | 0.12 – 0.42 – 0.48 | 0.59 | 9.90 – 9.90 – 10.98 | 10.15 | 4.17 – 6.69 – 10.83 | 8.52 |
| 50 | 0.06 – 0.06 – 0.12 | 0.27 | 6.42 – 10.62 – 10.86 | 9.06 | 2.76 – 4.95 – 6.54 | 5.78 |
| 51 | 0.06 – 0.06 – 0.12 | 1.49 | 13.14 – 13.20 – 13.20 | 12.69 | 3.21 – 3.30 – 3.36 | 3.14 |

Table 6.2: Quartiles and RMSE values for each test position when using Kasami sequences (cont.).

| | $d_{TDOA}$1-2 | | $d_{TDOA}$2-3 | | $d_{TDOA}$3-4 | |
|---|---|---|---|---|---|---|
| Test points | Quartiles | RMSE | Quartiles | RMSE | Quartiles | RMSE |
| 1 | 0.12 – 0.18 – 0.24 | 0.26 | 0.18 – 0.24 – 0.84 | 0.55 | 0.12 – 0.12 – 0.84 | 0.61 |
| 2 | 0.06 – 0.12 – 0.48 | 0.30 | 0.06 – 0.06 – 0.21 | 0.22 | 0.12 – 0.18 – 0.24 | 0.20 |
| 3 | 0.12 – 0.18 – 0.30 | 0.25 | 0.00 – 0.42 – 0.48 | 0.45 | 0.12 – 0.18 – 0.36 | 0.45 |
| 4 | 0.18 – 0.27 – 2.16 | 1.61 | 0.18 – 0.36 – 0.48 | 0.80 | 0.15 – 0.18 – 0.30 | 0.66 |
| 5 | 0.00 – 0.06 – 0.12 | 0.97 | 0.06 – 0.18 – 0.36 | 0.51 | 0.12 – 0.48 – 0.60 | 0.64 |
| 6 | 0.18 – 0.24 – 0.30 | 0.44 | 0.06 – 0.12 – 0.30 | 0.27 | 0.12 – 0.12 – 0.18 | 0.43 |
| 7 | 0.06 – 0.06 – 0.54 | 0.62 | 0.06 – 0.18 – 0.42 | 0.49 | 0.06 – 0.18 – 0.30 | 0.56 |
| 8 | 0.06 – 0.06 – 1.68 | 1.23 | 0.06 – 0.12 – 0.18 | 0.23 | 0.06 – 0.06 – 0.12 | 0.24 |
| 9 | 0.24 – 0.78 – 2.40 | 2.00 | 0.12 – 0.24 – 0.33 | 1.53 | 0.06 – 0.12 – 0.18 | 0.23 |
| 10 | 1.20 – 1.26 – 2.25 | 1.86 | 0.18 – 0.24 – 0.30 | 0.48 | 0.12 – 0.18 – 0.24 | 0.26 |
| 11 | 0.12 – 0.96 – 1.80 | 1.50 | 0.06 – 0.72 – 1.38 | 0.91 | 0.00 – 0.06 – 0.36 | 0.29 |
| 12 | 0.18 – 1.50 – 3.06 | 2.80 | 0.12 – 0.18 – 0.30 | 1.22 | 0.06 – 0.06 – 0.30 | 0.18 |
| 13 | 1.26 – 1.56 – 2.97 | 3.20 | 2.64 – 2.76 – 3.72 | 3.06 | 0.18 – 0.24 – 0.24 | 0.24 |
| 14 | 4.38 – 7.38 – 11.64 | 8.44 | 0.06 – 0.12 – 4.14 | 2.81 | 0.24 – 0.30 – 0.48 | 0.43 |
| 15 | 0.24 – 0.96 – 1.56 | 2.34 | 0.12 – 0.24 – 1.08 | 0.97 | 0.06 – 0.09 – 0.78 | 0.69 |
| 16 | 0.27 – 1.95 – 6.48 | 4.26 | 0.81 – 1.08 – 1.26 | 2.42 | 0.24 – 0.36 – 0.42 | 0.35 |
| 17 | 0.06 – 0.27 – 0.30 | 0.26 | 1.26 – 3.06 – 3.75 | 2.81 | 0.24 – 1.26 – 4.47 | 3.08 |
| 18 | 0.06 – 0.12 – 0.12 | 0.17 | 0.06 – 0.48 – 0.66 | 1.31 | 0.48 – 0.66 – 1.44 | 1.60 |
| 19 | 0.12 – 0.24 – 0.30 | 0.23 | 0.00 – 0.18 – 0.51 | 1.77 | 0.24 – 0.90 – 1.86 | 1.96 |
| 20 | 0.12 – 0.18 – 0.54 | 0.38 | 0.00 – 0.24 – 0.30 | 0.44 | 0.06 – 0.12 – 1.20 | 0.95 |
| 21 | 0.06 – 0.06 – 0.12 | 0.23 | 0.12 – 0.12 – 1.38 | 1.15 | 0.21 – 0.96 – 1.05 | 1.21 |
| 22 | 0.06 – 0.12 – 0.42 | 1.16 | 0.06 – 0.12 – 0.90 | 0.77 | 0.06 – 0.06 – 0.24 | 0.75 |
| 23 | 0.06 – 0.30 – 0.42 | 0.31 | 0.00 – 0.06 – 5.19 | 2.99 | 0.18 – 0.30 – 5.34 | 2.85 |
| 24 | 0.18 – 0.18 – 0.54 | 0.35 | 0.18 – 0.24 – 0.30 | 0.27 | 0.06 – 0.18 – 0.42 | 0.45 |
| 25 | 0.12 – 0.18 – 0.24 | 0.70 | 0.00 – 0.06 – 1.50 | 0.95 | 0.09 – 0.18 – 0.42 | 0.70 |

Table 6.3: Quartiles and RMSE values for each test position when using LS sequences.

| | $d_{TDOA}$1-2 | | $d_{TDOA}$2-3 | | $d_{TDOA}$3-4 | |
|---|---|---|---|---|---|---|
| Test points | Quartiles | RMSE | Quartiles | RMSE | Quartiles | RMSE |
| 26 | $0.06 - 0.18 - 0.24$ | 0.45 | $0.00 - 0.06 - 0.36$ | 0.78 | $0.18 - 0.18 - 0.81$ | 0.77 |
| 27 | $0.12 - 0.18 - 0.72$ | 0.63 | $0.21 - 0.42 - 0.90$ | 0.87 | $0.12 - 0.18 - 0.24$ | 0.59 |
| 28 | $0.30 - 0.60 - 0.78$ | 0.77 | $0.06 - 0.06 - 0.12$ | 0.16 | $0.06 - 0.12 - 0.24$ | 0.21 |
| 29 | $0.06 - 0.18 - 0.30$ | 0.27 | $0.24 - 0.30 - 0.63$ | 0.53 | $0.30 - 0.36 - 0.48$ | 0.42 |
| 30 | $0.21 - 0.66 - 0.72$ | 0.58 | $0.12 - 0.24 - 0.75$ | 2.65 | $0.54 - 1.08 - 1.86$ | 3.06 |
| 31 | $0.06 - 0.12 - 0.18$ | 0.17 | $0.12 - 0.24 - 0.30$ | 0.58 | $0.06 - 0.12 - 0.33$ | 0.52 |
| 32 | $0.00 - 0.06 - 0.48$ | 0.37 | $0.12 - 0.18 - 0.30$ | 0.73 | $0.12 - 0.18 - 0.30$ | 0.66 |
| 33 | $0.24 - 0.78 - 0.96$ | 0.81 | $0.06 - 0.12 - 0.66$ | 0.60 | $0.06 - 0.18 - 0.24$ | 0.54 |
| 34 | $0.48 - 0.66 - 1.56$ | 1.22 | $0.12 - 0.36 - 1.02$ | 0.65 | $0.06 - 0.12 - 0.12$ | 0.32 |
| 35 | $0.12 - 0.18 - 0.21$ | 0.21 | $0.06 - 0.12 - 0.30$ | 0.42 | $0.06 - 0.12 - 0.66$ | 0.49 |
| 36 | $0.12 - 0.18 - 0.81$ | 0.93 | $0.00 - 0.93 - 2.13$ | 1.57 | $0.00 - 0.93 - 2.10$ | 1.53 |
| 37 | $0.06 - 0.39 - 1.44$ | 0.94 | $0.06 - 1.74 - 2.43$ | 1.94 | $0.00 - 0.06 - 2.34$ | 1.73 |
| 38 | $0.66 - 0.72 - 0.84$ | 0.89 | $0.24 - 0.30 - 0.36$ | 0.51 | $0.06 - 0.12 - 0.18$ | 0.34 |
| 39 | $0.06 - 0.12 - 1.50$ | 0.96 | $0.06 - 0.06 - 0.12$ | 0.33 | $0.06 - 0.18 - 0.54$ | 0.34 |
| 40 | $0.00 - 0.06 - 1.17$ | 0.99 | $0.18 - 0.24 - 0.24$ | 0.23 | $0.06 - 0.60 - 2.22$ | 1.41 |
| 41 | $0.06 - 0.12 - 0.42$ | 0.65 | $0.12 - 0.128 - 0.24$ | 0.70 | $0.06 - 1.26 - 2.97$ | 2.46 |
| 42 | $0.06 - 0.12 - 0.42$ | 0.89 | $0.12 - 0.12 - 0.24$ | 0.26 | $0.12 - 0.18 - 0.42$ | 0.31 |
| 43 | $0.24 - 0.24 - 0.30$ | 0.59 | $0.12 - 0.18 - 1.56$ | 0.89 | $0.15 - 0.24 - 1.62$ | 1.15 |
| 44 | $0.12 - 0.18 - 0.60$ | 0.86 | $0.12 - 0.18 - 0.24$ | 0.21 | $0.12 - 0.30 - 0.72$ | 0.61 |
| 45 | $0.12 - 0.18 - 0.18$ | 0.39 | $0.00 - 0.06 - 0.51$ | 0.66 | $0.00 - 0.12 - 0.48$ | 0.61 |
| 46 | $0.06 - 0.12 - 0.12$ | 0.18 | $0.06 - 0.06 - 0.33$ | 0.45 | $0.06 - 0.18 - 1.20$ | 1.01 |
| 47 | $0.18 - 0.18 - 0.24$ | 0.26 | $0.18 - 0.42 - 6.57$ | 4.71 | $2.64 - 2.82 - 4.50$ | 4.47 |
| 48 | $0.18 - 0.18 - 0.24$ | 0.38 | $0.12 - 0.30 - 2.16$ | 2.12 | $0.24 - 0.45 - 2.34$ | 2.22 |
| 49 | $0.06 - 0.30 - 0.36$ | 0.33 | $0.18 - 0.42 - 1.80$ | 1.25 | $0.12 - 0.39 - 1.80$ | 1.40 |
| 50 | $0.00 - 0.06 - 0.36$ | 0.61 | $0.06 - 0.30 - 3.21$ | 1.99 | $0.06 - 1.50 - 2.46$ | 1.98 |
| 51 | $0.06 - 0.06 - 0.30$ | 1.86 | $0.42 - 1.32 - 3.60$ | 3.01 | $1.44 - 5.70 - 5.82$ | 4.87 |

Table 6.3: Quartiles and RMSE values for each test position when using LS sequences (cont.).

# Chapter 7

# Application to Ultrasonic Ranging Systems

In this chapter we compare the performance of several GO spreading sequences in a real scenario. The objective is to analyze the trade-offs in the design of spreading sequences, specifically between the flexibility of the sequence length, the ZCZ size or set size, the energy efficiency and hardware simplicity. Furthermore the use of a mismatched filter is proposed in the experimental system. The use of GO spreading sequences jointly with this filter achieves ranging errors in the millimetre range.

## 7.1 Global structure of the experimental system

The ultrasonic LPS is composed of an emitter module, formed of a computer, three arbitrary waveform generators and five emitting beacons placed on the ceiling. The ultrasonic LPS has also a receiver module which is composed of an ultrasonic microphone, an amplifier, an acquisition board and a computer. In the tests, the receiver module is placed on known positions of the coverage area. It receives the ultrasonic signals synchronously emitted by the beacons and computes the TDOAs. The ground truth is achieved by a handmade grid of dimensions $3 \times 3$ metres in steps of 0.5 metres. Figure 7.1 shows the environment in which the ranging tests have been carried out.

## 7.2 Emitter module

The emitter module is composed of the following elements:

- Five beacons (B$a$, $1 \leq a \leq 5$), placed on the ceiling and arranged as depicted in Figure 7.2. The position of the beacons are calibrated by using the algorithm

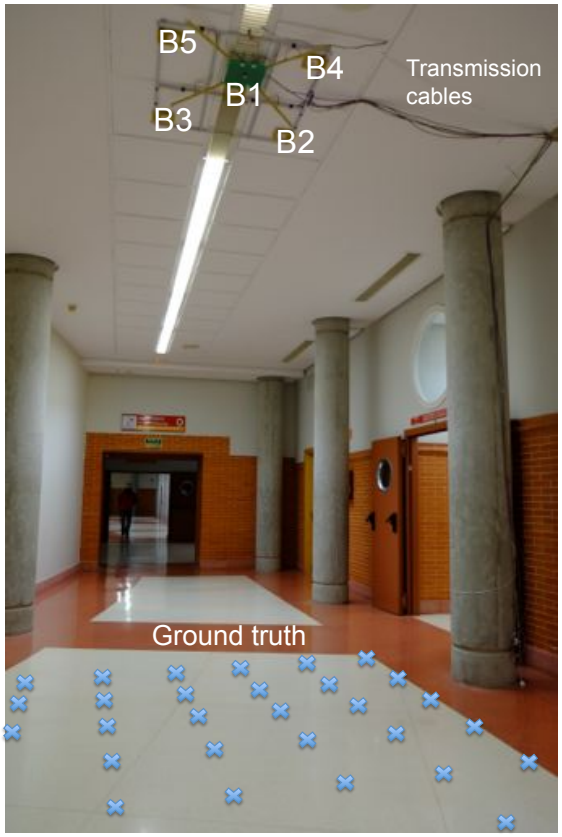


Figure 7.1: Environment used to perform the ranging tests.

proposed in [Ruiz 11] and their positions are shown in Table 7.1. These beacons were originally designed to work with TDMA and Kasami sequences [Villa 13]. For the ranging test developed here, the emitter module has been modified in order to work with CDMA and easily change the spreading sequence transmitted. Each beacon has an ultrasonic ceramic transducer Prowave 328ST160, with an aperture angle of $\pm 80^{o}$. According to the manufacturer, this transducer has a resonance peak at 32.8 kHz, a bandwidth of 2.5 kHz measured at $-6$ dB and it is capable of transmitting 120 dB Sound Pressure Level (SPL) at the resonance frequency. Nevertheless, this transducer has been characterized for larger frequencies and Figure 7.3 shows the frequency response experimentally obtained.

The cross mark situated at 32.8 kHz and the intersection of the horizontal line at 115 dB SPL with the frequency response correspond with the resonance peak and the frequency bandwidth given by the manufacturer, respectively. The intersection of the horizontal line at 96 dB SPL with the frequency response, represents the

| Beacon | $x$ | $y$ | $z$ |
|---|---|---|---|
| B1 | 0.200 | −0.029 | 3.484 |
| B2 | 0.533 | −0.401 | 3.463 |
| B3 | 0.564 | 0.305 | 3.474 |
| B4 | −0.1657 | −0.378 | 3.460 |
| B5 | −0.141 | 0.333 | 3.447 |

Table 7.1: Beacons position in the test area (in metres).

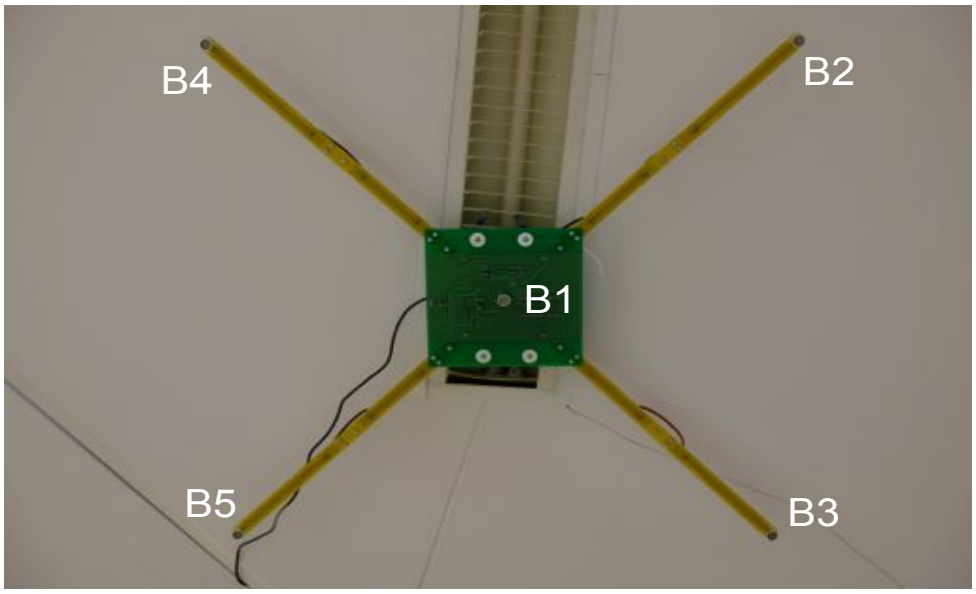


Figure 7.2: Beacons used to perform the ranging test.

lower and upper frequency at −6 dB when we choose a center frequency of 40 kHz. Consequently, in this case the bandwidth is approximately equal to 18 kHz.

- Arbitrary waveform generators Tabor WW5062 [Tabor 13]. Each generator has two programable outputs with a maximum sampling frequency of 50 MSps and has a maximum output of 10 V peak-to-peak. Since the emitter system is composed of five beacons, we have used three synchronized arbitrary waveform generators. The output of these generators are directly connected to the transducers, without using power amplifiers. The sampling frequency used for all the tests is equal to 400 kHz. Considering that the transducers have a center frequency of 40 kHz, each modulation symbol will have 10 samples to fit in the transducer bandwidth.

- Laptop used for sending the signals to the arbitrary waveform generators. For the sake of clarity, Figure 7.4 shows a scheme of the emitter module.

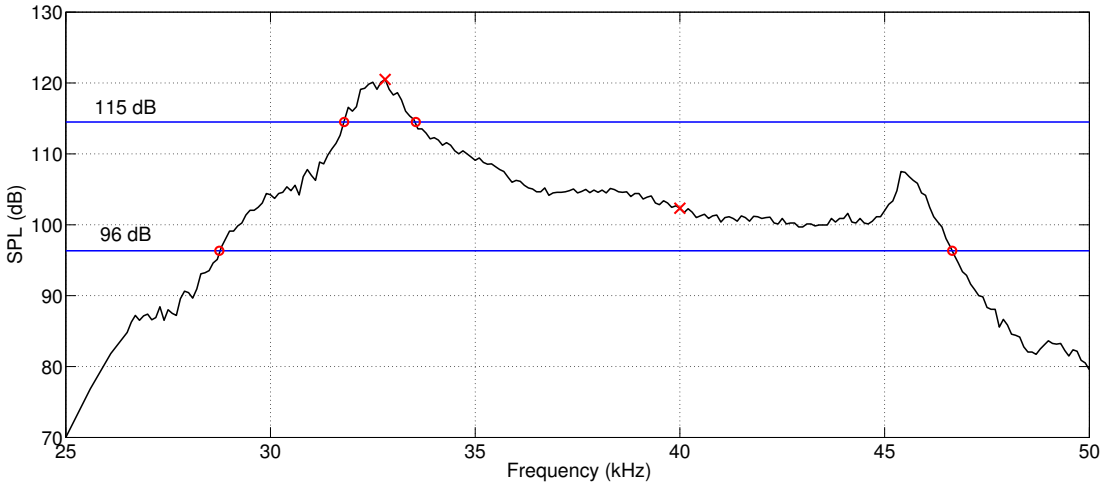


Figure 7.3: Experimental frequency response of the Prowave 328ST160.

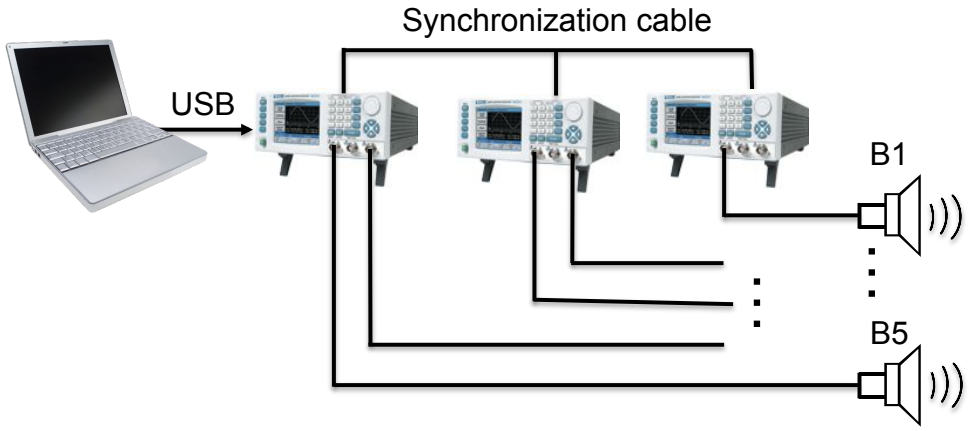


Figure 7.4: Scheme of the emitter module.

## 7.3 Receiver module

The receiver module is formed of the following elements:

- Ultrasonic microphone Brüel&Kjær 4939 [Brüel 13]. It has a sensitivity of 4mV/Pa in the frequency range that goes from 4 Hz to 100 kHz. For each GO sequence, this microphone will be placed on 21 known positions of the grid and at height of 11.85 centimetres.

- Avisoft 1/4" preamplifier [Aviso 13]. It amplifies the received signal with a gain of 30 dB in the frequency range from 20 Hz to 200 kHz. It also has a high-pass filter with a cut-off frequency of 15 kHz.

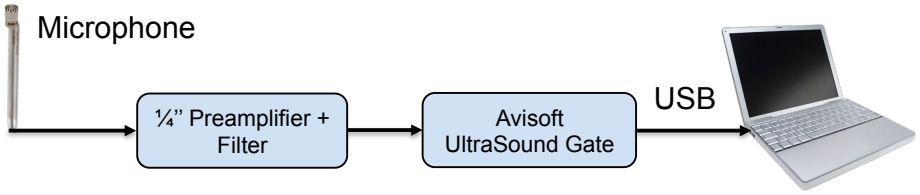


Figure 7.5: Scheme of the receiver module.

- Avisoft UltraSound Gate 116Hm. It has a maximum sample rate of 1 MHz. It also has an adjustable gain up to 40 dB. The sampling frequency selected for the tests is 400 kHz.
- Laptop for storing and processing the received signals. Figure 7.5 shows a scheme of the receiver module.

The received signal is non-coherently demodulated, and passed through a mismatched filter. Later, this output is correlated with each sequence to be detected. Afterwards, the absolute value of the filtered correlation output is carried out and finally the first arriving path detection algorithm proposed in [Perez 09a] is employed. It is similar to the one used in Chapter 6, with the exception that now the threshold is equal to the maximum peak value within the window, whose length is adjusted for each correlation signal. Figure 7.6 shows the signal processing stages carried out in the laptop.

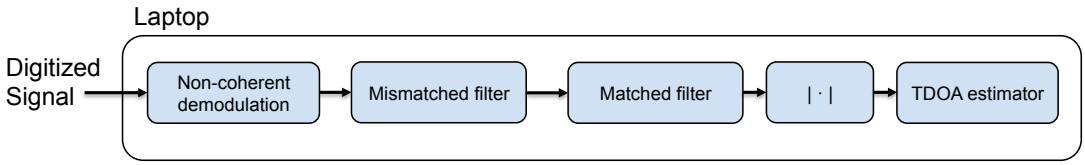


Figure 7.6: Scheme of the stages involved in the signal processing.

As stated previously, in the following tests we propose the use of a mismatched filter (traditionally employed in the radar field) to minimize non-desired effects due to the non-coherent demodulation and the non-ideal response of the transducers. This proposal provides highly precise ranging measurements as it will be shown later.

To compute the filter coefficients, we capture an ultrasonic transmission, then we correlate it with the appropriate sequence and introduce into the minimization algorithm a window of 255 samples centred around the maximum correlation peak (and therefore it must be correctly centred to avoid the introduction of a bias in the TOA estimation). The coefficients of the mismatched filter have been worked out by following the least

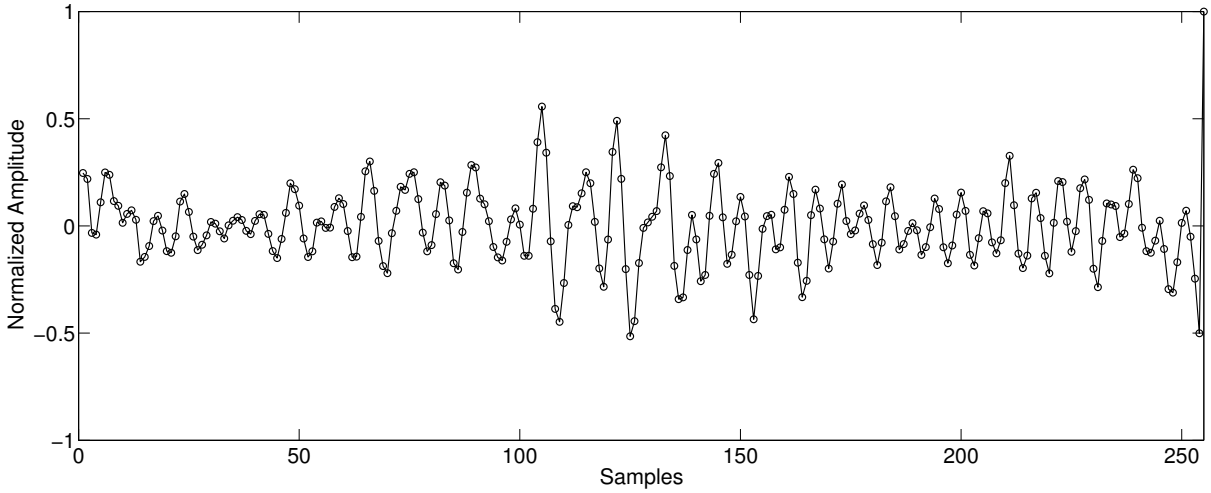


Figure 7.7: Coefficients of the mismatched filter of 255 taps.

square minimization method explained in Chapter 2, section 2.2.4 (refer to equation 2.8). The coefficients derived from this minimization method are shown in Figure 7.7. The same coefficients have been used for all the tests, independently of the spreading sequence transmitted.

Figure 7.8 depicts how the mismatched filter copes with the undesired sidelobes due to the non-coherent demodulation and the non-ideal behaviour of the transducers. The first graph represents a simulated scenario where the correlation signal has been obtained without considering the transducer or channel effects. The second plot depicts the correlation signal obtained in a real scenario, whereas the third graph represents the correlation signal obtained by adding a mismatched filter in cascade with the matched filter in a real scenario. Observe how the correlation sidelobes have diminished by using the mismatched filter and the ringing artefacts almost disappear.

The mismatched filter minimizes the energy sidelobes by using a weighting matrix and a Least Squares minimization (refer to Chapter 2, section 2.2.4). Figure 7.8 shows how the output of the mismatched filter has changed the sign of the correlation peak. This is because in the optimization process, we have selected a correlation peak with a negative sign (i.e. with a phase change due to the transducers response), so when the input of the mismatched filter is a correlation with a phase change, the product of negative numbers leads to a change of the correlation peak sign. This does not happened if we select for determining the filter coefficients a correlation with a positive peak (i.e. without phase change).

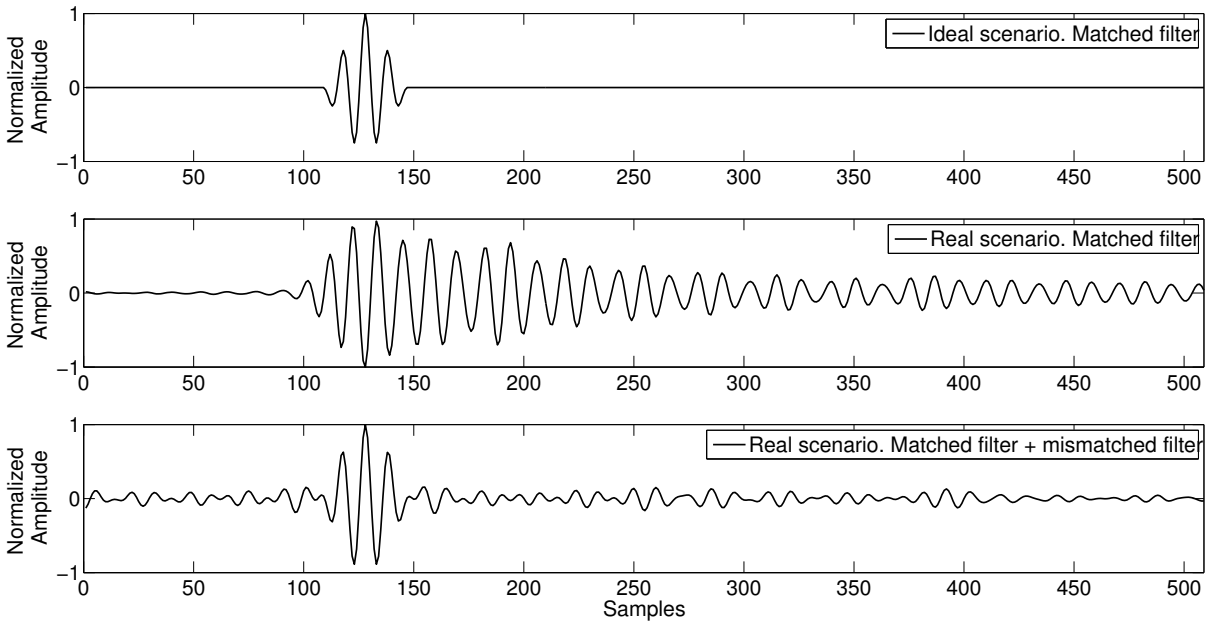


Figure 7.8: Comparison of the aperiodic correlations obtained in different scenarios.

## 7.4 Results

We have carried out ranging tests for five different GO spreading sequences. For all of them, the sequences are modulated by using two carrier cycles per sequence bit, in order to accommodate the transmitted signals into the transducer bandwidth. Figure 7.9 shows the test positions and the projection of the beacons on the working area. For each one of the 21 positions and for each GO sequence, we have measured four TDOAs at 100 different time instances: TDOA 1-2, TDOA 2-3, TDOA 3-4 and TDOA 4-5. The term TDOA $a - b$ represents the Time Difference of Arrival between beacon $a$ and beacon $b$ (i.e. TOA $a$ - TOA $b$).

Due to geometrical restrictions, the maximum theoretical TDOA (in bits of the spreading sequence) in the ground truth is equal to 64 bits (considering a room temperature of 20$^o$C). To ensure that all TOAs are within the IFW we have established a minimum ZCZ length of 79 bits. Table 7.2 depicts the spreading sequences used for the ranging test. It also indicates the number of sequences in the set ($K$), ZCZ length, their processing gain, their energy efficiency and the modulation used to transmit each sequence.

[1]Notice that the number of transmitted signals is five (one per beacon).

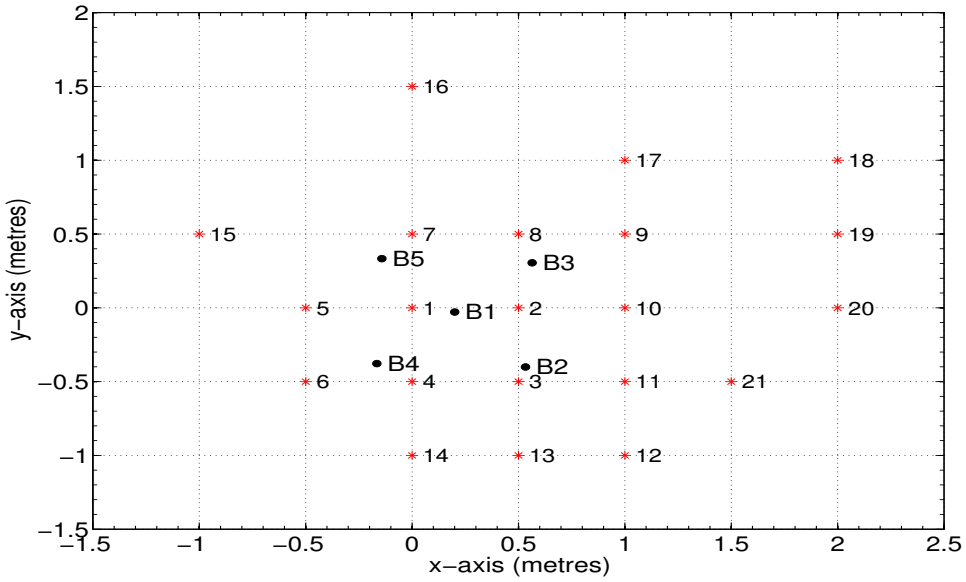


Figure 7.9: Test positions and beacon projections on the ground.

| Sequence | Binary LS | Multilevel LS | Binary CSS | Multilevel CSS | GPC |
|---|---|---|---|---|---|
| # Spreading bits | 640 | 680 | $64 \times 8$ | $85 \times 5$ | $416 \times 2$ |
| $K^1$ | 8 | 8 | 8 | 5 | 8 |
| ZCZ | 79 | 84 | 84 | 84 | 103 |
| Total length (bits) | 719 | 764 | 1100 | 761 | 416 |
| Processing Gain (dB) | 27.55 | 24.01 | 23.72 | 17.75 | 29.20 |
| Efficiency | 89% | 37% | 46% | 7.8% | 100% |
| Modulation | BPSK | BPSK | BPSK | BPSK | QPSK |

Table 7.2: GO sequences and modulations used in the ranging tests.

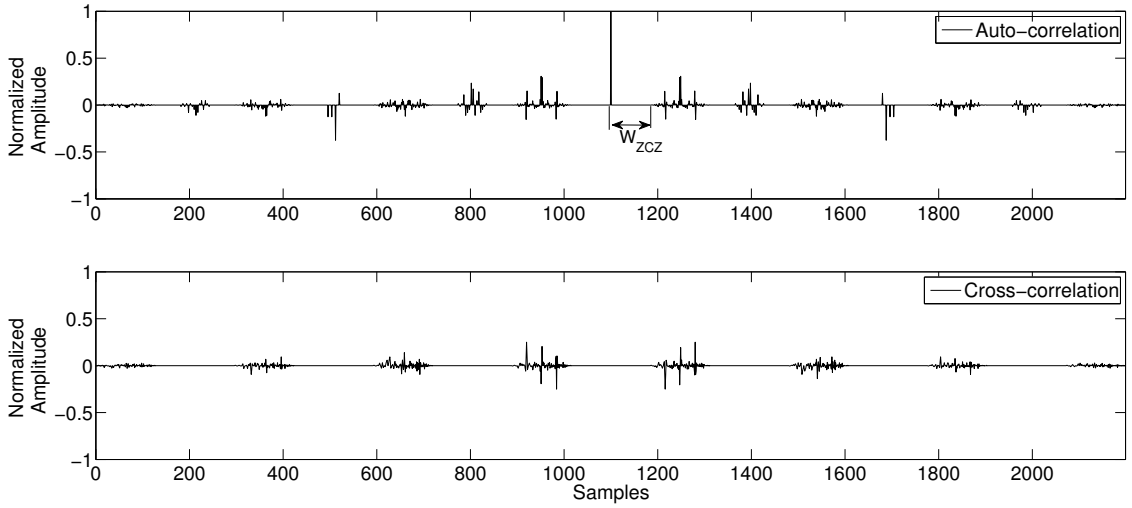


Figure 7.10: Aperiodic correlation functions of a binary CSS with the concatenation method indicated in [Perez 12].

For the transmission of the CSS, we have carried out the same method shown in [Perez 12]. The sequences $j$ $(0 \leq j \leq K-1)$ of a set $i$ $(s_{i,j}[l])$ have been concatenated by inserting $W_{ZCZ}$ zeros between them, so the new sequence is equal to $\sum_{j=0}^{K-1} s_{i,j}[l] \cdot z^{-j\cdot(L+W_{ZCZ})}$ and has a length equal to $K \cdot L + (K-1) \cdot W_{ZCZ}$, where $L$ is the number of spreading bits of the sequence $s_{i,j}[l]$ (i.e. its length). Figure 7.10 shows the aperiodic correlation functions of a given binary CSS of 8 sequences of length 64 bits, concatenated with the previous method. Observe that with this method the aperiodic correlation functions have a ZCZ of length equal to $W_{ZCZ}$, i.e. the concatenated sequences have GO properties.

Figure 7.11 depicts the reduction in the transmitted power when the energy efficiency is lower than 100%. Given a real sequence $s[l]$ of length $L$, the energy efficiency is defined as

$$\varepsilon = \frac{\sum_{l=0}^{L-1} |s[l]|^2}{L \cdot [\max(s[l])]^2} \tag{7.1}$$

Considering that the energy of a binary sequence is equal to its length $(L)$, and by normalizing the real sequence $s[l]$ to its maximum, i.e. $max(s[l]) = 1$, we have that the reduction in the transmitted power when multilevel sequences are used is equal to $\triangle Power = 10 \cdot \log_{10}(\varepsilon)$. The normalization of the sequence $s[l]$ is carried out considering

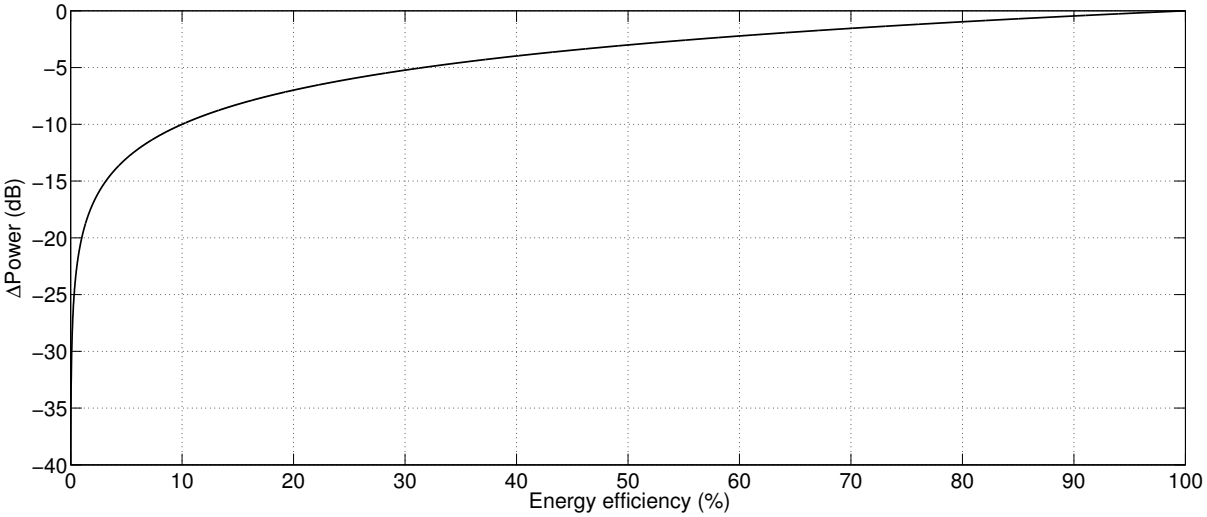


Figure 7.11: Reduction in the transmitted power when the energy efficiency is lower than 100%.

that the same power amplifier is used for both binary and multilevel sequences and that both sequences use the maximum linear range of the amplifier.

Finally, Figure 7.12 depicts the CRLB for the estimation of TDOA for different SNR and two effective bandwidths (defined by the kind of modulation employed) and a room temperature of 20ºC. As stated, the best theoretical precision is in the millimetre range for both effective bandwidths.

The following sections show the ranging test results for each spreading sequence, represented by the RMSE values of each TDOA measurement and by the first (25%), second (50%) and third (75%) quartile, expressed as $Q_1 - Q_2 - Q_3$. All the errors are given in millimetres.

### 7.4.1 Binary LS Sequences

Figure 7.13 shows the RMSE values in millimetres of four TDOA measurements (refer to Table 7.3 for their specific values and distributions). Observe that most of these errors are lower than 8 millimetres, even in those positions where there is near-far effect and that are situated far away from the beacons.

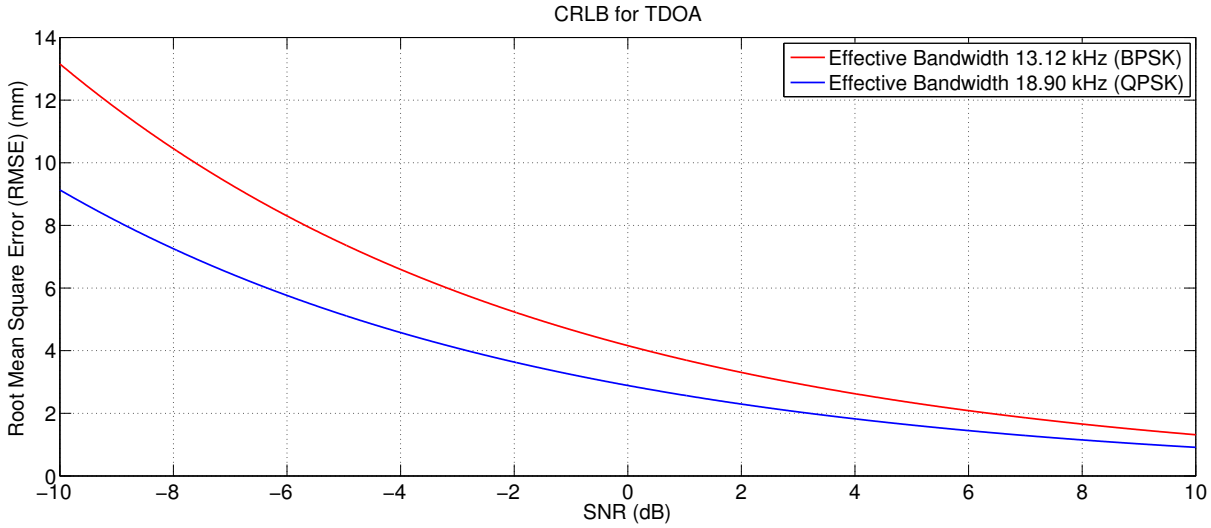


Figure 7.12: CRLB for two different bandwidths.

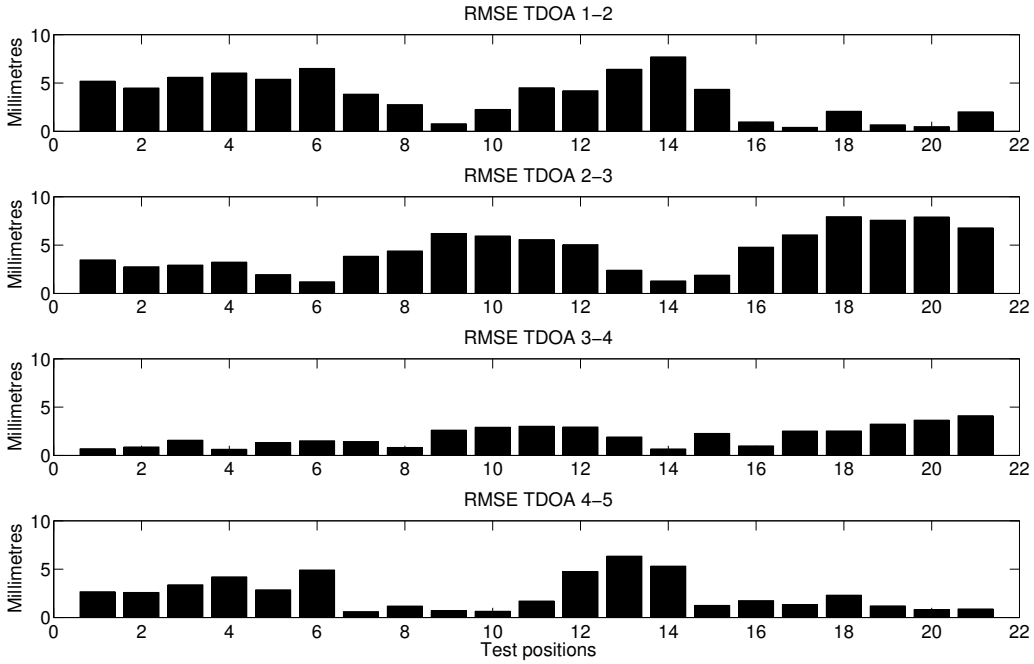


Figure 7.13: RMSE values obtained in each test position for the four TDOA measurements when using binary LS sequences of 719 bits.

### 7.4.2 Multilevel LS Sequences

We have transmitted five multilevel LS sequences of length 764 bits and with a ZCZ length of 84 bits. These sequences have been generated by using the following parameter values:

$Q = 7$, $A^{(q)} = \{1, 1, 1, 1, 1, 1, 2\}$, $W^{(1,q)} = \{\pm 1, -1, -1, -1, -1, -1, -1\}$ and the delay distribution $D^{(q)}$ defined in Chapter 5, equation 5.4, $(0 \leq q \leq Q-1)$. If we compare the efficiency of the multilevel LS sequences with the one of binary LS sequences, it turns out that with these sequences we are transmitting 3.54 dB less of power. Figure 7.14 shows the RMSE values of the TDOA measurements in millimetres (for a detailed analysis of the errors refer to Table 7.4). Observe how the errors are very similar to those with binary LS sequences, even in positions that are far away from the beacons. The error differences can be mainly due to two factors: the first one is the lower power transmitted with multilevel LS sequences; the second factor is that the differences in the TDOA errors are so low that they can be caused by errors in the positioning of the microphone in the ground truth. The use of these parameters $Q$, $A^{(q)}$, $D^{(q)}$ and $W^{(1,q)}$ leads to an efficient hardware implementation (reduced number of stages and only one multiplier that can be implemented by shifting). Nonetheless, if other parameter values were chosen, the multilevel LS sequences generated could have a larger energy efficiency and thus transmit both sequences almost the same power for a given length, with the additional advantage of having a flexible ZCZ length.

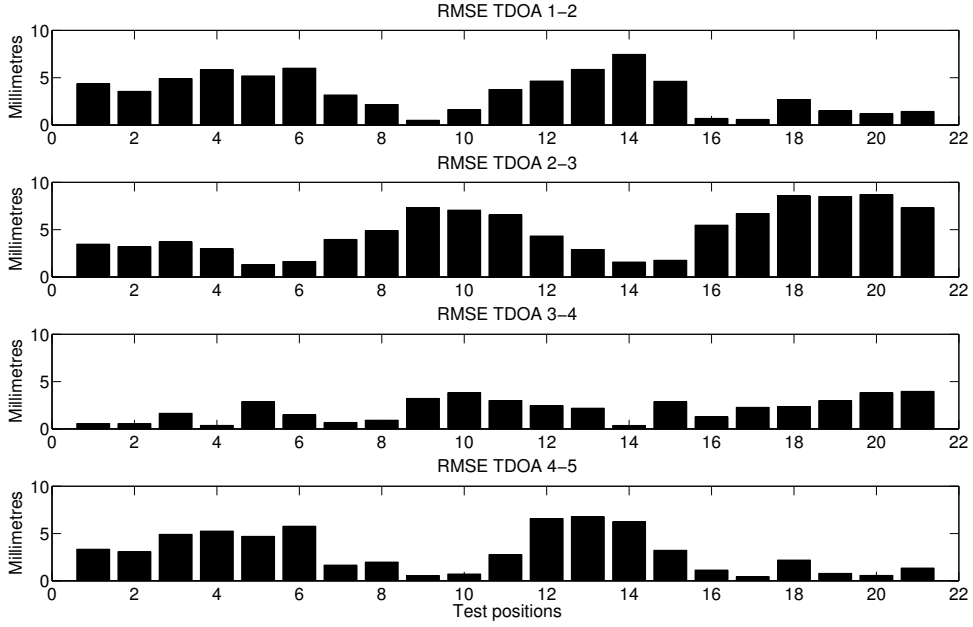


Figure 7.14: RMSE values obtained in each test position for the four TDOA measurements when using multilevel LS sequences of 764 bits.

### 7.4.3 Binary CSS Sequence

Five sets of eight binary sequences of length 64 bits have been concatenated following the procedure indicated in this chapter and have been transmitted simultaneously by the ultrasonic beacons. The processing gain of the concatenated sequences is only 0.29 dB lower than the one of multilevel LS sequences; both of them have the same ZCZ length but the concatenated binary CSS have a total length of 1100 bits, instead of the 764 bits of multilevel LS sequences. It has been demonstrated experimentally in [Pared 11] that this difference in length has important implications when there are Doppler shifts due to the relative movement emitter-receiver. The longer the length of the sequence the larger its sensitivity to Doppler shifts. Figure 7.15 shows the RMSE values in the TDOA estimation for each test position, whereas Table 7.5 includes the RMSE values and their quartiles (both of them in millimetres). As depicted, the errors are in the same order of magnitude than the previous sequences.

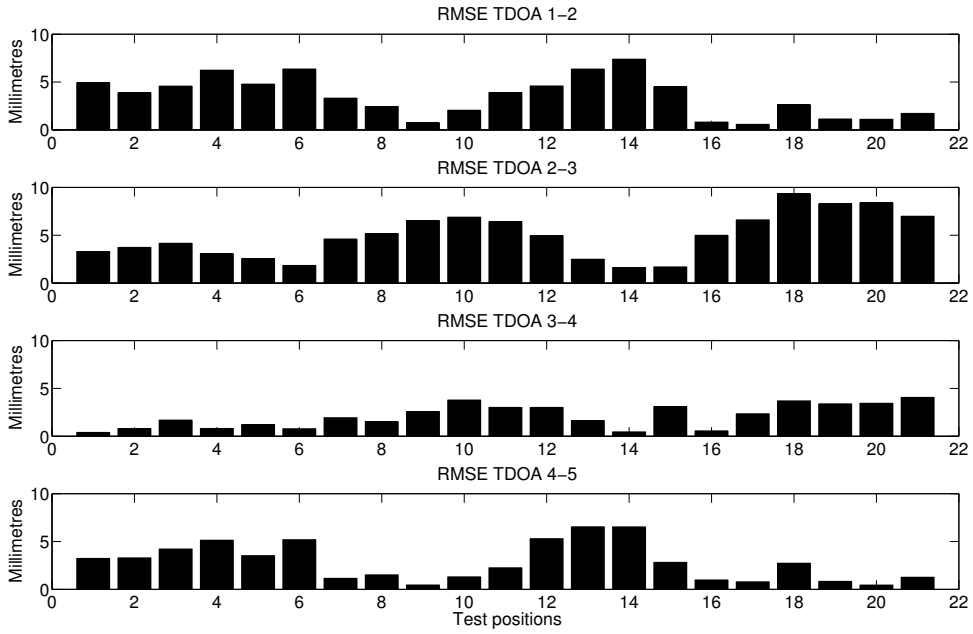


Figure 7.15: RMSE values obtained in each test position for the four TDOA measurements when using $K = 8$ binary CSS of 64 bits.

### 7.4.4 Multilevel CSS Sequences

Five multilevel CSS have been transmitted by using the same concatenation method than binary CSS, and they have been generated in $Q = 3$ stages by using a circulant

Hadamard matrix $\boldsymbol{\mathcal{C}}_{K_{|MultCSS}}$ defined by the first row [ 3 −2 −2 −2 −2 ], a delay distribution defined in Chapter 3 equation 3.46 and initial conditions defined also by the same matrix $\boldsymbol{\mathcal{C}}_{K_{|MultCSS}}$. Contrary to the binary case, the use of multilevel CSS allows to have a set size adapted to the number of beacons, which gives more flexibility to the system. Nevertheless, the energy efficiency of the concatenated multilevel CSS generated with the previous parameters are very low. Maybe there exist other parameter values for generating multilevel CSS sequences with both flexible length and set size, and a larger energy efficiency, but it is needed an exhaustive search. Figure 7.16 shows the RMSE values in millimetres for each test position. Due to the high SNR conditions, these errors are in the same range of those obtained with binary sequences (for a detailed representation of these errors and their distribution refer to Table 7.6)

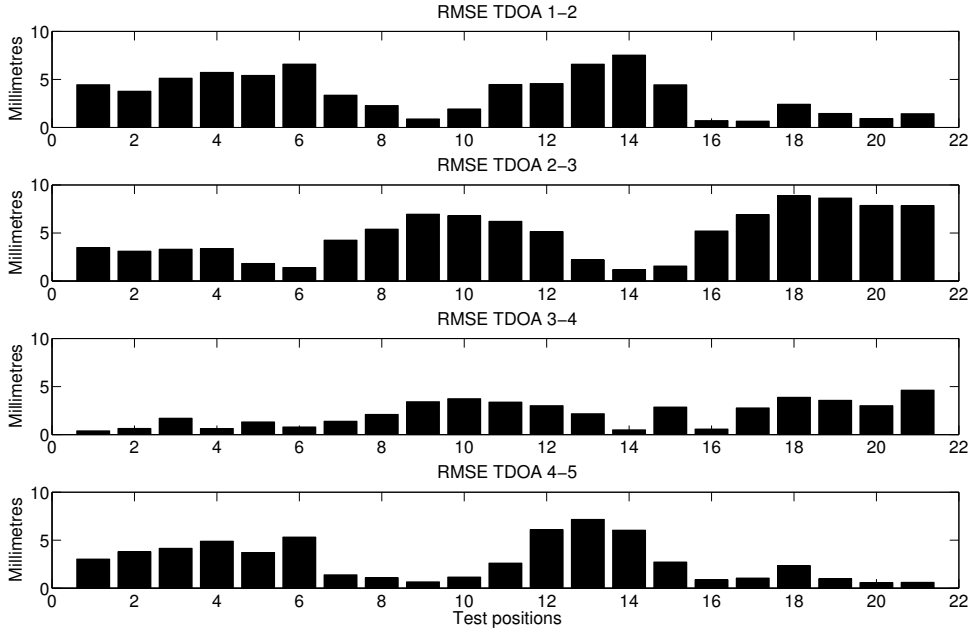


Figure 7.16: RMSE values obtained in each test position for the four TDOA measurements when transmitting $K = 5$ multilevel CSS of 85 bits.

### 7.4.5 Binary GPC Sequences

These sequences have been transmitted by using a non-coherent QPSK modulation to avoid the carrier phase recovery. Figure 7.17 depicts a scheme of the modulation-demodulation used to transmit GPC sequences.

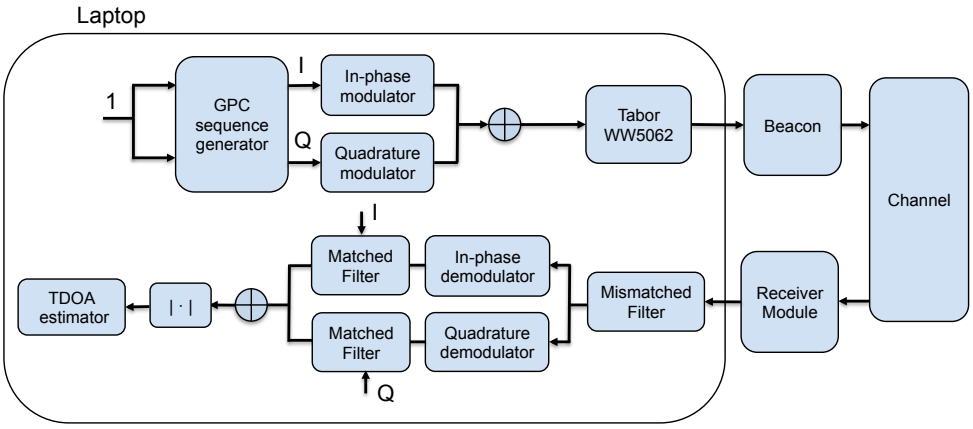


Figure 7.17: Scheme of the signal processing scheme used with GPC sequences.

Figure 7.18 shows the RMSE values in millimetres for each test position. In the second and twentieth positions, the RMSE values are larger than 10 millimetres for measurements TDOA 2-3, TDOA 3-4 and TDOA 4-5 (refer to Table 7.7 for their specific values), while in the other positions these values are below 8.85 millimetres. Notice that despite the large processing gain, GPC sequences have a worse performance than the previous spreading sequences. This is mainly due to the non-coherent demodulation process, which degrades the IFW. Nevertheless, with an appropriate modulation scheme, GPC sequences are very promising as they have the largest ZCZ length for a given sequence length and the largest energy efficiency.

Figure 7.19 will help to understand what happens in the second and twentieth positions. This Figure shows the sum of aperiodic correlation functions for each of the GPC spreading sequences transmitted by the beacons. As stated in section 7.3, a very similar first arriving path estimation algorithm to the one of Chapter 6 is employed [Perez 09a], where the maximum correlation peak among all the aperiodic correlations is used to determine a searching window. As depicted in Figure 7.19, there are sidelobes that are of the same magnitude than the largest correlation peak (i.e. the one situated at zero time shift $\tau = 0$). This implies that the algorithm could search the first arriving path in an erroneous window centred around a sidelobe.

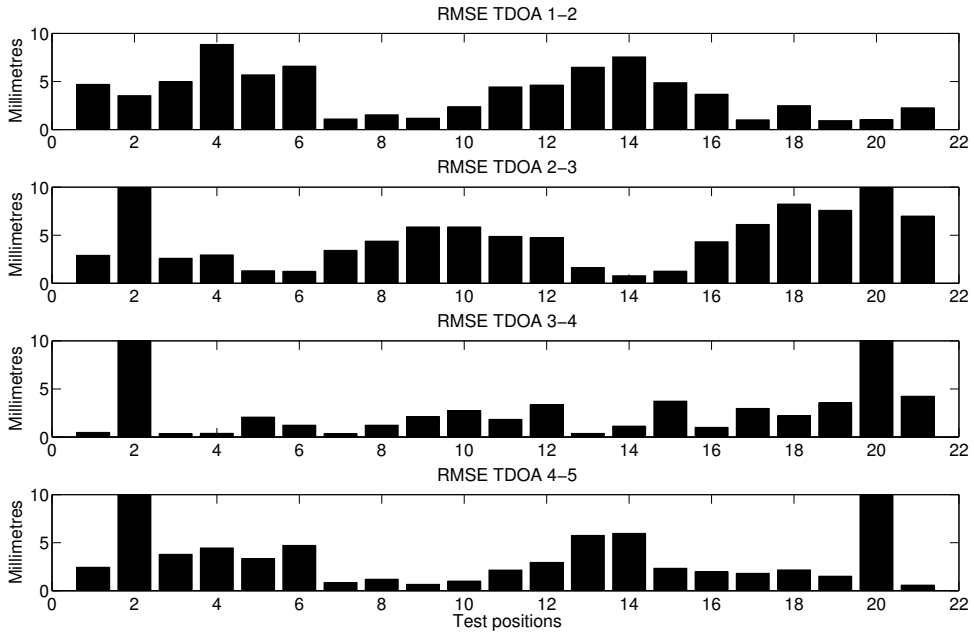


Figure 7.18: RMSE values obtained in each test position for the four TDOA measurements when transmitting GPC sequences of 416 bits.

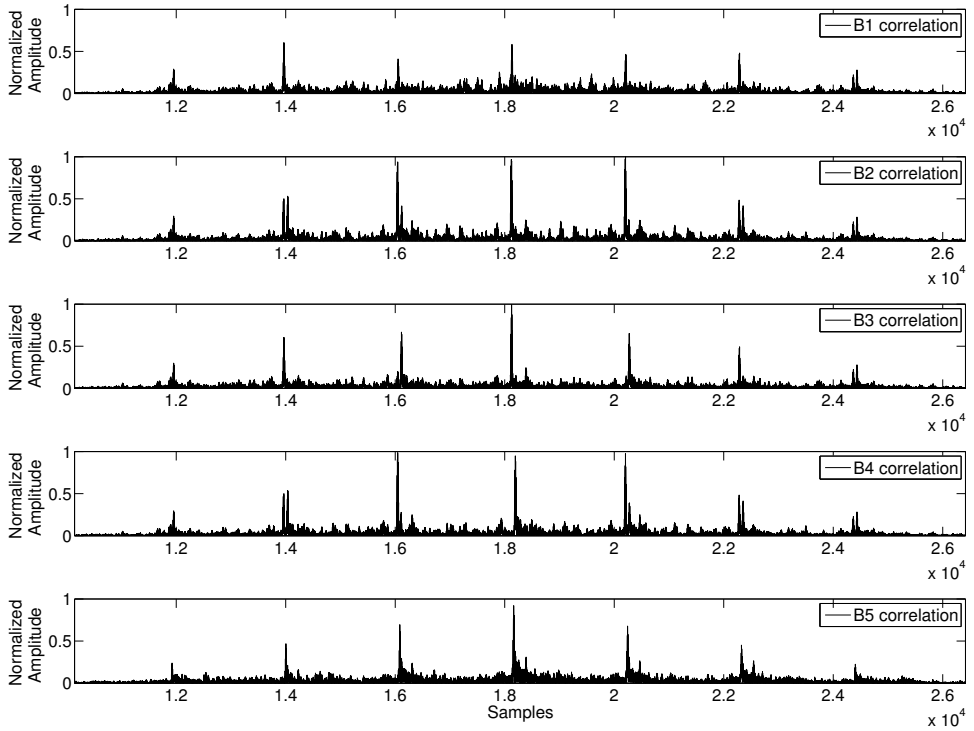


Figure 7.19: Aperiodic correlations in the test position 2 for a given measurement instance when transmitting GPC sequences of 416 bits.

## 7.5 Conclusions

We have analyzed the trade-offs of five different spreading sequences in a real scenario: binary LS, multilevel LS, binary CSS, multilevel CSS and GPC sequences. The energy efficiency of the multilevel signals can be improved with a different modulation scheme, as MC-CDMA, by assigning each level of the sequence to a particular carrier. Nonetheless, this solution increases the energy efficiency at the expense of reducing the spectral efficiency. This solution is only feasible in systems with a large bandwidth, which is not the case of ultrasonic ranging systems. Multilevel sequences are a promising solution only if the efficient architectures proposed in this thesis are used as a basis for the search of near-binary CSS (and therefore near-binary LS). This would permit the efficient generation of high energy efficient sequences with both flexible length and flexible number of sequences (in the case of multilevel CSS).

On the other hand, GPC sequences have both the highest energy efficiency and the largest ZCZ length for a given sequence length. Nevertheless the use of an appropriate modulation-demodulation scheme is a fundamental issue. We have used non-coherent QPSK modulation to avoid the recovery of the carrier frequency and phase, but this scheme degrades the correlation properties and it hinders the TDOA estimation. The ranging errors obtained with GPC sequences are in some positions larger than those obtained with other sequences that have lower processing gain.

The high SNR in the system, makes the errors on the TDOA estimation to be very similar for all the spreading sequences used. Nonetheless, in low SNR conditions, the value of the processing gain would make a difference between multilevel and binary sequences. Moreover the use of a mismatched filter reduces the correlation sidelobes caused by transducer effects and therefore, it increases the precision of the TDOA estimation.

To sum up, the ranging tests performed in this chapter allows to illustrate the trade-offs between energy efficiency, spectral efficiency, hardware complexity, ZCZ length and sequence length.

| | TDOA 1-2 | | TDOA 2-3 | | TDOA 3-4 | | TDOA 4-5 | |
|---|---|---|---|---|---|---|---|---|
| Test position | Quartiles | RMSE | Quartiles | RMSE | Quartiles | RMSE | Quartiles | RMSE |
| 1 | 5.14 – 5.14 – 5.14 | 5.19 | 3.43 – 3.43 – 3.43 | 3.46 | 0.00 – 0.86 – 0.86 | 0.69 | 2.57 – 2.57 – 2.57 | 2.66 |
| 2 | 4.28 – 4.28 – 4.71 | 4.48 | 2.57 – 2.57 – 2.57 | 2.75 | 0.86 – 0.86 – 0.86 | 0.88 | 2.57 – 2.57 – 2.57 | 2.59 |
| 3 | 5.14 – 5.57 – 6.00 | 5.59 | 2.57 – 2.57 – 3.43 | 2.92 | 0.86 – 1.71 – 1.71 | 1.57 | 3.43 – 3.43 – 3.43 | 3.38 |
| 4 | 6.00 – 6.00 – 6.00 | 6.03 | 3.00 – 3.43 – 3.43 | 3.23 | 0.00 – 0.86 – 0.86 | 0.63 | 4.29 – 4.29 – 4.29 | 4.20 |
| 5 | 5.14 – 5.14 – 6.00 | 5.38 | 1.71 – 1.71 – 2.57 | 1.95 | 0.86 – 0.86 – 1.71 | 1.34 | 2.57 – 2.57 – 3.43 | 2.86 |
| 6 | 6.00 – 6.86 – 6.86 | 6.50 | 0.86 – 0.86 – 1.71 | 1.21 | 0.86 – 1.71 – 1.71 | 1.51 | 4.29 – 5.14 – 5.14 | 4.90 |
| 7 | 3.43 – 3.43 – 4.28 | 3.84 | 3.43 – 3.43 – 4.29 | 3.84 | 0.86 – 1.71 – 1.71 | 1.43 | 0.00 – 0.86 – 0.86 | 0.61 |
| 8 | 2.57 – 2.57 – 2.57 | 2.76 | 4.29 – 4.29 – 4.29 | 4.39 | 0.86 – 0.86 – 0.86 | 0.82 | 0.86 – 0.86 – 1.71 | 1.18 |
| 9 | 0.86 – 0.86 – 0.86 | 0.78 | 6.00 – 6.00 – 6.86 | 6.19 | 2.57 – 2.57 – 2.57 | 2.62 | 0.00 – 0.86 – 0.86 | 0.72 |
| 10 | 1.71 – 2.57 – 2.57 | 2.26 | 6.00 – 6.00 – 6.00 | 5.94 | 2.57 – 2.57 – 3.43 | 2.92 | 0.00 – 0.86 – 0.86 | 0.64 |
| 11 | 4.28 – 4.28 – 5.14 | 4.51 | 5.14 – 5.14 – 6.00 | 5.56 | 2.57 – 2.57 – 3.43 | 3.01 | 0.86 – 1.71 – 1.71 | 1.70 |
| 12 | 4.29 – 4.29 – 4.29 | 4.20 | 5.14 – 5.14 – 5.14 | 5.05 | 0.86 – 3.43 – 3.43 | 2.94 | 2.57 – 2.57 – 6.86 | 4.75 |
| 13 | 6.00 – 6.00 – 6.86 | 6.42 | 2.57 – 2.57 – 2.57 | 2.40 | 1.71 – 1.71 – 1.71 | 1.90 | 5.14 – 5.14 – 6.00 | 6.34 |
| 14 | 7.72 – 7.72 – 7.72 | 7.69 | 0.86 – 0.86 – 1.71 | 1.29 | 0.00 – 0.86 – 0.86 | 0.67 | 5.14 – 5.14 – 5.57 | 5.31 |
| 15 | 4.29 – 4.29 – 4.29 | 4.35 | 1.71 – 1.71 – 1.71 | 1.88 | 1.71 – 2.14 – 2.57 | 2.27 | 0.86 – 0.86 – 1.71 | 1.25 |
| 16 | 0.86 – 0.86 – 086 | 0.97 | 4.29 – 5.14 – 5.14 | 4.78 | 0.86 – 0.86 – 0.86 | 0.99 | 1.71 – 1.71 – 1.71 | 1.74 |
| 17 | 0.00 – 0.00 – 0.00 | 0.41 | 6.00 – 6.00 – 6.00 | 6.05 | 2.57 – 2.57 – 2.57 | 2.52 | 0.86 – 0.86 – 1.71 | 1.34 |
| 18 | 1.71 – 1.71 – 2.57 | 2.07 | 7.72 – 7.72 – 8.57 | 7.93 | 2.57 – 2.57 – 2.57 | 2.52 | 1.71 – 2.57 – 2.57 | 2.31 |
| 19 | 0.00 – 0.86 – 0.86 | 0.67 | 7.72 – 7.72 – 7.72 | 7.57 | 2.57 – 3.43 – 3.43 | 3.24 | 0.86 – 0.86 – 1.71 | 1.19 |
| 20 | 0.00 – 0.00 – 0.86 | 0.49 | 7.72 – 7.72 – 7.72 | 7.90 | 3.43 – 3.43 – 4.29 | 3.65 | 0.00 – 0.86 – 0.86 | 0.82 |
| 21 | 1.71 – 1.71 – 2.57 | 2.02 | 6.86 – 6.86 – 6.86 | 6.77 | 4.29 – 4.29 – 4.29 | 4.11 | 0.00 – 0.00 – 0.86 | 0.88 |

Table 7.3: Quartiles and RMSE values for each test position when using binary LS sequences of 719 bits.

| | TDOA 1-2 | | TDOA 2-3 | | TDOA 3-4 | | TDOA 4-5 | |
|---|---|---|---|---|---|---|---|---|
| Test position | Quartiles | RMSE | Quartiles | RMSE | Quartiles | RMSE | Quartiles | RMSE |
| 1 | 4.29 – 4.29 – 4.29 | 4.35 | 3.43 – 3.43 – 3.43 | 3.46 | 0.00 – 0.00 – 0.86 | 0.57 | 2.57 – 3.43 – 3.43 | 3.34 |
| 2 | 3.43 – 3.43 – 3.43 | 3.56 | 2.57 – 3.43 – 3.43 | 3.18 | 0.00 – 0.00 – 0.86 | 0.55 | 2.57 – 3.43 – 3.43 | 3.07 |
| 3 | 4.29 – 5.14 – 5.15 | 4.90 | 3.43 – 3.43 – 4.29 | 3.70 | 0.86 – 1.71 – 1.71 | 1.65 | 4.29 – 4.29 – 5.14 | 4.91 |
| 4 | 5.57 – 6.00 – 6.00 | 5.84 | 2.57 – 2.57 – 3.43 | 2.97 | 0.00 – 0.00 – 0.00 | 0.37 | 5.14 – 5.14 – 5.14 | 5.25 |
| 5 | 5.14 – 5.14 – 5.14 | 5.18 | 0.86 – 0.86 – 1.71 | 1.30 | 2.57 – 2.57 – 3.43 | 2.87 | 4.29 – 4.29 – 5.14 | 4.70 |
| 6 | 6.00 – 6.00 – 6.00 | 6.00 | 0.86 – 1.71 – 1.71 | 1.63 | 0.86 – 1.71 – 1.71 | 1.48 | 5.14 – 6.00 – 6.00 | 5.77 |
| 7 | 2.57 – 3.43 – 3.43 | 3.17 | 3.43 – 4.29 – 4.29 | 3.97 | 0.00 – 0.86 – 0.86 | 0.68 | 1.71 – 1.71 – 1.71 | 1.66 |
| 8 | 1.71 – 1.71 – 2.57 | 2.16 | 4.29 – 5.14 – 5.14 | 4.89 | 0.86 – 0.86 – 0.86 | 0.92 | 1.71 – 1.71 – 2.57 | 1.98 |
| 9 | 0.00 – 0.00 – 0.86 | 0.50 | 6.86 – 7.72 – 7.72 | 7.34 | 2.57 – 3.43 – 3.43 | 3.22 | 0.00 – 0.00 – 0.86 | 0.56 |
| 10 | 1.71 – 1.71 – 1.71 | 1.64 | 6.86 – 6.86 – 7.72 | 7.05 | 3.43 – 4.29 – 4.29 | 3.82 | 0.00 – 0.86 – 0.86 | 0.72 |
| 11 | 3.43 – 3.43 – 4.29 | 3.75 | 6.00 – 6.86 – 6.86 | 6.55 | 2.57 – 2.57 – 3.43 | 3.00 | 1.71 – 2.57 – 2.57 | 2.77 |
| 12 | 4.29 – 4.29 – 5.14 | 4.64 | 4.29 – 4.29 – 4.29 | 4.32 | 1.71 – 2.57 – 2.57 | 2.46 | 4.29 – 5.14 – 9.00 | 6.57 |
| 13 | 6.00 – 6.00 – 6.00 | 5.87 | 2.57 – 2.57 – 3.43 | 2.90 | 1.71 – 1.71 – 2.57 | 2.19 | 5.14 – 6.00 – 6.00 | 6.76 |
| 14 | 6.86 – 7.72 – 7.72 | 7.45 | 1.71 – 1.71 – 1.71 | 1.58 | 0.00 – 0.00 – 0.00 | 0.36 | 6.00 – 6.00 – 6.86 | 6.23 |
| 15 | 4.29 – 4.29 – 5.14 | 4.61 | 1.71 – 1.71 – 1.71 | 1.76 | 2.57 – 2.57 – 3.43 | 2.86 | 2.57 – 3.43 – 3.43 | 3.23 |
| 16 | 0.00 – 0.86 – 0.86 | 0.70 | 5.14 – 5.14 – 6.00 | 5.47 | 0.86 – 0.86 – 1.71 | 1.26 | 0.86 – 0.86 – 1.71 | 1.13 |
| 17 | 0.00 – 0.00 – 0.86 | 0.59 | 6.00 – 6.86 – 6.86 | 6.70 | 1.71 – 2.57 – 2.57 | 2.27 | 0.00 – 0.00 – 0.86 | 0.43 |
| 18 | 2.58 – 2.58 – 2.58 | 2.69 | 8.57 – 8.57 – 8.57 | 8.56 | 1.71 – 2.57 – 2.57 | 2.36 | 1.71 – 1.71 – 2.57 | 2.19 |
| 19 | 0.86 – 1.71 – 1.71 | 1.50 | 8.57 – 8.57 – 8.57 | 8.49 | 2.57 – 3.43 – 3.43 | 2.96 | 0.86 – 0.86 – 0.86 | 0.78 |
| 20 | 0.86 – 0.86 – 1.71 | 1.19 | 8.57 – 8.57 – 8.57 | 8.70 | 3.43 – 3.43 – 4.29 | 3.80 | 0.00 – 0.00 – 0.86 | 0.57 |
| 21 | 0.86 – 1.71 – 1.71 | 1.43 | 6.86 – 7.29 – 7.72 | 7.30 | 3.43 – 4.29 – 4.29 | 3.96 | 0.86 – 0.86 – 1.71 | 1.35 |

Table 7.4: Quartiles and RMSE values for each test position when using multilevel LS sequences of 764 bits.

| | TDOA 1-2 | | TDOA 2-3 | | TDOA 3-4 | | TDOA 4-5 | |
|---|---|---|---|---|---|---|---|---|
| Test position | Quartiles | RMSE | Quartiles | RMSE | Quartiles | RMSE | Quartiles | RMSE |
| 1 | 4.29 – 5.14 – 5.14 | 4.91 | 3.43 – 3.43 – 3.43 | 3.29 | 0.00 – 0.00 – 0.00 | 0.40 | 2.57 – 3.43 – 3.43 | 3.24 |
| 2 | 3.43 – 3.43 – 4.29 | 3.87 | 3.43 – 3.43 – 4.29 | 3.73 | 0.43 – 0.86 – 0.86 | 0.80 | 3.43 – 3.43 – 3.43 | 3.29 |
| 3 | 4.29 – 4.29 – 5.14 | 4.57 | 3.43 – 4.29 – 4.29 | 4.16 | 1.71 – 1.71 – 1.71 | 1.69 | 4.29 – 4.29 – 4.29 | 4.21 |
| 4 | 6.00 – 6.00 – 6.86 | 6.23 | 2.57 – 2.57 – 3.43 | 3.05 | 0.00 – 0.86 – 0.86 | 0.81 | 5.14 – 5.14 – 5.14 | 5.14 |
| 5 | 4.29 – 5.14 – 5.14 | 4.78 | 1.71 – 2.57 – 2.57 | 2.55 | 0.86 – 0.86 – 1.71 | 1.20 | 3.43 – 3.43 – 3.43 | 3.53 |
| 6 | 6.00 – 6.00 – 6.86 | 6.36 | 0.86 – 1.71 – 2.57 | 1.84 | 0.86 – 0.86 – 0.86 | 0.78 | 5.14 – 5.14 – 5.14 | 5.19 |
| 7 | 2.57 – 3.43 – 3.43 | 3.31 | 4.29 – 4.29 – 5.14 | 4.60 | 1.71 – 1.71 – 2.57 | 1.93 | 0.86 – 0.86 – 1.71 | 1.15 |
| 8 | 2.14 – 2.57 – 2.57 | 2.44 | 5.14 – 5.14 – 5.14 | 5.16 | 0.85 – 1.71 – 1.71 | 1.52 | 0.86 – 1.71 – 1.71 | 1.52 |
| 9 | 0.00 – 0.86 – 0.86 | 0.73 | 6.00 – 6.86 – 6.86 | 6.52 | 2.57 – 2.57 – 2.57 | 2.57 | 0.00 – 0.00 – 0.86 | 0.45 |
| 10 | 1.71 – 1.71 – 2.57 | 2.05 | 6.00 – 6.86 – 6.86 | 6.89 | 3.43 – 3.43 – 4.29 | 3.78 | 0.86 – 0.86 – 1.71 | 1.30 |
| 11 | 3.43 – 4.29 – 4.29 | 3.91 | 6.00 – 6.00 – 6.86 | 6.40 | 2.57 – 2.57 – 3.43 | 3.02 | 1.71 – 1.71 – 2.57 | 2.25 |
| 12 | 4.29 – 4.29 – 5.14 | 4.58 | 5.14 – 5.14 – 5.14 | 4.97 | 2.57 – 3.43 – 3.43 | 3.01 | 3.43 – 4.29 – 4.72 | 5.30 |
| 13 | 6.00 – 6.00 – 6.86 | 6.35 | 1.71 – 2.57 – 2.57 | 2.49 | 0.86 – 0.86 – 1.71 | 1.63 | 6.00 – 6.00 – 6.86 | 6.54 |
| 14 | 6.86 – 7.72 – 7.72 | 7.38 | 1.29 – 1.71 – 1.71 | 1.63 | 0.00 – 0.00 – 0.86 | 0.45 | 6.00 – 6.86 – 6.86 | 6.53 |
| 15 | 4.29 – 4.29 – 5.14 | 4.50 | 1.71 – 1.71 – 1.71 | 1.69 | 2.57 – 2.57 – 3.43 | 3.10 | 2.57 – 2.57 – 3.43 | 2.82 |
| 16 | 0.86 – 0.86 – 0.86 | 0.81 | 4.71 – 5.14 – 5.14 | 4.99 | 0.00 – 0.00 – 0.86 | 0.56 | 0.86 – 0.86 – 0.86 | 0.98 |
| 17 | 0.00 – 0.00 – 0.86 | 0.58 | 6.00 – 6.86 – 6.86 | 6.60 | 1.71 – 2.57 – 2.57 | 2.35 | 0.00 – 0.86 – 0.86 | 0.78 |
| 18 | 2.57 – 2.57 – 2.57 | 2.62 | 9.43 – 9.43 – 9.43 | 9.32 | 3.43 – 3.43 – 4.29 | 3.70 | 2.57 – 2.57 – 2.57 | 2.73 |
| 19 | 0.86 – 0.86 – 1.71 | 1.13 | 7.71 – 8.57 – 8.57 | 8.28 | 3.43 – 3.43 – 3.43 | 3.39 | 0.86 – 0.86 – 0.86 | 0.83 |
| 20 | 0.86 – 0.86 – 0.86 | 1.10 | 7.71 – 8.57 – 8.57 | 8.38 | 3.43 – 3.43 – 3.43 | 3.44 | 0.00 – 0.00 – 0.86 | 0.44 |
| 21 | 1.71 – 1.71 – 1.71 | 1.72 | 6.86 – 6.86 – 6.86 | 6.98 | 3.43 – 4.29 – 4.29 | 4.06 | 0.86 – 0.86 – 1.71 | 1.27 |

Table 7.5: Quartiles and RMSE values for each test position when using binary $K = 8$ CSS of 64 bits.

| | TDOA 1-2 | | TDOA 2-3 | | TDOA 3-4 | | TDOA 4-5 | |
|---|---|---|---|---|---|---|---|---|
| Test position | Quartiles | RMSE | Quartiles | RMSE | Quartiles | RMSE | Quartiles | RMSE |
| 1 | 4.29 – 4.29 – 4.29 | 4.45 | 3.43 – 3.43 – 3.43 | 3.49 | 0.00 – 0.00 – 0.00 | 0.39 | 2.57 – 3.00 – 3.43 | 3.03 |
| 2 | 3.43 – 3.43 – 4.29 | 3.77 | 2.57 – 3.43 – 3.43 | 3.11 | 0.00 – 0.00 – 0.86 | 0.64 | 3.43 – 3.43 – 4.29 | 3.79 |
| 3 | 5.14 – 5.14 – 5.14 | 5.12 | 3.43 – 3.43 – 3.43 | 3.31 | 1.71 – 1.71 – 1.71 | 1.70 | 4.29 – 4.29 – 4.29 | 4.15 |
| 4 | 5.14 – 6.00 – 6.00 | 5.73 | 3.43 – 3.43 – 3.43 | 3.38 | 0.00 – 0.86 – 0.86 | 0.63 | 4.29 – 5.14 – 5.14 | 4.89 |
| 5 | 5.14 – 5.14 – 6.00 | 5.42 | 1.71 – 1.71 – 1.71 | 1.82 | 0.86 – 0.86 – 1.71 | 1.31 | 3.43 – 3.43 – 4.29 | 3.72 |
| 6 | 6.00 – 6.86 – 6.86 | 6.59 | 0.86 – 1.71 – 1.71 | 1.40 | 0.00 – 0.86 – 0.86 | 0.79 | 5.14 – 5.14 – 5.14 | 5.32 |
| 7 | 3.43 – 3.43 – 3.43 | 3.36 | 4.29 – 4.29 – 4.29 | 4.25 | 0.86 – 1.71 – 1.71 | 1.39 | 0.86 – 1.71 – 1.71 | 1.39 |
| 8 | 1.71 – 2.57 – 2.57 | 2.27 | 5.14 – 5.14 – 6.00 | 5.40 | 1.71 – 1.71 – 2.57 | 2.10 | 0.86 – 0.86 – 0.86 | 1.10 |
| 9 | 0.86 – 0.86 – 0.86 | 0.89 | 6.86 – 6.86 – 6.86 | 6.95 | 3.43 – 3.43 – 3.43 | 3.42 | 0.00 – 0.00 – 0.86 | 0.66 |
| 10 | 1.71 – 1.71 – 1.71 | 1.92 | 6.86 – 6.86 – 6.86 | 6.80 | 3.43 – 3.43 – 4.28 | 3.73 | 0.86 – 0.86 – 1.71 | 1.15 |
| 11 | 4.29 – 4.29 – 4.29 | 4.47 | 6.00 – 6.00 – 6.86 | 6.21 | 2.57 – 3.43 – 3.85 | 3.38 | 1.71 – 2.57 – 2.57 | 2.61 |
| 12 | 4.29 – 4.29 – 5.14 | 4.56 | 5.14 – 5.14 – 5.14 | 5.15 | 0.86 – 3.43 – 3.43 | 3.01 | 3.43 – 4.29 – 8.57 | 6.09 |
| 13 | 6.00 – 6.86 – 6.86 | 6.58 | 1.71 – 1.71 – 2.57 | 2.20 | 1.72 – 1.72 – 2.57 | 2.17 | 6.00 – 6.00 – 6.00 | 7.16 |
| 14 | 7.72 – 7.72 – 7.72 | 7.53 | 0.86 – 0.86 – 1.71 | 1.18 | 0.00 – 0.00 – 0.86 | 0.49 | 6.00 – 6.00 – 6.00 | 6.04 |
| 15 | 4.29 – 4.29 – 4.29 | 4.43 | 1.71 – 1.71 – 1.71 | 1.56 | 2.57 – 2.57 – 3.43 | 2.87 | 2.57 – 2.57 – 2.57 | 2.72 |
| 16 | 0.00 – 0.86 – 0.86 | 0.71 | 5.14 – 5.14 – 5.14 | 5.20 | 0.00 – 0.00 – 0.86 | 0.57 | 0.86 – 0.86 – 0.86 | 0.88 |
| 17 | 0.00 – 0.86 – 0.86 | 0.66 | 6.86 – 6.86 – 6.86 | 6.91 | 2.57 – 2.57 – 3.43 | 2.78 | 0.86 – 0.86 – 0.86 | 1.05 |
| 18 | 1.71 – 2.57 – 2.57 | 2.41 | 8.57 – 8.57 – 9.43 | 8.87 | 3.43 – 4.29 – 4.29 | 3.88 | 1.71 – 2.57 – 2.57 | 2.34 |
| 19 | 0.86 – 1.71 – 1.71 | 1.46 | 8.57 – 8.57 – 8.57 | 8.63 | 3.43 – 3.43 – 4.29 | 3.56 | 0.86 – 0.86 – 0.86 | 0.98 |
| 20 | 0.86 – 0.86 – 0.86 | 0.93 | 7.72 – 7.72 – 8.57 | 7.86 | 2.57 – 2.57 – 3.43 | 3.01 | 0.00 – 0.00 – 0.86 | 0.58 |
| 21 | 0.86 – 1.71 – 1.71 | 1.43 | 7.72 – 7.72 – 7.72 | 7.84 | 4.29 – 4.29 – 5.14 | 4.62 | 0.00 – 0.86 – 0.86 | 0.61 |

Table 7.6: Quartiles and RMSE values for each test position when using multilevel $K = 5$ CSS of 85 bits.

| | TDOA 1-2 | | TDOA 2-3 | | TDOA 3-4 | | TDOA 4-5 | |
|---|---|---|---|---|---|---|---|---|
| Test position | Quartiles | RMSE | Quartiles | RMSE | Quartiles | RMSE | Quartiles | RMSE |
| 1 | 4.29 – 4.29 – 5.14 | 4.70 | 2.57 – 2.57 – 3.43 | 2.91 | 0.00 – 0.00 – 0.86 | 0.48 | 2.57 – 2.57 – 2.57 | 2.44 |
| 2 | 0.00 – 0.00 – 4.29 | 3.52 | 2.57 – 2.57 – 56.59 | 34.31 | 0.86 – 0.86 – 117.48 | 68.49 | 3.43 – 3.43 – 55.74 | 32.65 |
| 3 | 5.14 – 5.14 – 5.14 | 4.99 | 2.57 – 2.57 – 2.57 | 2.60 | 0.00 – 0.00 – 0.00 | 0.34 | 3.43 – 3.43 – 4.29 | 3.79 |
| 4 | 6.00 – 6.86 – 11.14 | 8.85 | 2.57 – 2.57 – 3.43 | 2.94 | 0.00 – 0.00 – 0.00 | 0.38 | 4.29 – 4.29 – 4.29 | 4.45 |
| 5 | 5.14 – 6.00 – 6.00 | 5.69 | 0.86 – 0.86 – 1.71 | 1.30 | 1.71 – 1.71 – 2.57 | 2.06 | 3.43 – 3.43 – 3.43 | 3.35 |
| 6 | 6.00 – 6.86 – 6.86 | 6.59 | 0.86 – 0.86 – 1.71 | 1.24 | 0.86 – 0.86 – 1.71 | 1.23 | 4.29 – 4.29 – 5.14 | 4.72 |
| 7 | 0.86 – 0.86 – 0.86 | 1.10 | 3.43 – 3.43 – 3.43 | 3.42 | 0.00 – 0.00 – 0.00 | 0.34 | 0.86 – 0.86 – 0.86 | 0.86 |
| 8 | 0.86 – 1.71 – 1.71 | 1.54 | 4.29 – 4.29 – 4.29 | 4.38 | 0.86 – 0.86 – 1.71 | 1.23 | 0.86 – 0.86 – 1.71 | 1.20 |
| 9 | 0.86 – 0.86 – 1.71 | 1.18 | 6.00 – 6.00 – 6.00 | 5.86 | 1.71 – 1.71 – 2.57 | 2.12 | 0.00 – 0.86 – 0.86 | 0.66 |
| 10 | 1.71 – 2.57 – 2.57 | 2.38 | 6.00 – 6.00 – 6.00 | 5.86 | 2.57 – 2.57 – 2.57 | 2.74 | 0.86 – 0.86 – 0.86 | 1.00 |
| 11 | 4.29 – 4.29 – 4.29 | 4.43 | 4.29 – 5.14 – 5.14 | 4.88 | 1.71 – 1.71 – 1.71 | 1.83 | 1.71 – 1.71 – 2.57 | 2.15 |
| 12 | 4.29 – 4.29 – 5.14 | 4.62 | 4.29 – 5.14 – 5.14 | 4.74 | 3.43 – 3.43 – 3.43 | 3.35 | 2.57 – 2.57 – 3.43 | 2.95 |
| 13 | 6.00 – 6.86 – 6.86 | 6.48 | 1.71 – 1.71 – 1.71 | 1.64 | 0.00 – 0.00 – 0.00 | 0.37 | 5.14 – 6.00 – 6.00 | 5.76 |
| 14 | 7.72 – 7.72 – 7.72 | 7.55 | 0.86 – 0.86 – 0.86 | 0.78 | 0.86 – 0.86 – 1.71 | 1.13 | 6.00 – 6.00 – 6.00 | 5.96 |
| 15 | 4.29 – 5.14 – 5.14 | 4.87 | 0.00 – 0.86 – 0.86 | 1.26 | 3.43 – 3.43 – 3.43 | 3.73 | 1.71 – 2.57 – 2.57 | 2.33 |
| 16 | 0.86 – 1.71 – 6.00 | 3.67 | 4.29 – 4.29 – 4.29 | 4.32 | 0.86 – 0.86 – 0.86 | 1.00 | 1.71 – 1.71 – 2.57 | 1.98 |
| 17 | 0.00 – 0.00 – 0.86 | 1.01 | 6.00 – 6.00 – 6.86 | 6.12 | 2.57 – 2.57 – 3.43 | 2.97 | 1.71 – 1.71 – 1.71 | 1.81 |
| 18 | 2.57 – 2.57 – 2.57 | 2.49 | 7.72 – 8.57 – 8.57 | 8.23 | 1.71 – 2.57 – 2.57 | 2.21 | 1.71 – 1.71 – 2.57 | 2.17 |
| 19 | 0.86 – 0.86 – 0.86 | 0.93 | 6.86 – 7.72 – 7.72 | 7.58 | 3.43 – 3.43 – 3.43 | 3.55 | 0.86 – 1.71 – 1.71 | 1.51 |
| 20 | 0.00 – 0.00 – 0.86 | 1.04 | 6.86 – 6.86 – 6.86 | 34.88 | 1.71 – 2.57 – 2.57 | 67.27 | 0.00 – 0.00 – 0.00 | 33.44 |
| 21 | 1.71 – 2.57 – 2.57 | 2.26 | 6.86 – 6.86 – 6.86 | 6.98 | 4.29 – 4.29 – 4.29 | 4.23 | 0.00 – 0.00 – 0.86 | 0.58 |

Table 7.7: Quartiles and RMSE values for each test position when using binary GPC sequences of 416 bits.

# Chapter 8

# Conclusions and Future Works

In this chapter we analyze the most significant conclusions derived from this thesis. Furthermore, we include the papers published (or in review for publication) in indexed international journals and international conferences about the work carried out in the thesis. Finally, we propose some novel research lines which could be tackled with the contributions of the thesis.

## 8.1 Conclusions

Due to the intensively use of CSS in a broad range of applications, a great effort has been made to find both CSS with more different lengths and set sizes and efficient architectures for their generation and correlation. Nevertheless, the majority of contributions to the efficient generation/correlation of CSS available in literature (with the notable exception of the recent contribution by Budišin for $K_{|CSS} = 2$ binary CSS of lengths $L_{|CSS} = 2^N \cdot 10^M$) focuses on $K_{|CSS} = 2^k$ binary CSS of length $L_{|CSS} = K^Q_{|CSS}$. This thesis contributes to the study of the efficient generation/correlation algorithms of CSS with flexible length and set size. The most significant contributions of this thesis can be summarized as

1. The existence of both multilevel Hadamard matrices of any order and multilevel CSS for more lengths than binary CSS have led us to propose generation/correlation architectures for multilevel CSS. We have proposed two architectures for the generation/correlation of multilevel CSS, the first one for $K_{|MultCSS} = 2^k$ CSS ($k \in \mathbb{N} - \{0\}$) and the second one for $K_{|MultCSS} \geq 3 - \{4\}$ CSS. The parameters of these architectures can be tuned to generate/correlate efficiently multilevel CSS with a low PAPR.

2. The proposed architecture for $K_{|MultCSS} = 2$ multilevel CSS has allowed the decomposition of the Golay kernel 26. By using this decomposition and the one proposed by Budišin for the Golay kernel 10, we have proposed an efficient generation/correlation algorithm of $K_{|CSS} = 2^k$ binary CSS of lengths $L_{|CSS} = (\frac{K_{|CSS}}{2}) \cdot 2^N \cdot 10^M \cdot 26^P$.

3. Generalization of the previous generation algorithms of LS sequences to multilevel alphabet. This proposal permits to design energy efficient multilevel LS sequences with many more length than the binary ones, by finding the appropiate parameter values of the architecture.

4. Proposal of an efficient generator/correlator of GPC sequences. We have taken advantage of the modular architecture for the correlation of Golay binary pairs of lengths $L_{|Gol} = 2^N \cdot 10^M \cdot 26^P$ and the easy generation of $E$-sequences to propose a generator/correlator of GPC sequences. We have also shown the theoretical link between GPC sequences and LS sequences and interestingly it derives to a very efficient generator/correlator of LS sequences. From the real test performed in an ultrasound ranging system with asynchronous detection, we conclude that GPC sequences are promising only with an appropiate modulation scheme, which does not introduces ISI. The non-coherent QPSK demodulation carried out, degrades the IFW due to ISI.

5. The design of an UWB-based indoor positioning system which has been used as test-bed for the performance comparison of Kasami and LS sequences. We conclude that the use of CDMA in UWB is only feasible if there exists a power control in the emission, which would increase the system complexity, or if GO sequences (as LS ones) are used and their ZCZ length is large enough to ensure that the maximum TDOA is within the IFW. In spite of the good aperiodic correlation properties of Kasami sequences, they are sensitive to near-far effect. It is noteworthy that near-far effect in UWB is much more severe than in other local positioning systems as the ones based on ultrasound. Finally, the use of an adaptive first arriving path estimator, robust to NLOS conditions is necessary in UWB positioning systems for accurate measurements.

## 8.2 Publications Derived from the Thesis

The following papers has been derived from the proposals of this thesis:

### 8.2.1 International Journals

1. E. García, J. J. García, J. Ureña, M. C. Pérez, A. Hernández, "Generation algorithm for multilevel LS codes," *Electronics Letters*, vol. 46, no. 21, pp. 1465-1467, Oct. 2010.

2. E. García, J. Ureña, J. J. García, M. C. Pérez, D. Ruiz, "Efficient generator/correlator of GPC sequences for QS-CDMA," *IEEE Communications Letters*, vol. 16, no. 10, pp. 1676-1679, Oct. 2012.

3. E. García, J. Ureña, J. J. García, D. Ruiz, M. C. Pérez, J. C. García, "Efficient filter for the generation/correlation of Golay binary sequence pairs," *International Journal of Circuit Theory and Applications*, available online, DOI: 10.1002/cta.1901, 2013.

4. E. García, J. Ureña, J. J. García, M. C. Pérez, "Efficient architectures for the generation and correlation of CSS derived from different kernel lengths," *IEEE Transactions on Signal Processing*, in review.

5. E. García, J. Ureña, J. J. García, "Generation and correlation architectures of multilevel complementary sets of sequences," *IEEE Transactions on Signal Processing*, in review.

### 8.2.2 International Conferences

1. E. García, J. J. García, J. Ureña, M. C. Pérez, D. Ruiz, "Multilevel complementary sets of sequences and their application in UWB," *IEEE Conference on Indoor Positioning and Indoor Navigation* (IPIN), 2010.

2. E. García, S. Holm, J. J. García, J. Ureña, "Link budget for low bandwidth and coded ultrasonic indoor location systems," *IEEE International Conference on Indoor Positioning and Indoor Navigation* (IPIN), 2011.

3. E. García, J. Ureña, J. J. García, M. C. Pérez, D. Ruiz, C. Diego, J. Aparicio, "Multilevel LS sequences with flexible ZCZ length and their application to local positioning systems," *IEEE International Instrumentation and Measurement Technology Conference* (I2MTC), 2012.

4. E. García, J. Ureña, J. J. García, M. C. Pérez, D. Ruiz, D. Gualda, R. Gutiérrez, F. J. Álvarez, "Genetic algorithm for searching a doppler resilient multilevel complementary waveform," *IEEE International Symposium on Intelligent Signal Processing* (WISP), 2011.

## 8.3 Future Works

This thesis has contributed to the efficient design of flexible CSS and GO sequences. Nevertheless, there is still a large amount of effort to be made, as

1. Find the parameters of the proposed architectures that reduce the PAPR of the multilevel CSS. In this way, we could generate and correlate efficiently near-binary CSS of flexible length. Particularly, it would be interesting to find more multilevel $2-$CSS kernels with low PAPR and with a prime-number length, so as to combine with the Golay kernels of lengths 2, 10 and 26 and to generate near-binary CSS of flexible length.

2. One of the limitations in the use of OFDM in mobile communications is the large PAPR, which constraints the system portability. In the last years, one of the main objectives of some researchers (mostly mathematicians and communication engineers) is to reduce PAPR in OFDM communications systems. One promising solution is the use of complementary sequences directly mapped in the QAM alphabet [Lee 06, Chang 10, Huang 11]. This approach bounds the PAPR and gives error-correcting capabilities due to the connection to Reed-Muller codes found by Davis and Jedwab [Davis 99]. An interesting approach would be to consider seed values $W^{(k,q)}$ in the unitary circle (and not limited to the real axis) in order to propose efficient architectures for CSS mapped in the QAM alphabet.

3. Analyze further novel spreading sequences with good correlation properties, that cope with undesired effects. We propose the study of mismatched sequences for QS-CDMA, as LS and GPC ones to increase the ZCZ size. Mismatched sequences for the generation of flexible CSS have been recently proposed in [Bi 12].

4. Study methods to increase the number of GO sequences in a set. This directly depends on the orthogonal matrix construction employed.

5. Propose new architectures for CSS-based signatures. From the theoretical and practical point of view it would be interesting to unify in the same architecture the generation of CSS and Z-complementary sequences, which are a suboptimal solution with ZCZ and flexible length [Fan 07, Li 11a].

6. The performance of the UWB test-bed can be improved by implementing more advanced TOA estimators as the ones shown in [Guven 05, Falsi 06, Kuhn 10] and by combining the use of TDOA with AOA.

7. The application of GPC sequences to other fields such as QS-CDMA based sensor arrays, that would minimize interferences between pairs of sensors, or to Power-Line-Communication (PLC) systems.

# Appendix A
# Other Spreading Sequences

## A.1 Pseudo-Random Sequences

This group of sequences, also known as Pseudo-Noise (PN) sequences, are periodic sequences, with a random-like behaviour but generated deterministically and with properties similar to AWGN. To evaluate the randomness of a sequence, it is defined the following criteria [Fan 96]:

- Correlation property: A sequence $s[l]$, $0 \leq l \leq L_{|PN}$; $s[l] \in \{+1, -1\}$ of length $L_{|PN}$ should have the following periodic auto-correlation function:

$$R_{s,s}[\tau] = \sum_{l=0}^{L_{|PN}-1} s[l] \cdot s[l+\tau] = \begin{cases} L_{|PN} & \text{for } \tau = 0 \\ \varepsilon & \text{for } \tau \neq 0 \end{cases} \tag{A.1}$$

  where $\varepsilon$ is a constant $\varepsilon \in \mathbb{R}$, which represents the sidelobes of the periodic auto-correlation function.

- Balance property: In a PN sequence, the number of $+1$ should not exceed the number of $-1$ in more than one element.

- Run property: In a PN sequence, half of the consecutive identical bits (runs) have length 1, one-quarter of the block have length 2, one-eighth have length 3 and so on. The number of runs of $-1$ are the same as the number of runs of $+1$ and the total number of consecutive identical bits in a sequence should be an integer.

In the following subsections, it is briefly review the properties of the most commonly used PN sequences.

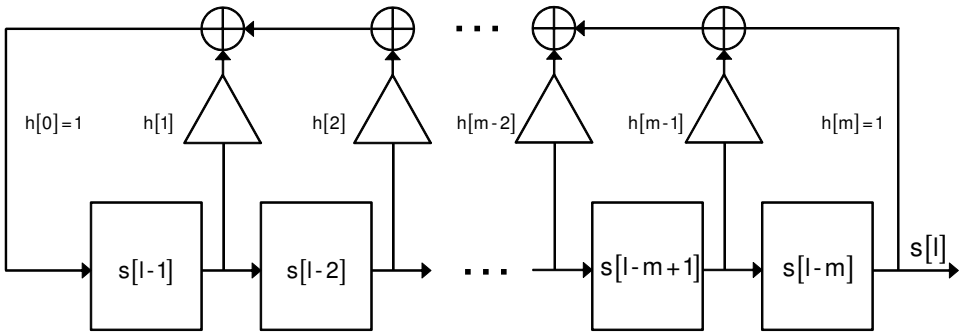


Figure A.1: Linear Feedback Shift Register.

### A.1.1 $m$-Sequences

$m$-sequences have good pseudo-random properties as they satisfy the three previous randomness criteria. They are easily generated by means of a Linear Feedback Shift Register (LFSR) [Golom 82] as the one depicted in Figure A.1, where the values $\{s^{(0)}[m-1], s^{(0)}[m-2], \ldots, s^{(0)}[0]\}$ are the initial state of the LFSR and the symbol $\oplus$ represents a modulo-2 adder. A LFSR is composed of a set of $m$ flip-flops and a feedback function which generates in each step the most significant bit. At each step (i.e. clock event), all the bits stored in the flip-flops are shifted one place to the right and the entry of the most significant bit is generated by means of the feedback function. This function is controlled by the *primitive polynomial* of degree $m$, $h(x) = \sum_{i=0}^{m} h[i] \cdot x^{m-i}$; $h[i] \in \{0, +1\}$, with $h[0]$ and $h[m]$ equal to $+1$, in such a way that the terms $h[i]$ are modulo-2 added and back-propagated to the left. The terms $h[i]$ manages the feedback of each cell. So a value of $h[i] = +1$ means that there is feedback at the output of the cell $i$; on the contrary, a value of $h[i] = 0$ means that there are no feedback at the tap $i$. Consequently, the generated $m$-sequence can be expressed as follows:

$$s[l] = \begin{cases} s^{(0)}[l] & \text{for } 0 \leq l \leq m \\ \sum_{i=1}^{m} h[i] \cdot s[l-i] & \text{for } l \geq m \end{cases} \tag{A.2}$$

If the LFSR is composed of $m$ stages, the maximum period of the resultant $m$-sequence (without repeating the sequence and avoiding the state "all-zeros", i.e. its length) is equal to $L_{|m-seq} = 2^m - 1$. For this reason, $m$-sequences are also known as maximal length sequences.

The periodic auto-correlation function of $m$-sequences is given by equation A.1 where $\varepsilon = -1$. Unfortunately, the periodic cross-correlation function of two $m$-sequences are not favourable. Nevertheless it is possible to find *preferred pairs* of $m$-sequences with reasonably good periodic cross-correlation properties. A pair of $m$-sequences, $s_1[l]$ and $s_2[l]$, are a *preferred pair* with a three-level periodic cross-correlation function if the following conditions hold [Fan 96]:

- $m$ is not divisible by 4.
- The sequence $s_2[l]$ can be obtained by decimating $s_1[l]$ by a factor $d$: $s_2[l] = s_1[d \cdot l]$, with $d = 2^k + 1$ or $d = 2^{2 \cdot k} - 2^k + 1$
- The great common division of $l$ and $k$, which is equal to $\gcd(l, k)$, has a value so as to $m/\gcd(l,k)$ is odd.

In this way, the levels of the periodic cross-correlation function of the *preferred pair,* $R_{s_1,s_2}[\tau]$ are $\{-1, -1 - 2^{\frac{m+1}{2}}, -1 + 2^{\frac{m+1}{2}}\}$ for $m$ odd and $\{-1, -1 - 2^{\frac{m+2}{2}}, -1 + 2^{\frac{m+2}{2}}\}$ for $m$ even.

If the first condition does not hold, i.e. $m$ is a multiple of 4, there no exist *preferred pairs* with three-level periodic cross-correlation functions, but it is possible to find them with four-level periodic cross-correlation functions if the decimating factor $d$ is equal to $d = -1 + 2^{\left(\frac{m+2}{2}\right)}$. In this case the values of $R_{s_1,s_2}[\tau]$ are $\{-1, -1 + 2^{\frac{m+2}{2}}, -1 + 2^{\frac{m}{2}}, -1 - 2^{\frac{m}{2}}\}$.

Finally, $m$-sequences can be generalized to non-binary sequences of length $L_{|m-seq} = \ell^m - 1$ by using a primitive polynomial of degree $m$ over $\mathrm{GF}(\ell)$. The periodic auto-correlation properties of the non-binary $m$-sequences are the same as those of binary ones.

Despite of the fact that there exist sets of $m$-sequences where all the sequences of the sets are *preferred pairs* between them, the major drawback of $m$-sequences is the limited number of sequences with reduced periodic cross-correlation functions, which makes difficult their use in multi-user environments.

### A.1.2 Gold Sequences

Gold sequences are derived from a *preferred pair* of $m$-sequences and cope with the limitation that have $m$-sequences in the number of sequences with reduced cross-correlation levels. Unfortunately, the increase in the number of sequences with reduced periodic cross-correlation levels is accomplished at the expense of increasing the sidelobe levels of the

periodic auto-correlation functions. Notice that this implies that Gold sequences do not satisfy the first randomness criteria. In practice, it is difficult that the three randomness criteria are satisfied at the same time. However, Gold sequences as other sequences (as Kasami ones, discussed latter) are broadly admitted as pseudo-random sequences.

Given a *preferred pair* of $m$-sequences, $s_1[l]$ and $s_2[l]$, of length $L_{|m-seq} = 2^m - 1$, it is possible to generate a set $\mathbf{G}[l] = \{g_0[l], g_1[l], \ldots, g_{K_{|Gold}-1}[l]\}$ of $K_{|Gold} = 2^m + 1$ Gold sequences of length $L_{|Gold} = 2^m - 1$ [Gold 67]. The set $\mathbf{G}[l]$ is formed of the following sequences:

$$\mathbf{G}[l] = \left\{s_1[l],\ s_2[l],\ s_1[l] \oplus D^1 s_2[l],\ s_1[l] \oplus D^2 s_2, \ldots,\ s_1[l] \oplus D^{L_{|Gold}-1} s_2[l]\right\} \quad \text{(A.3)}$$

Where the symbol $\oplus$ is the modulo-2 addition and $D^k s_2[l]$ is the cyclic shift of $k$ bits to the sequence $s_2[l]$. The periodic auto-correlation properties of Gold sequences, represented in equation A.4, are not as good as those of $m$-sequences, as the sequences of the set $\mathbf{G}[l]$ are not maximal length sequences, with the exception of the sequences $s_1[l]$ and $s_2[l]$.

$$R_{g_i,g_j}[\tau] = \begin{cases} L & \text{for } \tau = 0 \\ \varepsilon & \text{for } \tau \neq 0 \end{cases} \quad \text{(A.4)}$$

Where $\varepsilon$ is equal to $\{-1,\ -1-2^{\frac{m+1}{2}},\ -1+2^{\frac{m+1}{2}}\}$ for $m$ odd and $\{-1,\ -1-2^{\frac{m+2}{2}},\ -1+2^{\frac{m+2}{2}}\}$ for $m$ even not divisible by 4[Fan 96]. So the periodic cross-correlation values and the sidelobes of the periodic auto-correlation functions of Gold sequences are the same as those of the *preferred pairs* of $m$-sequences, with $m$ not divisible by 4.

### A.1.3 Kasami Sequences

Kasami sequences are normally classified into two groups according to the set size, namely:

- Small sets of Kasami sequences [Kasam 66]: The sidelobes of the periodic correlation functions of the small set of Kasami sequences are lower than those of the Gold sequences but the set size of this group of Kasami sequences is smaller. Given a $m$-sequence $s_1[l]$, of length $L_{|m-seq} = 2^m - 1$, with $m$ even, and another $m$-sequence $s_2[l]$ of length $L_{|m-seq} = 2^m - 1$, generated by decimating $s_1[l]$ by a factor $d = 1 + 2^{\frac{m}{2}}$ and concatenating it $d$ times, the small set of Kasami sequences is defined as follows:

$$\mathbf{F}[l] = \left\{s_1[l],\ s_1[l] \oplus s_2[l],\ s_1[l] \oplus D^1 s_2[l], \ldots,\ s_1[l] \oplus D^{\frac{2 \cdot m}{2}-2} s_2[l]\right\} \quad \text{(A.5)}$$

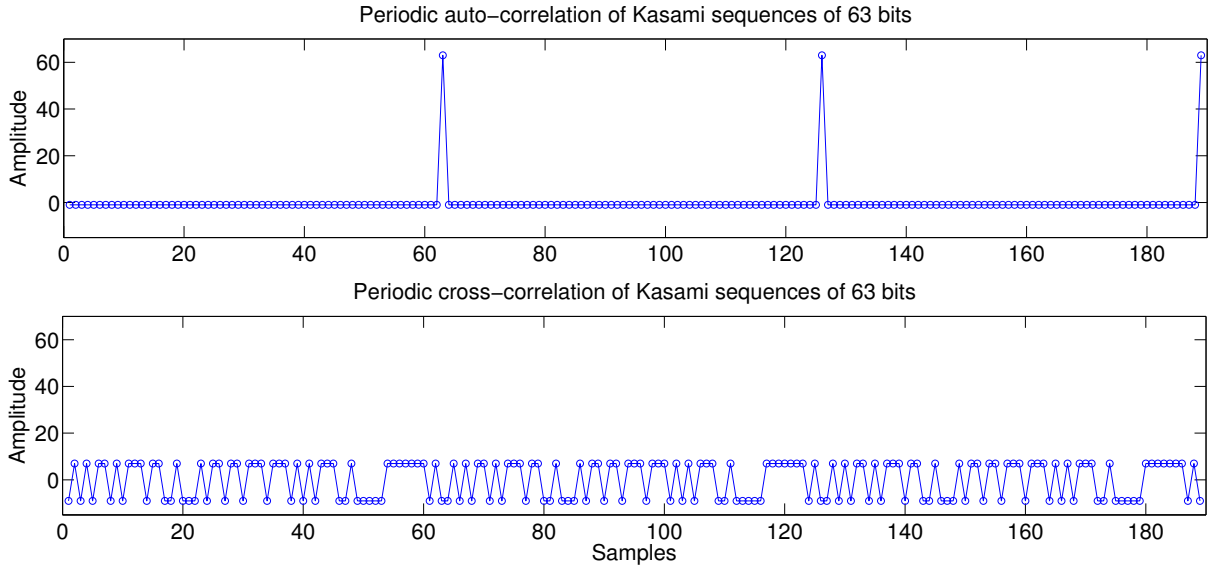


Figure A.2: Periodic correlation functions of the small set of Kasami sequences of length 63.

The sidelobes of the periodic correlation functions of the small set of Kasami sequences are equal to $\{-1, -1-2^{\frac{m}{2}}, -1+2^{\frac{m}{2}}\}$, which are almost two times lower than the periodic correlation sidelobes of the Gold sequences. Moreover, despite of the fact that the correlation properties deteriorate when the sequences are emitted in an aperiodic mode, the small set of Kasami sequences still have good aperiodic correlation functions [Lahto 95, Sun 11] and are commonly used in aperiodic CDMA schemes [Diego 11, Villa 07]. For the sake of clarity, Figure A.2 depicts the periodic and Figure A.3 shows the aperiodic correlation functions of Kasami sequences.

- Large sets of Kasami sequences: This group of Kasami sequences have the small set of Kasami sequences and the Gold sequences as a subset. They have a set size equal to $K_{|LargeKasami} = 2^{\frac{m}{2}} \cdot (2^m + 1)$ when generated from Gold sequences but the periodic correlation sidelobes are the same as those of the *preferred pairs* of $m$-sequences.

In general, the term Kasami sequences refers to the small set of Kasami sequences [Perez 09a, Diego 11]. Finally, remark that Kasami sequences have also an algorithm for its generalization to non-binary alphabet [Liu 92].

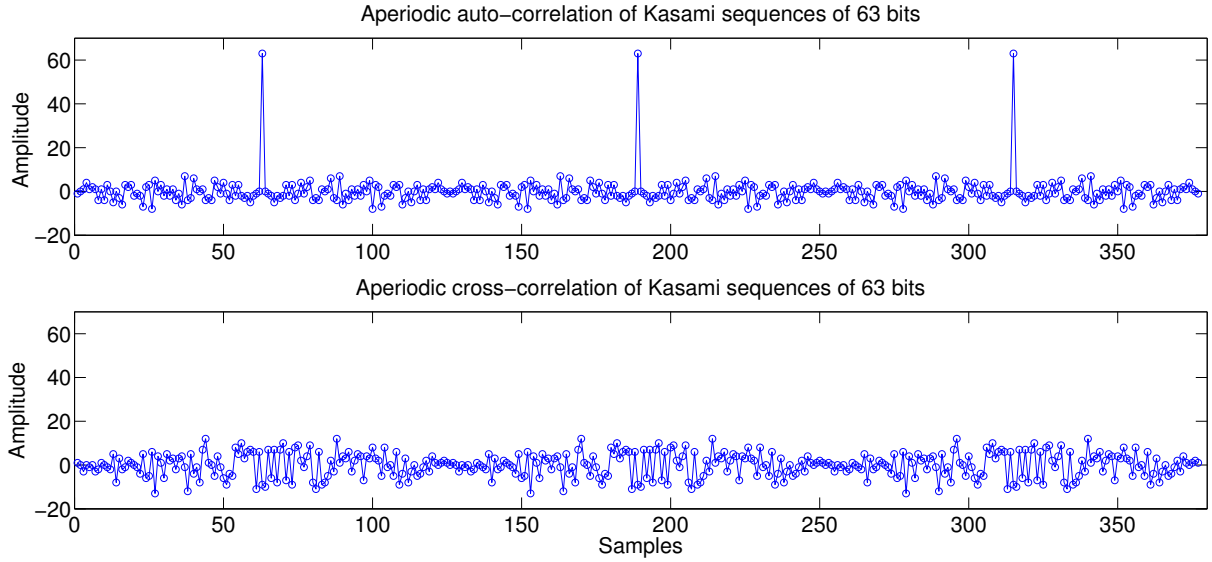


Figure A.3: Aperiodic correlation function of small set of Kasami sequences of length 63 bits.

## A.2 Chaotic Sequences

In the last years, there has been a great interest in the analysis of the dynamical systems. This interest boosted in the 60s, mainly due to the publication of the paper "Predictability: Does the Flap of a Butterfly's Wing in Brazil Set Off a Tornado in Texas?". In this paper, the importance of the effects of the initial conditions in the weather forecasting (modelled as dynamical systems) was demonstrated.

For given parameter values of certain dynamical systems (and deterministics), small changes in the initial conditions can generate completely uncorrelated solutions. Those solutions are known in the signal processing field as chaotic sequences, which have an infinite period and a noise-like behaviour. The former properties (sensitivity to initial conditions and noise-like behaviour) make chaotic sequences interesting for their use as spreading sequences in CDMA, as theoretically it is possible to obtain infinite uncorrelated sequences of infinite length. In what follows, some definitions are introduced for a better understanding of the chaotic sequences and their advantages and limitations as spreading sequences for CDMA systems.

### A.2.1 Definitions

Dynamical systems are those whose behaviour change with time and can be continuous or discrete. The first one are described by differential equations, and the second one by difference equations. Given a state vector $\mathbf{x}(t) = (x_1(t), ..., x_n(t))$ and a vectorial function, (also known as vector field in continuous systems) $\mathbf{f}(f_1, ..., f_n)$, which ascertains the evolution of the system, the continuous dynamical system is defined as stated in equation A.6 [Garci 06]:

$$\frac{d\mathbf{x}(t)}{dt} = \mathbf{f}(t, \mathbf{x}(t)) \tag{A.6}$$

The components of the state vector $\mathbf{x}(t)$ are the dependent variables of the differential system and determine in a given instant the state of the dynamic system, whereas the vectorial function $\mathbf{f}(f_1, ..., f_n)$ determines the evolution of the system.

If the dynamic system is discrete, it is represented as difference equations (equation A.7), and the functions $f$ are known as maps.

$$\mathbf{x}[n] = \mathbf{f}(\mathbf{x}[n-1], n) \tag{A.7}$$

- *Space State*: Represents all the feasible values of a dynamical system for an infinite set of initial conditions.

- *Orbit*: It is the trajectory that follows the state vectors and they are obtained by iterating the map $f$. That is to say, it is the domain of definition of all the feasible values of the state vectors for a given initial condition. The objective of the Chaos Theory is the asynthotic analysis of the infinite orbits that follows a dynamical system.

- *Chaotic System:* In accordance with the most accepted definition [Devan 89], a dynamical system defined by a map $f$, has a chaotic behaviour if the following conditions are held:

    1. The map $f$ has a strong dependency to initial conditions. That is to say, initially close orbits, leads to uncorrelated states when they separate at the iteration $n$.
    2. The map $f$ is topologically transitive. This means that the map has states which are moving from a local point to another in an arbitrary form. So the map can not be decomposed into two disjointed open sets that stay invariant.

3. Despite of the complexity of the map $f$, it presents a regularity.

- *Attractor*: According to [Sobot 06], they are the regions of the state space towards the orbits of the map converge. If the orbits tends to a region of $f$, they are known as attractor basin. When the regions of the state space are formed by the points of a periodic orbit, the attractor is known as limit cycle of the map $f$. Furthermore, if the regions towards the orbits converges are composed by an unique point of the map $f$, the attractor is known as equilibrium point. Finally, if the attractor has a regular structure in the state space, with a pseudo-random behaviour in the time domain, the attractor is known as fractal or chaotic.

### A.2.2 Statistical Analysis of Chaos

- *Ergodicity*: A map $f(x)$, with probability density function $p(x)$ is ergodic if the average over the time of an integrable function, $g(x)$ is equal to its mathematical expectation [Berli 92], i.e.

$$\lim_{N\to\infty}\frac{1}{N}\sum_{i=0}^{N-1}g\left(f^i(x)\right)=\int g(x)\,p(x)\,dx \tag{A.8}$$

  A fundamental consequence of this property is the feasibility of computing the statistics of the maps for only one orbit (i.e. one iteration of a given initial condition) and independently of the initial condition chosen. A priori demonstrations of the ergodicity of a dynamical system is difficult and it is commonly assumed the ergodicity and then it is checked that the probability density function of a map for a large number of iterations and a given initial condition is the same than the probability density function of the same map at a given iteration for a large number of initial conditions.

- *Lyapunov exponent*: The Lyapunov exponent is an indicator of the system sensitivity to the initial conditions [Berli 92]. It is defined as depicted in equation A.9.

$$\lambda_{x_0}=\lim_{T\to\infty}\sum_{k=0}^{T-1}\log\left|\frac{df(x_k)}{x_k}\right| \tag{A.9}$$

  This parameter quantifies the level of chaos as it represents the level of separation between orbits when varying the initial conditions a quantity $dx_0$. Therefore, the

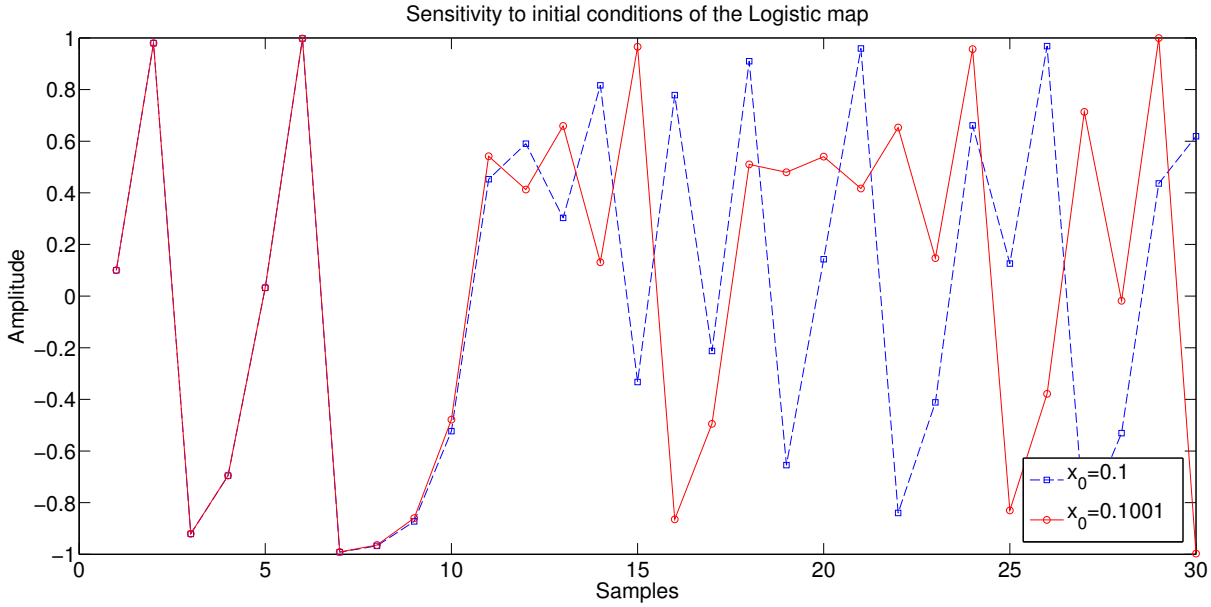


Figure A.4: Sensitivity to the initial conditions of the Logistic map.

larger the Lyapunov exponent $\lambda_{x_0}$, the larger degree of chaoticity in the dynamical system. On the contrary, if the Lyapunov exponent $\lambda_{x_0}$ is lower than zero, the dynamical system will have a regular behaviour.

### A.2.3 Chaotic Maps

The most known dynamical systems used for the generation of chaotic sequences are the logistic map, Lorenz map and Rössler map. In what follows, these maps are presented in order to analyse the performance of the chaotic sequences generated with them.

- *Logistic Map*: Logistic map in one the most studied maps due to its simplicity. This map is a discrete unidimensional function and it was designed to model how the population grows. It is expressed as stated in equation A.10.

$$x\left[t\right] = \mu \cdot \left(1 - x\left[t-1\right]\right) \cdot x\left[t-1\right] \;\; 0 < x < 1 \tag{A.10}$$

  Where $\mu$ is a parameter whose value must be $3.45 < \mu < 4$ in order to obtain a chaotic behaviour. Figure A.4 depicts the sensitivity to the initial conditions of the logistic map. A slight variation of the initial condition implies a completely different behaviour. In Figure A.5 the bifurcation diagram, or state space of the logistic map is shown. Notice the chaotic behaviour for values of the parameter $\mu > 3.45$.

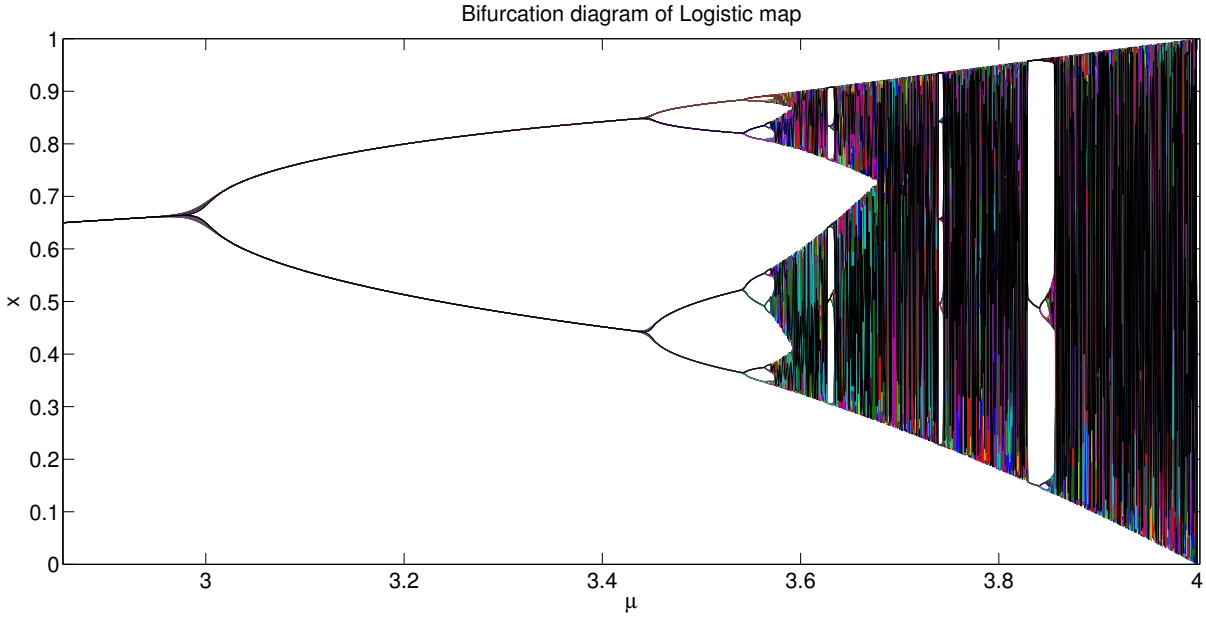


Figure A.5: Bifurcation diagram of the Logistic map.

In order to show the ergodicity of the logistic map and for better understanding of the ergodicity concept, the histogram of the logistic map for 4000 iterations with the initial condition $x[0] = 0.1$ and $\mu = 4$ has been computed. Also the histogram of the map at iteration 2000 for 4000 initial conditions, with $x[0] \in \{0.1, \ldots, 0.5\}$ and $\mu = 4$ has been derived. As shown in Figure A.6, the histogram for both cases are quite similar, independently of the initial condition chosen, and therefore the map is ergodic [Berli 92].

- *Rössler Map*: Wang and He propose the use of the Rössler map to generate chaotic sequences and their use in UWB communications [Wang 08]. Rössler dynamic system is defined as stated in the equation A.11.

$$\begin{cases} \dot{x} &= -y - z \\ \dot{y} &= x + ay - du \\ \dot{z} &= bxz - cz + k \\ \dot{u} &= exu - fz + g \end{cases} \tag{A.11}$$

Where $a$, $b$, $c$, $d$, $e$, $f$, $g$, and $k$ are the system parameters. For values $a = 0.2$, $b = 28/13$, $c = 7$, $d = 1.5$, $e = 0.01$, $f = 0.1$, $g = 0.18$ y $k = 0.2$, the dynamical

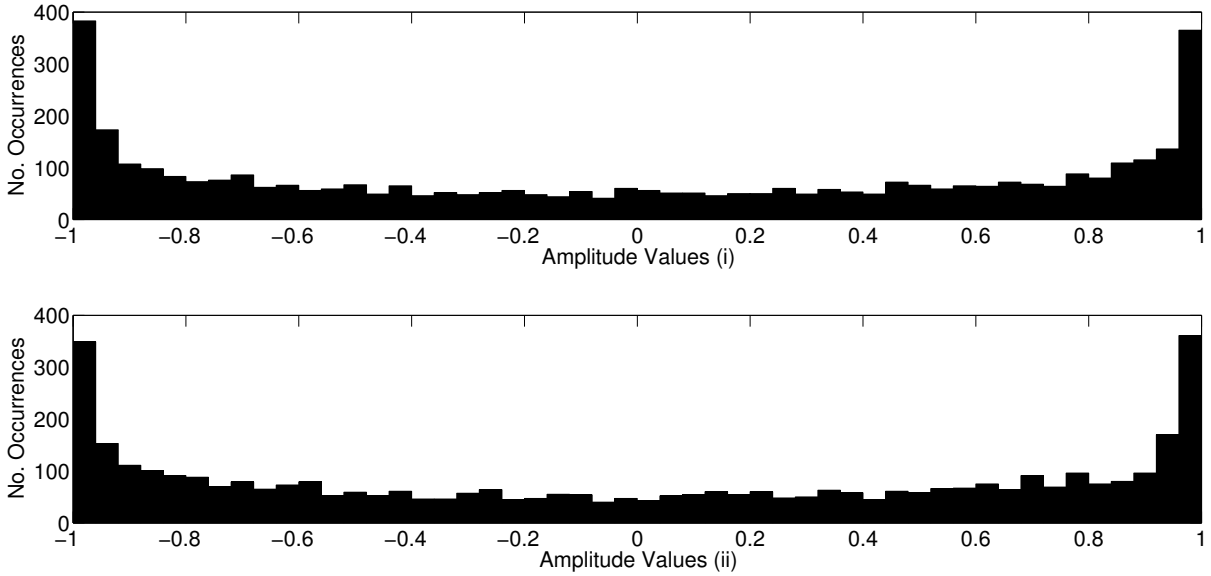


Figure A.6: Ergodicity of logistic map. (i) Histogram of the map for 4000 iterations, with $x[0] = 0.1$ and $\mu = 4$. (ii) Histogram of the map at iteration 2000 for 4000 initial conditions $x[0] \in \{0.1, \ldots, 0.5\}$ and $\mu = 4$.

system has a chaotic behaviour as it presents two positive Lyapunov exponents. Figure A.7 shows the state space and the chaotic attractor of the Rössler map.

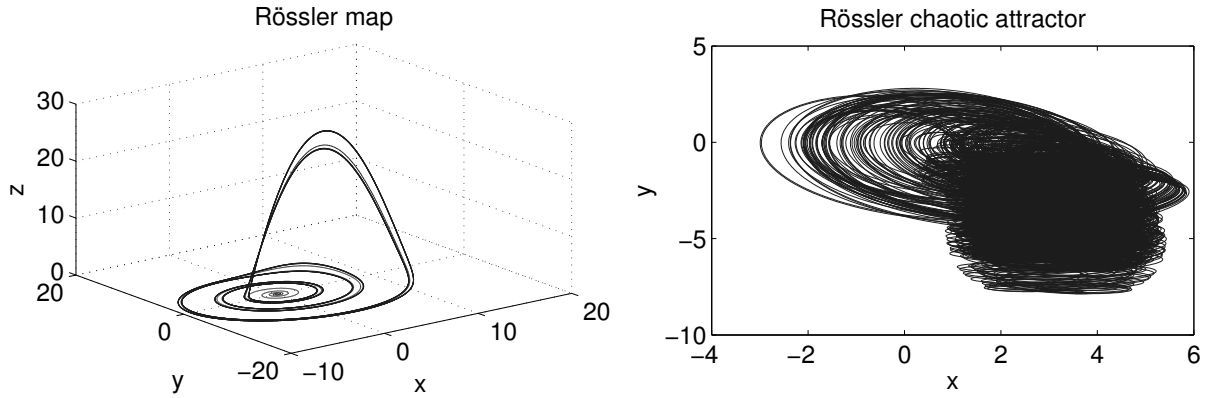


Figure A.7: State space and attractor of the Rössler map.

- *Lorenz Map*: One of the most known chaotic maps is the Lorenz one, introduced by Lorenz in 1963 as an approximate model of the dynamic of the terrestrial atmo-

sphere. This map is expressed in equation A.12.

$$\begin{cases} \dot{x} &= -\sigma x + \sigma y \\ \dot{y} &= Rx - y - xz \\ \dot{z} &= -Bz + xy \end{cases} \tag{A.12}$$

Where $\sigma$, $R$ and $B$ are constant parameters. Figure A.8 shows the projection of the Lorenz map in the plane $x - z$. The constants used to plot the projection have been equal to $\sigma = 10$, $R = 28$, $B = 8/3$. For these values, all the orbits tends to the attractor known as "The Butterfly".

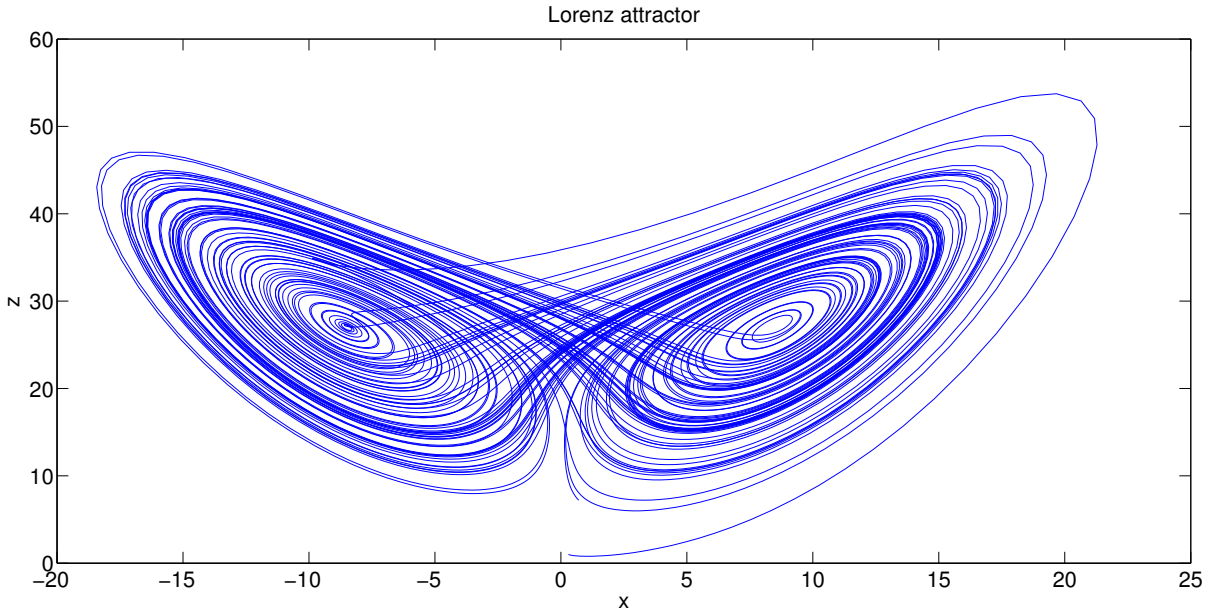


Figure A.8: Projection in the plane $x - z$ of the Lorenz map.

.

Refer to [Garci 06] for a comprehensive analysis of further chaotic maps.

### A.2.4 Design of Chaotic Maps by Means of Genetic Programming

Varadan and Leung carries out an exhaustive search of functions that generates optimum chaotic sequences for certain work conditions by means of Genetic programming

[Varad 02]. In this way, for a sequence length of $L_{|Genetic} = 1023$ and 10 users, the optimum map is represented by equation A.13.

$$x[n+1] = mod1[mod1(2x[n]) - mod1[(40.6681 + 8.6655 \cdot x[n]) \cdot mod1(2x[n])]] \tag{A.13}$$

For this map, the auto-correlation bound is equal to $\theta_{AC} = 0.0898$, while the cross-correlation bound is $\theta_{CC} = 0.0965$. The search of an ad-hoc map for its use in given conditions results in a better performance when compared to the typical chaotic maps used, as the Logistic map. Table A.1 presents a comparison of the correlation bounds between the chaotic map of [Varad 02] and the Logistic map.

| Map | $\theta$ | $\theta_{AC}$ | $\theta_{CC}$ |
|---|---|---|---|
| [Varad 02]$L_{\|Genetic} = 1023$, $K_{\|Genetic} = 10$ | 0.0965 | 0.0898 | 0.0965 |
| Logistic $L_{\|Logistic} = 1023$, $K_{\|Logistic} = 10$ | 0.1144 | 0.0978 | 0.1144 |

Table A.1: Comparison between the correlation bounds of Kasami sequences and the chaotic map of [Varad 02].

Furthermore, if the chaotic map of [Varad 02] is compared with a set of 8 Kasami sequences of length $L_{|Kasami} = 1023$, in terms of the correlation bounds, the results are very similar. Table A.2 shows the correlation bounds of both sets of sequences.

| Map | $\theta$ | $\theta_{AC}$ | $\theta_{CC}$ |
|---|---|---|---|
| [Varad 02]$L_{\|Genetic} = 1023$, $K_{\|Genetic} = 10$ | 0.0965 | 0.0898 | 0.0965 |
| Kasami $L_{\|Kasami} = 1023$, $K_{\|Kasami} = 8$ | 0.0626 | 0.0626 | 0.0587 |

Table A.2: Comparison between the correlation bounds of Kasami sequences and the chaotic map of [Varad 02].

### A.2.5 Transmission of Chaotic Sequences

An advantage of chaotic sequences is that, theoretically, they are not limited both in the number of uncorrelated sequences or in the length. The sequences generated by the chaotic maps are real sequences, which can imply the necessity of highly-linear amplifiers to avoid the distortion of the sequences and a reduction of the energy efficiency of the system. For that reason, chaotic sequences are binarized to obtain a constant envelope signal. This implies a degradation of the correlation properties as can appear periodicities

in the sequence. So multilevel quantization is sometimes assumed as a trade-off between the correlation properties and complexity of implementation.

**Quantization**

The methods commonly used to quantize chaotic sequences are:

1. Thresholding [Sando 98]: The binary sequence $s_k$ is generated from the chaotic sequence, by defining the following function $s_k = g\left\{x\left(t\right) - E_t\left(x\left[t\right]\right)\right\}|_{t=kT}$. Where $g\left(x\right) = 1$ for $x > 0$ and $g\left(x\right) = -1$ for $x < 0$. $E_t\left(x\left[t\right]\right)$ represents the mean value of the real chaotic sequence and $T$ is the period of $x\left[t\right]$.

2. Multilevel thresholding [Sando 98]: The previous discretization can be generalized to $\ell_n$ levels by introducing $n-1$ thresholds levels $\Gamma_i$, $1 \leq i \leq n-1$ as follows:

$$g\left(x\right) = \begin{cases} \ell_1 & \Gamma_1 < x \leq x \\ \ell_2 & \Gamma_2 \leq x < \Gamma_1 \\ & \vdots \\ \ell_n & x < \Gamma_{n-1} \end{cases} \tag{A.14}$$

   According to [Sando 98], the number of binary chaotic sequences obtained with this method for a given correlation bound is larger than the previous method.

3. Direct binarization of the sequences [Wang 05] by means of the method of equation A.15:

$$\begin{aligned} M\left(n\right) &= int\left[x\left(n\right) \cdot 10^{\mu}\right] mod\left(2^{\nu}\right) \\ K\left(n\right) &= bin\left[M\left(n\right)\right] \end{aligned} \tag{A.15}$$

   Where $\upsilon$ is the number of bits used in the data conversion, $\mu$ is an integer that represents the number of decimals used in the quantization and $K\left(n\right)$ is the binarized version of $M\left(n\right)$. The drawback of this method is that the computer precision is finite, and consequently the correlation properties of the chaotic sequences will be degraded.

Another common option is the use of Direct Chaotic Communication (DCC) methods. This method consists on the direct transmission of the real sequences, i.e. without any kind of quantization nor up-conversion. They are generated and transmitted in baseband

by means of analog circuits that model the dynamical system. One of the most common circuits is the one designed by Chua [Chua 92]. Due to the fact that these sequences, in chaotic regimen, are noise-like sequences (they have an almost flat power spectrum). Therefore, in DCC, chaotic sequences are passed through a band-pass filter to use only the required spectrum. The filtering process has the drawback of degrading the correlation properties of the chaotic sequences. Nonetheless, DCC method gives priority to simple implementation over performance. In fact, DCC receivers are in practice non-coherent, as they are based on envelope detection [Chong 05]. This implies lower accuracy and robustness in the position estimation in a LPS.

# Appendix B

# Useful Tables

| | | | $L_{\|CSS}$ | | | | |
|---|---|---|---|---|---|---|---|
| $N$ | $M$ | $P$ | $K_{\|CSS}=2$ | $K_{\|CSS}=4$ | $K_{\|CSS}=8$ | $K_{\|CSS}=16$ | $K_{\|CSS}=32$ |
| 1 | 0 | 0 | 2 | 4 | 8 | 16 | 32 |
| 2 | 0 | 0 | 4 | 8 | 16 | 32 | 64 |
| 3 | 0 | 0 | 8 | 16 | 32 | 64 | 128 |
| 0 | 1 | 0 | 10 | 20 | 40 | 80 | 160 |
| 4 | 0 | 0 | 16 | 32 | 64 | 128 | 256 |
| 1 | 1 | 0 | 20 | 40 | 80 | 160 | 320 |
| 0 | 0 | 1 | 26 | 52 | 104 | 208 | 416 |
| 5 | 0 | 0 | 32 | 64 | 128 | 256 | 512 |
| 2 | 1 | 0 | 40 | 80 | 160 | 320 | |
| 1 | 0 | 1 | 52 | 104 | 208 | 416 | |
| 6 | 0 | 0 | 64 | 128 | 256 | 512 | |
| 3 | 1 | 0 | 80 | 160 | 320 | | |
| 0 | 2 | 0 | 100 | 200 | 400 | | |
| 2 | 0 | 1 | 104 | 208 | 416 | | |
| 7 | 0 | 0 | 128 | 256 | 512 | | |
| 4 | 1 | 0 | 160 | 320 | | | |
| 1 | 2 | 0 | 200 | 400 | | | |
| 3 | 0 | 1 | 208 | 416 | | | |
| 8 | 0 | 0 | 256 | 512 | | | |
| 0 | 1 | 1 | 260 | | | | |
| 5 | 1 | 0 | 320 | | | | |
| 2 | 2 | 0 | 400 | | | | |
| 4 | 0 | 1 | 416 | | | | |
| 9 | 0 | 0 | 512 | | | | |

Table B.1: CSS lengths up to 512 bits generated with the proposals of Chapter 4.

| | $K_{\|LS}=4$ | | $K_{\|LS}=8$ | | $K_{\|LS}=16$ | | $K_{\|LS}=32$ | |
|---|---|---|---|---|---|---|---|---|
| $L_{\|CSS}$; $(K_{\|CSS}=2)$ | $L_{\|LS}$ | $ZCZ$ | $L_{\|LS}$ | $ZCZ$ | $L_{\|LS}$ | $ZCZ$ | $L_{\|LS}$ | $ZCZ$ |
| 2 | 19 | 3 | 35 | 3 | 67 | 3 | 131 | 3 |
| 4 | 39 | 7 | 71 | 7 | 135 | 7 | 263 | 7 |
| 8 | 79 | 15 | 143 | 15 | 271 | 15 | 527 | 15 |
| 10 | 99 | 19 | 179 | 19 | 339 | 19 | 659 | 19 |
| 16 | 159 | 31 | 287 | 31 | 543 | 31 | 1055 | 31 |
| 20 | 199 | 39 | 359 | 39 | 679 | 39 | 1319 | 39 |
| 26 | 259 | 51 | 467 | 51 | 883 | 51 | 1715 | 51 |
| 32 | 319 | 63 | 575 | 63 | 1087 | 63 | | |
| 40 | 399 | 79 | 719 | 79 | 1359 | 79 | | |
| 52 | 519 | 103 | 935 | 103 | 1767 | 103 | | |
| 64 | 639 | 127 | 1151 | 127 | | | | |
| 80 | 799 | 159 | 1439 | 159 | | | | |
| 100 | 999 | 199 | 1799 | 199 | | | | |
| 104 | 1039 | 207 | 1871 | 207 | | | | |
| 128 | 1279 | 255 | | | | | | |
| 160 | 1599 | 319 | | | | | | |
| 200 | 1999 | 399 | | | | | | |

Table B.2: LS sequences parameters for $L_{|LS} < 2000$ generated with the algorithm proposed in Chapter 5.

| | $K_{\|GPC} = 4$ | | $K_{\|GPC} = 8$ | | $K_{\|GPC} = 16$ | | $K_{\|GPC} = 32$ | |
|---|---|---|---|---|---|---|---|---|
| $L_{\|CSS}$; $(K_{\|CSS} = 2)$ | $L_{\|GPC}$ | $ZCZ$ | $L_{\|GPC}$ | $ZCZ$ | $L_{\|GPC}$ | $ZCZ$ | $L_{\|GPC}$ | $ZCZ$ |
| 2 | 8 | 3 | 16 | 3 | 32 | 3 | 64 | 3 |
| 4 | 16 | 7 | 32 | 7 | 64 | 7 | 128 | 7 |
| 8 | 32 | 15 | 64 | 15 | 128 | 15 | 256 | 15 |
| 10 | 40 | 19 | 80 | 19 | 160 | 19 | 320 | 19 |
| 16 | 64 | 31 | 128 | 31 | 256 | 31 | 512 | 31 |
| 20 | 80 | 39 | 160 | 39 | 320 | 39 | 640 | 39 |
| 26 | 104 | 51 | 208 | 51 | 416 | 51 | 832 | 51 |
| 32 | 128 | 63 | 256 | 63 | 512 | 63 | 1024 | 63 |
| 40 | 160 | 79 | 320 | 79 | 640 | 79 | 1280 | 79 |
| 52 | 208 | 103 | 416 | 103 | 832 | 103 | 1664 | 103 |
| 64 | 256 | 127 | 512 | 127 | 1024 | 127 | | |
| 80 | 320 | 159 | 640 | 159 | 1280 | 159 | | |
| 100 | 400 | 199 | 800 | 199 | 1600 | 199 | | |
| 104 | 416 | 207 | 832 | 207 | 1664 | 207 | | |
| 128 | 512 | 255 | 1024 | 255 | | | | |
| 160 | 640 | 319 | 1280 | 319 | | | | |
| 200 | 800 | 399 | 1600 | 399 | | | | |
| 208 | 832 | 415 | 1664 | 415 | | | | |
| 256 | 1024 | 511 | | | | | | |
| 260 | 1040 | 519 | | | | | | |
| 320 | 1280 | 639 | | | | | | |
| 400 | 1600 | 799 | | | | | | |
| 416 | 1664 | 831 | | | | | | |

Table B.3: GPC sequences parameters with $L_{|GPC} < 2000$ generated with the algorithm proposed in Chapter 5.

# Bibliography


[4DSP 13] 4DSP. `http://www.4dsp.com`, 2013. Accessed on January 8, 2013.

[Ackro 70] M. H. Ackroyd. "The design of Huffman sequences". *IEEE Transactions on Aerospace and Electronic Systems*, Vol. AES-6, No. 6, pp. 790–796, 1970.

[Ackro 72] M. H. Ackroyd. "Synthesis of efficient Huffman sequences". *IEEE Transactions on Aerospace and Electronic Systems*, Vol. AES-8, No. 1, pp. 2–8, 1972.

[Ackro 73] M. H. Ackroyd. "Optimum mismatched filters for sidelobe suppression". *IEEE Transactions on Aerospace and Electronic Systems*, Vol. AES-9, No. 2, pp. 214–218, 1973.

[Aczél 89] J. Aczél and J. Dhombres. *Functional Equations in Several Variables*. Cambridge University Press, 1989.

[Alvar 04] F. J. Álvarez, J. Ureña, M. Mazo, A. Hernández, J. J. García, and J. A. Jiménez. "Efficient generator and pulse compressor for complementary sets of four sequences". *Electronics Letters*, Vol. 40, No. 11, pp. 703–704, 2004.

[Alvar 05] F. J. Álvarez. *Codificación de emisiones ultrasónicas con secuencias complementarias para uso en exteriores*. PhD thesis, University of Alcalá. Department of Electronics, 2005.

[Alvar 06] F. J. Álvarez, J. Ureña, M. Mazo, A. Hernández, J. J. García, and C. De Marziani. "High reliability outdoor sonar prototype based on efficient signal coding". *IEEE Transactions on Ultrasonics, Ferroelectrics, and Frequency Control*, Vol. 53, No. 10, pp. 1862–1872, 2006.

[Analo 13] Analog Devices. `http://www.analog.com/en/index.html`, 2013. Accessed on January 8, 2013.

[Aviso 13] Avisoft Bioacoustics. `http://www.avisoft.com`, 2013. Accessed on January 17, 2013.

[Berli 92] L. M. Berliner. "Statistics, probability and chaos". *Statistical Science*, Vol. 7, No. 1, pp. 69–90, Feb. 1992.

[Bi 12] J. Bi and H. Rohling. "Complementary binary code design based on mismatched filter". *IEEE Transactions on Aerospace and Electronic Systems*, Vol. 48, No. 2, pp. 1793–1797, 2012.

[Boren 88] J. Borenstein and Y. Koren. "Obstacle avoidance with ultrasonic sensors". *IEEE Journal of Robotics and Automation*, Vol. 4, No. 2, pp. 213–218, 1988.

[Borwe 03] P. B. Borwein and R. A. Ferguson. "A complete description of Golay pairs for lengths up to 100". *Mathematics of Computation*, Vol. 73, No. 246, pp. 967–985, 2003.

[Brüel 13] Brüel & Kjær. `http://www.bksv.es`, 2013. Accessed on January 17, 2013.

[Budis 11] S. Z. Budišin. "Golay kernel 10 decomposition". *Electronics Letters*, Vol. 47, No. 15, pp. 853–855, 2011.

[Budis 87] S. Z. Budišin. "Supercomplementary sets of sequences". *Electronics Letters*, Vol. 23, No. 10, pp. 504–506, 1987.

[Budis 89] S. Z. Budišin. "Fast PN sequence correlation by using FWT". In: *Proceedings of the 1989 Mediterranean Electrotechnical Conference, MELECON'89*, pp. 513–515, 1989.

[Budis 90a] S. Z. Budišin. "New complementary pairs of sequences". *Electronics Letters*, Vol. 26, No. 13, pp. 881–883, 1990.

[Budis 90b] S. Z. Budišin. "New multilevel complementary pairs of sequences". *Electronics Letters*, Vol. 26, No. 22, pp. 1861–1863, 1990.

[Budis 91] S. Z. Budišin. "Efficient pulse compressor for Golay complementary sequences". *Electronics Letters*, Vol. 27, No. 3, pp. 219–220, 1991.

[Casti 13] J. M. Castilla. *Implementación en hardware configurable de correladores eficientes para parejas Golay derivadas de kernels de longitud 2,10 y 26.*

Master's thesis, University of Alcalá. Department of Electronics, 2013. To be presented.

[Chang 10] C.-Y. Chang. "New 64-QAM Golay complementary sequences". *IEEE Transaction on Information Theory*, Vol. 56, No. 5, pp. 2479–2485, 2010.

[Chen 01] H.-H. Chen, J.-F. Yeh, and N. Suehiro. "A multicarrier CDMA architecture based on orthogonal complementary codes for new generations of wideband wireless communications". *IEEE Communications Magazine*, Vol. 39, No. 10, pp. 126–135, 2001.

[Chen 04] H.-H. Chen. "Design of perfect complementary codes to implement interference free CDMA systems". In: *Proceedings of the 2004 IEEE Global Telecommunications Conference, GOBLECOM'04.*, pp. 1096–1100, 2004.

[Chen 06] H.-H. Chen, Y.-C. Yeh, X. Zhang, A. Huang, Y. Yang, J. Li, Y. Xiao, H. R. Sharif, and A. J. H. Vinck. "Generalized pairwise complementary codes with set-wise uniform interference-free windows". *IEEE Journal on Selected Areas in Communications*, Vol. 24, No. 1, pp. 65–74, 2006.

[Chen 07] H.-H. Chen. *The next generation CDMA technologies*. John Wiley, 2007.

[Chong 05] C.-C. Chong, S. K. Yong, and S. S. Lee. "UWB direct chaotic communication technology". *IEEE Antennas and Wireless Propagation Letters*, Vol. 4, pp. 316–319, 2005.

[Chu 72] D. Chu. "Polyphase codes with good periodic correlation properties (Corresp.)". *IEEE Transactions on Information Theory*, Vol. 18, No. 4, pp. 531–532, 1972.

[Chua 92] L. O. Chua. "The genesis of Chua's circuit". Tech. Rep. UCB/ERL M92/1, EECS Department, University of California, Berkeley, 1992.

[Coker 10] J. D. Coker and A. Tewfik. "Simplified ranging systems using discrete wavelet decomposition". *IEEE Transactions on Signal Processing*, Vol. 58, No. 2, pp. 575–582, 2010.

[Coole 65] J. W. Cooley and J. W. Tukey. "An algorithm for machine calculation of complex Fourier series". *Mathematics of Computation*, Vol. 19, No. 90, pp. 297–301, 1965.

[Craig 06] R. Craigen, S. Georgiou, W. Gibson, and C. Koukouvinos. "Further explorations into ternary complementary pairs". *Journal of Combinatorial Theory, Series A*, Vol. 113, No. 6, pp. 952–965, 2006.

[Darda 09] D. Dardari, A. Conti, U. Ferner, A. Giorgetti, and M. Z. Win. "Ranging with ultrawide bandwidth signals in multipath environments". *Proceedings of the IEEE*, Vol. 97, No. 2, pp. 404–426, 2009.

[Darne 88] M. Darnell and A. H. Kemp. "Synthesis of multilevel complementary sequences". *Electronics Letters*, Vol. 24, No. 19, pp. 1251–1252, 1988.

[Davis 99] J. A. Davis and L. Jedwab. "Peak-to-mean power control in OFDM, Golay complementary sequences, and Reed-Muller codes". *IEEE Transaction on Information Theory*, Vol. 45, No. 7, pp. 2397–2417, 1999.

[De Ma 06] C. De Marziani, J. Ureña, A. Hernández, M. Mazo, J. J. García, A. Jiménez, J. M. Villadangos, M. C. Pérez, A. Ochoa, and F. J. Álvarez. "Inter-symbol interference reduction on macro-sequences generated from complementary set of sequences". In: *Proceedings of the IEEE 32nd Annual Conference of the Industrial Electronics Society, IECON '06*, pp. 3367–3372, 2006.

[De Ma 07] C. De Marziani, J. Ureña, A. Hernández, M. Mazo, F. J. Álvarez, J. J. García, and P. Donato. "Modular architecture for efficient generation and correlation of complementary set of sequences". *IEEE Transactions on Signal Processing*, Vol. 55, No. 5, pp. 2323–2337, 2007.

[De Ma 11] C. De Marziani, J. Ureña, A. Hernández, J. J. García, F. J. Álvarez, A. Jiménez, and M. C. Pérez. "Recursive algorithm to directly obtain the sum of correlations in a CSS". *Signal Processing*, Vol. 91, No. 5, pp. 1343–1346, 2011.

[Devan 89] R. L. Devaney. *An introduction to chaotic dynamical systems.* Addison-Wesley, 2 Ed., 1989.

[Diaz 02] V. Díaz, D. Hernanz, and J. Ureña. "Using complementary sequences for direct transmission path identification". In: *Proceedings of the IEEE 28th Annual Conference of the Industrial Electronics Society, IECON '02*, pp. 2764–2767, Nov. 2002.

[Diego 11] C. Diego, Á. Hernández, A. Jiménez, F. J. Álvarez, R. Sanz, and J. Aparicio. "Ultrasonic array for obstacle detection based on CDMA with Kasami codes". *Sensors*, Vol. 11, No. 12, pp. 11464–11475, 2011.

[Donat 09a] P. Donato, M. A. Funes, M. N. Hadad, and D. O. Carrica. "Optimised Golay correlator". *Electronics Letters*, Vol. 45, No. 7, pp. 380–381, 2009.

[Donat 09b] P. G. Donato, M. A. Funes, M. N. Hadad, and D. O. Carrica. "Simultaneous correlation of orthogonal pairs of complementary sequences". *Electronics Letters*, Vol. 45, No. 25, pp. 1332–1334, 2009.

[Dummi 04] D. S. Dummit and R. M. Foote. *Abstract algebra.* John Wiley & Sons, 3 Ed., 2004.

[Europ 98] European Telecommunications Standards Institute, ETSI. "ETSI Technical Report: UMTS XX.12 v0.1.0 (1998-12). UTRA TDD; radio transmission and reception". 1998.

[Falsi 06] C. Falsi, D. Dardari, L. Mucchi, and M. Z. Win. "Time of arrival estimation for UWB localizers in realistic environments". *EURASIP Journal on Applied Signal Processing*, Vol. 2006, No. 032082, pp. 1–13, 2006.

[Fan 03] P. Fan, J. Li, and Y. Pan. "Special issue: coding and its applications in CDMA wireless systems". *Wireless Communications and Mobile Computing*, Vol. 3, No. 5, pp. 549–551, 2003.

[Fan 04] P. Fan. "Spreading sequence design and theoretical limits for quasisynchronous CDMA systems". *EURASIP Journal on Wireless Communications and Networking*, Vol. 2004, No. 1, pp. 19–31, 2004.

[Fan 07] P. Fan, W. Yuan, and Y. Tu. "Z-complementary binary sequences". *IEEE Signal Processing Letters*, Vol. 14, No. 8, pp. 509–512, 2007.

[Fan 96] P. Fan and M. Darnell. *Sequence design for communications applications.* Research Studies Press, 1996.

[Feder 02] Federal Communications Commission. "First report and order. FCC 02-48". Tech. Rep., FCC, 2002.

[Fonta 03] R. J. Fontana, E. Richley, and J. Barney. "Commercialization of an ultra wideband precision asset location system". In: *Proceedings of the IEEE Conference on Ultra Wideband Systems and Technologies*, pp. 369–373, 2003.

[Fract 13] Fractus. `http://www.fractus.com`, 2013. Accessed on January 8, 2013.

[Frank 62] R. Frank, S. Zadoff, and R. Heimiller. "Phase shift pulse codes with good periodic correlation properties (Corresp.)". *IRE Transactions on Information Theory*, Vol. 8, No. 6, pp. 381–382, 1962.

[Frank 63] R. Frank. "Polyphase codes with good nonperiodic correlation properties". *IEEE Transactions on Information Theory*, Vol. 9, No. 1, pp. 43–45, 1963.

[Frank 80] R. Frank. "Polyphase complementary codes". *IEEE Transactions on Information Theory*, Vol. 26, No. 6, pp. 641–647, 1980.

[Funes 10] M. A. Funes, P. G. Donato, M. N. Hadad, and D. O. Carrica. "Reduced architecture for simultaneous correlation of orthogonal sets of complementary sequences". *Electronics Letters*, Vol. 46, No. 22, pp. 1502–1504, 2010.

[Garci 06] D. L. García. *Estimación óptima de secuencias caóticas con aplicación en comunicaciones*. PhD thesis, Universidad de Cantabria. Grupo de Tratamiento Avanzado de Señal, 2006.

[Garci 11] E. García, S. Holm, J. J. García, and J. Ureña. "Link budget for low bandwidth and coded ultrasonic indoor location systems". In: *Proceedings of the 2011 IEEE International Conference on Indoor Positioning and Indoor Navigation, IPIN '11*, 2011.

[Gavis 94] A. Gavish and A. Lempel. "On ternary complementary sequences". *IEEE Transaction on Information Theory*, Vol. 40, No. 2, pp. 522–526, 1994.

[Golay 61] M. J. E. Golay. "Complementary series". *IRE Transactions on Information Theory*, Vol. 7, No. 2, pp. 82–87, 1961.

[Golay 62] M. J. E. Golay. "Note on 'Complementary series'". *Proceedings of IRE*, Vol. 50, p. 84, 1962.

[Golay 72] M. J. E. Golay. "A class of finite binary sequences with alternate autocorrelation values equal to zero (Corresp.)". *IEEE Transactions on Information Theory*, Vol. 18, No. 3, pp. 449–450, 1972.

[Gold 67] R. Gold. "Optimal binary sequences for spread spectrum multiplexing (Corresp.)". *IEEE Transactions on Information Theory*, Vol. 13, No. 4, pp. 619–621, 1967.

[Golom 82] S. W. Golomb. *Shift register sequences.* Aegean Park Press, revised second Ed., 1982.

[Gonza 09] M. González, L. Prados, J. A. Rubio, J. C. Segura, Á. De la Torre, J. M. Moya, P. Rodríguez, and M. J. L. "ATLINTIDA: A robust indoor ultrasound location system: design and evaluation". In: *Advances in Soft Computing. 3rd symposium of ubiquitous computing and ambient intelligence*, pp. 180–190, 2009.

[Green 84] P. J. Green. "Iteratively reweighted least squares for maximum likelihood estimation, and some robust and resistant alternatives". *Journal of the Royal Statistical Society. Series B (Methodological)*, Vol. 46, No. 2, pp. 149–192, 1984.

[Griep 95] K. R. Griep, J. A. Ritcey, and J. J. Burlingame. "Polyphase codes and optimal filters for multiple user ranging". *IEEE Transactions on Aerospace and Electronic Systems*, Vol. 31, No. 2, pp. 752–767, 1995.

[Guven 05] I. Guvenc and Z. Sahinoglu. "Threshold-based TOA estimation for impulse radio UWB systems". In: *Proceedings of the IEEE International Conference on Ultra-Wideband, ICU '05*, pp. 420–425, 2005.

[Gysin 01] M. Gysin and J. Seberry. "On ternary complementary pairs". *Australasian Journal of Combinatorics*, Vol. 23, pp. 153–170, 2001.

[Hazas 02] M. Hazas and A. Ward. "A novel broadband ultrasonic location system". In: Springer-Verlag, Ed., *Proceedings if the 4th International Conference on Ubiquitous Computing, UbiComp '02*, pp. 264–280, 2002.

[Hazas 03] M. Hazas and A. Ward. "A high performance privacy-oriented location system". In: *Proceedings of the 1st IEEE International Conference on Pervasive Computing and Communications, PerCom '03*, pp. 216–223, 2003.

[He 11] L. He, Z. Wang, F. Yang, S. Chen, and L. Hanzo. "Preamble design using embedded signaling for OFDM broadcast systems based on reduced complex-

ity distance detection". *IEEE Transaction on Vehicular Technology*, Vol. 60, No. 3, pp. 1217–1222, 2011.

[Herna 04] A. Hernández, J. Ureña, J. J. García, M. Mazo, D. Hernanz, J.-P. Derutin, and J. Serot. "Ultrasonic ranging sensor using simultaneous emissions from different transducers". *IEEE Transactions on Ultrasonics, Ferroelectrics and Frequency Control*, Vol. 51, No. 12, pp. 1660–1670, 2004.

[Holm 05] S. Holm. "Airborne ultrasound data communications: the core of an indoor positioning system". In: *Proceedings of the 2005 IEEE Ultrasonics Symposium*, pp. 1801–1804, 2005.

[Holm 09] S. Holm. "Hybrid ultrasound-RFID indoor positioning: combining the best of both worlds". In: *Proceedings of the 2009 IEEE International Conference on RFID*, pp. 155–162, 2009.

[Huang 11] Y.-W. Huang and Y. Li. "16-QAM Golay complementary sequences with new sequence lengths". In: *Proceedings of the IEEE International Symposium on Information Theory, ISIT '11*, 2011.

[Huffm 62] D. Huffman. "The generation of impulse-equivalent pulse trains". *IRE Transactions on Information Theory*, Vol. 8, No. 5, pp. 10–16, 1962.

[IDTec 12] IDTechEx. `http://www.idtechex.com`, 2012. Accessed on December 2, 2012.

[IEEE 05] IEEE-SA Standards Board. "IEEE Std. 802.15.1, part 15.1: wireless Medium Access Control (MAC) and Physical Layer (PHY) specifications for Wireless Personal Area Networks (WPANs)". 2005.

[IEEE 99] IEEE-SA Standards Board. "IEEE Std. 802.11.b, part 11: wireless LAN Medium Access Control (MAC) and Physical Layer (PHY) specifications: Higher-speed physical layer extension in the 2-4 GHz band". 1999.

[Irahh 06] Z. Irahhauten, G. Bellusci, G. J. M. Janssen, H. Nikookar, and C. Tiberius. "Investigation of UWB ranging in dense indoor multipath environments". In: *Proceedings of the 10th IEEE Singapore International Conference on Communication systems, ICCS '06*, pp. 1–5, 2006.

[Jaure 62] S. J. Jauregui. "Complementary sequences of length 26 (Corresp.)". *IRE Transactions on Information Theory*, Vol. 8, No. 4, p. 323, 1962.

[Jedwa 04] J. Jedwab. "A survey of the merit factor problem for binary sequences". In: *Proceedings of the 3rd International Conference on Sequences and Their Applications, SETA '04*, pp. 30–55, Springer-Verlag Berlin, 2004.

[Jian 07] W. Jian, L. Jianguo, and D. Li. "Synchronization for MIMO OFDM systems with Loosely Synchronized (LS) codes". In: *Proceedings of the 2007 International Conference on Wireless Communications, Networking and Mobile Computing, WiCom '07.*, pp. 254–258, 2007.

[Johns 98] J. Johnson, R., P. Schniter, T. J. Endres, J. D. Behm, D. R. Brown, and R. A. Casas. "Blind equalization using the constant modulus criterion: a review". *Proceedings of the IEEE*, Vol. 86, No. 10, pp. 1927–1950, 1998.

[Kasam 66] T. Kasami. "Weight distribution formula for some class of cyclic codes". Tech. Rep. R-285, Coordinated Science Laboratoy, University of Illinois, 1966.

[Kemp 89] A. H. Kemp and M. Darnell. "Synthesis of uncorrelated and nonsquare sets of multilevel complementary sequences". *Electronics Letters*, Vol. 25, No. 12, pp. 791–792, 1989.

[Kerdo 72] A. M. Kerdock. "A class of low-rate nonlinear binary codes". *Information and Control*, Vol. 20, No. 2, pp. 182–187, 1972.

[Kim 06] W. Kim, H. K. Chung, K. C. Lee, H. Jeon, J. Cha, and H. Lee. "LS codes aided channel estimation for MIMO-OFDM systems in multipath environment". In: *Proceedings of the 2006 Vehicular Technology Conference, VTC '06.*, pp. 1–5, 2006.

[Knapp 76] C. Knapp and G. Carter. "The generalized correlation method for estimation of time delay". *IEEE Transactions on Acoustics Speech and Signal Processing*, Vol. 24, No. 4, pp. 320–327, 1976.

[Krets 88] F. F. Kretschmer and K. R. Gerlach. "Low sidelobe pulse compression waveforms". In: *Proceedings of the 22nd Asilomar Conference on Signals, Systems and Computers*, pp. 663–667, 1988.

[Kuhn 10] M. J. Kuhn, J. Turnmire, M. R. Mahfouz, and A. E. Fathy. "Adaptive leading-edge detection in UWB indoor localization". In: *Proceedings of the 2010 IEEE Radio and Wireless Symposium, RWS '10*, pp. 268–271, 2010.

[Lahto 95] J. Lahtonen. "On the odd and the aperiodic correlation properties of the Kasami sequences". *IEEE Transaction on Information Theory*, Vol. 41, No. 5, pp. 1506–1508, 1995.

[Leave 09] C. Leavens, R. Willams, P. Burns, and M. Sherar. "The use of phase codes in ultrasound imaging: SNR gain and bandwidth requirements". *Applied Acoustics*, Vol. 70, No. 10, pp. 1340–1351, 2009.

[Lee 06] H. Lee and S. H. Golomb. "A new construction of 64-QAM Golay complemetary sequences". *IEEE Transactions on Information Theory*, Vol. 52, No. 4, pp. 2479–2485, May 2006.

[Levan 04] N. Levanon and E. Mozeson. *Radar signals*. John Wiley & Sons, 2004.

[Levan 05] N. Levanon. "Cross-correlation of long binary signals with longer mismatched filters". *IEE Proceedings- Radar, Sonar & Navigation*, Vol. 152, No. 6, pp. 377–382, 2005.

[Leven 99] V. I. Levenshtein. "New lower bounds on aperiodic crosscorrelation of binary codes". *IEEE Transactions on Information Theory*, Vol. 45, No. 1, pp. 284–288, 1999.

[Lewis 81] B. L. Lewis and F. F. Kretschmer. "A new class of polyphase pulse compression codes and techniques". *IEEE Transactions on Aerospace and Electronic Systems*, Vol. AES-17, No. 3, pp. 364–372, 1981.

[Lewis 82] B. L. Lewis and F. F. Kretschmer. "Linear frequency modulation derived polyphase pulse compression codes". *IEEE Transactions on Aerospace and Electronic Systems*, Vol. AES-18, No. 5, pp. 637–641, 1982.

[Li 00] D. Li. "LAS-CDMA meeting". Tech. Rep., Third Generation Partnership Project 2, CWTS, WG-1, April 10, 2000.

[Li 02] D. Li. "A method for spread spectrum multiple access coding with zero correlation window". European Patent: EP 1257077, 2002.

[Li 03] D. Li. "The perspectives of large area synchronous CDMA technology for the fourth-generation mobile radio". *IEEE Communications Magazine*, Vol. 41, No. 3, pp. 114–118, 2003.

[Li 08] J. Li, A. Huang, M. Guizani, and H.-H. Chen. "Inter-group complementary codes for interference-resistant CDMA wireless communications". *IEEE Transactions on Wireless Communications*, Vol. 7, No. 1, pp. 166–174, 2008.

[Li 10] S. F. Li, J. Chen, and L. Q. Zhang. "Optimisation of complete complementary codes in MIMO radar system". *Electronics Letters*, Vol. 46, No. 16, pp. 1157–1159, 2010.

[Li 11a] X. Li, P. Fan, X. Tang, and Y. Tu. "Existence of binary Z-complementary pairs". *IEEE Signal Processing Letters*, Vol. 18, No. 1, pp. 63–66, 2011.

[Li 11b] X. D. Li, P. Z. Fan, W. H. Mow, and M. Darnell. "Multilevel perfect sequences over integers". *Electronics Letters*, Vol. 47, No. 8, pp. 496–497, 2011.

[Lie 05] J. P. Lie, M. S. Chong, and P. N. Boon. "UWB ranging with high robustness against dominant jammer and multipath". *IEEE Microwave and Wireless Components Letters*, Vol. 15, No. 12, pp. 907–909, 2005.

[Lim 99] Y. C. Lim, R. Yang, D. Li, and J. Song. "Signed power-of-two term allocation scheme for the design of digital filters". *IEEE Transactions on Circuits and Systems II: Analog and Digital Signal Processing*, Vol. 46, No. 5, pp. 577–584, May 1999.

[Liu 11a] Z. L. Liu, Y. L. Guan, and W. H. Mow. "Improved lower bound for quasi-complementary sequence set". In: *Proceedings of the IEEE International Symposium on Information Theory, ISIT '11*, pp. 489–493, 2011.

[Liu 11b] Z. L. Liu, Y. L. Guan, B. C. Ng, and H.-H. Chen. "Correlation and set size bounds of complementary sequences with low correlation zone". *IEEE Transactions on Communications*, Vol. 59, No. 12, pp. 3285–3289, 2011.

[Liu 92] S.-C. Liu and J. J. Komo. "Nonbinary Kasami sequences over GF(p)". *IEEE Transactions on Information Theory*, Vol. 38, No. 4, pp. 1409–1412, 1992.

[Mahfo 08] M. R. Mahfouz, C. Zhang, B. C. Merkl, M. J. Kuhn, and A. E. Fathy. "Investigation of high-accuracy indoor 3-D positioning using UWB technology". *Microwave Theory and Techniques, IEEE Transactions on*, Vol. 56, No. 6, pp. 1316–1330, 2008.

[Meyer 01] U. Meyer-Bäese. *Digital signal processing with filed programmable gate arrays*. Springer-Verlag Berlin, 2001.

[Mini 13] Mini-Circuits. `http://minicircuits.com/`, 2013. Accessed on January 2, 2013.

[Misar 05] T. Misaridis and J. A. Jensen. "Use of modulated excitation signals in medical ultrasound. Part I: basic concepts and expected benefits". *IEE Transactions on Ultrasonics, Ferroelectrics, and Frequency Control*, Vol. 52, No. 2, pp. 177–191, 2005.

[Pared 11] J. A. Paredes, T. Aguilera, F. J. Álvarez, J. Lozano, and J. Morera. "Analysis of Doppler effect on the pulse compression of different codes emitted by an ultrasonic LPS". *Sensors (Basel)*, Vol. 11, No. 11, pp. 10765–10784, 2011.

[Peng 04] D. Y. Peng and P. Z. Fan. "Generalised Sarwate bounds on the aperiodic correlation of sequences over complex roots of unity". *IEE Proceedings- Communications*, Vol. 151, No. 4, pp. 375–382, 2004.

[Perez 07a] M. C. Pérez, J. Ureña, A. Hernández, and W. P. De Marziani, C. Jiménez A. Marnane. "Hardware implementation of an efficient correlator for interleaved complementary sets of sequences". *Journal of Universal Computer Science*, Vol. 13, No. 3, pp. 388–406, 2007.

[Perez 07b] M. C. Pérez, J. Ureña, A. Hernández, A. Jiménez, W. P. Marnane, and F. J. Álvarez. "Efficient real-time correlator for LS sequences". In: *Proceedings of the 2007 IEEE International Symposium on Industrial Electronics, ISIE '07*, pp. 1663–1668, 2007.

[Perez 08] M. C. Pérez, J. Ureña, A. Hernández, F. J. Álvarez, A. Jiménez, and C. De Marziani. "Efficient correlator for LS codes generated from orthogonal CSS". *IEEE Communications Letters*, Vol. 12, No. 10, pp. 764–766, 2008.

[Perez 09a] M. C. Pérez. *Generación y correlación eficiente de códigos binarios derivados de conjuntos de secuencias complementarias para sistemas ultrasónicos*. PhD thesis, University of Alcalá. Department of Electronics, 2009.

[Perez 09b] M. C. Pérez, J. Ureña, A. Hernández, A. Jiménez, and C. De Marziani. "Efficient generation and correlation of sequences pairs with three zero-correlation zones". *IEEE Transactions on Signal Processing*, Vol. 57, No. 9, pp. 3450–3465, 2009.

[Perez 09c] M. C. Pérez, J. Ureña, A. Hernández, A. Jiménez, D. Ruiz, F. J. Álvarez, and C. De Marziani. "Performance comparison of different codes in an ultrasonic positioning system using DS-CDMA". In: *Proceedings of the 6th IEEE International Symposium on Intelligent Signal Processing, WISP '09*, pp. 125–130, 2009.

[Perez 10] M. C. Pérez, J. Ureña, C. De Marziani, A. Hernández, J. J. García, and F. J. Álvarez. "Very efficient correlator for loosely synchronised codes". *Electronics Letters*, Vol. 46, No. 16, pp. 1127–1129, 2010.

[Perez 11] M. C. Pérez, J. Ureña, A. Hernández, C. De Marziani, J. J. García, and A. Jiménez. "Optimized correlator for LS codes-based CDMA systems". *IEEE Communications Letters*, Vol. 15, No. 2, pp. 223–225, 2011.

[Perez 12] M. C. Pérez, R. Serrano, J. Ureña, A. Hernández, C. De Marziani, and F. J. Álvarez. "Correlator implementation for orthogonal CSS used in an ultrasonic LPS". *IEEE Sensors Journal*, Vol. 12, No. 9, pp. 2807–2816, 2012.

[Phoon 05] S.-M. Phoong and K.-Y. Chang. "Antipodal paraunitary matrices and their application to OFDM systems". *IEEE Transactions on Signal Processing*, Vol. 53, No. 4, pp. 1374–1386, 2005.

[Pietr 10] M. M. Pietrzyk and T. von der Grun. "Experimental validation of a TOA UWB ranging platform with the energy detection receiver". In: *Proceedings of the 2010 International Conference on Indoor Positioning and Indoor Navigation, IPIN '10*, pp. 1–8, 2010.

[Pinke 92] R. Pinkel and J. A. Smith. "Repeat-sequence coding for improved precision of Doppler sonar and sodar". *Journal of Atmospheric and Oceanic Technology*, Vol. 9, No. 2, pp. 149–163, 1992.

[Popov 87] B. M. Popovic and S. Z. Budišin. "Generalised subcomplementary sets of sequences". *Electronics Letters*, Vol. 23, No. 8, pp. 422–424, 1987.

[Popov 99a] B. M. Popovic. "Efficient Golay correlator". *Electronics Letters*, Vol. 35, No. 17, pp. 1427–1428, 1999.

[Popov 99b] B. M. Popovic. "Spreading sequences for multicarrier CDMA systems". *IEEE Transactions on Communications*, Vol. 47, No. 6, pp. 918–926, 1999.

[Priet 07] J. C. Prieto, A. R. Jiménez, and J. I. Guevara. "Subcentimeter-accuracy localization through broadband acoustic transducers". In: *Proceedings of the 2007 IEEE International Symposium on Intelligent Signal Processing, WISP '07*, pp. 1–6, 2007.

[Priya 00] N. B. Priyantha, A. Chakraborty, and H. Balakrishnan. "The Cricket location-support system". In: *Proceedings of the 6th Annual ACM International Conference on Mobile Computing and Networking, MOBICOM '00*, 2000.

[Proak 00] J. G. Proakis. *Digital communications*. McGraw-Hill, 2000.

[Proak 96] J. G. Proakis and D. G. Manolakis. *Digital signal processing*. Prentice-Hall, 3rd Ed., 1996.

[Rade 04] L. Råde and B. Westergren. *Mathemathics handbook for science and engineering*. Springer-Verlag Berlin, 5th Ed., 2004.

[Regal 89] P. A. Regalia and S. K. Mitra. "Kronecker products, unitary matrices and signal processing applications". *Society for Industrial ans Applied Mathematics*, Vol. 31, No. 4, pp. 586–613, 1989.

[Rihac 71] A. W. Rihaczek and R. M. Golden. "Range sidelobe suppresion for Barker codes". Vol. AES-7, No. 6, pp. 1087–1092, 1971.

[Rudin 59] W. Rudin. "Some theorems on Fourier coefficients". *Proceedings of the American Mathematical Society*, Vol. 10, pp. 855–859, 1959.

[Ruiz 11] D. Ruiz, J. Ureña, J. C. García, A. Jiménez, A. Hernández, and J. J. García. "LPS auto-calibration algorithm with predetermination of optimal zones". *Sensors*, Vol. 11, No. 11, pp. 10398–10414, 2011.

[Saad 12] M. M. Saad, C. J. Bleakley, T. Ballal, and S. Dobson. "High-accuracy reference-free ultrasonic location estimation". *IEEE Transactions on Instrumentation and Measurement*, Vol. 61, No. 6, pp. 1561–1570, 2012.

[Sahin 08] Z. Sahinoglu, S. Gezici, and I. Guvenc. *Ultra-wideband positioning systems. Theoretical Limits, ranging algorithms and protocols*. Cambridge University Press, 2008.

[Sando 98] D. Sandoval-Morantes and D. Muñoz-Rodríguez. "Chaotic sequences for multiple access". *Electronics Letters*, Vol. 34, No. 3, pp. 235–237, Feb. 1998.

[Sarwa 79] D. Sarwate. "Bounds on crosscorrelation and autocorrelation of sequences (Corresp.)". *IEEE Transactions on Information Theory*, Vol. 25, No. 6, pp. 720–724, 1979.

[Schol 00] D. P. Scholnik. "Optimal filters for range-time sidelobe suppresion". In: *X European Signal Processing Conference, EUSIPCO*, 2000.

[Schro 05] J. Schroeder, S. Galler, and K. Kyamakya. "A low-cost experimental ultra-wideband positioning system". In: *Proceedings of the 2005 IEEE International Conference on Ultra-Wideband, ICU '05*, pp. 632 – 637, 2005.

[Seber 92] J. Seberry and M. Yamada. *Contemporary design theory: A collection of surveys*, Chap. Hadamard matrices, sequences, and block designs, pp. 431–560. John Wiley & Sons, 1992.

[Segur 10] M. Segura, H. Hashemi, C. Sisterna, and V. Mut. "Experimental demonstration of self-localized ultra wideband indoor mobile robot navigation system". In: *Proceedings of the 2010 IEEE International Conference on Indoor Positioning and Indoor Navigation, IPIN '10*, 2010.

[Shapi 51] H. S. Shapiro. *Extremal problems for polynomials and power series*. Master's thesis, Massachusets Institute of Technology, 1951.

[Sirol 10] N. Sirola. "Close-form algorithms in mobile positioning: myths and misconceptions". In: *Proceedings of the 7th Workshop on Positioning Navigation and Communication, WPNC '10*, pp. 38–44, 2010.

[Sivas 78a] R. Sivaswamy. "Digital and analog subcomplementary sequences for pulse compression". *IEEE Transactions on Aerospace and Electronic Systems*, Vol. AES-14, No. 2, pp. 343–350, 1978.

[Sivas 78b] R. Sivaswamy. "Multiphase complementary codes". *IEEE Transactions on Information Theory*, Vol. 24, No. 5, pp. 546–552, 1978.

[Sivas 82] R. Sivaswamy. "Self-clutter cancellation and ambiguity properties of subcomplementary sequences". *IEEE Transactions on Aerospace and Electronic Systems*, Vol. AES-18, No. 2, pp. 163–181, 1982.

[Sobot 06] M. Sobottka and L. P. L. De Oliveira. "Periodicity and predictability in chaotic systems". *The American Mathematical Monthly*, Vol. 113, No. 5, pp. 415–424, May 2006.

[Stanc 01] S. Stanczak, H. Boche, and M. Haardt. "Are LAS-codes a miracle?". In: *Proceedings of the 2001 IEEE Global Telecommunications Conference, GLOBECOM '01*, pp. 589–593, 2001.

[Stoic 06] L. Stoica, A. Rabbachin, and I. Oppermann. "A low-complexity noncoherent IR-UWB transceiver architecture with TOA estimation". *IEEE Transactions on Microwave Theory and Techniques*, Vol. 54, No. 4, pp. 1637–1646, 2006.

[Suehi 88] N. Suehiro and M. Hatori. "N-shift cross-orthogonal sequences". *IEEE Transaction on Information Theory*, Vol. 34, No. 1, pp. 143–146, Jan. 1988.

[Suehi 94] N. Suehiro. "A signal design without co-channel interference for approximately synchronized CDMA systems". *IEEE Journal on Selected Areas in Communications*, Vol. 12, No. 5, pp. 837–841, 1994.

[Sun 11] Z. Sun, X. Zeng, and L. Hu. "Aperiodic correlation of Kasami sequences in the small set". *Applicable Algebra in Engineering, Communication and Computing*, Vol. 4, No. 4, pp. 311–320, 2011.

[Sylve 67] J. J. Sylvester. "Thoughts on inverse orthogonal matrices, simultaneous sign successions, and tesselated pavements in two or more colours, with applications to Newton's rule, ornamental tile-work, and the theory of numbers". *Phylosophical Magazine*, Vol. 34, pp. 461–475, 1867.

[Tabor 13] Tabor Electronics. `http://www.taborelec.com`, 2013. Accessed on January 17, 2013.

[Taki 69] Y. Taki, H. Miyakawa, M. Hatori, and S. Namba. "Even-shift orthogonal sequences". *IEEE Transactions on Information Theory*, Vol. 15, No. 2, pp. 295–300, March 1969.

[Tang 01a] X. H. Tang and P. Fan. "Bounds on aperiodic and odd correlations of spreading sequences with low and zero correlation zone". *Electronics Letters*, Vol. 37, No. 19, pp. 1201–1203, 2001.

[Tang 01b] X. H. Tang and P. Z. Fan. "A class of pseudonoise sequences over GF(P) with low correlation zone". *IEEE Transaction on Information Theory*, Vol. 47, No. 4, pp. 1644–1649, May 2001.

[Tang 06] X. Tang and W. H. Mow. "Design of spreading codes for quasi-synchronous CDMA with intercell interference". *IEEE Journal on Selected Areas in Communications*, Vol. 24, No. 1, pp. 84–93, 2006.

[Times 13] Times Microwave Systems. `http://www.timesmicrowave.com/cgi-bin/calculate.pl`, 2013. Accessed on January 2, 2013.

[Trinh 06] Q. K. Trinh, P. Fan, and E. M. Gabidulin. "Multilevel Hadamard matrices and zero correlation zone sequences". *Electronics Letters*, Vol. 42, No. 13, pp. 748–750, 2006.

[Tseng 00] S.-M. Tseng and M. R. Bell. "Asynchronous multicarrier DS-CDMA using mutually orthogonal complementary sets of sequences". *IEEE Transactions on Communications*, Vol. 48, No. 1, pp. 53–59, 2000.

[Tseng 72] C.-C. Tseng and C. Liu. "Complementary sets of sequences". *IEEE Transactions on Information Theory*, Vol. 18, No. 5, pp. 644–652, 1972.

[Turyn 61] R. Turyn and J. Storer. "On binary sequences". *Proceedings of the American Mathematical Society*, Vol. 12, No. 3, pp. 394–399, 1961.

[Turyn 67] R. J. Turyn. *Error correcting codes*, Chap. Sequences with small correlation, pp. 195–228. Wiley, 1967.

[Turyn 74] R. J. Turyn. "Hadamard matrices, Baumert-Hall units, four-symbol sequences, pulse compression, and surfave wave encodings". *Journal of Combinatorial Theory, Series A*, Vol. 17, No. 3, pp. 313–333, 1974.

[Ubise 12] Ubisense. `http://ubisense.net`, 2012. Accessed on December 4, 2012.

[Ullah 10] M. H. Ullah, M. N. Bari, and A. U. Priantoro. "FPGA implementation of LS code generator for CDM based MIMO channel sounder". *Journal of Computing*, Vol. 2, No. 2, pp. 55–61, 2010.

[Urena 07] J. Ureña, A. Hernández, A. Jiménez, J. M. Villadangos, M. Mazo, J. C. García, J. J. García, F. J. Álvarez, C. De Marziani, M. C. Pérez, A. R. Jiménez, and F. Seco. "Advanced sensorial system for an acoustic LPS". *Microprocessors and Microsystems*, Vol. 31, No. 6, pp. 393–401, 2007.

[Vaidy 90] P. P. Vaidyanathan. "Multirate digital filters, filter banks, polyphase networks, and applications: a tutorial". *Proceedings of the IEEE*, Vol. 78, No. 1, pp. 56–93, 1990.

[Vaidy 93] P. P. Vaidyanathan. *Multirate systems and filter banks*. Prentice Hall, 1993.

[Van N 91] D. J. R. Van Nee. "New fast GPS code-acquisition technique using FFT". *Electronics Letters*, Vol. 27, No. 2, pp. 158–160, 1991.

[Varad 02] V. Varadan and H. Leung. "Design of piecewise maps for chaotic spread-spectrum communications using genetic programming". *IEEE Transactions on Circuits and Systems I: Fundamental Theory and Applications*, Vol. 49, No. 11, pp. 1543–1553, 2002.

[Villa 07] J. M. Villadangos, J. Ureña, M. Mazo, A. Hernández, C. De Marziani, M. C. Pérez, F. Álvarez, J. J. García, A. Jiménez, and I. Gude. "Ultrasonic local positioning system with large covered area". In: *Proceedings of the 2007 IEEE International Symposium on Intelligent Signal Processing, WISP '07*, pp. 1–6, 2007.

[Villa 11] J. M. Villadangos, J. Ureña, J. J. García, M. Mazo, A. Hernández, A. Jiménez, D. Ruiz, and C. De Marziani. "Measuring time-of-flight in an

ultrasonic LPS system using generalized cross-correlation". *Sensors*, Vol. 11, No. 11, pp. 10326–10342, 2011.

[Villa 13] J. M. Villadangos. *Contribución Contribución al diseño de un LPS ultrasónico de amplia cobertura empleando técnicas de codificación*. PhD thesis, University of Alcalá. Department of Electronics, 2013.

[Viter 02] A. J. Viterbi. "Very low rate convolution codes for maximum theoretical performance of spread-spectrum multiple-access channels". *IEEE Journal on Selected Areas in Communications*, Vol. 8, No. 4, pp. 641–649, 2002.

[Wang 05] X. Wang, Z. M., Y.-C. Lai, X. Gong, and C. H. Lai. "Spread-spectrum communication using binary spatiotemporal chaotic codes". *Physics Letters A*, Vol. 334, No. 1, pp. 30–36, 2005.

[Wang 08] G. Wang and H. He. "A new hyperchaotic sequence for DS-UWB systems". In: *Proceedings of the 11th IEEE Singapore International Conference on Communication Systems, ICCS '08*, pp. 54–58, 2008.

[Ward 97] A. Ward, A. Jones, and A. Hopper. "A new location technique for the active office". *IEEE Personal Communications*, Vol. 4, No. 5, pp. 42–47, 1997.

[Wei 05] H. Wei, L. L. Yang, and L. Hanzo. "Interference-free broadband single- and multicarrier DS-CDMA". *IEEE Communications Magazine*, Vol. 43, No. 2, pp. 68–73, 2005.

[Welch 74] L. Welch. "Lower bounds on the maximum cross correlation of signals (Corresp.)". *IEEE Transactions on Information Theory*, Vol. 20, No. 3, pp. 397–399, 1974.

[Wentz 06] D. D. Wentzloff and A. P. Chandrakasan. "Gaussian pulse generators for subbanded ultra-wideband transmitters". *IEEE Transactions on Microwave Theory and Techniques*, Vol. 54, No. 4, pp. 1647–1655, 2006.

[White 77] D. J. White, J. N. Hunt, and L. A. G. Dresel. "Uniform Huffman sequences do not exist". *Bulletin of the London Mathematical Society*, Vol. 9, No. 2, pp. 193–198, 1977.

[White 92] J. D. H. White and R. E. Challis. "A Golay sequencer based NDT system for highly attenuating materials". In: *Proceedings of the IEE Colloquium on Non-Contacting and Remote NDT*, pp. 7/1 –7/7, Nov. 1992.

[Woodw 53] P. M. Woodward. *Probability and information theory with applications to RADAR.* New York: Pergamon, 1953.

[Worne 95] G. W. Wornell. "Spreading signature CDMA: Efficient multiuser communication in the presence of fading". *IEEE Transaction on Information Theory*, Vol. 41, No. 5, pp. 1418–1438, 1995.

[Xilin 07] Xilinx Inc. "Virtex-II Pro and Virtex-II Pro X FPGA user guide". `http://www.xilinx.com/support/documentation/user_guides/ug012.pdf`, 2007. Accessed on January 8, 2013.

[Xilin 12a] Xilinx Inc. "Virtex-5 FPGA user guides". `http://www.xilinx.com/support/documentation/virtex-5_user_guides.htm`, 2012. Accessed on February 20, 2013.

[Xilin 12b] Xilinx Inc. "Virtex-6 FPGA user guides". `http://www.xilinx.com/support/documentation/virtex-6.htm`, 2012. Accessed on January 8, 2013.

[Yang 00] K. Yang, K. Y. K., and P. V. Kumar. "Quasi-orthogonal sequences for code-division multiple-access systems". *IEEE Transactions on Information Theory*, Vol. 46, No. 3, pp. 982–993, 2000.

[Yokog 13] Yokogawa Electric Corporation. `http://www.yokogawa.com`, 2013. Accessed on January 8, 2013.

[Zebra 12] Zebra Enterprise Solutions. `http://zes.zebra.com/`, 2012. Accessed on December 4, 2012.

[Zejak 91] A. J. Zejak, E. Zentner, and P. B. Rapajic. "Doppler optimised mismatched filters". *Electronics Letters*, Vol. 27, No. 7, pp. 558–560, 1991.

[Zhang 04] C. Zhang, X. Lin, and M. Hatori. "New sequence pairs with ear zero correlation windows". In: *Proceedings of the 2004 IEEE International Conference on Communications*, pp. 3261–3264, 2004.

[Zhang 05] C. Zhang, X. Lin, S. Yamada, and M. Hatori. "General method to construct LS codes by complete complementary sequences". *IEICE Transactions on Communications*, Vol. E88-B, No. 8, pp. 3484–3487, 2005.

[Zhao 07] H. Zhao, L. Y. L. Mo, and S. Gao. "Barker-coded ultrasound flow imaging: theoretical and practical design considerations". *IEEE Transactions on Ultrasonics, Ferroelectrics and Frequency Control*, Vol. 54, No. 2, pp. 319–331, 2007.